Kinetic and thermodynamic considerations on the formation of heteromolecular layers on metal surfaces

Caroline Henneke

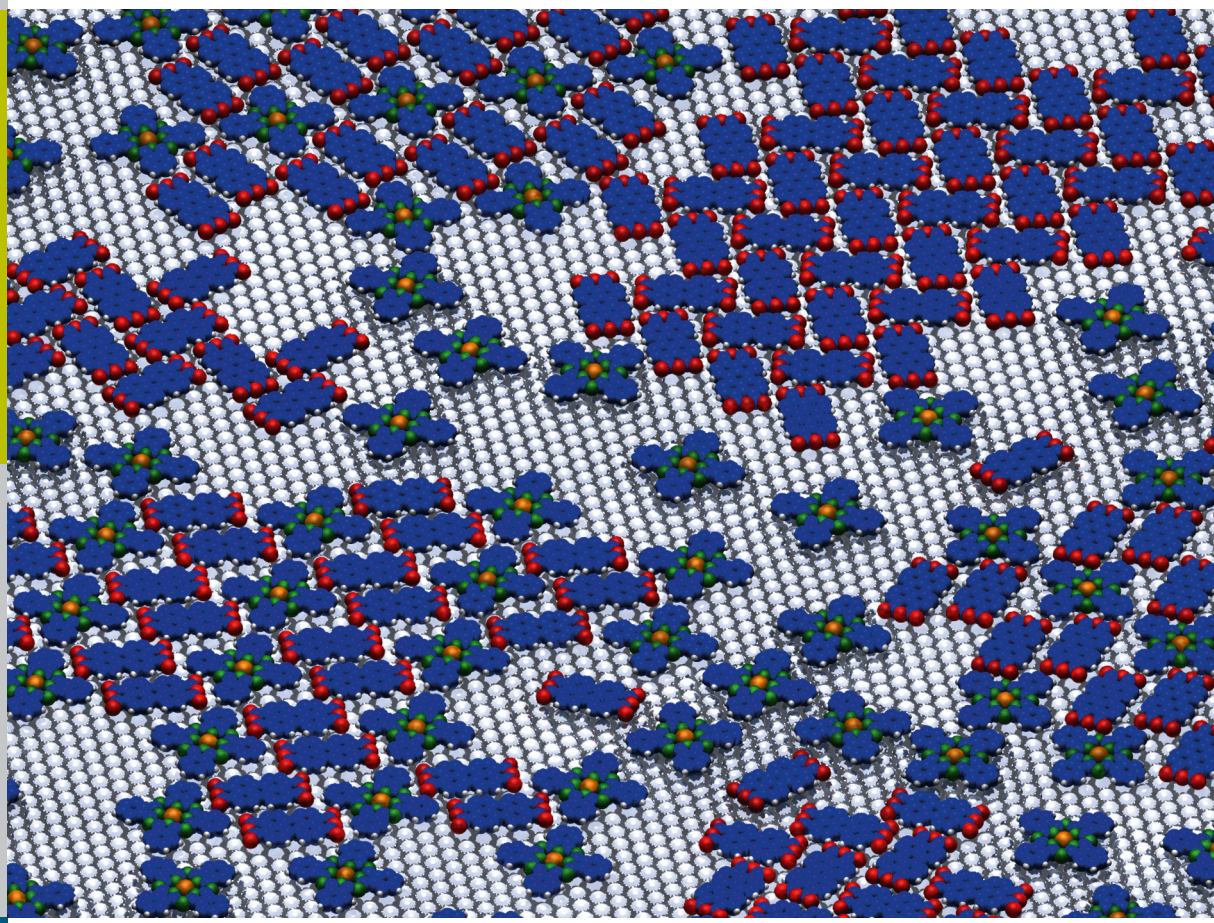

Schlüsseltechnologien / Key Technologies
Band / Volume 149
ISBN 978-3-95806-245-0

JÜLICH FORSCHUNGSZENTRUM

Schriften des Forschungszentrums Jülich
Reihe Schlüsseltechnologien / Key Technologies Band / Volume 149

Forschungszentrum Jülich GmbH
Peter Grünberg Institute (PGI)
Functional Nanostructures at Surfaces (PGI-3)

Kinetic and thermodynamic considerations on the formationof heteromolecular layers on metal surfaces

Caroline Henneke

Schriften des Forschungszentrums Jülich
Reihe Schlüsseltechnologien / Key Technologies Band / Volume 149

ISSN 1866-1807 ISBN 978-3-95806-245-0

Bibliographic information published by the Deutsche Nationalbibliothek.
The Deutsche Nationalbibliothek lists this publication in the Deutsche
Nationalbibliografie; detailed bibliographic data are available in the
Internet at http://dnb.d-nb.de.

Publisher and Distributor:	Forschungszentrum Jülich GmbH Zentralbibliothek 52425 Jülich Tel: +49 2461 61-5368 Fax: +49 2461 61-6103 Email: zb-publikation@fz-juelich.de www.fz-juelich.de/zb
Cover Design:	Grafische Medien, Forschungszentrum Jülich GmbH
Printer:	Grafische Medien, Forschungszentrum Jülich GmbH
Copyright:	Forschungszentrum Jülich 2017

Schriften des Forschungszentrums Jülich
Reihe Schlüsseltechnologien / Key Technologies, Band / Volume 149

D 82 (Diss. RWTH Aachen University, 2015)

ISSN 1866-1807
ISBN 978-3-95806-245-0

The complete volume is freely available on the Internet on the Jülicher Open Access Server (JuSER)
at www.fz-juelich.de/zb/openaccess.

It was one of my more brilliant ideas,
and between you and me, that's saying something.

– *Albus Dumbledore*

Harry Potter and the Philosopher's Stone
by J. K. Rowling

Contents

1 Introduction

An introduction to the system investigated in this work is given in this chapter.

organic electronics

The market for organic electronics is growing fast since the properties of these devices offer a multitude of new applications. Flexible or transparent devices are feasible which is impossible with conventional Si-based materials [For04]. The ability to produce organic electronics by inkjet printing techniques might lead to very low production costs in the future [SKF+00, For04, KB09]. Understanding the fundamental mechanisms that govern the formation of the active layer of such devices is the goal of this work.

self-assembly

Different production methods exist for the fabrication of organic devices [GXS+05]. They can be created by a "top-down" approach and a prominent example for this is photolithography. Also scanning tunneling microscopy (STM) techniques are discussed for direct manipulation in context with proof-of-principle experiments of prototypical devices [ES90, GEW+14]. Both of these methods are prone to errors and, in the latter case, are very time consuming. A quicker "bottom-up" method would be the self-assembly of organic materials which is a standard technique in supramolecular chemistry [WMS91, PS96, WG02]. This method has a built-in error correction since molecules that are bound at a wrong site can detach and reattach again at a different site due to the relatively small, mostly van der Waals, forces between the molecules. A better understanding of the self-assembly of organic layers could simplify the fabrication of organic electronic devices and may even enable the production of devices with specific properties.

heteromolecular system

The active organic layer in electronic devices usually consists of two or more different organic materials acting as charge acceptors and donors. These two types of materials are necessary for organic electronic devices since charge separation and recombination in organic solar cells and organic light emitting diodes [TV87, FFG+99, SBF+99, BTF00, GMN+00], respectively, occur at the donor-acceptor interface. Understanding the fundamental properties of this interface is crucial for improving the device performance. Such a heteromolecular layer consisting of two materials is chosen for this investigation. The focus of this work is on the self-assembly of such heteromolecular films.

(sub-) monolayer regime

The growth or self-assembly is investigated in the (sub-)monolayer regime for two reasons. Firstly, the first layer is the connection between the active layer and the electrodes. It influences the efficiency of organic devices significantly since the band alignment determines the electronic transport through the interface [Zhu04, ZGS07, UK08]. Secondly, it also acts as a template for the growth of the rest of the active layer that is deposited on top. This means that the crystal structure of the entire active layer can be regulated by it.

in-situ observation

Low energy electron microscopy (LEEM) is the chosen method in this investigation since it allows the observation of the film growth *in-situ* during the deposition process of the organic layer. This *in-situ* observation is crucial for understanding the film formation which is the main goal of this work. An additional advantage is the observation of the organic films on a mesoscopic scale which is difficult with other microscopy methods. The combination of theses two advantages allows the observation and understanding of growth dynamics [MRT01, HPF$^+$08]. Low energy electron diffraction (LEED) is also employed in this work since it allows the identification of the different phases on the surface. STM is used when a detailed knowledge of the position and orientation of the molecules on the surface is of crucial importance. These techniques together allow a thorough investigation of the sample in real and reciprocal space.

model system

The heteromolecular system consisting of the molecules 3,4,9,10-perylenetetracarboxylic dianhydride (PTCDA) and copper phthalocyanine (CuPc) is investigated in this work. These molecules are chosen since they represent a model for a donor-acceptor system and the investigation of such systems is important for applications. The homomolecular systems of these molecules have been investigated for more than 20 years, and the electronic as well as the geometric properties of PTCDA [Tau07, EST03, USF96, BMW$^+$12, KUS04, KUS06, GSL$^+$00, HTS$^+$10, SGE$^+$00, ZKS$^+$06, TES$^+$02a, TSS$^+$00, SA94, SSCA95, ATNIK08, GFB$^+$14, SZJ$^+$04, RNP$^+$09] and CuPc [SA94, SPG$^+$02, KSS$^+$10, KSW$^+$11b, KLS$^+$09, SKRK11, HLWM96, SHD$^+$07] are known in detail. First studies of the growth of PTCDA on Ag(111) exist as well [Mar06, MGS$^+$06b]. Heteromolecular systems of the two molecules were started to be investigated about 10 years ago [BWBM03, CMG$^+$12, SLW$^+$14, SHS$^+$15, SSB$^+$14, SWnSR14, GSP$^+$15]. The three heteromolecular phases of the PTCDA-CuPc system on Ag(111) were found at the institute of the author and their electronic and geometric properties are known [SHS$^+$15]. This knowledge about the properties of the final structures of the homomolecular and heteromolecular phases is one of the reasons for choosing this system since it allows the investigation of the growth of the system without the need for additional determinations of basic properties.

different intermolecular interactions

Another reason for selecting these two molecules is their different intermolecular interactions which allow the study of a multitude of different phenomena. The attraction between PTCDA molecules leads to island growth, while the repulsion between the CuPc molecules is the reason for forming a disordered phase up to high submonolayer coverages. This combination of intermolecular attraction and repulsion creates a complex system where different fundamental interactions, which govern the self-assembly, can be studied.

molecule-substrate interaction

The influence of different molecule-substrate interactions on the growth is studied by employing two different substrates, namely Ag(111) and Cu(001). The first substrate is chosen since the structure of the heteromolecular phases of PTCDA and CuPc is known for Ag(111). The second substrate is employed in the investigation to manipulate the interplay between the intermolecular and the molecule-substrate interaction by changing the latter.

growth dynamics

Although many studies have been performed on this and similar systems, only little is known about the actual growth process of the layers. Some knowledge about the

occurrence of the different phases exists, but the driving force for the formation of the different phases is unknown. The growth dynamics are analyzed in this work in detail for the mentioned systems to gain information about their growth kinetics and thermodynamic properties. This gives valuable insights into the crucial parameters for the growth which help identifying the fundamental physical forces behind them.

Outline

The experimental LEEM setup is introduced in chapter 2 and some additional aspects concerning the sample preparation and the data processing are discussed. experimental setup

The theoretical background of growth processes that is frequently used throughout this work is explained in chapter 3. Different growth regimes, the analysis of island densities and island size distributions are introduced. These concepts are important for the determination of interaction energies which is performed in this work. theoretical background

The homomolecular systems of PTCDA and CuPc are discussed in the next two chapters. Important factors for the growth in these systems are determined, which is necessary, since the growth of the heteromolecular system consisting of these two molecules cannot be understood otherwise. results

The growth of PTCDA is described in chapter 4. PTCDA islands grow on both substrates due to the attractive interaction between the molecules. Nucleation theory is successfully applied to the growth and interaction energies are determined. Note that the growth of PTCDA on Ag(111) was already investigated by Marchetto [Mar06, MGS+06b] and is found to be in good agreement with the results presented in this work. PTCDA

The growth of CuPc on both substrates is investigated in chapter 5. The different phases for CuPc on Cu(001) are described in detail including the corresponding phase transitions. The focus is on the disorder-order phase transitions with increasing coverage for the CuPc/Ag(111) system. It is found that this transition is also temperature dependent which is explained by thermodynamic considerations. CuPc

The growth of heteromolecular layers is discussed in the main part of this work (chapter 6). New heteromolecular phases on Cu(001) are presented, and the influence of the concentrations of the two molecules on the occurrence of the different phases is investigated. It is found that the stable phases strongly depend on the deposition sequence of the molecules due to the strong interaction with the Cu(001) substrate. This is different on Ag(111). The weaker substrate interaction allows the thermodynamic equilibrium to be reached in the experiments which in turn enables the determination of a phase diagram for the PTCDA-CuPc system on Ag(111). This was the main goal of this research since such a phase diagram enables the fabrication of heteromolecular layers with distinct properties by looking up the different coverages of the two molecules necessary for the specified layer. heteromolecular layers

This work concludes with a summary of the most important results and an outlook describing the necessary next steps for improving the understanding of the studied system. summary

2 Experimental setup

An overview over the experimental setup that was used in this work is given in this section. Low energy electron microscopy (LEEM) is introduced in the first part. The sample preparation, the temperature measurement, and the beam damage are discussed afterwards. The chapter closes with a detailed description of the image processing methods applied to analyze the image data.

2.1 Experimental methods

The main measurement technique, low energy electron microscopy, used in this work is briefly explained in this section and its measurement modes are described.

2.1.1 Low energy electron microscopy

A short overview over the general measurement principles of LEEM and its possible contrast mechanisms is given in this section. The special characteristics of LEED measurements with a LEEM instrument are explained. The section closes with a description of dark field LEEM measurements.

instrument

All LEEM experiments were carried out with a commercial Elmitec LEEM-III with a Schottky field emitter, an aberration corrector, and an energy analyzer which can be seen in Fig. 2.1. The Schottky field emitter produces a highly coherent electron beam with low energy dispersion. The aberration corrector is a tetrode mirror improving the lateral resolution to $< 2\,\mathrm{nm}$. The energy analyzer delivers an energy resolution $< 150\,\mathrm{meV}$. These three features make this LEEM instrument one of only a handful of microscopes with comparable capabilities. The microscope itself consists of a main chamber and an imaging column. An additional preparation chamber is connected to the main chamber where the sample can be sputtered and annealed and where up to four samples can be stored. The LEEM instrument is also equipped with a Hg- and a He-lamp for photoelectron emission microscopy (PEEM) measurements in the UV radiation range.

working principle

LEEM usually measures the elastically backscattered electrons. A complicated setup is necessary for this which is not described here. The energy the electrons have, when they interact with the sample, can be set by the start voltage, which is closely related to the energy of the electrons, when they reach the sample. This energy changes the contrast in the image, as discussed in the next sections. A detailed description of the physical principles of LEEM and its applications can be found in Ernst Bauer's textbook [Bau14].

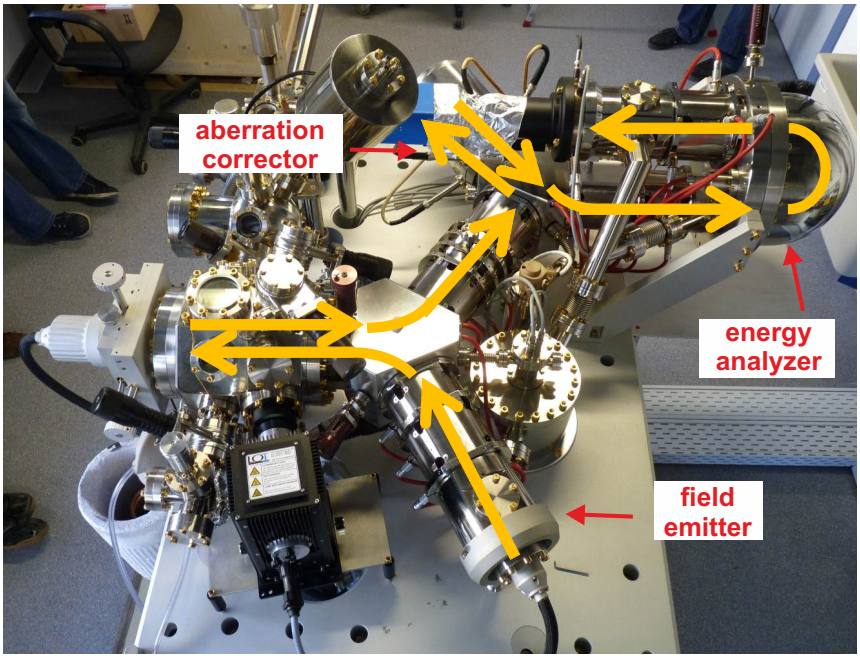

Fig. 2.1: A picture of the LEEM instrument. The yellow arrows indicate the path the electrons travel on through the optics until they hit the detector. The Schottky field emitter, the energy analyzer, and the aberration corrector, which make it one of a handful of instruments with comparable capabilities, are marked.

beam path

The path of the electrons in the microscope is depicted by the yellow arrows in Fig. 2.1. The electrons are emitted by the Schottky field emitter and accelerated to 20 keV. They travel through the illumination column and are deflected by the first sector field. They are decelerated to a specified low energy after they have passed the objective lens and hit the sample at normal incidence (or under a small angle for dark-field LEEM). They interact with the sample and a large part of the electrons is reflected or diffracted. They are reaccelerated on their way to the objective lens, pass the sector field again but are now deflected into the intermediate optics, which guide the electrons through a second sector field to the aberration corrector, where they are reflected. They travel again through the second sector field to the image column and then through the energy analyzer. They are projected onto the detector in the last step.

image and focal plane

The spatial and momentum information of the electrons are maintained while the electrons travel through the optics. This allows the measurement of a spatially resolved image of the surface in a single shot without having to scan over the surface. Image and focal planes are present at different points in the electrons' path. The

image at the detector is affected differently when apertures are inserted in the image or the focal plane. Only certain areas of the sample are imaged when an aperture is inserted in an image plane. The image created by a specific emission angle can be obtained when an aperture is inserted in a focal plane. The effect caused by different positions of an aperture in the focal plane is explained in section 2.1.1.3.

2.1.1.1 Contrast in LEEM mode

There are two different contrast mechanisms in the LEEM mode which are explained in this section, the amplitude or diffraction contrast and the phase contrast. The influence of the focus on the contrast is also discussed.

amplitude contrast

The amplitude contrast is due to different reflection coefficients of the materials on the surface. The organic films investigated in this work reflect the electrons differently than the metal substrates. This reflectivity changes strongly with the energy of the electrons. These changes can cause an inversion of the contrast between the organic film and the metal or a complete disappearance of any contrast. These changes can be quantified by measuring the intensity of LEEM images in a specific range of electron energies to get LEEM-IV curves. Their measurement is crucial for this work, since they help determining, which electron energy gives the best contrast between the organic layers and the metal or the different organic layers themselves. An example, where a change in electron energy changes the contrast within an organic islands consisting of two different phases, can be seen in Fig. 6.25 (e) and (f). Besides these practical applications, LEEM-IV curves can be used to investigate the geometric an electronic structure of the surface [FKM$^+$13, FK14].

phase contrast

The phase contrast is the second type of contrast. It is due to interference effects of the reflected electron waves. Phase shifts of the electron wave occur at step edges where electrons travel differently long paths when they are reflected at the lower or upper terrace of the step edge. This leads to interference effects, e.g. to destructive interference visible as dark lines at the step edges of the Ag(111) surface, as can be seen in Fig. 2.4 (a). Depending on the phase shift of the waves, which can be tuned by selecting the start energy, different interference patterns can be seen at the step edges. This can be used to determine on which side of a step edge the upper and lower terrace is located [Alt10, ACL98].

focus

The focusing conditions of the objective lens also change the contrast in LEEM images. The contrast can invert or the size of features can change significantly when the objective lens current, which determines the focus length, is changed. This is discussed in [DTKT14] where images of a heteromolecular layer are taken at different focusing conditions. They are used to reconstruct an image with improved contrast and more realistic island sizes. Fig. 6.11 shows two images of the same area on the surface at different focusing conditions. The heteromolecular islands, which appear black in Fig. 6.11 (a), turn white in Fig. 6.11 (b) when only the focus is changed. Different focusing conditions were used in this work to make the relevant objects more visible while maintaining a realistic representation of their size and shape.

2.1.1.2 LEED

Low energy electron diffraction (LEED) patterns give information about the geometric structure of the surface. Since it is a standard technique, its working principles are not described here, but only specific aspects for LEED data recorded with the LEEM instrument are addressed. LEED patterns can be obtained by changing a few lens settings in the LEEM instrument so that the focal plane instead of the image plane is projected onto the detector.

spots do not move

One special characteristic of the LEED pattern obtained by a LEEM instrument compared to a conventional LEED is that the spots do not move significantly when the electron energy is changed. This is due to the high energy the electrons get accelerated to by the voltage between the sample and the objective lens. This simplifies the data extraction of LEED-IV curves since the integration area does not have to follow the movement of the LEED spot.

µLEED

Another specialty of the LEED measurements with the LEEM instrument is that only small areas on the surface can be measured. This allows the determination of the geometric structure of individual islands on the surface. Such LEED measurements from areas of less than a few square micrometers are called µLEED. All LEED measurements in this work are µLEED measurements of areas of 18 µm^2 or less.

2.1.1.3 Bright-field and dark-field LEEM

The methods and opportunities of bright-field and dark-field LEEM are described in this section.

position of contrast aperture

It was already mentioned that the selection of electrons with a specific emission angle is possible by inserting an aperture, the contrast aperture, in a focal plane. A sketch of the beam path at normal incidence in the microscope is shown in Fig. 2.2 (a). The direction of the incoming electrons on the sample is depicted by the wide light gray arrow. Electrons are reflected at the sample with different emission angles. The path of those electrons the momentum of which parallel to the surface does not change upon reflection is shown by the thick black line while electrons with a certain momentum transfer parallel to the surface are depicted by the red and blue lines depending on their emission direction. They travel through the LEEM optics, which is indicated by the light blue ellipse, and the image plane is projected onto the detector. The beams with the same emission angles intersect in the focal planes. One focal plane is depicted in the image.

BF-LEEM

Bright-field (BF) LEEM images are obtained when the aperture is inserted in a way that the 00-beam (intersection of thick black lines) passes the contrast aperture, see Fig. 2.2 (a). Only electrons emitted normal to the surface can pass the aperture and are projected onto the detector. BF-LEEM images are just called "LEEM images" in this work.

DF-LEEM

Dark-field (DF) LEEM images are obtained when not the (00)-beam but a different beam is selected. This is shown in Fig. 2.2 (b) where only the red beams pass the aperture and reach the detector. This selection of specific beams can be done by changing the position of the contrast aperture or by tilting the incidence beam on the

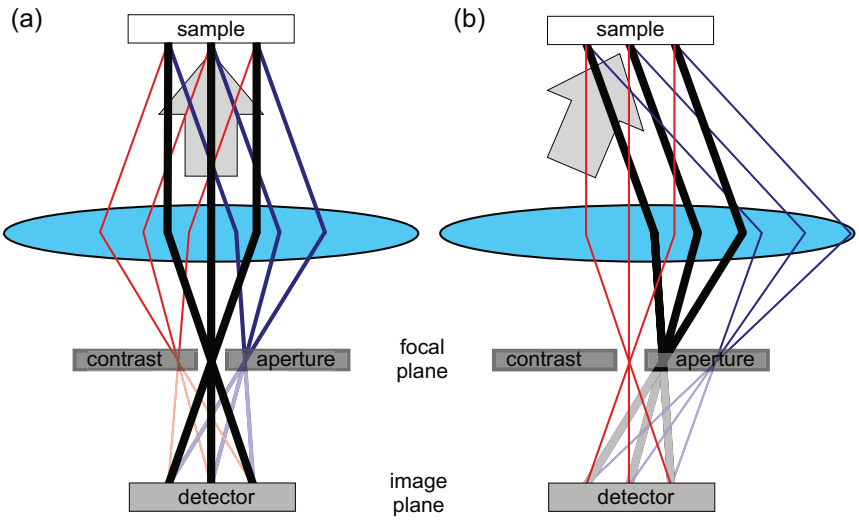

Fig. 2.2: Paths of the electrons at different incident angles. (a) Bright-field LEEM: the 00-spot passes the aperture. (b) Dark field-LEEM: a higher order diffraction spot is selected by the contrast aperture.

sample. The first method leads to a worse image quality since the chosen beam does not travel on the optical axis through the microscope which increases aberrations. Furthermore, it is almost impossible to position the contrast aperture reproducibly. Hence, the second method is usually applied. This creates an image that only contains the information in the red beam. Different incident angles can be applied so that different LEED spots can pass the aperture.

opportunities

The ability to choose specific beams for the image formation gives additional information about the surface such as the orientation of domains or the structures of different parts on the surface. An example is the measurement of two different rotational domains of CuPc on Cu(001) with DF-LEEM, as shown in Fig. 2.3. The areas that appear bright in each image belong to the domain the selected diffraction spot belongs to. The areas that appear bright in Fig. 2.3 (a) are dark in (b) and vice versa since only two different rotational domains exist on this surface due to symmetry reasons. The individual DF-LEEM images are often superimposed to create a composite image. This process is described in section 2.5.2.

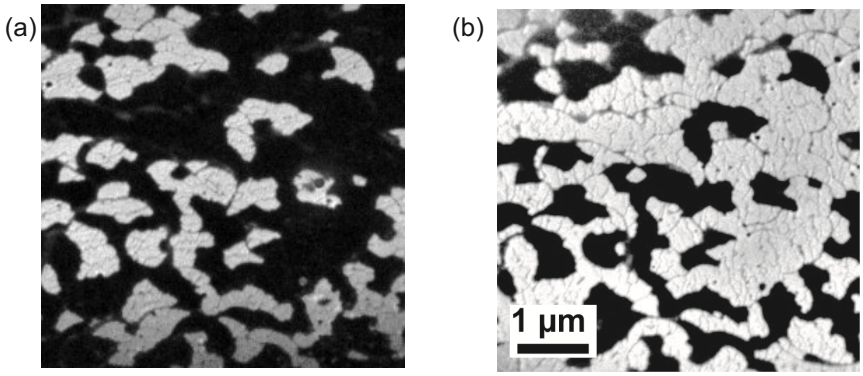

Fig. 2.3: The two rotational domains of CuPc on Cu(001) measured at $U_{\text{start}} = 3.0\,\text{V}$. The bright areas belong to the domain of the selected LEED spot. A spot of each domain was chosen for the two images. Adapted from [vB14].

2.2 Sample preparation

The sample preparation is described in this section.

cleaning procedure of crystals

The metal substrates were prepared by sputtering and annealing cycles in the preparation chamber of the LEEM instrument. The Cu(001) crystal was cleaned by sputtering with a 1:1 mixture of Ar and H_2 at 1 keV and subsequent annealing to 900 K. Better results regarding terrace width were obtained with this mixture of gases compared to standard Ag-sputtering. The Ag(111) crystal was sputtered with Ar or Ne ions at 1 keV and He ions in the final cycle. The crystal was annealed to 750 K and, in the last cycle, to 850 K to create large terraces.

step edges

An image of the clean Ag(111) crystal is shown in Fig. 2.4 (a). The terraces are clean and only a few pinning centers of the step edges can be observed. The upper terrace is located on the concave side of a step edge, as is marked in Fig. 2.4 (b). This was determined by the movement of the step edges during annealing experiments. The step edges move into the direction of the red arrow during the heating process. This determines the lower terrace as the left side since molecules desorb during the annealing process leading to movement of the step edges towards the higher terraces. The curvature of the steps does not change significantly during the cooling of the Cu(001) and Ag(111) crystals back to room temperature, which made the identification of the upper and lower side of the step edges possible, without watching the annealing process at that particular area. The upper and lower terrace can also be determined by analyzing the intensity directly around the step edges [CA98].

deposition parameters

All samples were prepared under UHV conditions with a base pressure of $5 \cdot 10^{-10}$ Torr. The PTCDA and CuPc powders were purified by at least three sublimation cycles. They were evaporated onto the sample in the main chamber of the LEEM instrument with custom-made Knudsen cell evaporators. The evaporators were preheated for at least one hour to guarantee constant deposition rates. They were calibrated before-

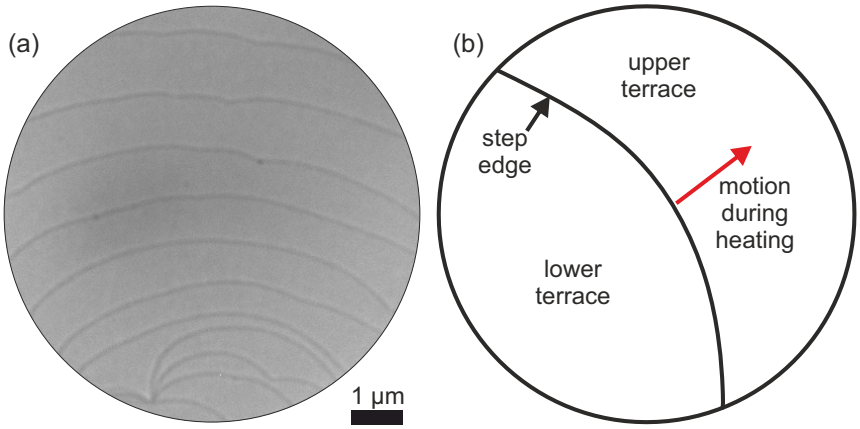

Fig. 2.4: (a) LEEM image of the clean Ag(111) surface ($U_{\text{start}} = 0.5\,\text{V}$). (b) Sketch of the movement direction of the step edge during annealing which determines the upper and lower terrace.

hand by measuring the time it took to deposit a monolayer film of each substance. It was checked regularly that the deposition rate did not change due to different filling levels of the crucibles containing the molecules. The uncertainty on the deposition rates depends strongly on the type of molecule and the evaporator used. The deposition rate of PTCDA was almost constant during many months while the CuPc deposition rate changed from experiment to experiment by up to 10% even though the same heating conditions were used.

2.3 Temperature measurement

How the temperature measurement of the sample in the experiments was performed is briefly explained in this section. A more detailed description of the temperature calibration can be found in the Master's thesis of Jonas van Bebber [vB14].

instrument

The sample temperature is measured by a tungsten rhenium thermo couple which is spot welded to the sample holder. The measurement is complicated by the sample holder (together with sample), which is biased with approximately 20 kV, since this voltage is needed to decelerate the electrons to the start voltage of only a few volts. The readout of the temperature is therefore performed in the high voltage (HV) rack of the LEEM with the right electronics which are also floating at 20 kV.

influence of room temperature

The sample temperature in the cage of the HV-rack influences the measured sample temperature strongly. It was found that the measured sample temperature increases with increasing temperature in the cage of the HV-rack. This is a problem, since the laboratory is not air conditioned, which leads to a fluctuation of the temperature in the HV-rack. The temperature of a sample that was not heated or cooled but in equilibrium with its surroundings, which was assumed to be always 300 K, was determined

for many different temperatures in the HV-rack which were measured by a digital thermometer taped to the inside of the front plane of the HV-rack. A linear trend between the two temperatures was found and a calibration curve was obtained that could be used to calculate the "real" room temperature. A temperature difference of 1 K in the HV-rack leads to a measured temperature difference of around 30 K [vB14]. The temperature in the HV-rack was always noted when experiments were performed to compensate for this. It is assumed that this difference between the measured and the actual temperature only depends on the temperature in the HV-rack and not on the sample temperature as well. This leads to a specific offset at a certain HV-rack temperature for all sample temperatures which is important for heating experiments. There is still a lag between the temperature that was measured on the inside of the HV-rack and on the inside of the cage of the HV-rack where the connection point of the thermo couple is located. This introduces an additional uncertainty into this calibration.

heating The heating of the sample in the experiments was performed with tungsten filaments leading to slightly different heating rates for each filament since the filaments were not all exactly the same. A calibration curve was determined giving the temperature-current dependency for each filament. This calibration helped diminish the uncertainty on the temperature measurement, since the values from this calibration and the actually measured temperature, which could be corrected with the previously explained linear calibration, could be compared.

uncertainty Despite these efforts, the uncertainty on the temperature is still between 5 K and 15 K. This is not a significant uncertainty when working with large temperature difference, but most experiments in this work were performed in a temperature range between 300 K and 400 K. This makes the quantitative analysis of temperature dependent phenomena difficult.

2.4 Beam damage

Beam damage in organic or molecules thin films is always a big concern.

visible changes The influence of the electrons on the sample manifests itself in different ways. The intensity of LEED spots decreases, when the sample is illuminated for prolonged time with electrons of an energy above 5 eV, since the long range order of the organic film becomes worse. It was also observed that some parts of the islands change their contrast in LEEM showing that different parts of the islands are affected differently. Both are discussed in [Sch12] on pages 14 - 17. The organic film can also show a different contrast in the areas that were illuminated, as can be seen in Fig. 2.5 (a). The red circle marks the area that was previously illuminated by electrons with an energy of 5 eV. A difference in contrast between the inside and the outside of the circle can be seen.

changed physics Another possibility is that the conditions on the sample are changed due to the presence of the LEEM electrons which could lead to a change in growth. These differences in the growth conditions only become visible if a different part of the sample is imaged.

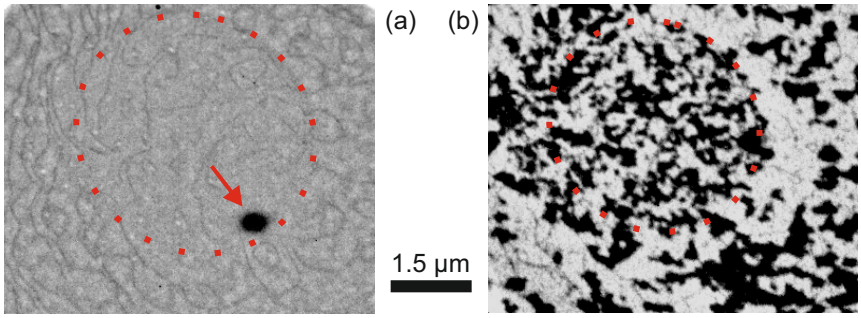

Fig. 2.5: (a) Changed LEEM image contrast of a CuPc film on Cu(001) at $U_{\text{start}} = 3.0\,\text{V}$. The red arrow marks a defect of the channel plates. (b) Electron beam induces change in the nucleation density as can be seen be the decreased size of the rotational domains of CuPc on Cu(001) (DF-LEEM at $U_{\text{start}} = 2.0\,\text{V}$).

Fig. 2.5 (b) shows such a case with a DF-LEEM image taken after the deposition of CuPc on Cu(001). The bright and dark areas belong to the two rotational domains of CuPc. The area, where the electron beam has illuminated the sample during the growth, is marked by a red circle. No intensity difference between the domains inside and outside of the circle can be observed but the domain sizes are different. The domains are much smaller inside the circle than outside. This shows that the nucleation density of CuPc was influence by the presence of the electron beam during the growth.

savety measures

Several precautions were taken during the experiments to prevent beam damage to influence the results. Small start voltages of 2 V and below were used for LEEM measurement which proved to not damage the organic films. After LEED measurements„ which were performed at higher energies between 4 V and 30 V, it was always checked in LEEM for any changes before and after the measurement and the position on the sample was changed if damage was observed.

2.5 Image processing

The LEEM data was analyzed using the open source *ImageJ* program [SRE12] and the related *Fiji* [SACF+12] image processing package. Important processing steps of the LEEM data are described in the next three sections.

2.5.1 Image correction

The images can be corrected to simplify their analysis. The following procedures can be used for LEEM and LEED images and was already described by Schwarz *et al.* [SvGZP12a].

flat field correction

The channel plates exhibit different sensitivities at different areas. This area dependent factor is constant over several month if the channel plates are not exposed to high intensities or ambient condition and are operated with the same parameters. A flat field correction compensates for the different sensitivities of the channel plates. An image the intensity of which does not depend on the sample morphology is needed for this correction. LEEM images in the mirror mode at negative start voltages are a possible source. Several of such images should be measured and then averaged to get good statistics for this background image. The measured images are divided by this image canceling the inhomogeneities due to the different sensitivities on the channel plates.

backgound in LEED

Secondary electrons and diffuse intensity sometimes obscure the LEED patterns of crystalline structures. The secondary electrons are not very prominent in the images taken with the employed LEEM instrument since it has an energy analyzer and most of the secondary electrons can be cut off by an energy slit. There are nonetheless still secondary electrons present and visible diffuse intensity. The background correction was only performed to make LEED patterns of crystalline structures more visible. The background was not corrected when the diffuse intensity was important, as in the case of the presence of CuPc on Ag(111) and Cu(001) (chapter 5). The LEED images are processed in the following way to improve the visibility of the LEED spots. The minimal value in a specified region of several pixels is found and is plotted with an appropriate filter with *Fiji*. The size of the region depends on the sharpness of the spots and the resolution of the image. The region has to be big enough so that all LEED spots have disappeared after this procedure. The maximum in regions of the same size are then determined and plotted with a different filter. A Gaussian blur is then applied to smooth the modified image. The measured image is divided by the modified LEED image to remove the diffuse background signal. This procedure can significantly improve the visibility of the LEED spots, an example of this can be found in [SvGZP12a].

2.5.2 Composite images

There are up to six rotational domains present in the molecular films investigated in this work. Composite images (based on up to six DF-LEEM images) are created

showing rotational domains in different colors to allow the comparison of the individual domains.

image alignment

It is important for this method that there is no misalignment between the individual DF-LEEM images. This means that the outlines of the domains have to fit between the images. This is not always the case, since the images shift due to the tilt of the incident beam when the LEEM instrument is not perfectly aligned. The images have to be matched before they can be processed further if this is the case.

merge color channels

The different DF-LEEM images can be merged in a false-color composite image with the *Fiji* program. An example of this can be seen in Fig. 4.13 for two rotational domains and Fig. 5.14 for six rotational domains. Each color channel (blue, red, green, magenta, cyan, and yellow) represents one of the DF-LEEM images.

2.5.3 Step edges

The step edges play an important role in the the growth of organic films, as is discussed in this work. They are usually not clearly visible in the best focusing conditions for imaging the molecular islands. This makes them (almost) invisible in most images that focus on the organic islands, but they are visible under different conditions. Hence, the outline of the step edges are, in this work, usually measured in a separate LEEM image and then superimposed to the actual image. Two methods to determine these outlines are described now.

threshold method

Images of the step edges of the substrate with a very clear contrast can be processed using the threshold method. The background was first subtracted with the method described in section 2.5.1. The step edges now have all approximately the same intensity. They can be selected by applying a threshold in *Fiji*. This creates a black and white image where the selected areas (step edges) are black and the other areas (terraces) are white. Such binary images can easily be superimposed to the LEEM images. This method requires are very good image quality. An example of step edges determined by this method can be seen in Fig. 5.17.

manually

The image contrast was sometimes not good enough to employ the threshold method. Thin lines can be drawn manually in the image in such cases if the step edges are only barely visible. This modified image can be easily processed with the threshold method in *Fiji* to get the outlines of the step edges. This leads to very clear lines, as can be seen in Fig. 5.20. The drawback of this method is that it is more time consuming.

3 Theoretical background

Theoretical models that describe the growth of thin films are discussed in this section. The different growth regimes of island growth are first explained. Then a method to determine the binding energy of small clusters and the activation energy for diffusion is described. The critical island size is needed for that and its determination by analyzing the island size distribution (ISD) is demonstrated in the last part.

3.1 Growth regimes at submonolayer coverages

The growth of the first layer of an adsorbate on a surface can be categorized into different growth regimes. Using Smoluchowski's approach with rate equation [vS16, vS17], four different regimes of the growth can be identified [AFL94].

complete condensation

When adsorbates, in this case molecules, are deposited on a surface, they can either get adsorbed on the surface and stay there, or get adsorbed and then desorb again. Only the case of complete condensation, in which the molecule will not leave the surface once it is adsorbed on it, is considered in the following. This means that the sticking coefficient, which gives the percentage of molecules that stay on the surface from the amount of molecules that hit the surface, is 1.0. This case of complete condensation is a good approximation for the systems investigated in this work.

growth regimes

The different regimes during the island growth of adsorbates on a surface are described in the following paragraphs. The number of islands versus the coverage is plotted in Fig. 3.1 to give an overview over the different regimes. This data from a kinetic Monte Carlo simulation is taken from the Master's thesis of Felix Lublasser [Lub15].

low coverage regime

Only a few molecules are present on the surface in the beginning of the deposition process. They diffuse on the surface and, if they meet each other and the total energy for forming a cluster is smaller than that of the individual molecules, they will stick together forming an island. In some cases, two molecules together already form a stable island and in other cases many molecules have to meet to become a stable island. Details of this critical size of stable clusters are discussed in section 3.3. In the low coverage regime, many stable clusters form leading to the nucleation of many new islands. This leads to a strong increase in the number of islands on the surface.

intermediate regime

When the deposition is continued, the number of islands increases until there are more islands than single molecules. This is where the intermediate regime starts. Single molecules still meet each other and form new stable clusters but the majority of molecules gets adsorbed at the edges of already existing islands leading to a growth of these islands. The number of islands still increases in this regime but not as strongly as in the previous regime.

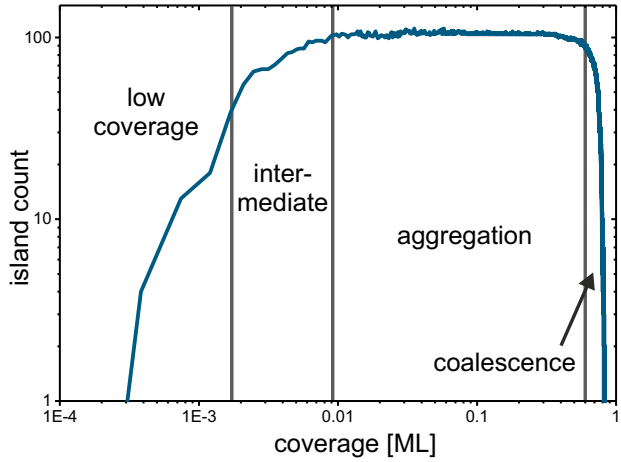

Fig. 3.1: The number of islands is shown at different coverages to illustrate the different regimes during island growth. It starts with a low coverage regime, followed by the intermediate regime. The island density is constant in the aggregation regime and when islands start to grow together, coalescence begins. The data is taken from a kinetic Monte Carlo simulation from [Lub15].

aggregation regime

Once the distance between the islands' edges is in the range of the diffusion length of the molecules, all deposited molecules attach to existing islands. In this regime, called the aggregation regime, the islands grow in size while the number of islands is constant. This leads to a constant island density, which is a characteristic property of the system and can be used to determine the critical island size, diffusion barriers, and binding energies of clusters.

coalescence

The islands continue to grow and, at some point, they touch each other and coalesce. The islands grow together leading to a decrease in the island density. The decrease in island numbers continues until nucleation in the second layer starts leading again to an increase in the number of islands.

3.2 Island density, binding energies, and diffusion barrier

The island density gives important information about the properties of the adsorbate-substrate system. Information about the diffusion barrier and binding energies can be obtained by analyzing the island density of thin films that were deposited at different substrate temperatures.

In the last section, it was shown that the island density strongly depends on the coverage of the adsorbate on the surface. The number of islands is only constant in the aggregation regime. This island density is determined by the interaction of the substrate with the adsorbate, the interadsorbate interaction, and the deposition rate. In the aggregation regime, the number of islands is given by

critical island size i

$$N \propto \left(\frac{F}{D}\right)^{\chi} \tag{3.1}$$

where D is the diffusion constant, F the deposition flux, and $\chi = \frac{i}{i+2}$ [VSH84]. The critical nucleus size i gives the maximal number of entities in a cluster that is still more likely to break apart again than to stick together. That means that a cluster of size i is unstable. If one more entity is added to the cluster, giving it a size of $i+1$, it becomes stable.
The diffusion constant is given by

energy dependence

$$D = D_0 e^{-E_D/k_B T} \tag{3.2}$$

with the diffusion prefactor D_0, the activation energy for diffusion E_D, and the temperature T. Substituting (3.2) in (3.1) gives

$$N \propto e^{\chi \frac{E_D}{k_B T}}. \tag{3.3}$$

This only takes into account the activation energy for diffusion and not binding energies between molecules, which means that it is only valid for $i = 1$. If the binding energy between the molecules is also considered [Bru98, TKKT04]

$$\rho \propto e^{\frac{\sum_{s=2}^{i} E_B^{(s)} + i \cdot E_D}{(i+2) k_B T}}, \tag{3.4}$$

is obtained, where $E_B^{(s)}$ is the binding energy difference between cluster of size s and $s-1$.
Information about the exponent in Eq. (3.4) is obtained by plotting the logarithm of the island density versus the inverse of the temperature in an Arrhenius-type diagram and determining the slope of that curve. But it can be seen that without further information about the critical island size, i, neither the binding energy nor the activation energy for diffusion can be determined. One way to determine the critical island size is explained in the next section.

data evaluation

3.3 Critical island size determined by island size distribution

The island size distribution can be used to obtain the critical island size since it has a characteristic shape which is determined only by the critical island size in the

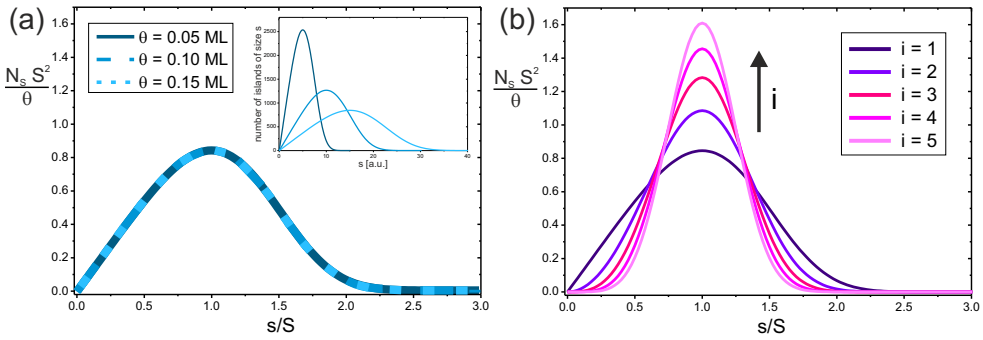

Fig. 3.2: (a) Island size distribution of $i = 1$. Inset: Histogram of islands of size s for different coverages. After the normalization all three curves collapse into one curve with a peak at 1.0 and a characteristic shape depending on the critical island size i. (b) Island size distribution for different i. With increasing critical nucleus size, the peak gets sharper and the maximal value increases, while the area of the curve stays constant.

aggregation regime. The method outlined here was developed by Amar, Family and Lam [AFL94].

island size distribution function

The island size distribution function, N_s, gives the number of islands of size s per site at a certain coverage. This function depends on the coverage, θ, as can be seen in the inset in Fig. 3.2 (a), which shows the number of islands of size s versus the size of the islands for three different coverages. The peak of the distribution moves to bigger island sizes with increasing coverage and it becomes broader while the area under the curve stays constant. This is not surprising since the number of islands is constant in the aggregation regime and the islands only increase in size. The goal is to obtain a function that only depends on the critical island size but not on the coverage. One way to accomplish this is described now. The total island density, N, is defined as

$$N = \sum_{s \geq 2} N_s(\theta)\,. \tag{3.5}$$

The mean island size, S, and the coverage, θ, are given by

$$S = \frac{\sum\limits_{s \geq 2} s N_s(\theta)}{\sum\limits_{s \geq 2} N_s(\theta)} \quad \text{and} \quad \theta = \sum_{s \geq 1} s N_s(\theta)\,. \tag{3.6}$$

The dynamic scaling assumption [VF84, Mul86, FM88, FM89] proposes that there is one characteristic property that determines the island size distribution. This is the mean island size S. This leads to

$$f\left(\frac{s}{S}\right) = \frac{N_s S^2}{\theta} \qquad \text{for} \qquad s \geq 2, \tag{3.7}$$

i	a_i	C_i
1	0.2715	1.1091
2	0.2976	1.9678
3	0.3086	3.2385
4	0.3145	5.1214
5	0.3182	7.9036
6	0.3207	11.9963

Table 3.1: Values for a_i and C_i determined by (3.9)

where f only depends on i. This means that all island size distribution functions for different coverages will collapse into one function when $N_s S^2/\theta$ is plotted versus s/S. Equation (3.7) was applied to the data in the inset of Fig. 3.2 (a) and the result can be seen in Fig. 3.2 (a). All three function overlap after this normalization.

scaling function

The next step is to calculate the critical island size from the shape of the island size distributions. One ansatz for a scaling function for different i is

$$f_i(u) = C_i u^i e^{\left(-i a_i u^{1/a_i}\right)}, \tag{3.8}$$

where C_i and a_i are given by the implicit equations

$$(i a_i)^{a_i} = \frac{\Gamma\left[(i+2)\, a_i\right]}{\Gamma\left[(i+1)\, a_i\right]} \quad \text{and} \quad C_i = \frac{(i a_i)^{(i+1) a_i}}{a_i \Gamma\left[(i+1)\, a_i\right]}. \tag{3.9}$$

The values for a_i and C_i are given in Table 3.1 [PLN+11]. The scaling functions for different i are plotted in Fig. 3.2 (b). It can be seen that the peak gets sharper and the maximum value increases with increasing critical island size.

data evaluation

In order to apply this theory to an experiment, the individual island sizes in the aggregation regime during the growth have to be measured. By applying Eq. (3.7), the data can be scaled. In the last step, the data has to be compared to the theoretical scaling curves. The data and the theoretical curves should overlap without further scaling meaning that they should have the same absolute values. In chapter 4.1.1, the critical nucleus for PTCDA on Cu(001) are determined for different temperatures and in chapter 6.1.2 the limits of this theory are discovered.

4 Growth of PTCDA

The growth of PTCDA is discussed in this chapter. The attractive intermolecular interaction of the PTCDA molecules leads to island growth at already very low coverages. The analysis of the growth dynamics of these islands allows the determination of interaction energies between the PTCDA molecules as well as the molecule-substrate interaction. The growth is investigated on two different substrates, namely Cu(001) (section 4.1) and Ag(111) (section 4.2). This change in substrates enables the study of the influence of the different molecule-substrate interaction strength on the growth of the molecular islands.

4.1 Growth of PTCDA on Cu(001)

The growth of PTCDA on a bare Cu(001) surface is discussed in this section.
The geometric and electronic structure of PTCDA on Cu(001) was already investigated by intensive LEED, thermal desorption mass spectrometry (TDMS) and X-ray photoelectron spectroscopy (XPS) studies [SA94, SSCA95]. PTCDA grows on Cu(001) with a commensurate rectangular $(4\sqrt{2} \times 5\sqrt{2})$-$R45°$ superstructure. The unit cell dimension are $b_1 = 14.5\,\text{Å}$ and $b_2 = 18.1\,\text{Å}$ leading to a unit cell size of $262\,\text{Å}^2$. The superstructure can be described by the superstructure matrix

previous studies

$$M_{\text{PTCDA, Cu(001)}} = \begin{pmatrix} 4 & 4 \\ -5 & 5 \end{pmatrix}.$$

In an ARPES study, it was proposed that PTCDA molecules loose one oxygen atom when it comes in contact with the reactive Cu(001) surface [ATNIK08]. The authors of another recent publication raised doubts about this finding since they cannot find any evidence of this change in the PTCDA molecule in their STM studies [GFB+14]. They also found that the crystallinity of the PTCDA layer is strongly influenced by the temperature during the deposition. At deposition temperatures between 300 K and 350 K, there are many domain boundaries that develope when two differently oriented islands or islands with a slight lateral translation grow together.
In the following subsections, the growth of PTCDA up to coverages of one monolayer is discussed. The first subsection (4.1.1) focuses on the growth at substrate temperatures of 300 K-390 K during the deposition. A change of the critical nucleus size with increasing substrate temperature is determined and a diffusion barrier of 0.45 eV and a binding energy of 1.6 eV are found. The second part describes the growth at more elevated substrate temperatures of around 460 K (4.1.2). Growth kinetics and

contents

nucleation processes are analyzed. The anisotropy of the growth is explained by a preferential adsorption at certain island edges. It is shown that single molecules can cross step edges while the crystalline islands cannot grow across them. A concentration necessary for the nucleation of new islands of $1.02 \cdot 10^{-3}$ molecules/nm^2 is determined.

4.1.1 Growth at temperatures between 300 K and 390 K

The growth of PTCDA on Cu(001) at room temperature and slightly above is analyzed in this section.

growth process

The growth process of PTCDA at 350 K on Cu(001) at coverages from 0 monolayers (ML) to 1.01 ML is shown in Fig. 4.1.[1] The first islands nucleate soon after the deposition is started. The islands that are present at a coverage of 0.03 ML can be seen in Fig. 4.1 (a). New islands continue to nucleate until a coverage of 0.08 ML is reached. The number of islands is constant from this point on until the islands start to coalesce. This regime with a constant number of islands is called the aggregation regime and the analysis of the island size distribution is carried out there. Fig. 4.1 (b) shows the islands in the aggregation regime at a coverage of 0.43 ML. Some islands that nucleated after image Fig. 4.1 (a) was taken are marked by the white arrows in Fig. 4.1 (b). The islands that are present in Fig. 4.1 (b) continue to grow and their shape at a coverage of 0.60 ML can be seen in Fig. 4.1 (c). The islands continue to grow until they start to grow together and coalesce at a coverage of 0.65 ML. This marks the end of the aggregation regime. More islands grow together (Fig. 4.1 (d)) until almost the whole surface is covered by a PTCDA layer (Fig. 4.1 (e)). The dark contrast in the image marks the last areas not jet covered by the PTCDA layer. The dark lines give the boundaries between the individual domains. The nucleation of the second layer starts once the first layer is completely closed, as can be seen as the dark contrast in Fig. 4.1 (f).

layer-by-layer growth

The fact that the second layer only starts to nucleate when the first layer is completely closed shows that PTCDA exhibits a layer-by-layer growth on Cu(001) at 350 K. This agrees with the findings of the growth on Ag(111) (section 4.2 and [Mar06]).

nucleation at step edges

It can be seen in Fig. 4.1 (b) and (c) that islands nucleate preferentially at step edges since the two edges (upper right corner and on the left) are almost completely decorated by islands.

supersaturation

It was already mentioned that the first islands nucleate soon after the deposition is started. The time delay before the first clusters appear is so short that they are already visible in the third measured image after the shutter of the evaporator is opened. This means that the necessary coverage for nucleation for PTCDA is below 0.002 ML since the acquisition time for each image is 1 s and the deposition rate is 0.039 ML/min. How this supersaturation is influenced by the temperature of the substrate during the deposition is discussed in section 4.1.2.

[1] One monolayer (1 ML) is defined as the coverage at which the whole surface is covered by a crystalline PTCDA film.

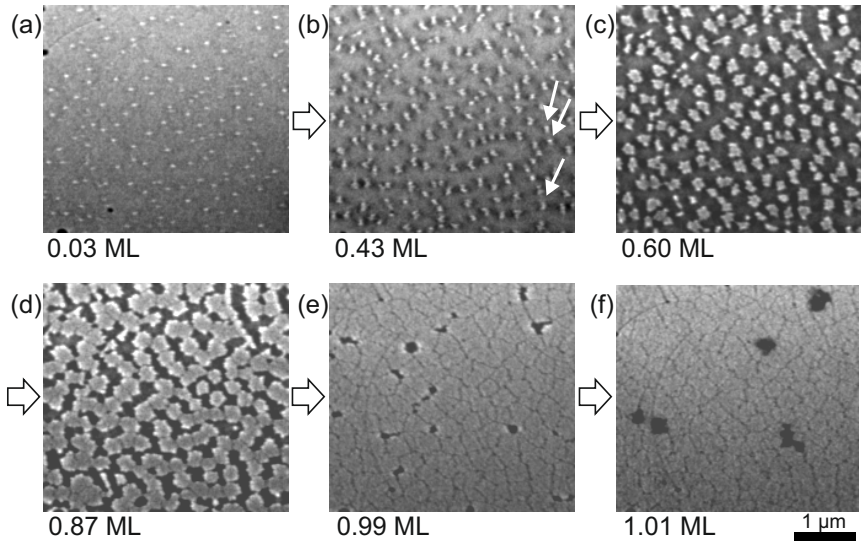

Fig. 4.1: LEEM images taken during the growth of PTCDA on Cu(001) at 350 K. (a) Nucleation of PTCDA islands (bright contrast) starts soon after the deposition is started and many PTCDA islands have already nucleated at a coverage of 0.03 ML. (b) New islands continue to nucleate until a constant number of islands is present on the sample and the aggregation regime of the growth is reached. (c) The existing islands grow. (d) The islands start growing together making the end of the aggregation regime. (e) The surface is almost completely covered by the PTCDA layer. (f) As soon as the first layer is complete, but not before, nucleation of the second layer starts (dark contrast). Images were taken at 2 V (a, b) and 1.3 V (c-f) with a slight under focus.

4.1.1.1 Determination of critical island size

The critical island size of the PTCDA islands at different temperatures is determined in this section.

strong intermolecular attraction

The fact that PTCDA molecules already form clusters at low coverages indicates that there is a relatively strong intermolecular attraction. One way to quantify the strength of the interaction is the determination of the critical island size i since a stronger attractive interaction leads to smaller stable clusters. Another measure of the strength of the interaction is the binding energy. Both were determined and are reported in this work.

applicablity of ISD analysis

The theory to determine the critical island size was developed for adatoms on surfaces. It was already successfully applied to a few systems where molecular films were deposited on surfaces [RNK$^+$03, SHMH06, CCMS07, TKKT04]. Exploratory experiments were carried out to see if the critical nucleus can be determined by analyzing

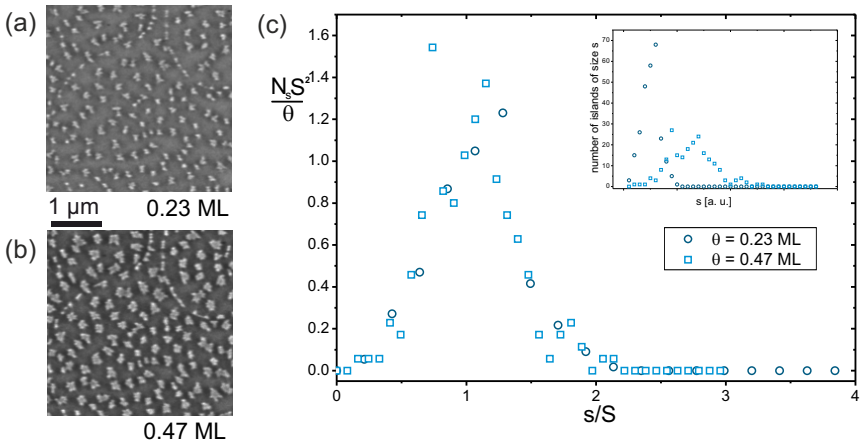

Fig. 4.2: (a) PTCDA islands deposited at 350 K at a coverage of 0.23 ML and (b) 0.47 ML. (c) Island size distribution of PTCDA at different coverages. The inset shows the island size distribution at different coverages before normalization.

the island size distribution (ISD) for PTCDA on Cu(001). PTCDA molecules were deposited at two different temperatures on the Cu(001) surface for this.

prerequisites

Fig. 4.2 shows PTCDA islands (bright contrast) that were deposited at 350 K on Cu(001) in the aggregation regime for two different coverages. Both images were taken at the same position on the sample. The coverages are 0.23 ML in Fig. 4.2 (a) and 0.47 ML in Fig. 4.2 (b). It can be seen that the number of islands is the same. The islands that are present in Fig. 4.2 (a) are still at the same positions in Fig. 4.2 (b) and no new islands have nucleated showing that these images were indeed taken in the aggregation regime. The islands have just grown in size and have changed their shape. It can also be seen that there are very few step edges present on the sample which influence the growth of the islands. The step edges can be identified as the locations where the islands are very small and seem to form curved lines. Only islands that did not grow along step edges are used for the analysis since it is important that the size of the islands is not mainly influenced by the substrate morphology. In order to achieve this, there have to be several islands on each terrace since otherwise the size of the islands is determined by the size of the terrace and not by the interaction between the molecules and between the molecules and the substrate.

image analysis

The images were processed to extract the island size distribution in the following way. Firstly, the background was subtracted by the method described in [SvGZP12b] and in section 2.5.1. Then, a threshold was set and the image was converted into a binary image. With the "Analyse Particle" routine of Fiji [SACF+12], the image was processed with size and roundness constraints to only pick single islands and not noise or other image defects. Only areas that were not influenced by step edges were selected.

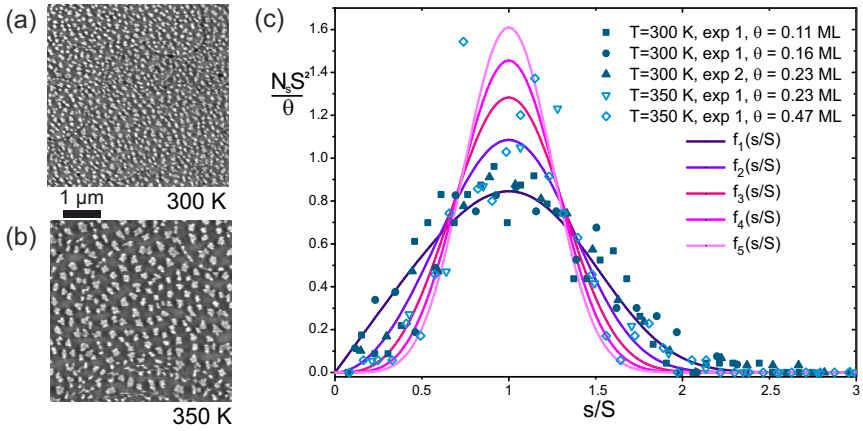

Fig. 4.3: (a) PTCDA islands deposited at 300 K and (b) at 350 K. (c) Island size distribution of PTCDA at different temperatures. The filled symbols show data of two experiments measured at 300 K and the open symbols show data measured at 350 K. The curves depict the scaling function for different critical nuclei.

scaling works

The results of the analysis of the island sizes is plotted in the inset in Fig. 4.2 (c). The number of islands of a certain size s are plotted versus their size making it a histogram of the island sizes. It is clearly visible that the peak of the size distribution at 0.23 ML (dark blue circles) shifts to bigger island sizes for the higher coverage of 0.47 ML (light blue squares). This is expected since the islands that existed at 0.23 ML increase in size. The peak also becomes broader as is also predicted by theory. These curves still depend on the coverage and a curve that only depends on the critical island size is needed for the analysis. Equation (3.7) was applied to the data in the inset to normalize it. The normalized data is given in Fig. 4.2 (c). The clear overlap of the two data sets shows that the normalization works nicely. This proves that the scaling theory can be applied to our data.

island density

This procedure is repeated for PTCDA islands that were deposited at 300 K. In Fig. 4.3, a LEEM image of the islands grown at 300 K (a) and 350 K (b) can be seen. The deposition rate of the molecules was the same in both experiments. The nucleation density decreases with increasing temperature. This is the expected behavior since the diffusion coefficient of the molecules increases with increasing temperature (comp. Eq. (3.1)). This also makes the island size distribution analysis impossible at high temperatures because the island size is then strongly influenced by the terrace size since only very few (if any) islands nucleate on each terrace.

critical island size

The island size distribution data for both temperatures after proper normalization is plotted in Fig. 4.3 (c). The filled dark blue symbols represent the results from two different experiments performed at 300 K and one of these experiments is analyzed at two different coverages. All three data sets overlap nicely. The 350 K data is plotted

with open light blue symbols. It is obvious that the shape of the two data sets for the two different temperatures is different. This shows that there is a difference in the critical island size between the deposition at 300 K and 350 K. To determine the critical nucleus size, the data has to be compared with theoretical predictions. Scaling functions for different critical nucleus sizes given by Eq. (3.8) are plotted as pink and purple curves in Fig. 4.3 (c). It can be seen that the 300 K data is described well by the scaling function of a critical cluster size of $i = 1$. This clear agreement between the theoretical model and the experimental data shows that the theory is applicable to our molecular system. It is more difficult to determined the critical nucleus size for the 350 K data set since there is more noise. A critical cluster size of two or three seems to have the smallest deviation from the data. The theoretical curve for $i = 2$ seems to fit a little better to the data.

increasing i with increasing T

An increase in the critical island size with increasing temperature is an expected result. When two molecules meet on the surface at 300 K, they stick together. When the substrate temperature is increased, the thermal energy of the molecules increases. That means that a dimer that was stable at lower temperatures can dissolve again. This makes a higher energy gain by forming larger clusters necessary to compensate for the increased thermal energy. Such an increase of the critical nucleus with increasing temperature was also found for pentacene on SiO_2 [TKKT04].

4.1.1.2 Determination of interaction energies

The previous experiments at the two different temperatures showed that the island size distribution analysis can be applied to the growth of PTCDA on Cu(001) and the critical nucleus size can be identified by it. Additionally, binding energies between the molecules and the diffusion barrier can be determined by looking at island densities at different temperatures if the critical nucleus size is known. This means that further experiments were necessary. PTCDA was deposited at different temperatures and the island density as well as the island size distribution were measured. Twelve deposition experiments were carried out with substrate temperatures between 300 K and 390 K. It was not possible to go to higher temperatures since the island density decreases with increasing temperature until only one island grows on each terrace. The growth at temperatures above 390 K is discussed in section 4.1.2. The island densities determined by these experiments cannot be compared to the previous experiments since the deposition rates were different.

complete condensation

It was checked that the sticking coefficient, which gives the relative amount of molecules that stay on the surface after they are adsorbed, was constant in this temperature regime by comparing the time it took to complete the first monolayer at 300 K and 390 K. The full monolayer is the best reference for this test since lensing and focusing effects play no significant role here. The necessary deposition time for the deposition of 1 ML was 38 min at 310 K and 43 min at 390 K proving that the sticking coefficient does not decrease with increasing temperature as it might have been the case. Assuming that all molecules stick to the surface at room temperature, which is very likely

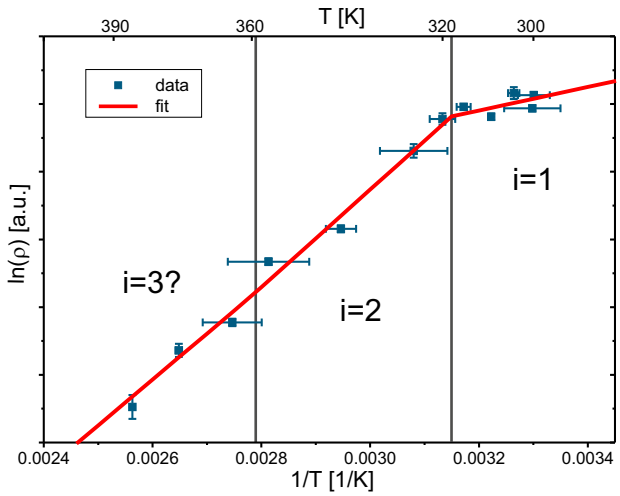

Fig. 4.4: Island density plotted against the substrate temperature during deposition. A clear change in slope can be identified at 320 K. The linear fits give the diffusion barrier and binding energies between the molecules, as is discussed in the text.

due to the strong interaction between the substrate and the molecules, all experiments were carried out in the regime of complete condensation, which is a necessary prerequisite for the usage of the rate equations described in chapter 3.

island densities

The island densities were determined in the aggregation regime for all experiments and are plotted in Fig. 4.4. The data points show a linear trend between 300 K and 315 K and another linear trend with a different slope for temperatures above 320 K. This indicates that there are most likely two different critical island sizes present in this temperature range.

critical island size

The island size distributions are determined to obtain the critical island size of PTCDA deposited at different substrate temperatures. A critical nucleus size of $i = 1$ is found for temperatures below 315 K since the ISD for the temperatures 315 K and 310 K shown in Fig. 4.5 (a) clearly exhibit a good fit to the theoretical curve of $i = 1$. At lower temperatures, the critical nucleus stays one, as was already discussed in the previous section. Between temperatures of 320 K and 350 K, the critical nucleus size is $i = 2$ as the two data sets shown in Fig. 4.5 (b) prove. The shape as well as the amplitude of the peak fit very well to the $f_2(s/S)$ function. This change in critical nucleus size coincides with the change in slope at 320 K of the curve shown in Fig. 4.4. The critical island size seems to change again at 365 K to $i = 3$ as shown in Fig. 4.5 (c). This is not an expected result since the slope in Fig. 4.4 does not change in this temperature region. It can be seen in Fig. 4.5 (c) that the noise is higher in this temperature region compared to the lower temperatures. This is due to the reduced number of islands on each terrace in this temperature range leading

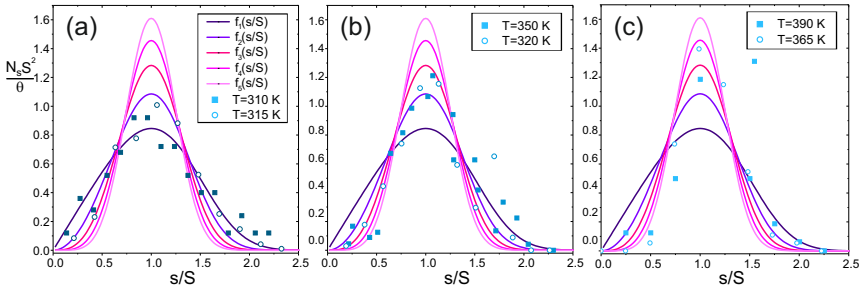

Fig. 4.5: Island size distributions for different substrate temperatures during the deposition. The critical island size increases from $i = 1$ in (a) for temperatures up to 315 K to $i = 2$ in (b) until the critical nucleus size seems to become $i = 3$ in (c) at temperatures above 365 K. The data points represent the shape of the theoretical curves very well for $i = 1$ and 2. The noise for $i = 3$ is much higher making it more difficult to judge the agreement between theory and experiment.

to worse statistics. The shape of the curve is not represented very well by both data sets either due to the high noise or due to the fact that it is not actually represented by the theoretical curve for $i = 3$. The absolute value of the maximum of the curve (the average of the two points with the highest value) on the other hand fits very well to the theoretical prediction of $i = 3$.

data fitting

Three lines are fitted to the island densities at different temperatures and can be seen as the red curve in Fig. 4.4. The first line in the temperature range of 300 K - 315 K, the second between 320 K - 350 K, and the third between 365 K - 390 K. The only constraint on the fit is that the lines have to connect between the temperatures, at which the critical island size changed, i.e. at 317 K and at 358 K.

diffusion barrier

Equation (3.4) gives a relation between the slope of the Arrhenius-type plot of the island density and the diffusion barrier and the binding energies. For a critical island size $i = 1$, the slope a_1 of the linear fit is

$$a_1 = \frac{E_D}{3k_B} \tag{4.1}$$

giving $E_D = 3k_B a_1$. Fitting a line to the data for temperatures below 315 K determined E_D to be 0.45 ± 0.21 eV. The uncertainty on this fit is quite high. This is not surprising since the data scatters a lot. One possible explanation for this is the uncertainty on the temperature that is present in the experiments. The sample heats up when it is moved to the working distance of the objective lens. The deposition was always started approximately half an hour after the sample was moved to the working distance to minimize this effect but it was not always possible to rigorously stick to this routine. The sample was not kept at the working distance for longer times due to time constraints and the increased probability of flash arcs, which would destroy the sample, at this distance. The diffusion barrier determined here is slightly higher

than that determined by Tejima *et al.*, who found a range of $0 < E_D < 0.20\,\text{eV}$ for pentacene on SiO_2 [TKKT04].
The Einstein-Smoluchowski relation [Ein05, vS06] mobility

$$D = \mu k_B T \tag{4.2}$$

gives the relation between the diffusion coefficient $D = D_0 exp(-E_D/k_B T)$ (equation (3.2)) and the mobility μ. It is not possible to determine the absolute value of the mobility of the molecules on the sample from the diffusion barrier E_D alone since the attempt frequency for hopping, D_0, is also necessary for it. But it is possible to determine the relative change of the mobility with temperature. Using the diffusion barrier and equations (4.2) and (3.2), it can be seen that the mobility doubles when the temperature is increases from 300 K to only 313 K.

$$\frac{\mu_{313\text{ K}}}{\mu_{300\text{ K}}} = \frac{D_{313\text{ K}}}{D_{300\text{ K}}} = 2.0$$

The mobility is even 43 times higher at 390 K compared to 300 K.

$$\frac{\mu_{390\text{ K}}}{\mu_{300\text{ K}}} = \frac{D_{390\text{ K}}}{D_{300\text{ K}}} = 43.1$$

This shows that the temperature has a very large influence on the mobility of the PTCDA molecule in the investigated temperature regime.
The slope in the temperature range from 320 K to 350 K, where the critical cluster size is two, is given by binding energy

$$a_2 = \frac{E_B^{(2)} + 2E_D}{4k_B}. \tag{4.3}$$

Since the diffusion barrier has already been determined by the slope for $i = 1$, the energy difference $E_B^{(2)}$ of a cluster of two molecules compared to the energy of two single molecules alone on the surface could be determined to be $1.6 \pm 0.5\,\text{eV}$. The high uncertainty on the determined binding energy is mostly due to the large uncertainty of the diffusion barrier which is propagated to the binding energy since the fitted slope for $i = 2$ only has an uncertainty of 8%. The reason for this high binding energy is explained later.
The slope of the third line fitted to the three data points belonging to the critical island size of $i = 3$ is given by high T

$$a_3 = \frac{E_B^{(3)} + E_B^{(2)} + 3E_D}{5k_B}. \tag{4.4}$$

With E_D and $E_B^{(2)}$ already determined, $E_B^{(3)}$ is found to be $-0.01 \pm 0.83\,\text{eV}$. The lack of a change in slope in this temperature range and the relatively high deviation of the ISD from the theoretical curves that were mentioned earlier already indicated that something went wrong in the analysis. This low value for the binding energy is the final proof that $i = 3$ is not the critical island size in this temperature range. $E_B^{(3)}$

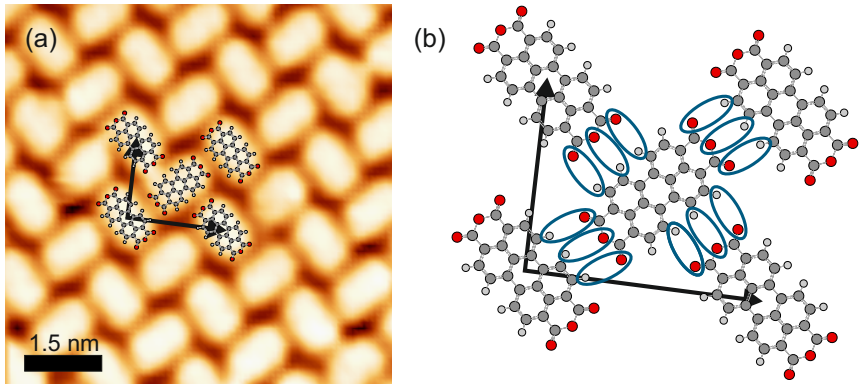

Fig. 4.6: (a) STM image of the filled states of a crystalline PTCDA island. The unit cell determined by LEED and the orientation of the PTCDA islands are drawn to illustrate the molecular arrangement (Bias = 50 mV, Set Point = 0.033 nA). (b) Hydrogen bonds (blue ellipses) between the molecules can possibly explain the high binding energy between the molecules.

gives the energy difference between a cluster of three molecules and a cluster of two molecules and one single molecule. There is no obvious reason why the binding energy between the first two molecules should be much different from the one between the third molecule and the dimer it attaches to. The high noise of the island size distributions determined by the few islands present on each terrace at these temperatures might obscure the fact that they actually belong to a critical cluster size of two. This would explain the very similar slope in this temperature region compared to the $i = 2$ region.

strong H-bond

The binding energy of the PTCDA molecules in small clusters was determined to be 1.6 ± 0.5 eV. This value is significantly larger than the binding energy for pentacene on SiO_2 of < 0.40 eV [TKKT04] and of *para*-hexaphenyl on amourphous mica of 0.74 eV (calculations) [PLN+11]. How can this high energy be explained? A closer look at the molecular arrangement gives an insight into this high binding energy. A scanning tunneling microscopy (STM) image of the PTCDA structure within one island on Cu(001) can be seen in Fig. 4.6 (a). The image was taken at room temperature with a commercially available Omicron VT STM (Variable Temperature Scanning tunneling Microscope) where the sample was grounded. The image was processed with the program *WSxM* [HFGR+07, WSx14]. The herringbone structure with a perpendicular orientation of the molecules to each other is clearly visible. The unit cell fits to that determined by LEED, which was given in the beginning of this chapter, and is indicated in the image by the black arrows. This arrangement of the molecules was also found by Gärtner *et al.* [GFB+14]. Fig. 4.6 (b) gives a closer look at the arrangement of the PTCDA molecules within the unit cell. Pair potential calculations result in a maximal energy gain of 0.62 eV for such a perpendicular orientation of the molecules as it is found here [KSW+11b]. This value is much smaller than the one determined

by the measurements performed in this work. But these calculations only take into account van der Waals and electrostatic interactions. This shows that a large part of the binding energy must be contributed by other interactions. It is proposed here that the rest of the energy can be attributed to hydrogen bonds that form between the PTCDA molecules. The three oxygen atoms on each side of the PTCDA molecule can form hydrogen bonds with the neighboring PTCDA molecule, as is marked by the blue ellipses in Fig. 4.6 (b). Hence, the difference in binding energy would be explained if each hydrogen bond contributed 0.33 eV. This value seems to be slightly too high considering that the energy of a hydrogen bond formed by a hydrogen atom that is attached to a carbon atom and an oxygen atom should normally be very low since the electronegativities of hydrogen and carbon are very similar. The situation in PTCDA is different though. PTCDA exhibits a strong quadrupole moment since the oxygen atoms at the anhydride groups accumulate electrons leading to a positively charged perylene core. This leads to a stronger partial charge of the hydrogens and thus to a strengthening of the hydrogen bonds. This effect could explain the unusually strong hydrogen bonds and the high binding energy. This, and the fact that the experimental uncertainty of the measurement of 0.5 eV is quite high, can explain the high binding energy of 1.6 eV. There might be other effects which also contribute to the binding strength to various degrees. The influence of image charges, for example, is neglected in the proposed model. It is very difficult to determine the contribution of image charges to the system without numerical simulations. This made it impossible to quantify their part in the binding energy. DFT calculations of PTCDA on Cu(001) would be very helpful in clarifying the reasons for the high binding energy.

summary

The analysis of the island size distribution and the island density measured in a temperature range between 300 K and 390 K allow the determination of crucial interaction energies. A diffusion barrier of 0.45 eV is determined which shows the large influence of the temperature on the mobility in this temperature range which strongly influence the growth. A binding energy between two PTCDA molecules on the Cu(001) surface of 1.6 eV is found and could be explained by the strong hydrogen bonds between the molecules.

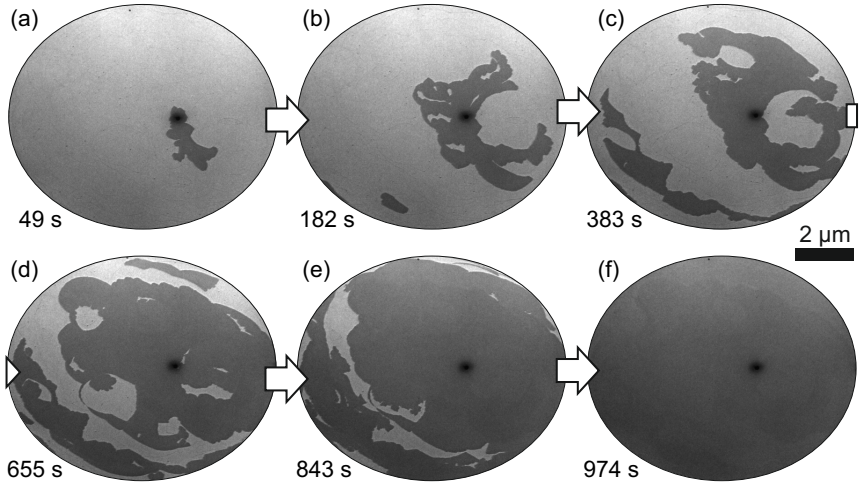

Fig. 4.7: Snapshots of LEEM images taken at different times after the deposition was started ($U_{start} = 2\,\text{eV}$). The PTCDA islands are the dark contrast that spreads across the surface until it is completely covered. The unchanging dark spot present in all images is a defect on the channel plates.

4.1.2 Growth at 460 K

The growth of PTCDA at higher substrate temperatures during the deposition is discussed in this section. At 460 K, PTCDA has a higher mobility and it is likely that the critical nucleus size is bigger than it was at 390 K. This should lead to a reduction of the nucleation density if the deposition rate is kept constant and only one or a few islands should nucleate on each terrace.

overview over deposition process

The deposition process of one monolayer of PTCDA on the Cu(001) surface at 460 K can be seen in Fig. 4.7. The first image was taken 49 s after the deposition was started. A single islands has nucleated up to this point and can be seen as the dark contrast in Fig. 4.7 (a). The dark spot, which is present in all images, is a defect on the detector. The first PTCDA island spreads across the terrace and a second island nucleates on a different terrace (Fig. 4.7 (b)). The shape of the islands is influenced by the step edges that are on the sample which are not visible in this focusing condition. An image with the step edges superimposed can be seen in Fig. 4.9. More islands nucleate on the surface while the existing islands continue to grow until they are spread across the whole terrace they nucleated on (Fig. 4.7 (c)-(e)). The monolayer is complete after 974 s (Fig. 4.7 (f)). It can be seen that no islands in the second layer nucleate while the first layer is being completed. The following pages give a detailed analysis of the growth process shown here.

deposition rate

The percentage of the area covered by PTCDA islands over time is plotted in Fig. 4.8 (a). The modulation between 5 s and 45 s and the outliers between 700 s and 900 s are due to changes of the focusing conditions of the microscope and have no physical relevance

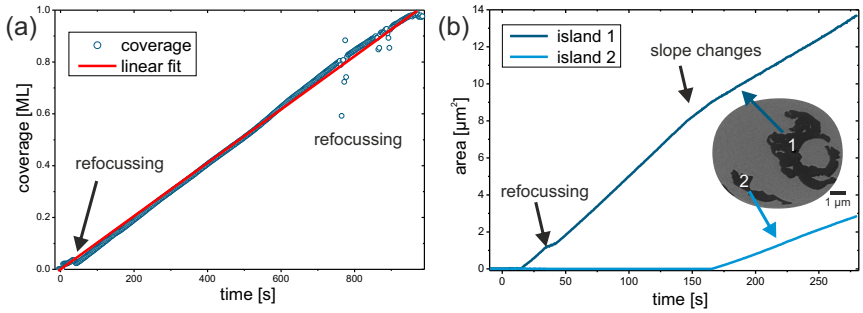

Fig. 4.8: (a) The coverage of PTCDA increases linearly with time. The modulation between 5 s and 45 s and the outliers between 700 s and 900 s are due to a change in focus. (b) The area of two PTCDA islands plotted individually. The slope of the first island changes, when the second island nucleates, since the molecules have two islands they can attach at thus decreasing the growth rate of the first island.

for the coverage. It can be seen that the slope deviates slightly from a linear increase. Reasons for this are explained in the next two paragraphs. The deposition rate is calculated by fitting a linear function $\theta = a*t$ to the data resulting in a deposition rate of 0.0618 ML/min. This corresponds very well to the value of $1/t_{1\mathrm{ML}} = 0.0617$ ML/min which is the inverse of the deposition time until a complete monolayer is achieved.

lensing effects

The coverage measured below 0.6 ML is below the fitted line in Fig. 4.8 (a). It is most likely that these are deviations due to artifacts of the measurement technique. Different focusing conditions can make islands appear larger or smaller than they actually are [DTKT14]. A focusing condition where these lensing effects make islands appear smaller than they actually are would lead to an underestimation of the covered area at low coverages where the islands are small and edge effects are important. When bigger islands are present on the surface, these effects become less significant since the ratio between the island edges and island area is decreased. Furthermore, an increase of the PTCDA concentration leads to a change in the work function of the copper surface which also affects the focus.

sticking coefficient

The decrease in slope for higher coverages can be explained by a reduced adsorption rate of the PTCDA molecules at higher coverages. This indicates that the sticking coefficient of PTCDA molecules on a PTCDA layer is smaller than on the copper surface, which would explain why the growth rate seems to slow down at coverages close to one monolayer. Another reason might be that it takes the PTCDA molecules longer to diffuse to the few remaining holes in the PTCDA layer, which would slow down the growth rate at coverages very close to one monolayer as well. Even though there are small deviations from the linear fit, it is clear that the deposition rate is very stable and that the growth is not influenced by fluctuations in the deposition rate.

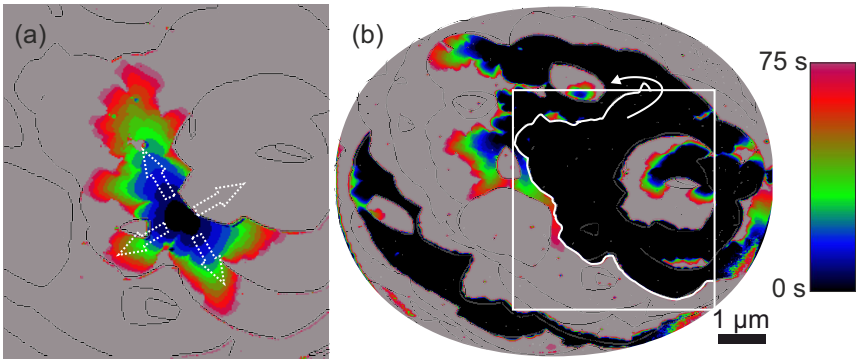

Fig. 4.9: The shape of the PTCDA islands during different stages of the growth. The colors give the size of the islands at the times specified by the color bar in the image. (a) The island growing across the terrace after its nucleation. The growth is anisotropic with clear preferential growth directions. (b) The island growth is also influenced by the topography of its surroundings. It grows the fastest where the most admolecules can diffuse to. The section of (b), which is shown in (a), is marked by a white frame.

interlayer transport

The linear increase in coverage also shows that molecules that are deposited on the PTCDA island are able to move across the islands edge and down to the bare Cu(001) substrate. This leads to the complete filling of the first monolayer for PTCDA on Cu(001) before the nucleation of the second layer can be observed. This layer-by-layer growth is observed for all substrate temperatures during the deposition experiments performed for this thesis. It is shown later in this section that this interlayer transport only enables the molecules to cross the island edge in one direction, i.e. from the top of the island to the metal substrate.

step edges permeable for molecules

Beside the total coverage, which has been shown to increase linearly, the growth rate of the individual islands is also investigated. The area of two individual islands is plotted versus the deposition time in Fig. 4.8 (b). The first island nucleates 13 s after the deposition is started. Its area increases linearly with time until a second island nucleates 170 s after the deposition is started. Why this island nucleates at this time is discussed later in this section. As soon as the second island is present, the growth of the first island slows down. This slower growth speed is also constant and leads to a linear increase in area. The second island also grows with a constant speed, but slightly slower than the first island. This behavior can be explained as follows: When only one island is present on the surface, all molecules diffuse to its island edges and attach there. Once there is a second island present, the molecules can attach to both islands effectively slowing down the growth of the first island. This change in growth speed due to the nucleation of a second island proves that the individual molecules can cross step edges. Adding the areas of both islands results in a linear increase in the total coverage that was already discovered in Fig. 4.8 (a).

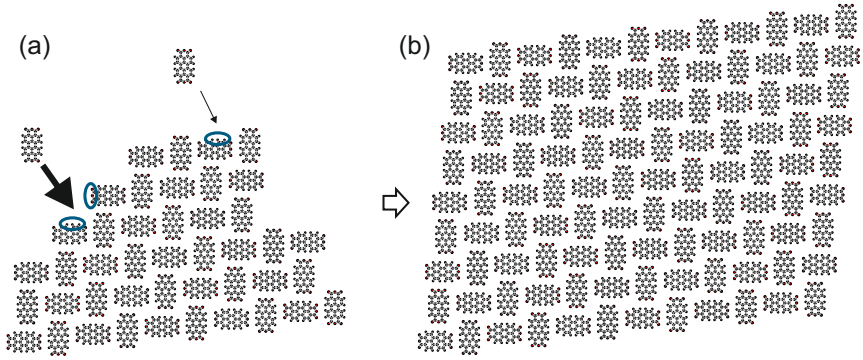

Fig. 4.10: Sketch to illustrate the different growth speeds of different islands edges. (a) There are two different adsorption sites at the island edge. One allows the formation of three hydrogen bonds (one ellipse) while the other allows six (two ellipses). This leads to a higher flux to the island edges where six hydrogen bonds can form. (b) The different fluxes to the two types of island edges lead to a rhomboid shape of the island.

step edges barriers for islands

In Fig. 4.9, the growth behavior of PTCDA is shown for two different stages of the growth. Fig. 4.9 (a) displays the growth directly after nucleation of the first island. The different colors depict the size and shape of the island in time intervals of 5 s going from dark blue to red. Step edges are marked as black lines. The island spreads across the terrace after its nucleation and does not grow across any step edges. The inability to grow across step edges in either direction is found for all islands growing at this or lower temperatures. To grow across a single step edge, the PTCDA island has to overcome a height difference of 2.08 Å and also a shift in the registry of 1.95 Å, which corresponds to a shift along two [110] directions by half a nearest neighbor distance. This inability to grow across even single step edges is also found for BDA on Cu(001) [SvGZP13a].

island shape

The growth of PTCDA islands at this temperature is anisotropic. Right after the island has nucleated, it displays a rectangular shape (Fig. 4.9 (a) dark blue contrast). A schematic image of the PTCDA molecules attaching to an existing PTCDA island is given in Fig. 4.10. It is shown in section 4.1.1.2 that the three hydrogen bonds that the three oxygen atom on each end of PTCDA can form are relatively strong with 0.3 eV per bond. This makes it much more beneficial for the PTCDA molecule to attach at an adsorption site which has the most bonds between oxygen and hydrogen atoms. There are two different adsorption sites depicted in Fig. 4.10 (a). The PTCDA molecules can form six new hydrogen bonds when it attaches at the site marked with the thick black arrow. The formation of only three hydrogen bonds is possible at the other site marked by the thin black arrow. It is proposed that the molecules prefer to attach at sites of the first type where six hydrogen bonds are formed. This leads to an increased flux to the first type of island edge. An elongation of the edges consisting

of adsorption sites of the second type is the result. This leads to a rhomboid shape of the island, which explains the initial shape of the island depicted in Fig. 4.9 (a) (dark blue contrast).

growth instabilities

Once a certain size of the island is reached, the incorporation of the molecules into the corners of the islands exceeds the growth of the flat edges as can be seen in Fig. 4.9 (a). This leads to an elongation of the corners of the island. This behavior can be explained by looking at the diffusion field of the molecules around the island. To get to a long flat edge of an island, molecules can only come from one direction which is perpendicular to this side. This is different at the corners of the islands. Here, molecules from different directions can reach the corner which leads to an increased attachment rate of molecules at the corners of the islands compared to the flat edges of the islands. The corners of the islands elongate. This process again increases the flux to the now even more exposed corners of the islands which makes them grow even faster. Such a behavior is called Mullins-Sekerka-type growth instabilities [MS63, MS64] and gives rise to an enhanced growth velocity at the corners of the islands leading to ramified islands. This type of instability was also observed for BDA on Cu(001) [SvGZP13b].

growth direction

The growth of PTCDA at a later stage during the deposition is shown in Fig. 4.9 (b), which shows a larger area of the sample than in Fig. 4.9 (a). The large black areas are the areas that are already covered by PTCDA islands at the beginning of this growth sequence. The colors depict the growth in 5 s-steps just as in Fig. 4.9 (a). The island from (a) has grown significantly without ever crossing a step edge. The island had to grow around a step edge (marked by a white arrow) to reach the left side of the sample shown in the image. The deposited molecules diffuse on the surface and if they find an edge of an already existing PTCDA island that is not bordered by a step edge at the point of impact they attach there. The growth velocity of the island edge in a certain direction depends on the morphology of the sample. When the edge is surrounded by empty copper terraces, it grows faster than when it is next to a growth front of another PTCDA island, which "steals" some admolecules to incorporate them into its own island edge, as was already discussed previously.

nucleation of additional islands

When there is no growth front of a PTCDA island in the vicinity, the local admolecule concentration increases and the nucleation of additional islands occurs. One of these islands can be seen as a large black area in the lower left part in Fig. 4.7 (b). This island nucleates after the first island completely covers the terrace where its growth is constrained by the large step edge marked by the white line in Fig. 4.9 (b). No further growth in that direction is possible once the island reaches the step edge. Molecules that are deposited on the lower left part of the area shown here are no longer able to attach to an existing PTCDA island since the only remaining growth front is far away in the upper right part of the depicted area (comp. Fig. 4.7 (b)). This leads to an increase in the admolecule concentration in the lower left area and the nucleation of the second island when a certain supersaturation is reached. This means that a supersaturation of PTCDA molecules is necessary for the nucleation of an island, which corresponds to the PTCDA coverage on the surface at the time of the first nucleation. With a deposition rate of 0.062 ML/min and the 13 s it takes the molecules to form the first island, a coverage of 0.013 ML at the maximal supersaturation is obtained

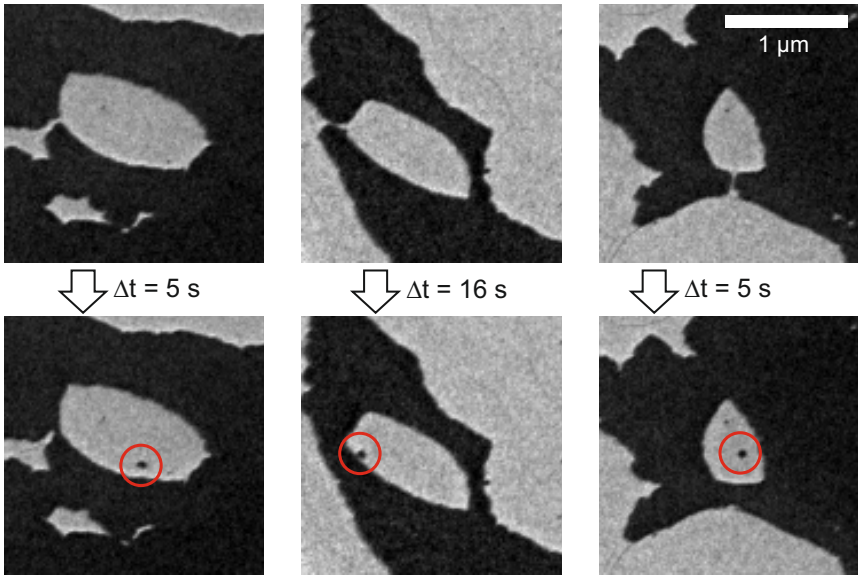

Fig. 4.11: PTCDA islands nucleate shortly after terraces are surrounded by PTCDA islands. The nucleation occurs faster when the terraces are surround by larger PTCDA islands leading to a greater flux in admolecules to the terrace.

that is necessary for nucleation of islands at this temperature. This is equivalent to a concentration of 0.001 molecules/nm^2. The supersaturation at this concentration is high enough to overcome the nucleation barrier. This coverage is one order of magnitude higher than the coverage of 0.002 ML at 350 K indicating that a higher density of PTCDA molecules is present in the disordered phase at higher temperatures.

supersaturation

To demonstrate this necessary supersaturation for nucleation even better, the nucleation of islands on terraces that are completely surrounded by a PTCDA layer is analyzed. The top row of Fig. 4.11 shows small terraces on the Cu(001) surface that are almost surrounded by PTCDA islands. The step edges are not visible in the images but they are right at the border between the surrounding PTCDA island and the "empty" copper terrace. "Empty" means that there are only diffusing single molecules present and no islands. This means that there is already a certain concentration of diffusing PTCDA molecules on the terrace. This concentration of diffusion PTCDA molecules corresponds approximately to the equilibrium concentration of diffusing PTCDA molecules in thermodynamic equilibrium with PTCDA islands. Before the copper terraces are completely encased by the surrounding PTCDA island, the diffusing molecules can move away from the terrace and attach at a growth front of a PTCDA island. After the copper terraces are completely encased and adsorbed PTCDA molecules can no longer diffuse away from the terrace and attach at an al-

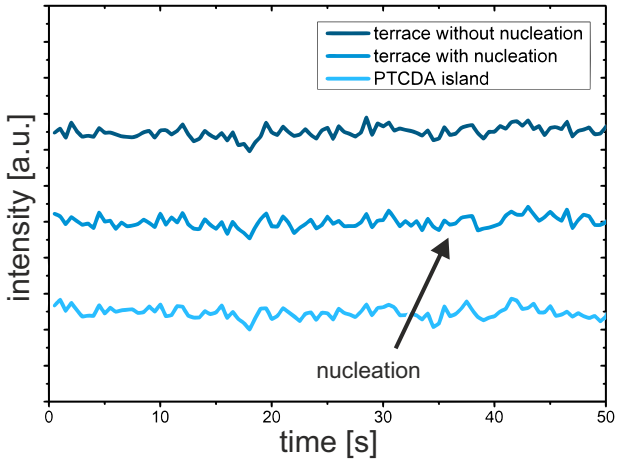

Fig. 4.12: Intensity of the sample during the nucleation of the islands on the left in Fig. 4.11. The intensity is measured on a terrace where no nucleation occurred, on a terrace where the nucleation occurred at 37 s, and on the PTCDA island around the terrace plotted as dark blue, blue, and light blue lines, respectively.

ready existing growth front, the concentration of molecules on these terraces increases until the concentration necessary for nucleation is reached and a new island starts to grow, marked with a red circle. The time it takes for the nucleation to occur depends on the morphology of the surrounding area and the size of the terrace. Molecules that adsorb on PTCDA islands diffuse on these islands until they reach the edge of the island and move to the Cu(001) surface. This leads to a stronger increase in the concentration of PTCDA molecules on terraces that are surrounded by large PTCDA islands or on smaller terraces surrounded by the same amount of PTCDA islands. The nucleation on the left and right images in Fig. 4.11 happens quicker than in the middle images because they have such an increased PTCDA flux due to the large surrounding PTCDA island.

one-way interlayer transport

This also shows that the interlayer transport discussed earlier is only possible in one direction (from on top of the PTCDA island to the copper terrace) or it is at least strongly preferred in this direction. Otherwise the PTCDA molecules would cross the surrounding PTCDA island and attach themselves at an already existing growth front preventing the strong increase in admolecule concentration that can be observed.

admolecule concentration

The LEEM intensity on the terrace on the left in Fig. 4.11 is measured during the deposition to see if the change in admolecule concentration can be seen in a change in intensity. The intensity should decrease with an increasing number of PTCDA molecules diffusing on the terrace and drop back to the equilibrium intensity after the nucleation has occurred. The intensity on the surrounded terrace far away from the nucleation point of the island as well as two reference intensities, one measured

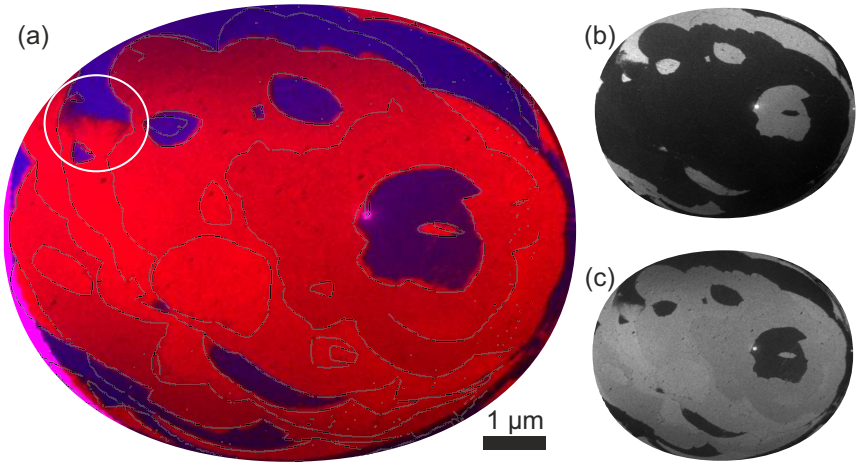

Fig. 4.13: Investigation of the orientation of the PTCDA islands. (a) The composite image is made up of the two DF-LEEM images ((b) + (c)). The two different domains can clearly be distinguished. The inhomogeneous contrast within one domain is due to a slight deviation of the unit cell from the commensurate superstructure. The step edges are superimposed as black lines in the composite image.

on a terrace where no nucleation occurred and one on an existing PTCDA island, are shown in Fig. 4.12. The curves are normalized and an offset is introduced for better visibility. No significant change in contrast can be observed before and after the nucleation of these islands. The slight changes in intensity are due to noise and, in the case of an intensity drop in all three curves, to slight instabilities of the LEEM instrument. This, combined with the very short time it takes the islands to nucleate, points to a very low supersaturation that is necessary for nucleation. An increase in intensity with a slight drop after the nucleation of a molecular island was observed for BDA on Cu(001) in [SvGZP12b].

orientational domains

To further prove that islands do not grow across step edges and that they keep their crystallinity over large areas during the growth, dark-field LEEM images were taken. Fig. 4.13 (b) and (c) show two dark field images corresponding to the two rotational domains of PTCDA islands on Cu(001). Fig. 4.13 (a) is a composite image of Fig. 4.13 (b) and (c) where (b) is colored blue and (c) red with the step edges superimposed in black. It can be seen that the two rotational domains add up to the whole layer meaning that there are no structures on the surface that are not described by these two domains.

nucleation

The orientation of the domains that nucleated on each terrace is randomly distributed as can be seen by the almost equal number of islands of each domain (18 red and 14 blue). Each domain covers the complete terrace it nucleated on indication that only one island nucleates on each terrace. There is only one area where there is a change

from one domain into the other domain within one terrace (marked with a white circle in Fig. 4.13 (a)). This is due to the nucleation of two different domains on one terrace and not a reorientation during the growth of one island. The nucleation of two islands on one terrace was possible because the terrace stretches over a very long distance and is at the same time very narrow. Additionally, the terrace was one of the last terraces without an island and at the same time being almost completely encased by terraces that themselves were almost completely covered by a PTCDA layer (see Fig. 4.7 (d) and (e)). This lead to a quick increase in the PTCDA concentration on the terrace since the molecules could not attach to a nearby growth front which induced the nucleation of one island on the terrace. The nucleation of this island could not decrease the PTCDA concentration quickly enough at the other end of the terrace and a second island nucleated there as well.

change of LEED spot position

The intensity of the bright domains in the dark-field images is not homogeneous which can be seen especially well in Fig. 4.13 (c). This slight change in contrast points to the fact the LEED spot corresponding to this domain is cut a little by the contrast aperture leading to an incomplete transmission of the intensity of the island to the detector. This suggests that the LEED spots of the different islands of the same rotational domain are not all exactly at the same position in the back focal plane indicating a slight change of the unit cell or its orientation with respect to the substrate. Further experiments would be necessary to investigate where this effect comes from.

4.2 Growth of PTCDA on Ag(111)

This chapter discusses the growth of PTCDA on Ag(111).
The structure of PTCDA on Ag(111) is already very well studied [Tau07, KUS04, ZKS+06, HTS+10, TES+02a, TSS+00, EST03, SMS+10, SSM+09, RNP+09, STS+00]. PTCDA has an attractive intermolecular interaction and thus grows in islands in the submonolayer regime at room temperature [GSS+98]. The islands exhibit a high crystallinity and the unit cell is described by the superstructure matrix

previous studies

$$M_{\text{PTCDA, Ag(111)}} = \begin{pmatrix} 6 & 1 \\ -3 & 5 \end{pmatrix}.$$

It has a size of 238.7 Å^2 and contains two PTCDA molecules that are arranged in a herringbone pattern meaning that they are oriented approximately perpendicular to each other [GSS+98]. There also exist some LEEM studies on the growth of PTCDA [Gro06, Mar06, MGS+06a].
New findings on the growth of PTCDA are discussed briefly in this chapter. The growth of PTCDA at 300 K is discussed in the first section. The island size distribution is measured although the critical island size cannot be determined. The growth at 400 K is discussed in the second part. It is found that the PTCDA islands are able to grow across step edges in only one direction and the growth dynamics are described in detail. This section closes with the analysis of the orientation of the rotational domains with respect to the step edges where they nucleated.

content

4.2.1 Deposition of PTCDA at different temperatures

The influence of the temperature on the growth of PTCDA on Ag(111) is analyzed in this section.

4.2.1.1 Deposition of PTCDA at 300 K

The growth process of PTCDA on Ag(111) at 300 K is discussed in this section.
LEEM images taken during the deposition of PTCDA on Ag(111), which was kept at 300 K, with the step edges of the Ag(111) substrate superimposed can be seen in Fig. 4.14. The PTCDA islands exhibit a bright contrast at a start voltage of 2.0 V which was used for the measurements of Fig. 4.14 (a)-(h). The start voltage was increased slightly to 2.1 V to increase the contrast between the first and second layer PTCDA islands in Fig. 4.14 (i). The first islands nucleate almost as soon as the deposition is started. These islands grow and new islands continue to nucleate, as can be seen in Fig. 4.14 while islands start to grow together at higher coverages. This leads to an almost constant number of islands on the surface in a certain coverage regime. The nucleation of the second layer can be seen in Fig. 4.14 (h). More details about the growth are discussed in the next few paragraphs.

overview over growth

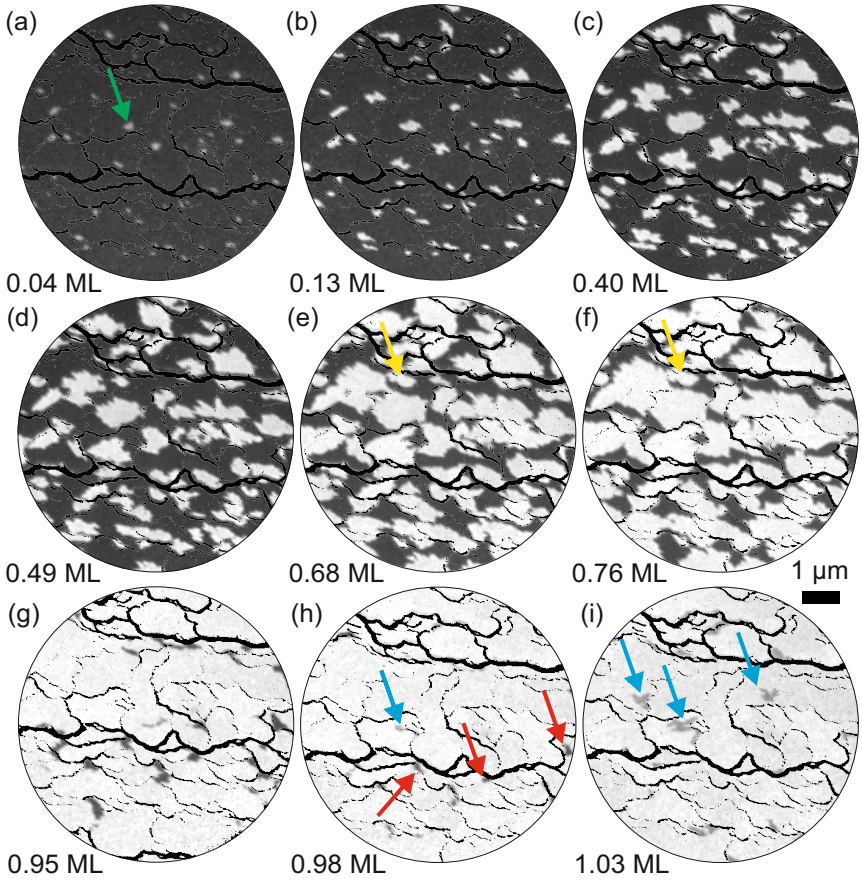

Fig. 4.14: LEEM images taken during the deposition of PTCDA on Ag(111) at 300 K with the step edges of the Ag(111) substrate superimposed in black. (a) The PTCDA islands, which exhibit a bright contrast (green arrow), nucleate at the lower side of step edges. (b)-(g) The islands grow across the terrace they nucleated on without crossing step edges. (h) PTCDA islands nucleate in the second layer (blue arrows) shortly before the first layer is completed. Some holes in the first layer are marked by red arrows. (i) The first layer is completed and the only contrast in the image is given by the second layer islands. ((a)-(h): $U_{\mathrm{start}} = 2.0\,\mathrm{V}$, (i): $U_{\mathrm{start}} = 2.1\,\mathrm{V}$)

nucleation at step edges

The PTCDA islands nucleate at the lower side of the step edges of the Ag(111) substrate, as can be seen by the curvature of the step edges in Fig. 4.14 (a). One of these islands is marked by a green arrow. This preferred nucleation at step edges is also found for PTCDA on Cu(001), as discussed in section 4.1.1. It can also be seen that the nucleation density is higher in areas with a high step edge density. This was also found by Marchetto [MGS+06a].

admolecule density

The nucleation of islands at already very low coverages indicates that the density of PTCDA molecules next to the islands is very low. This is similar to the growth of PTCDA on Cu(001) at comparable temperatures, as discussed in section 4.1.1.

diffusion across step edges

It can also be observed in Fig. 4.14 that islands do not nucleate at the same time. This indicates that the molecular density decreases in the areas surrounding a growth front of an island. The fact that islands do not nucleate on all terraces at the same time suggests that the PTCDA molecules can move across step edges at this temperature.

step edge barrier

The islands grow on the lower terrace next to the step edge they nucleated at. They spread across this terrace and never seem to grow across any step edges, as can be seen in Fig. 4.14 (b)-(h). When an island covers its terrace completely, it stops growing, as is marked by a yellow arrow in Fig. 4.14 (e)-(f). This is a surprising result since Marchetto proposed in [Mar06] that PTCDA islands can grow across step edges. This is explained by the slightly lower temperature in this experiment compared with the experiment in [Mar06].

nucleation of second layer

The islands continue to grow only in the first layer until almost the whole surface is covered. Islands start to nucleate in the second layer shortly before the first layer is completely closed, as can be seen in Fig. 4.14 (h) where holes in the first layer are marked by red arrows and an island in the second layer by a blue arrow. The deviation from a strict layer-by-layer growth can be explained by the high deposition rate of 0.12 ML/min. An experiment at the same temperature with a lower deposition rate shows that the first layer closes completely before the nucleation of the second layer starts. The observed nucleation of the second layer, before the first layer is closed, is due to kinetic effects of the growth that are more prominent at a higher deposition rate. This layer-by-layer growth agrees with the finding in [CSS+03].

island size distribution

The island size distribution was used to determine the critical nucleus size i for the growth of PTCDA on Cu(001), as was discussed in chapter 4.1.1. The same analysis is performed for the islands of this experiment in the coverage regime when the number of islands was approximately constant. The result can be seen in Fig. 4.15. It can clearly be observed that the data deviates qualitatively from all theoretical curves for $i \geq 1$. There are two reasons for this. The first is that there is no aggregation regime in the observed growth, since new islands continue to nucleate during the whole deposition process, as was already mentioned. The constant number of islands is only due to the fact that the increasing number of islands due to the nucleation of new islands is compensated for by the coalescence of existing islands. The same phenomenon is discussed in section 6.2.1.3 for the growth of heteromolecular islands. The second reason is that the size of the islands is strongly influenced by the substrate morphology. This leads to a size distribution that is no longer determined by the interaction between the molecules and the (defect free) substrate and by the intermolecular interaction.

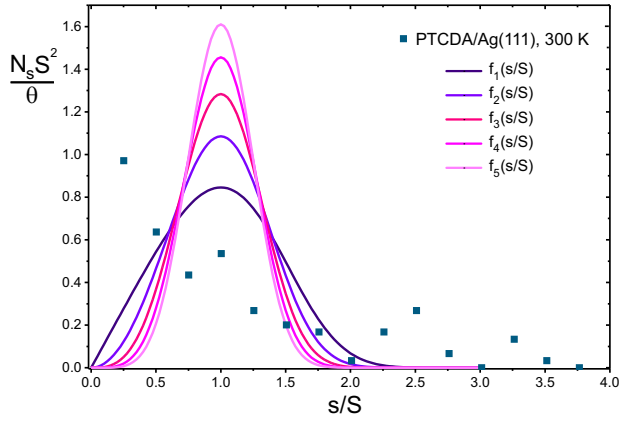

Fig. 4.15: Size distribution of the islands of the experiment shown in Fig. 4.14. The data points do not fit to any of the theoretical curves for critical nucleus sizes $i \geq 1$. This is most likely due to the fact that this system does not exhibit a clear aggregation regime and that the size of the islands is determined by the size of the terraces.

4.2.1.2 Deposition of PTCDA at 400 K

The deposition of a submonolayer film of PTCDA at elevated substrate temperatures of 400 K is discussed in this section.

overview over growth

LEEM images recorded during the growth of PTCDA on Ag(111) at 400 K are shown in Fig. 4.16. The PTCDA islands (green arrows) can be identified by their bright contrast. Step edges of the Ag(111) substrate are superimposed in black. The deposition rate of PTCDA is 0.12 ML/min just as in the last experiment (Fig. 4.14). The deposition was stopped after a coverage of PTCDA of 0.21 ML was reached.

low nucleation density

The nucleation of the first islands can be seen in Fig. 4.16 (a). The islands nucleate at step edges just, as was the case at 300 ML in the previously discussed experiment. New islands continue to nucleate up to coverages of 0.13 ML. The last islands that nucleate are marked by yellow arrows in Fig. 4.16 (d) and (e). The nucleation density is lower at this temperature than at 300 K. This is an expected result since the nucleation density decreases with increasing temperature (compare equation (3.3)).

growth across step edges

The islands start to grow after their nucleation. Some of them continue to grow until the deposition is stopped. Two of these islands are marked by blue arrows in Fig. 4.16 (i). It can be seen that they grow across many step edges at this temperature in contrast to the experiment at 300 K.

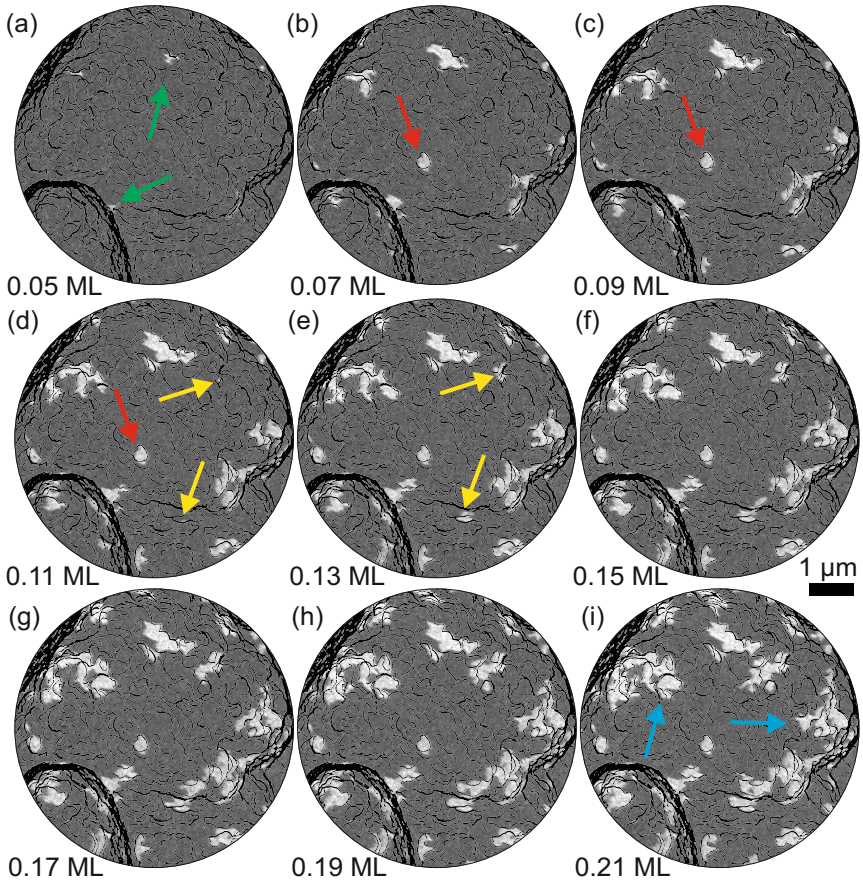

Fig. 4.16: LEEM images of the deposition of PTCDA at 400 K with the step edges of the Ag(111) substrate superimposed in black. The PTCDA islands (green arrow) can be identified as the bright contrast. Some islands (blue arrows) grow across many step edges while other islands (red arrows) stop growing when they reach a step edge. This can be explained by the fact that PTCDA islands can grow across step edges only in one direction. ($U_{\mathrm{start}} = 2.0\,\mathrm{V}$)

energy barrier

This temperature dependent growth across step edges suggests that a certain energy barrier has to be overcome by the islands to grow across a step edge. This would explain why the islands were not observed to grow across step edges at low temperatures and why they were at higher temperatures. This also solves the previously mentioned discrepancy between the results in this work for the growth at 300 K from section 4.2.1.1 and the one in [Mar06] since the lower temperature of 300 K prevented the observation of the growth across step edges in the experiment discussed in this work.

only crossing in one direction

It was already mentioned that only some islands continue to grow until the deposition is stopped. One island that stops growing, even though the deposition is continued, is marked by a red arrow in Fig. 4.16. It is spread across two terraces, one larger one and one small one located right under it. The island nucleated on the smaller terrace and grew across one step edge towards the larger terrace. As soon as the larger terrace is also completely covered, it stops growing. This stop in growth compared to the continued growth can be explained by the growth direction of the island across the step edges of the substrate. Islands can grow from an upper to a lower terrace, as can be seen by the islands that are marked by the blue arrows in Fig. 4.16. (Note that the upper terrace is located at the concave side of a step edges, as is marked in Fig. 2.4 (b) in chapter 2.2.) These island grow across many step edges but the growth direction of the islands is always downwards. The island marked by the red arrow nucleates on a terrace that only has one terrace that is lower and it does grow across the one downward step onto the lower terrace. It cannot continue to grow after it has spread across this terrace as well since it is then only bound by upward steps. This shows that the islands can only grow from an upper terrace to a lower terrace and not the other way around at this temperature.

delayed nucleation

The sizes of the islands at different times during the growth are shown in Fig. 4.17. The colors indicate the size and the shape of the islands at different times during the deposition, as specified by the color bar in Fig. 4.17. Fig. 4.17 (a) depicts the island during the whole deposition process. It can be seen very clearly that the islands nucleate at very different times. Islands containing blueish colors nucleate shortly after the deposition was started while islands containing only greenish and reddish colors nucleated later. Fig. 4.17 (b) depicts the size of the islands only in the second half of the deposition. The size of the islands after 110 s is depicted in black while the colors demonstrate the growth of the islands in the 100 s afterwards. It can be seen even more clearly in this image that some islands do not grow at all during the second part of the deposition while some islands nucleate only during this time.

influence of step edges

The influence of the step edges on the growth direction of the PTCDA can be seen in Fig. 4.17 as well. The islands can cross step edges but they seem to prefer growing across the terraces they are already on. This shows that a certain energy barrier has to be overcome to grow across a step edge.

influence of neighboring islands

The step edges are not the only factor influencing the growth of the islands. It can be seen in Fig. 4.17 (a) and (b) that the island marked by the red arrow starts growing after the growth of the island marked with the blue arrow has mostly stopped. This stop of the growth of the latter island leads to an increase in the concentration of

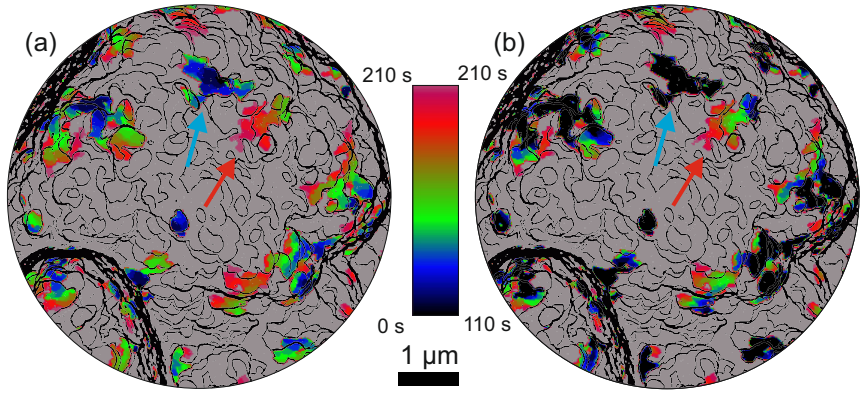

Fig. 4.17: The size of the islands at different times during the deposition are depicted by different colors (same experiment as Fig. 4.16). This allows a detailed analysis of the growth dynamics of the PTCDA islands.

PTCDA in the region around the island since molecules adsorbed there cannot attach to this island anymore since it is surrounded by upward steps in that area. This increased density of molecules in that area leads to the nucleation of an additional island there (red arrow in Fig. 4.17).

4.2.2 Orientation of individual islands

The orientation of individual islands with respect to the step edges they nucleated at is analyzed in this section.

different temperatures

Composite images of the six rotational domains of PTCDA islands deposited at two different temperatures on Ag(111) can be seen in Fig. 4.18. Some step edges are superimposed as white lines in small parts of the image to indicate their relation to the position of the islands. The orientation of the PTCDA islands that are deposited at 300 K and 400 K can be seen in Fig. 4.18 (a) and (b), respectively.

island shape

The islands in Fig. 4.18 (a) all nucleated at the lower side of a step edge, as discussed in the previous section. Each island has one slightly curved edge, which is nestled against the Ag(111) step edges, and ramified sides which are not bound by step edges. The same can be observed for the islands in Fig. 4.18 (b). They also exhibit slightly curved and more ramified sides.

island clusters with same orienation

One conclusion that can be drawn from these images is that there are areas where the islands have the same orientation. This observation is independent of whether the islands touch each other (Fig. 4.18 (b)) or not (Fig. 4.18 (a)). A growth of the islands across step edges could explain the observations at 400 K since many islands are connected, but it cannot explain why the individual islands at 300 K have the same orientation since all islands must have nucleated individually since none of the islands touch an island of a different terrace. Comparing the orientation of the islands with

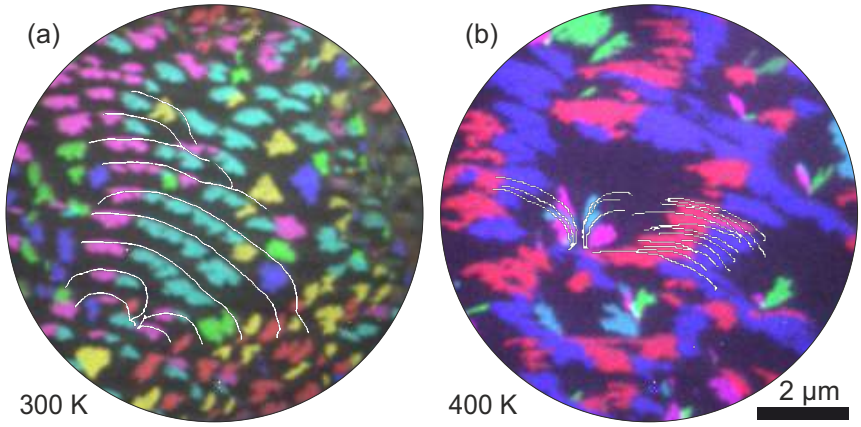

Fig. 4.18: Composite images of the orientational domains of PTCDA islands deposited at (a) 300 K and (b) 400 K. Domains with the same orientation nucleate at similarly oriented step edges. ($U_{\text{start}} = 10.5\,\text{V}$)

the orientation of the step edges shows that the islands that nucleated at similarly oriented step edges have the same domain orientation.

PTCDA molecules at step edges act as nucleation sites

It is known from literature that PTCDA molecules decorate the step edges of Ag(111) [Mar06, TES+02b, Tau07, GSS+98]. It is plausible that the orientation of PTCDA at the step edges is strongly influenced by orientation of the step edge which leads to similarly oriented PTCDA molecules at similarly oriented step edges. These molecules apparently act as nucleation sites for the islands so that the orientation of these molecules determines the orientation of the island which explains the observation from Fig. 4.18.

5 Growth of CuPc

The growth of CuPc is discussed in this chapter. The mostly repulsive intermolecular interaction of CuPc leads to a dilute disordered phase up to coverage of 0.8 ML. The different phases, disordered and ordered, that exist for the CuPc/Cu(001) system including the transitions between them are analyzed in section 5.1. The growth of the crystalline islands in the disordered phase is the focus of section 5.2.

5.1 Growth of CuPc on Cu(001)

The growth of CuPc on Cu(001) is discussed in this section.

previous studies

Several studies of the CuPc/Cu(001) system already exist. They focus on the final structure that forms after the end of the deposition and do not investigate the growth process itself. The unit cell of the structure formed at a coverage of 1.0 ML was determined by Schürlein *et al.* [SA94] to be squared with vector lengths of 13.7 Å tilted by 21.8° against the [110]-direction of the Cu(001) surface. They propose that the square lattice is continued for higher coverages since the spot positions do not change with increasing coverage. Ultraviolet photoelectron spectroscopy (UPS) measurements showed that CuPc interacts strongly with the underlying copper substrate leading to a partial filling of the lowest unoccupied molecular orbital (LUMO) of the CuPc in the first monolayer [ATNIK08]. TDMS spectra also showed a stronger binding of the first monolayer to the substrate compared to the second layer [Sch94].

contents

This section deals with the final structures of CuPc that are present after the deposition is stopped, but it is also discussed how the formation of and the transitions between the structures occur. This investigation of the growth process was not performed in any of the previous studies. The majority of the LEED and LEEM analyses presented in this chapter was performed in the framework of the Master's thesis of Jonas van Bebber [vB14].

5.1.1 Overview over different phases

During the deposition of CuPc on a Cu(001) surface that is kept at 460 K, different phases appear at different coverage of CuPc. Here, a short overview over the structures is given. Details are explained in more detail in the next sections.

phases

To monitor the growth of CuPc, LEED images were taken during the deposition of CuPc on Cu(001) and can be seen in Fig. 5.1. A strong change in the structure on the surface can be observed. At coverages up to 0.81 ML, a disordered phase is present

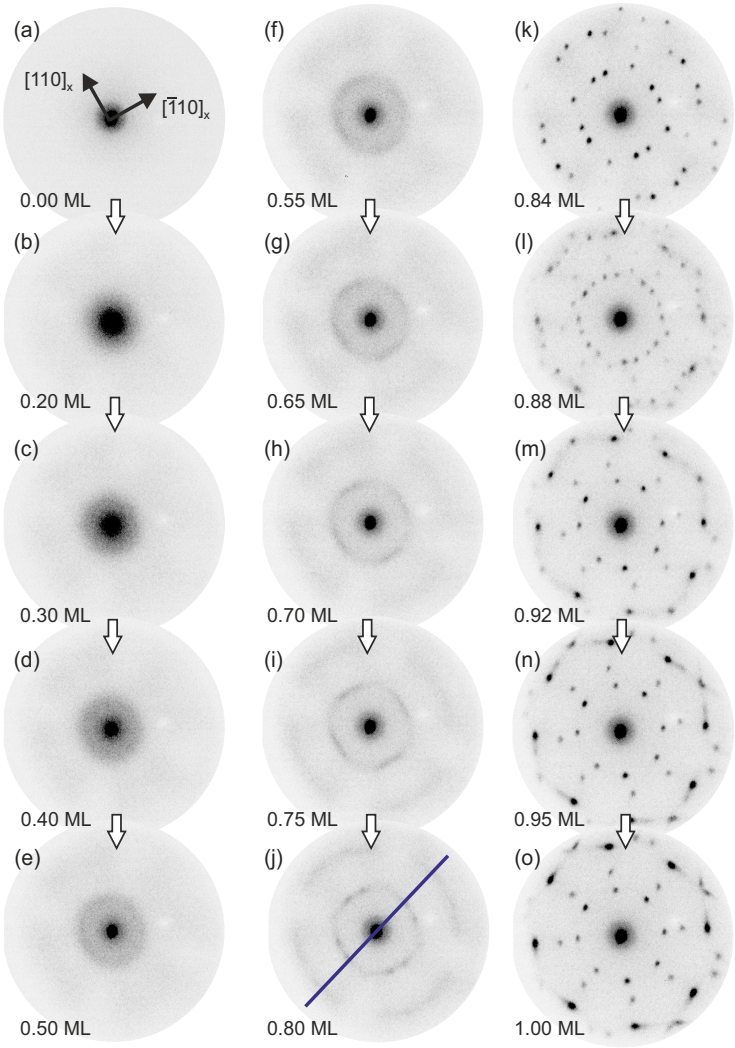

Fig. 5.1: LEED images taken during the deposition of CuPc on Cu(001) at 460 K. (a) the clean Cu(001) surface, (b)-(i) a dilute disordered phase forms, (j) the first crystalline phase called β phase emerges at coverages of 0.81 ML and (k) is spread across the whole surface, (l) a second crystalline phase, the δ phase, appears and (m) covers the whole surface, (n) the unit cell shrinks continuously (o) until the last crystalline phase, the ϵ phase, is reached.

on the surface, as can be seen by the diffuse intensity (Fig. 5.1 (a)-(j)). Then a first commensurate crystalline structure called β phase emerges in Fig. 5.1 (k). Increasing

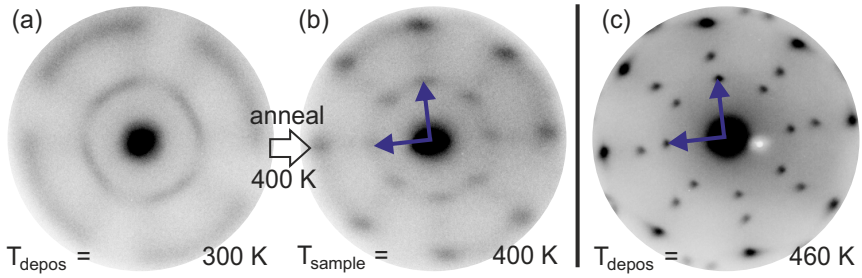

Fig. 5.2: (a) Only a diffuse LEED pattern is obtained after 1.1 ML CuPc are deposited at 300 K. (b) Annealing the sample to 400 K gives diffuse spots of the ϵ phase that keep their position after the sample is cooled down again. (c) High crystallinity is achieved when 1.0 ML is deposited at a substrate temperature of 460 K.

the coverage further leads to the appearance of a second crystalline structure called δ phase (Fig. 5.1 (m)), which slowly transforms into a third and final structure called ϵ phase (Fig. 5.1 (o)), which is present when the whole surface is closely packed with CuPc molecules. This last most densely packed structure defines a coverage of 1.0 ML. All coverages given in this chapter give the amount of CuPc molecules relative to this. A coverage of 0.5 ML means that 50% of the molecules that would be necessary to form the ϵ phase are present on the surface. It does not mean that 50% of the surface is not at all covered by CuPc molecules since CuPc molecules form structures of different densities on the surface. This means that the whole surface can be covered even though only a nominal coverage of 0.8 ML is present. LEEM, LEED, and STM measurements were performed to determine the domain sizes, the crystalline structure, and the orientation of the molecules in the different phases. The three crystalline structures described here are called β, δ, and ϵ phase, respectively. Two other structures of CuPc were also found by Franke [Fra14]. These five structures were ordered by their unit cell size and named consecutively leading to the sequence of the names of the phases in this work.

phase transitions

The transitions between the different structures are discussed in section 5.1.5. The phase transition from the diffuse phase to the β phase can be seen by a gradual transformation of the diffuse intensity of the LEED pattern into sharp spots (Fig. 5.1 (j)), the reorganization of the β phase into δ phase occurs without any intermediate structures (Fig. 5.1 (l)). Then the δ phase changes continuously into the ϵ phase (Fig. 5.1 (n)). DF-LEEM measurements combined with LEED measurements were applied to explain these different types of transitions.

5.1.2 Temperature dependence

Before the growth of the different phases can be analyzed, the influence of the substrate temperature during the deposition has to be discussed. It was already shown

in chapter 4.1 that a deposition temperature of 400 K was necessary to achieve highly crystalline films of PTCDA on Cu(001). CuPc is expected to have a low mobility at room temperature as well.

300 K When CuPc is deposited on Cu(001) at 300 K, a LEED pattern with diffuse ring structures that are modulated in intensity can be observed. The diffuse ring points to a preferred intermolecular distance and its modulation to a preferred orientation of the CuPc molecules. A detailed analysis of the radius of the diffuse ring and the mobility of CuPc molecules are given in the next section. The LEED pattern after 1.1 ML are deposited on the sample can be seen in Fig. 5.2 (a). The diffuse signal from Fig. 5.2 (a) turns into spots upon annealing to 400 K, which become sharper during the heating of the sample and keep their sharpness after the sample is cooled down again, as shown in Fig. 5.2 (b). By increasing the temperature, the CuPc molecules get more thermal energy and seem to be able to reorganize themselves into a more ordered structure. But the annealing process to only 400 K does not create a highly crystalline sample.

460 K A better lateral order can be achieved when the substrate temperature during deposition is increased. The LEED pattern in Fig. 5.2 (b) and Fig. 5.2 (c) belong to the structure present when the coverage is 1 ML. The direct comparison shows very clearly the strong influence of the deposition temperature on the quality of the crystal structure. The spots that are diffuse in Fig. 5.2 (b) are sharp in (c). If the film is kept at a constant temperature of 460 K, the intensity and sharpness of the LEED spots, i.e. the crystallinity of the film, stays the same for several hours.

$T > 460$ K When CuPc is deposited at temperatures above 460 K, the crystallinity of the structure is very good directly after the position. But the intensity of the LEED spots decreases quickly indicating a worse crystalline ordering. This can be due to desorption or the destruction of molecules at this high temperature.

optimal deposition temperature These experiments show that the temperature during deposition is crucial for the crystallinity of the film and its stability. All subsequent films were deposited at 460 K to achieve a high degree of crystallinity while keeping the damage to the molecules minimal.

5.1.3 Disordered phase

The disordered phase, which appears at coverages below 0.81 ML, is discussed first.

diffuse LEED intensity When CuPc is deposited on the Cu(001) surface at 460 K, a diffuse signal can be observed in the LEED pattern. This signal appears as soon as molecules are present on the surface (Fig. 5.1 (b)). It consists of a diffuse intensity around the (00)-spot, which transforms into a ring at coverages above 0.26 ML, and four outer lobes which each consist of two intensity maxima next to each other. The form of the diffuse signal changes when the coverage increases (see Fig. 5.1(c)-(i)). In the next paragraphs, the origin of these two features is explained.

intermolecular distance The intensity around the (00)-spot of the diffuse signal reflects intermolecular distances between the molecules. After the deposition is started, a broad disk-like intensity appears around the (00)-spot. This intensity is due to CuPc molecules that

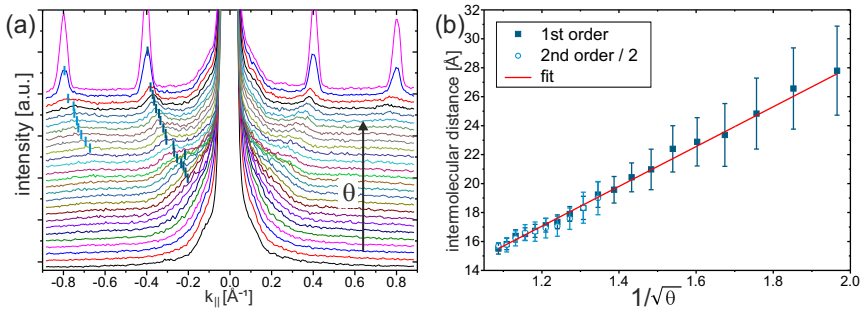

Fig. 5.3: (a) Line scans through the spots of the β phase and the 00-spot at coverages from 0.00 ML to 0.84 ML. (b) The distances calculated from the positions of the peaks in (a) plotted against the inverse of the square root of the coverage. A clear linear dependence can be observed and the slope of the fit gives an area, which is covered by one molecule, of 189.6 Å^2.

are relatively far away from each other and have no preferred intermolecular distance. When the coverage is increased, the broad peak changes into a diffuse ring around the (00)-spot. This indicates that the molecules start to have a preferred distance between them. The increasing radius of the ring shows that the molecules move more closely together. This is not surprising since the molecules have less space for themselves with increasing coverage. The radius of the ring can be employed to calculate the preferred intermolecular distance. It was determined by finding the first peak in the line scans shown in Fig. 5.3 (a). The direction in k-space, where the line scans were taken, can be seen in Fig. 5.1 (j). The positions of the peak are indicated by dark blue markers. These markers start at coverages of 0.26 ML since the peak is not present at lower coverages. With increasing coverage, the peak becomes sharper indicating that the distance between the molecules becomes better defined. With the distance in k-space, the real space distance d can be calculated by $d = \frac{2\pi}{k}$. Such an appearance of an inner ring, which reflects the decreasing distance between the molecules with increasing coverage, is also found for CuPc on Ag(111) [KSS$^+$10] and Au(111) [SKRK11], for SnPc on Ag(111) [SHK$^+$09], and H_2Pc on Ag(111) [Kro10].
The equation molecular size

$$\theta = A \cdot 1/d^2 + C$$

gives the theoretical relation between the coverage of particles of size A and their distance from each other when they form a gas on the surface. The added term C is zero when the whole surface can be covered by molecules. This means that the shape of the molecules must allow a close packing of the molecules. Measurements of CuPc on Ag(111) and Ag(110) [Sch15a] suggest that this is the case for CuPc. This gives

$$d = \sqrt{A}\sqrt{\frac{1}{\theta}}. \tag{5.1}$$

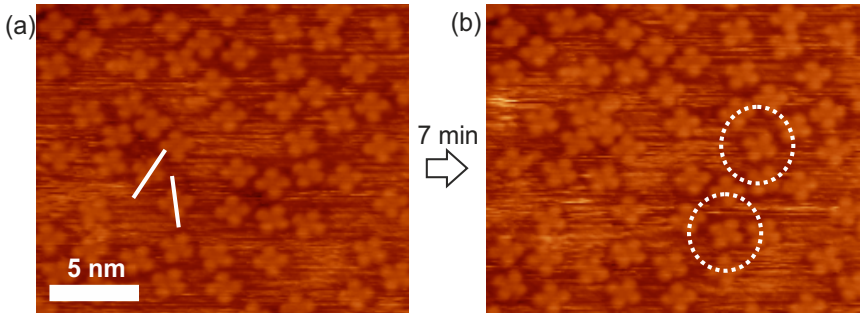

Fig. 5.4: (a) STM image of the filled states of the disordered phase at coverages of about 0.25 ML. It can clearly be seen that the CuPc molecules are oriented along two different directions as marked in the image. Image (b) was taken at the same place several minutes later. It can be seen that the CuPc molecules have not moved showing that the molecules have a very low mobility at room temperature. (Bias voltage = 50 mV, current = 0.033 nA)

The area occupied by a single molecule can be obtained by a linear fit of the measured distance d plotted versus the inverse of the square root of the coverage θ. The result is given in Fig. 5.3 (b). The uncertainty of d was estimated with the clearness of the peaks. The data shows a clear linear dependence of d with $\frac{1}{\sqrt{\theta}}$. This clear linear trend shows that the molecules are distributed evenly across the surface since the theoretically predicted linear trend needs the presence of a gas. It makes the growth of large amorphous islands or molecular chains unlikely since this would create a deviation from the linear trend. The linear fit results in a gradient of 13.75 ± 0.32 Å and an intercept of 0.55 ± 0.39 Å which give an area covered by an individual CuPc molecule of 189.1 ± 8.9 Å^2. Comparing this to the size of the most densely packed unit cell of CuPc of 189.6 Å^2 (see section 5.1.4) shows a remarkable agreement. This proves that the size of the molecule can be determined by analyzing these line scans and that the CuPc molecules are very densely packed in the monolayer phase. The fact that the intercept is not zero shows that there is some offset in the absolute value of the distances measured. This offset can be explained by a slight distortion of the LEED pattern that would lead to a systematic shift of 0.015 Å^{-1}.

orientation of intermolecular distance

At coverages above 0.6 ML, the inner ring also becomes modulated indicating that the preferred intermolecular distance occurs only in certain directions. This modulation becomes more prominent with increasing coverage until it turns into sharp LEED spots of the first crystalline structure.

molecular orientation

The outer lobes in the LEED pattern show a slightly different trend. They already appear at very low coverages where the inner ring is not present yet and do not change their position at low coverages. The lobes are hence due to intramolecular diffraction. The symmetry of the pattern points to one preferred orientation of the molecules on the surface, which is tilted by 15° with respect to the substrate's [110]-orientation. Together with its mirror orientation, it creates the twofold shape of the lobes. Room

temperature STM images were taken at a CuPc coverage of 0.25 ML (Fig. 5.4). They were taken to confirm that the molecules have two preferred orientations on the substrate. The molecules do indeed exhibit two different orientations on the surface (marked by the white lines in Fig. 5.4 (a)). Further analysis of STM images of the disordered phase can be found in Markus Franke's Master's thesis [Fra14]. These STM images together with other STM measurements of larger areas on different parts of the surface also prove that the molecules do not form islands or molecular chains, as was found for CuPc on Cu(111) in [KLS+09].

inter- and intramolecular distances

When the coverage is increased further, the outer lobes move away from the (00)-spot. This indicates that the outer lobes also have a component which is not caused by intramolecular but by intermolecular distances. This second component is the second order of the inner ring which becomes more pronounced at higher coverages. This leads to a superposition of both diffuse signals which shifts the outer lobes of the diffuse signal to higher k-values. The position of the second peak in the line scans (bright blue markers in Fig. 5.3 (a)) is used to calculate a distance as it was already done for the position of the diffuse ring. The results are divided by two and are plotted as open light blue circles in Fig. 5.3 (b). A clear overlap with the distances of the first order spot can be seen. This shows that the spots at higher coverages are mostly due to intermolecular distances.

mobility

STM can not only be used to determine the molecular orientation on the surface but also to investigate the mobility of the molecules. The fact that molecules can be imaged by STM at room temperature shows that the mobility of the molecules must be smaller than the time it takes to record the image. To get to larger time scales, an STM image was taken several minutes after the image in Fig. 5.4 (a) which can be seen in (b). These images show that the mobility of the CuPc molecules at room temperature is so low that only two molecules change their position in several minutes (marked by white dashed circles). Measurements of more molecules in larger scan areas confirm this result (not shown here).

strong molecule-substrate attraction

Combining the LEED analysis with the STM measurements of the disordered phase, several conclusions about the molecule-substrate and the intermolecular interaction can be drawn. The low mobility and the existence of two preferred orientations point to a strong molecule-substrate interaction. While the molecules can diffuse on the surface at high temperatures, when they have a higher thermal energy, the diffusion barrier is too high at room temperature to allow many movements of the molecules.

weak intermolecular interaction

The second conclusion is that there is no significant intermolecular attraction between the molecules on the Cu(001) surface. A strong intermolecular attraction would lead to island growth at low coverages. But the appearance of a diluted disordered phase is not proof for a repulsive interaction since the entropy might compensate for a weak attraction between the molecules. Investigating the other phases is necessary to draw conclusions about whether the intermolecular interaction is weakly attractive or repulsive.

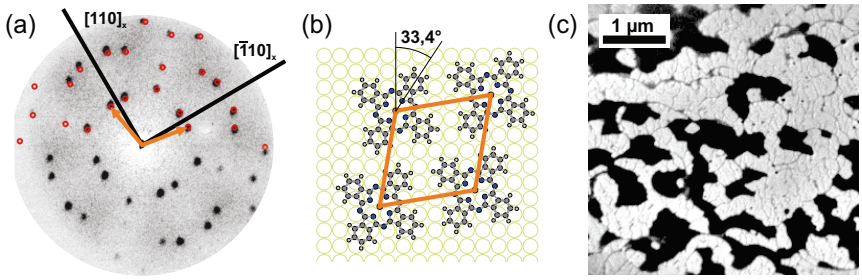

Fig. 5.5: β phase: (a) LEED pattern with the fitted superstructure unit cell and the substrate orientations. (b) CuPc molecules are tilted by 33.4° in the proposed structure model. (c) DF-LEEM image showing the size and orientation of the two rotational domains. The bright contrast belongs to one domain while the dark contrast indicates the other domain. The dark lines mark step edges and boundaries within one domain.

5.1.4 Crystalline phases

At coverages above 0.81 ML, CuPc forms long-range ordered structures. In this section, the three different crystalline structures that appear at a substrate temperature of 460 K during the deposition are presented.

5.1.4.1 β phase

At a coverage of 0.81 ML, see Fig. 5.1 (j) - (k), the diffuse intensity of the LEED image transforms into a sharp LEED pattern indicating that a crystalline phase has formed on the surface.

unit cell

The LEED pattern (see Fig. 5.5 (a)) was used to determine the superstructure matrix

$$M_{\beta \text{ phase, Cu(001)}} = \begin{pmatrix} 6 & 1 \\ 1 & 6 \end{pmatrix}$$

of the first crystalline phase called the β phase. The size of the unit cell is 228.7 Å^2 with unit vectors of a length of 15.5 Å with an angle of 108.9° between them. Considering the size of a CuPc molecule, only one CuPc molecule fits into this unit cell. A proposed structure model is shown in Fig. 5.5 (b). The molecules are tilted by 33.4° with respect to the [110] direction of the Cu(001) surface. This tilt angle is proposed due to the analysis of pair potential maps. A detailed explanation can be found in [vB14, Fra14]. Calculating what coverage is needed to cover the whole surface with the β phase by using the area of the unit cell results in a coverage of 0.83 ML. This fits very well with the maximum intensity of the corresponding LEED pattern at 0.83 ML and it shows that the whole surface is covered by this structure.

nucleation density

After the microscopic structure was determined, the domain structure was investigated. Due to the symmetry of the substrate and the superstructure, two rotational domains of the β phase exist. DF-LEEM was applied to determine the size of the domains that are present when the whole surface is covered by the β phase. One DF-LEEM image can be seen in Fig. 5.5 (c). One of the two domains is bright and the other is dark. It can be seen that the domains are big and spread over hundreds of nanometers. On large terraces, they can even be micrometers in diameter. Assuming that once an island nucleates, it spreads over its terrace while keeping its crystalline structure and orientation, the number of nucleation sites can be approximated by looking at the pattern created in the DF-mode. This is only a rough approximation since there are only two domains present and it is not possible to distinguish between two islands that exhibit the same rotational domain and nucleated next to each other. This leads to a lower number of perceived nucleation sites. It is nonetheless apparent that the nucleation density is low for the β phase, as can be seen in Fig. 5.5 (c). The number of nucleation sites is more strongly influenced by the surface morphology than by kinetic effects since the number of islands is smaller on large terraces and increases in areas with many step edges and smaller terraces.

step edge barrier

In many cases, the edges of the domains coincide with step edges of the substrate showing that domains, i.e. the growing CuPc islands, cannot grow across step edges. The step edges of Cu(001) seem to represent an insurmountable barrier for the growth of crystalline molecular islands, as was also the case for PTCDA on Cu(001) (section 4.1.2). That CuPc islands can grow across step edges on Ag(111) is discussed in 5.2.2.

line defects & stress

The DF-LEEM images also show that inner domain boundaries exist which separate each domain into smaller domains with the same orientation. These boundaries can be seen as dark lines in the bright domains in Fig. 5.5 (c). These boundaries are fairly straight and exhibit sharp corners and hardly any bending. This indicates that stress is building up in the domains that grew from a single nucleation site. This stress leads to defects within the domains. It seems that the stress is relieved by line defects that appear along the directions of the unit cell leading to straight boundary lines along certain directions. Similar line defects are seen in the ϵ phase of CuPc on Cu(001) [Fra14].

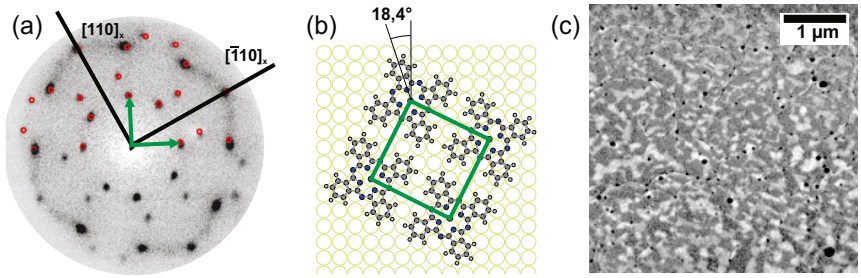

Fig. 5.6: δ phase: (a) LEED image and the corresponding fit of the superstructure unit cell. (b) Proposed structure model with the CuPc molecules tiled by 18.4° against the [110]- direction of the substrate. (c) DF-LEEM image of the two rotational domains. The domains are much smaller in the δ phase than in the β phase.

5.1.4.2 δ phase

The δ phase is present when the deposition is continued and a coverage of 0.93 ML is reached.

unit cell The LEED pattern of this second phase can be seen in Fig. 5.6 (a). It can be explained by a square unit cell of a size of 204.2 Å^2 and unit vectors of a length of 14.3 Å that are tilted by 26.57° with respect to the [110]-orientation of the substrate. The superstructure matrix is

$$M_{\delta \text{ phase, Cu(001)}} = \begin{pmatrix} 5 & 2.5 \\ -2.5 & 5 \end{pmatrix}.$$

This unit cell also contains only one CuPc molecule. The calculated coverage of a surface completely covered by the δ phase is 0.93 ML. This fits very nicely to the coverage of 0.94 ML at which the intensity of the LEED spots is the highest. A proposed structure model where the molecular are tilted by 18.4° is shown in Fig. 5.6 (b)

domain density A DF-LEEM image can be seen in Fig. 5.6 (c), where one rotational domain shows a bright and the other a darker contrast. It can be seen that the domains are much smaller than in the β phase. This can be due to a hindered ability of the CuPc molecules to reorganize themselves since they are already bound in the ordered β phase when they shift to form the δ phase.

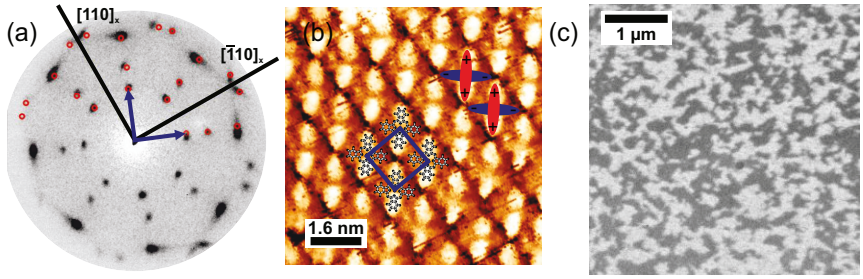

Fig. 5.7: ϵ phase: (a) LEED pattern with the accordant unit cell of the ϵ phase. (b) STM image showing the arrangement of the molecules in the unit cell and the different contrast of the CuPc wings within one molecule. (c) the size of the domain are between the size for the β and δ phases as can be seen by the two contrasts in the DF-LEEM image.

5.1.4.3 ϵ phase

When a coverage of 1.0 ML is reached, the ϵ phase is present on the surface.
The LEED pattern seen in Fig. 5.7 (a) was used to determine a unit cell with a superstructure matrix of unit cell

$$M_{\epsilon \text{ phase, Cu(001)}} = \begin{pmatrix} 5 & 2 \\ -2 & 5 \end{pmatrix}.$$

This corresponds to a square unit cell with a size of 189.6 Å^2 and unit vectors of a length of 13.7 Å. STM measurements were performed on this phase by Markus Franke [Fra14] and one image can bee seen in Fig. 5.7 (b). The molecules are tilted by 21.8° with respect to the [110]-direction of the substrate. The different contrast of the lobes of the CuPc molecules is due to different adsorption sites of the benzene rings of CuPc on the copper surface in this phase which lift the degeneracy of the two LUMO states of the molecule. A detailed analysis can be found in [Fra14].
A DF-LEEM image can be seen in Fig. 5.7 (c) which shows a nice contrast between the two rotational domains. The domains are bigger than in the δ phase. It is unclear why the domains increase in size again. One possible explanation is that the unequal adsorption sites, which cause an unequal partial filling of the two LUMO states, in turn induce a quadrupole moment which increases the interaction between the molecules. This stronger intermolecular interaction might lead to an alignment of the molecules with each other, thus, enlarging the domains. domain size
The unit cell data of the three different structures discussed in this work and the two structures discovered by Franke [Fra14] are summarized in Table 5.1. Four structures are commensurate and one is commensurate in the second order. This high degree of commensurability indicates a strong molecule-substrate interaction which confirms the finding for the disordered phase. There, the strong interaction was indicated by the low mobility and the preferred orientation of the molecules on the substrate. strong molecule-substrate interaction

	α phase	β phase	γ phase	δ phase	ϵ phase
M	$\begin{pmatrix} 6 & 3 \\ 0 & 7 \end{pmatrix}$	$\begin{pmatrix} 6 & 1 \\ 1 & 6 \end{pmatrix}$	$\begin{pmatrix} 5 & 3 \\ -3 & 5 \end{pmatrix}$	$\begin{pmatrix} 5 & 2.5 \\ -2.5 & 5 \end{pmatrix}$	$\begin{pmatrix} 5 & 2 \\ -2 & 5 \end{pmatrix}$
size	274.3 Å^2	228.7 Å^2	222.1 Å^2	204.2 Å^2	189.6 Å^2
vector length	17.9 Å & 18.4 Å	15.5 Å	14.9 Å	14.3 Å	13.7 Å
$\angle(b_1, b_2)$	63.4°	71.1°	90.0°	90.0°	90.0°
$\angle(b_1, a_1)$	26.6°	9.5°	31.0°	26.6°	21.8°
coverage	0.69 ML	0.83 ML	0.85 ML	0.93 ML	1.00 ML
c_{CuPc}[mol/nm^2]	0.37	0.44	0.45	0.49	0.53

Table 5.1: Overview over the five ordered phases that are found when CuPc is deposited on Cu(001).

5.1.5 Phase transitions

The transitions between the different phases exhibit very different behaviors. In the following paragraphs, the transition types are described and explained.

island growth: disordered $\rightarrow \beta$

When the CuPc coverage increases up to 0.81 ML, the LEED spots of the β phase slowly appear. Their intensity increases until a coverage of 0.83 ML is reached while the diffuse intensity of the disordered phase disappears. This continuous change is indicative of island growth. Islands nucleate once a certain density is reached and continue to grow until the whole surface is covered. During the growth of the island, two phases are present on the surface. One phase is the disordered dilute phase and the other is the crystalline β phase growing in islands within the dilute disordered phase. This explains both the increase of intensity of the LEED spots of the islands and the continuous decrease of the background intensity. This island growth was also observed in DF-LEEM at coverages from 0.81 ML to 0.83 ML. The corresponding DF-LEEM images can be found in [vB14].

abrupt reorganisation: $\beta \rightarrow \delta$

The change in unit cell from the β to the δ phase happens without any intermediate structures as illustrated in Fig. 5.8. At a coverage of 0.85 ML, new LEED spots belonging to the δ phase appear, which get more intense, while the intensity of the spots of the β phase decreases. From 0.85 ML to 0.93 ML both the β and the δ phase are present on the surface, which can also be seen in Fig. 5.1 (l). Only the δ phase is present on the surface when a coverage of 0.93 ML is reached and the LEED spots of the β phase have disappeared completely. This indicates that within the β phase new domains of the δ phase start to grow. Their overall area increases with increasing coverage until all of the β domains are gone and only the δ phase is present on the surface. This reorganization happens at the domain boundaries of the β phase where the molecules have fewer nearest neighbors and more space to move. This situation is similar to the first transition where islands of the β phase grow in the dilute

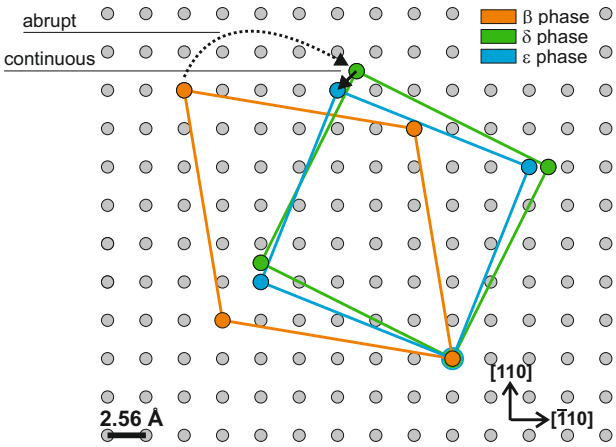

Fig. 5.8: Visualization of the change between the three different crystalline phases. The change in unit cell from the β to the δ phase happens without any intermediate phases while the unit cell of the δ phase changes continuously into that of the ϵ phase. Adapted from [vB14].

disordered phase. Here, the δ phase islands grow within the ordered β phase. The difference between these two transitions is that the molecules that already form an ordered structure have to break away from an existing ordered structure to form the new ordered structure in the second transition.

continuous reorientation: $\delta \rightarrow \epsilon$

The LEED pattern shows a continuous change in the unit cell during the transition from the δ to the ϵ phase (comp. Fig. 5.1 (m)-(o)). This continuous shrinking of the unit cell is visualized in Fig. 5.8. The molecules get pushed closer together with increasing coverage. This is an unusual behavior since otherwise structures do not change continuously. This behavior is also found, for example, for CuPc on Ag(111) [KSS+10] and Cu(111) and Au(111) [SKRK11] and for SnPc on Ag(111) [SHK+09].

intermolecular repulsion

This continuous decrease in unit cell size is the final proof for an intermolecular repulsion of CuPc on Cu(001) since the CuPc molecules always keep a maximal distance to each other.

5.2 Growth of CuPc on Ag(111)

The results of the analysis of the growth of CuPc on Ag(111) are presented in this section.

previous studies

The geometric and electronic structure of CuPc on Ag(111) was studied intensively by Kröger [KSS+10, Kro10, KSW+11a]. The results necessary for the research presented in this work are summarized here. CuPc grows in a disordered gas phase for coverages below 0.89 ML at 300 K and forms crystalline structures at higher coverages. A commensurate structure is present at a coverage of 0.89 ML. This structure changes continuously until a final point-on-line (p.o.l.) structure at a coverage of 1.0 ML is reached. Detailed SPA-LEED studies determined the unit cell of these two structures to

$$M_{\text{CuPc, comm., Ag(111)}} = \begin{pmatrix} 3 & 6 \\ 5 & 0 \end{pmatrix} \qquad M_{\text{CuPc, p.o.l., 1 ML, Ag(111)}} = \begin{pmatrix} 2.52 & 5.50 \\ 4.66 & -0.34 \end{pmatrix}.$$

The continuous change of the unit cell is a shrinking of the unit cell in a p.o.l. fashion. This continuous decrease in unit cell size indicates that a repulsive interaction between the CuPc molecules is present on the Ag(111) surface since the molecules always occupy the largest possible surface area. The commensurate structure also forms at lower coverages than 0.89 ML when the temperature is decreased. These findings are summarized in a phase diagram that can be found in [Kro10].

contents

This work focuses on the growth process of CuPc on Ag(111) and the influence of the temperature and the deposition rate. The influence of the temperature on the formation of different phases is analyzed in section 5.2.1. The observed phase transition with increasing temperature is explained by the entropy in the system. The growth process of the crystalline CuPc islands is discussed in section 5.2.2. The influence of the step edges on the growth is analyzed, and a reorganization of the rotational domains at high temperatures with time and continued deposition is described in detail.

5.2.1 Influence of temperature on formation of different phases

The influence of the substrate temperature on the formation of different phases of the CuPc layer is analyzed in this section.

sample preparation

CuPc molecules were deposited on a Ag(111) substrate which was kept at different temperatures (300 K, 380 K, and 400 K). The deposition rate was 0.17 ± 0.02 ML/min in all three experiments. This deposition rate is quite high compared to the deposition rates used later in this chapter but the system should nonetheless be close to the thermodynamic equilibrium since the structures do not change when the deposition is stopped.

gas phase

No strong deviation from the behavior that was already discussed in [KSS+10] could be observed for the gas phase of CuPc which is present at coverages below 0.83 ML.

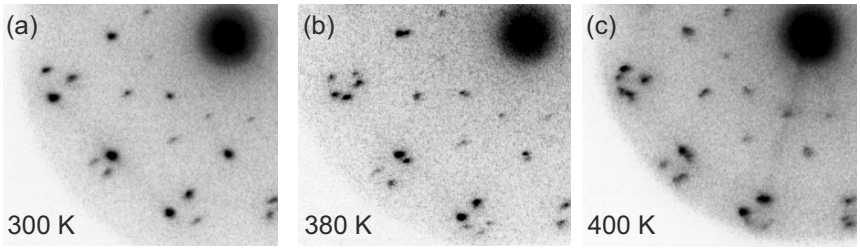

Fig. 5.9: LEED pattern of the first structure that forms when CuPc is deposited on Ag(111) at different substrate temperatures. (a) The commensurate structure appears at 300 K. No splitting of the spots can be observed. (b) The LEED spots, which are united in the commensurate structure, are already split when they appear when CuPc is deposited at 380 K. The intensity of domain-equivalent spots is different and some are even missing since the different rotational domains are not present in equal proportions in the small area that is investigated. (c) The same behavior that was already observed for 380 K is present when the temperature is increased further to 400 K.

But there are differences in the structure of the first islands that nucleate when the deposition is continued. These differences are discussed in the following paragraphs. crystalline phases
The LEED spots that appear at a coverage of 0.83 ± 0.01 ML, when CuPc is deposited on a substrate that is kept at 300 K, can be seen Fig. 5.9 (a). These spots belong to the commensurate structure of CuPc on Ag(111). The intensity of the spots increases until a coverage of 0.90 ± 0.01 ML is reached. The spots start to move when the deposition is continued until the p.o.l. structure that was observed at a coverage of 1.00 ML [Kro10] is reached demonstrating a continuous reduction of the unit cell. The presence of the commensurate structure at 0.89 ML and the shrinking of the unit cell agrees very nicely with the findings of Kröger [Kro10]. But the appearance of the spots of the commensurates structures already at 0.83 ML was not previously discovered. The increase in the intensity of the spots of the commensurate phase in the coverage regime from 0.83 ML to 0.90 ML indicates the nucleation of crystalline islands at 0.83 ML that grow until they cover the complete surface at 0.90 ML. Details about this growth process are discussed in 5.2.2. 300 K
A different situation is found when CuPc is deposited at an elevated substrate temperature of 380 K. The first LEED spots that appear at this temperature can be seen in Fig. 5.9 (b). They do not belong to the commensurate structure as can easily be seen when comparing Fig. 5.9 (a) and (b). Note that the spots belonging to one rotational domain are missing in the LEED pattern. This can be explained by the absence of one rotational domain in the measured area which only has a size of $18\,\mu m^2$. The structure that appears can be identified as the p.o.l. structure that was found at 0.95 ML at 300 K by Kröger [Kro10]. This p.o.l structure, and not the commensurate structure, is the first structure that nucleates at elevated temperatures at a coverage 380 K

of 0.86 ± 0.01 ML. This is an unexpected result since this p.o.l. structure was reported to appear only at higher coverages of 0.95 ML [KSS+10, Kro10]. The intensity of the first spots that appear increases until a coverage of 0.96 ± 0.01 ML is reached. This coverage is in good agreement with the coverage found by Kröger for the appearance of this structure at 0.95 ML at 300 K. The finding is also congruent with the presence of island growth that was already proposed to explain the observed increase in intensity of the LEED spots of the commensurate structure between 0.83 ML and 0.90 ML at 300 K.

400 K

The growth behavior present at 400 K is very similar to that at 380 K. The first spots, which belong to a p.o.l. structure, appear at a coverage of 0.87 ± 0.01 ML and can be seen in Fig. 5.9 (c). The determination of the exact structure these spots belong to is not possible since the image quality is not as good as in the previously discussed experiments and not all domains are present in the measured area leading to the absence of one domain. It can still be seen that the structure is very similar to the structure found at 380 K. The intensity of the spots increases until a coverage of 0.95 ± 0.01 ML is reached. These values coincide within the experimental uncertainties with the values found for 380 K. It seems that an increase in the temperature from 380 K to 400 K does not induce a strong change in the growth behavior.

phase transition

These experiments show that islands of different structures nucleate when CuPc is deposited at different substrate temperatures. The commensurate structure or a p.o.l. structure are present on the surface at coverages between 0.86 ML and 0.90 ML at different substrate temperatures. An explanation for this phase transition is given in the next paragraphs.

Gibbs free energy

The following argumentation uses thermodynamic equations that might not be strictly applicable to the system under investigation but are useful for illustrating the fundamental mechanisms. The Gibbs free energy, G, can be used to analyze the thermodynamics of this system. It is given by

$$G = U + pV - ST, \tag{5.2}$$

where U is the inner energy, p is the pressure, V the volume, S the entropy, and T the temperature. To explain the observations, it is differentiated between two cases which both have the same coverage, e.g. 0.88 ML, meaning the same overall density of molecules: one where the commensurate structure is present and one with a p.o.l. structure, both coexisting with a disordered phase. It is known that the commensurate structure is present below 0.89 ML at temperatures below 300 K [KSS+10]. This means that $G_{comm.} < G_{p.o.l.}$ at low temperatures. Increasing the temperature up to 380 K makes the p.o.l. energetically preferable showing that $G_{comm.} > G_{p.o.l.}$ for $T > 380\,K$. A sketch of the necessary trend of $G_{comm.}$ and $G_{p.o.l.}$ can be seen in Fig. 5.10 where the Gibbs free energy is plotted versus the temperature. Equation (5.2) contains a lot of unknown quantities and some simplifications are necessary. The pressure and volume of the system are considered to be the same in both cases since the coverage is the same. This means that the pV term can be neglected in the following since only the difference in the Gibbs free energy of the two cases is important. The simplified

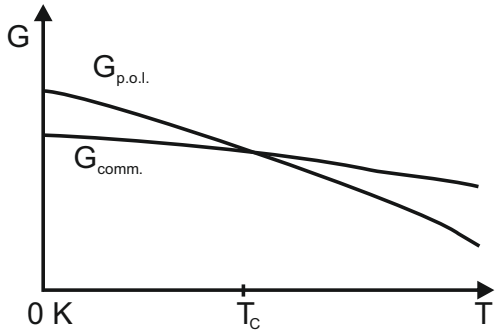

Fig. 5.10: The Gibbs free energy plotted versus the temperature of the substrate. The Gibbs free energy for a sample with coexisting commensurate islands and disordered areas, $G_{comm.}$, is smaller than for a sample with p.o.l instead of commensurate islands, $G_{p.o.l.}$, for temperatures below the critical temperature T_c. The p.o.l. structure is then preferred at temperature above T_c.

Gibbs free energies are defined as

$$G_{comm.} = U_{comm.} - S_{comm.}T \qquad \text{and} \qquad G_{p.o.l.} = U_{p.o.l.} - S_{p.o.l.}T. \tag{5.3}$$

The inner energy and the entropy consist in both cases of the contribution of the molecules that are in the disordered phase and of the contribution of the molecules in the ordered phase. This means that in the following argumentation the inner energy and the entropy of the molecules that form the disordered phase and of the molecules that form the ordered islands has to be taken into account for the two systems. The system where islands of the commensurate structure are present is called the commensurate system even though there exist also molecules that form a disordered phase and the system with p.o.l. islands and a disordered phase is called that p.o.l. system. The inner energy of the system is influenced by various factors, including interactions with the substrate as well as with other molecules and vibrational properties. Contributions that differ in strength are identified to find differences in the inner energy that determine which structure grows at which temperature. The interaction with the substrate as well as the vibrational properties should be almost the same for the molecules whether they are diffusing on the surface in the disordered phase or bound in a crystalline structure in the islands. This means that they are neglected here since they are the same for both systems. The interaction between the molecules in the disordered gas phase in both cases should also be the same. The interaction between the molecules in the two crystalline phases is different. Pair potential calculation of CuPc show that there is a weak attraction between the molecules in the commensurate structure while the interaction is slightly repulsive for the p.o.l. structures [KSW+11b]. Hence,

inner energy

$$U_{comm.} < U_{p.o.l.}.$$

It was already said that the commensurate structure is energetically preferable at temperatures down to 130 K. If this trend continues down to $T = 0$, then $G_{comm.}(T = 0) < G_{p.o.l.}(T = 0)$. Since $G_{comm.}(T = 0) = U_{comm.}$ and $G_{p.o.l.}(T = 0) = U_{p.o.l.}$, the proposed relation between $U_{comm.}$ and $U_{p.o.l.}$ is fulfilled.

entropy The second unknown quantity is the entropy. Two different types of entropies have to be considered for this system. The first entropy is the orientational entropy. It depends on the number of possible rotational orientations a molecules can have on the surface. In a crystalline phase, this entropy is very small since the molecules have fixed orientations. This means that the orientational entropy in both crystalline phases is the same and does not play a role for the phase transition. In the CuPc gas-phase at this coverage, the CuPc molecules also have a limited number of orientations due to the interaction with the substrate as can be seen by the inhomogeneous intensity distribution in the diffuse rings in the LEED pattern [Kro10]. The limited number of orientations is the same in both cases meaning that this entropy is also the same for the disordered phases for both cases. The second type of entropy is the positional entropy. It increases with increasing space the molecules can move on. This means that it decreases with increasing molecular density on the surface. The positional entropy of both crystalline phases is minimal and can be assumed to be identical since the molecules cannot move in the bound state. The final entropy that is left to consider is the positional entropy of the areas covered with the disordered phase in both cases. The density of CuPc in the commensurate islands is lower than in the p.o.l. islands. How does this affect the entropy of the areas covered by the disordered phase in both systems? When the surface is partially covered by the commensurate structure, the free molecules have a certain amount of space available to diffuse on. If the same amount of CuPc molecules that were bound in the commensurate system form islands with a p.o.l. structure, the available space for diffusion for the rest of the molecules is larger since CuPc molecules in the p.o.l. islands are more densely packed. This means that the positional entropy of the disordered phase in the p.o.l. system is larger than in the commensurate system. Since all other therms are equal or can be neglected, it can be concluded that

$$S_{comm.} < S_{p.o.l.}.$$

phase transition The necessary trend for the discovered phase transition, which is shown in Fig. 5.10, can be explained by taking the two relations from the last paragraphs into account. $G_{comm.} < G_{p.o.l.}$ at low temperatures since $U_{comm.} < U_{p.o.l.}$ and the entropy term does not have a big influence at low temperatures. $G_{p.o.l.}$ drops more quickly with increasing temperature than $G_{comm.}$ since its entropy term is higher. This leads to a crossing of the two Gibb's free energies and the phase transition from the commensurate to the p.o.l. structure with increasing temperature.

discussion These thermodynamic considerations can explain the phase transition from the commensurate structure present at 300 K to a p.o.l. structure at 380 K. An entropy-driven phase transition was also found for tetracene on Ag(111) [SKKT11]. Entropy is the driving force in the ordering of particle which are noninteracting or re-

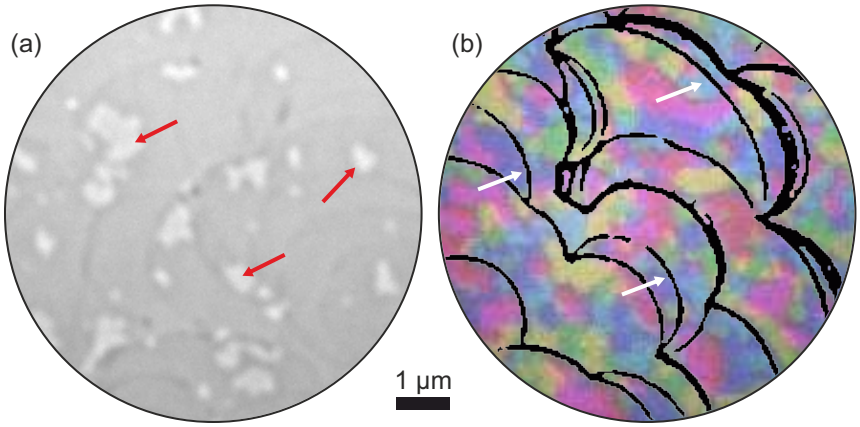

Fig. 5.11: Results of the deposition of CuPc at 300 K on Ag(111). (a) LEEM image showing the bright CuPc islands (some of which are marked by red arrows). Step edges of the Ag(111) substrate can be seen as dark lines. (U_{start} = 0.1 V) (b) Composite image of all six rotational domains with the step edges of the Ag(111) substrate superimposed. The white arrows mark locations where an island is spread over a step edge. (U_{start} = 2.0 V)

pelling [BOP92, EMF93, Sch01, Fre94, SPG00]. It is not surprising that it is applicable to this system since the interaction between the CuPc molecules on Ag(111) was also found to be very weak [KSS+10, KSW+11a].

5.2.2 Growth dynamics of crystalline phases

The LEED measurements of the previous section suggested that islands with different crystalline structures grow in the high coverage regime between 0.83 ML and 0.96 ML. The nucleation of these crystalline islands and their growth are discussed in this section. The influence of the substrate temperature during the deposition as well as the influence of the deposition rate on the growth are analyzed.

5.2.2.1 Growth dynamics at 300 K

The deposition of CuPc on a Ag(111) surface that is kept at 300 K is discussed first. LEED images were taken while CuPc was deposited on the Ag(111) surface. As soon as the first diffraction spots appeared, the deposition was stopped and the LEEM image shown in Fig. 5.11 (a) was taken.
It shows CuPc islands (bright contrast) that appear when 0.85 ML of CuPc are present islands
on the substrate. The dark lines are step edges of the silver substrate. This proves that there is indeed island growth, as was proposed in the previous section. It can be seen that more than one CuPc island nucleates on each terrace. Some islands nucleate

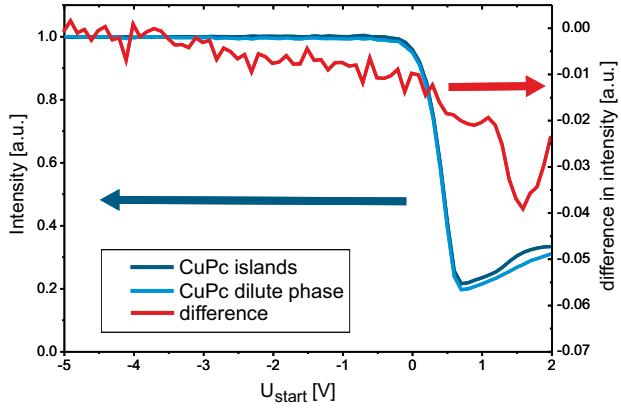

Fig. 5.12: LEEM-IV curves of the disordered gas phase and the ordered structure of the islands. The difference between the curves is also plotted to better see the maximal difference between the curves which is at 1.55 V.

at step edges and some in the middle of a terrace. The islands also have very different sizes indicating that the nucleation of the CuPc islands happens in a relatively wide time window or that the growth is strongly influenced by the sample morphology. Unfortunately, more CuPc was not deposited on this sample but it was continued with PTCDA to investigate the mixing behavior of PTCDA and CuPc which is discussed in chapter 6.2.1.

LEEM-IV

A LEEM-IV image sequence was measured at this coverage to determine the start voltage with the highest contrast between the disordered and the crystalline phase. The intensity from an area where the disordered phase was present and one where the ordered crystalline phase was present are plotted versus the start voltage in Fig. 5.12. Both curves follow almost the same trend up to a start voltage of 0.5 V. At higher start voltages, differences are clearly visible. The difference in intensity of the two curves is plotted as the red curve in Fig. 5.12. It can be seen that the difference is maximal at a start voltage of 1.55 V. This start voltage was used for the following experiments to get an optimal contrast between the two phases (the ordered islands and the disordered gas phase). The LEEM-IV curve was only measured up to 2.0 V since beam damage plays a role at higher start voltages.

rotational domains

Another experiment was done to get an idea about the growth and the structure of the complete layer. Images of the nucleation process of the islands are not shown here since the noise was so high that no islands could be discerned. DF-LEEM images were taken to differentiate between the different orientational domains. All DF-LEEM images shown in this chapter were taken with the first order diffracted spots that can be seen in Fig. 5.9 (b). Two spots are always very close together. This makes it difficult to get a good contrast between these two individual domains and explains the weak contrast between green and magenta domains in images Fig. 5.16 (b) and the vanishing contrast between the magenta and green domains in Fig. 5.20 (a). Fig. 5.11 (b) shows

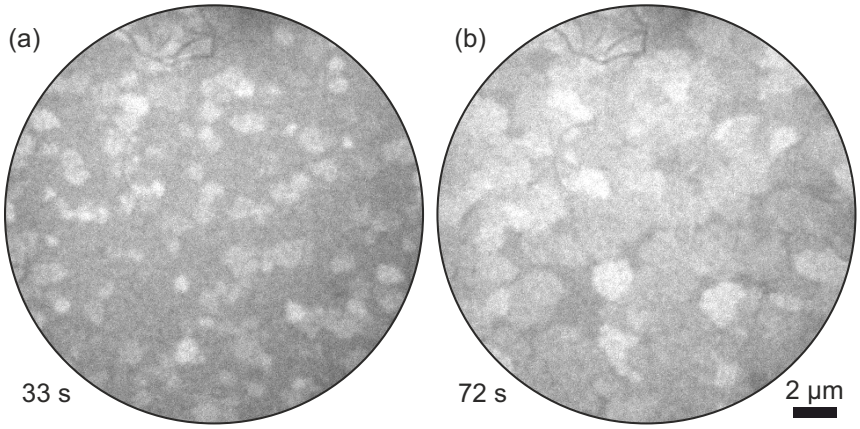

Fig. 5.13: LEEM images taken during the nucleation and growth of CuPc islands (bright contrast). The CuPc islands exhibit different contrast due to their different orientation. For details see text. ($U_{start} = 1.55\,\mathrm{V}$)

a composite image of all six orientational domains after the deposition of 1.0 ML. It can be seen that many differently oriented domains are present on each terrace. This suggests that many islands nucleate on each terrace, as could already be seen in Fig. 5.11 (a). All six rotational domains domains appear randomly distributed since no domain appears significantly more often than others. Some domains, which are marked by the white arrows, are spread across step edges. There are two possible explanations for this. One is that it is a coincidence that the edges of two individual domains align at the step edge. The other is that the islands can grow across step edges. It was already said that the nucleation at this deposition rate and temperature happens so quickly and that the islands are so small that it is impossible to determine if the islands just happened to align their borders at the step edges or if they grew across the step edges.

5.2.2.2 Growth dynamics at 430 K

The deposition experiment was repeated at higher temperatures since the nucleation density should decrease with increasing temperature. The expectation was that it would be possible to observe the growth of the individual islands if a more limited number of islands nucleated. CuPc was deposited on a Ag(111) substrate that was kept at 430 K to achieve this reduced nucleation density by increasing the temperature.

Fig. 5.13 shows two LEEM images taken during the growth of the crystalline CuPc islands. The CuPc islands appear brighter than the dilute disordered phase as expected from the LEEM-IV measurements (Fig. 5.12) for the selected start voltage of 1.55 V. It can be seen that some islands appear brighter than others. This is due to

island growth

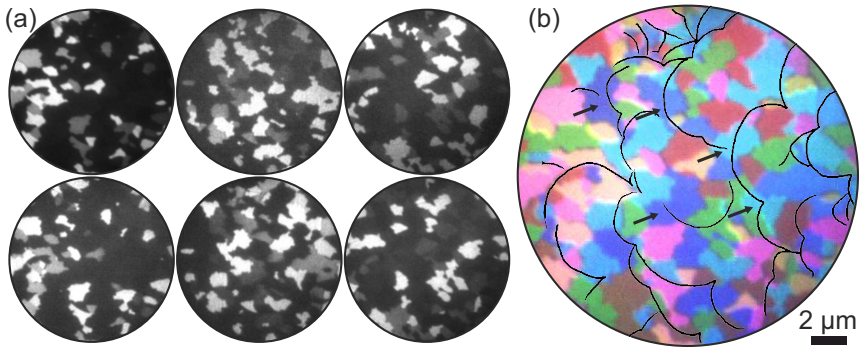

Fig. 5.14: DF-LEEM images corresponding to the growth experiment shown in Fig. 5.13. (a) Individual DF-LEEM images of all six domains. The image in the lower left represents the brightest domain from Fig. 5.13. (b) Composite image of all six domains with the step edges superimposed. Black arrows mark islands that spread across step edges. ($U_{\mathrm{start}} = 2.0\,\mathrm{V}$)

the different orientations of the CuPc islands. The measurement was performed with a contrast aperture to obtain a better contrast between the disordered and the crystalline phase. This contrast aperture decreased the intensity on the detector of some domains since it was not perfectly centered around the 00-spot and cut off some first order diffraction spots of the nucleated islands. Coincidentally, this makes it easier to follow the growth of some individual islands that appear brighter than others. It is shown later that the bright islands do in fact have the same orientation. The step edges are not visible in these images but can be seen in Fig. 5.14 (b). Even though it is possible to follow the growth of some islands, it is still not possible to analyze the growth in detail.

rotational domains

DF-LEEM images were taken to determine the orientation of the domains after a complete monolayer of CuPc was deposited on the surface. All six domains can be clearly distinguished in Fig. 5.14 (a). It can be observed that no orientation appears much more often than the others indicating that there is no preferred growth of islands with a specific orientation. The shapes of the islands do not seem to be influenced strongly by step edges since hardly any long and slightly curved island boundaries are visible. The domain shown in the lower left in Fig. 5.14 (a) can be identified as the island with the bright contrast from Fig. 5.13. Fig. 5.14 (b) is a composite image of all six domains with the step edges superimposed (black lines). It can be seen that some islands are spread across step edges and several of those islands are marked with black arrows. It is likely that the islands grew across the step edges since the edges of the domains of identical orientation align at the step edges as is can be seen clearly in the image which has a better contrast between the domains than Fig. 5.11 (b).

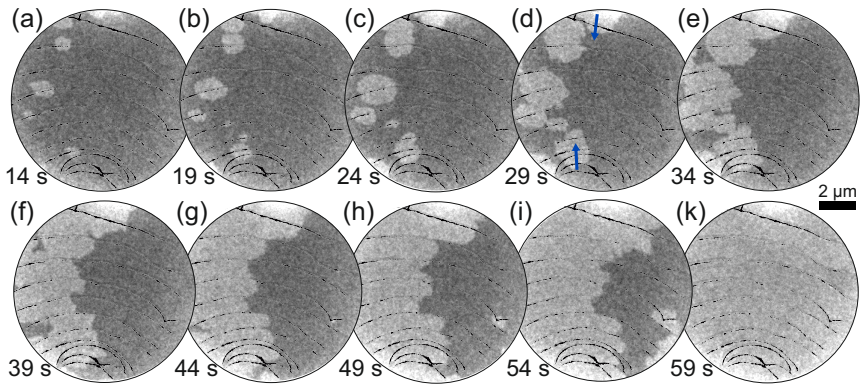

Fig. 5.15: A LEEM image sequence taken during the growth of the crystalline CuPc islands ($U_{\text{start}} = 1.55\,\text{V}$). The step edges of the silver substrate are superimposed in black. The time is given in seconds after the nucleation of the first islands. A detailed description of the images in given in the text.

5.2.2.3 Growth dynamics at 400 K

The next experiment was performed at a slightly lower substrate temperature but with a much lower deposition rate than the previous one to decrease the nucleation density further since a decreased island density makes the differentiation between individual islands easier. The results of the deposition at 400 K are discussed in this section.

growth

The growth process from the nucleation of the first islands to the completely covered surface is shown in Fig. 5.15. The crystalline CuPc islands appear bright while the gas phase of CuPc remains darker. The step edges of the Ag(111) surface are superimposed as black lines. The contrast between the islands and the disordered phase is very good making a detailed analysis of the growth possible.

nucleation at step edges

A few islands are visible on the left side of Fig. 5.15 (a). It can be seen that all islands nucleate at the silver step edges. It can also be observed that the nucleation sites are not spread evenly across the surface but are localized on the left side of the image where the step edges are all oriented approximately in the same direction. This suggests that the CuPc clusters prefer to nucleate at step edges where their orientation is similar to a specific direction in the unit cell. Such a behavior was also found for the growth of PTCDA on Ag(111) in section 4.2.2. In the case of PTCDA, it was suggested that the orientation of the islands was due to their nucleation at the PTCDA molecules that decorate the step edges. A decoration of CuPc at the step edges is not known from literature making it impossible to say for now if the same mechanism is responsible for the orientation of CuPc islands.

growth direction

The islands grow radially in all directions after they nucleated and no preference in growth direction can be observed (Fig. 5.15 (a)-(e)). This is in contrast to the growth of PTCDA on Ag(111), where the islands also nucleate at the step edges but only grow on the lower terrace (section 4.2.1.1).

growth across step edges

The islands continue to grow in all directions. They grow across step edges in both direction as can be seen in Fig. 5.15 (c)+(d) by the growth directions of the island at the bottom and at the top of the image (marked by blue arrows). The island located in the upper part of Fig. 5.15 (d) grows from upper to lower terraces while the island located in the lower part grows from lower to upper terraces. (The position of upper and lower terraces of the Ag(111) substrate was explained in section 2.2.)

influence of step edges

The shape of the islands is not yet influenced by the step edges in Fig. 5.15 (c). The islands continue to grow and start to grow together until they form one single island (Fig. 5.15 (d)-(f)). This bigger island finally shows that the step edges do influence the growth slightly since the growth front is not smooth at step edges. As the island expands to the right, the influence of the step edges becomes more apparent (Fig. 5.15 (f)-(h)). This is most likely a consequence of the growth direction of the island. Island edges that spread perpendicular to the step edges have a smaller angle between their growth front and the orientation of the step edges. This makes discontinuities of the island edge at the step edge appear smaller than when the island grows in the direction parallel to the step edges.

completion of monolayer

A second growth front appears in the field of view in Fig. 5.15 (i) in the lower right corner. The islands have grown together in Fig. 5.15 (j) covering the whole area with a crystalline film at a coverage of 0.95 ML. The deposition was continued until a complete monolayer was deposited.

orientational domains

DF-LEEM images were taken after the deposition of a complete monolayer. A composite image of the four different rotational domains present in this field of view can be seen in Fig. 5.16 (a). It was checked that only four different rotational domains grew in this area and that none of the colored areas in this image contains more than one domain. The step edges are superimposed to illustrate the relation between the step edges and the domain boundaries.

domains larger than terraces

The DF-LEEM image shows clearly that the domains are spread over large areas and that the step edges do not influence the domain boundaries significantly. The step edges represent boundaries of the domains only in some areas, e.g., on the right in Fig. 5.16 (a) between the blue and the magenta domain or between the red and the magenta domain.

similar nucleation sites lead to similar orientations

The positions of the LEED spots corresponding to the domains were determined. It is found that the red and the blue domains as well as the green and the magenta domains are mirror domains of each other. This means that there is only a misalignment of 8.8° between the axes of their unit cells and only 8° between the long axes of the molecules in both domains [Kro10]. Fig. 5.16 (b) shows a zoomed out image of the same area on the surface. The area from Fig. 5.16 (a) is marked in Fig. 5.16 (b) by a white circle. The preference for mirror domains to nucleate at similar areas becomes even more apparent here since the left of the image is dominated by magenta and green domains and the right by red and blue domains. This is the second indication - besides the

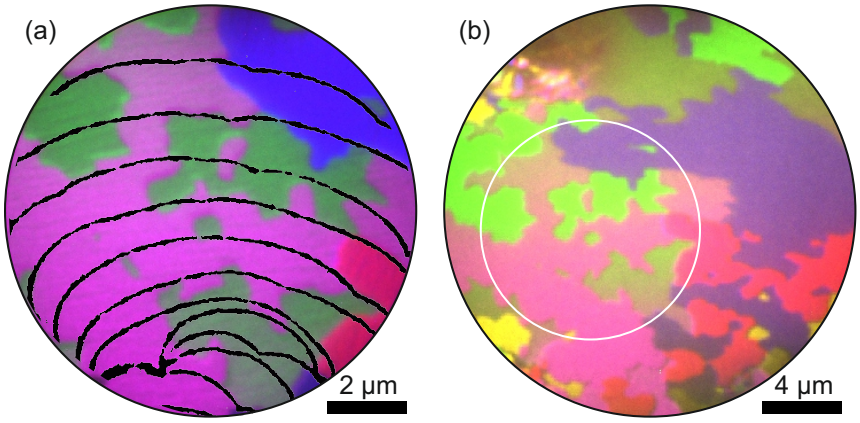

Fig. 5.16: Composite images of the rotational domains from the experiment shown in Fig. 5.15. (a) The four different domains present on this area on the sample can clearly be distinguished. The step edges are superimposed in black and do not seem to influence the domain boundaries significantly. (b) Composite image showing a larger part of the sample and the five domains present there. The area of part (a) is marked by a white circle. The left part of the image is dominated by the magenta and the green domain while the blue and the red domain dominate the right part. ($U_{\mathrm{start}} = 2.0\,\mathrm{V}$)

non-random distribution of nucleation sites - that the orientation of the step edge an island nucleates on determines the orientation of the domain. One additional domain orientation also becomes visible in this bigger field of view and it is colored yellow. These yellow domains grow in areas where the step edges have a different orientation than those present in Fig. 5.16 (a). This is another indication that the orientation of the step edges influences the orientation of the islands.

reorganization

Comparing the shape and the location of the domains with the growth sequence shown in Fig. 5.15 gives a large discrepancy between expected and existing domain boundaries. To illustrate this better, images of the growth sequence are superimposed in gray on the domain images in Fig. 5.17. Fig. 5.17 (a) shows the situation 35 s after the nucleation of the first islands. It can be seen that the largest island covers an area that later has two different orientations. But it can also be seen that this island spreads in two directions (marked by yellow arrows) that are later dominated by the green domains. This observation suggests that this island's original orientation corresponds to the green areas and that it forms the two large green domains in the upper part of the image. At the place where it nucleated, it transforms into a magenta domain. The growth of an additional island can be seen in Fig. 5.17 (b). Its growth direction is marked by a yellow arrow. This island will form the blue domain seen in the upper part of the image. Fig. 5.17 (c) shows how the islands have grown together and that it is no longer possible to follow the growth of the individual islands. These observations

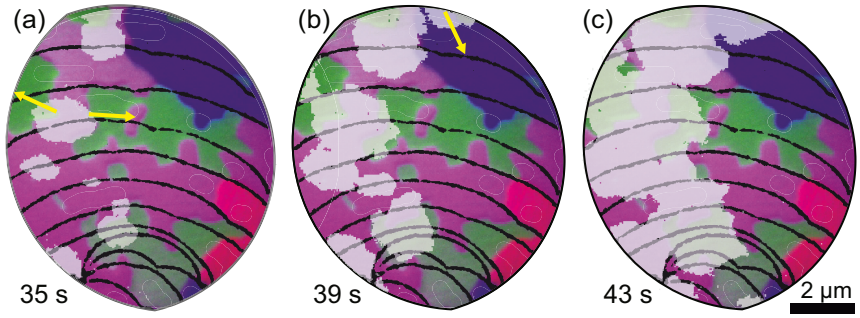

Fig. 5.17: The CuPc islands at different stages during the growth are superimposed in light gray over the composite image from Fig. 5.16 (a). The orientations of the domains after the deposition is not reflected very well by the growth of the islands.

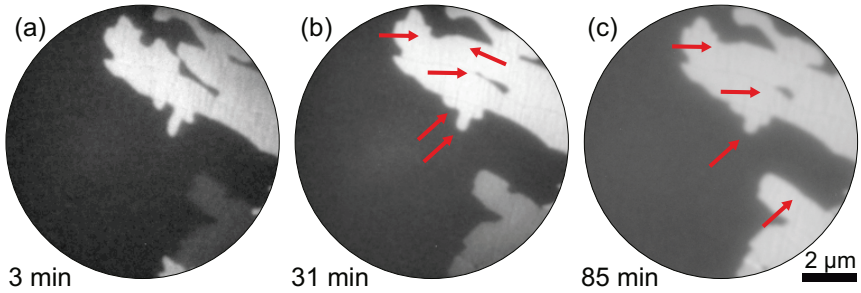

Fig. 5.18: DF-LEEM images of two domains at different times after the deposition was stopped. It is apparent that more drastic changes happen in the first 28 min after the deposition was stopped than in the next 54 min.

indicate that the orientation of the domains are given by the orientation of the first island that spreads over the area but that a lot of reorganization happens after the initial nucleation and growth.

time evolution of boundaries

Images of the domains were also taken in a long time interval after the deposition to investigate if this reorganization continues to happen even after the deposition is stopped. The substrate was kept at 400 K after the deposition. Three DF-LEEM images that were taken in a time range of 82 min are shown in Fig. 5.18. Several changes of the domain boundaries can be observed and are indicated by red arrows. The first image was taken 3 min after the deposition was stopped. It can be seen that more changes occur in the first time interval of 28 min than in the 54 min afterwards. It looks like the system tries to minimize the protrusions and, thus, the total length of the domain boundaries. This indicates that domain boundaries are energetically costly. There are more protrusions present right after the deposition is stopped leading to more prominent changes in the beginning.

different domain boundary types

It can be seen that boundaries between the green and the blue domains and the red and magenta domains exhibit changes while the other domain boundaries stay the same (color code from Fig. 5.16). Analyzing the orientation of the four domains with respect to each other, it is found that domains which can be transformed through rotation into each other (magenta-red, green-blue) change their boundaries and those which need a rotation and an additional mirror operation (blue-magenta, green-red) do not. The domain boundaries between the pure mirror domains where no rotation is involved (magenta-green and red-blue) do not change (not shown in a figure). Although this is a very tentative finding, since there are only four domains present in the field of view and only a few changes occur, it proves that the reorientation that is necessary to form the peculiar shape of the green and magenta domains must have happened during the deposition of the molecules.

reduced deposition rate

The experiment was repeated with a reduced deposition rate to get a better understanding of the reorientation of the domains. For this, a five times smaller deposition rate was chosen while the substrate temperature was identical. The growth of the first 0.95 ML was observed in LEEM mode and the last 0.05 ML in DF-LEEM mode. The LEEM image sequence is shown in Fig. 5.19. The time given in the images is the time after the nucleation of the first islands. The different time intervals between the images were chosen since the growth velocity of the island edges on the large terrace increases in the end.

defect

A larger field of view was chosen for this measurement since a lower nucleation density was expected due to the lower deposition rate compared to the previous experiment. Unfortunately, the nucleation density was even lower than expected and it had to be zoomed out during the deposition. A large defect on the substrate was then discovered which can be seen as the big black spot in the lower left part of the image. This spot looks even bigger than it was due to the small contrast aperture used and the necessary focus conditions to obtain a maximal contrast between the disordered and the ordered phase of CuPc. It should not affect the growth in the areas that show a good contrast in the image.

nucleation at step bunches

Fig. 5.19 (a) shows the bright crystalline CuPc islands 28 s after the nucleation of the first crystalline islands. The nucleation of the islands occurred at the step bunches of the silver substrate. The nucleation at step bunches is in agreement with the previous experiment, which also showed a preferred nucleation at step edges. This experiment even shows that step bunches are preferred to single step edges.

nucleation time

The nucleation of new islands occurs in a very narrow coverage window since no new islands can be seen to nucleate after the image in Fig. 5.19 (b) was taken. The nucleation behavior in relation to the CuPc density on the surface is discussed later in this section.

growth direction

The islands grow in all directions after their nucleation (Fig. 5.19 (b)-(c)). But they exhibit a higher growth speed in the direction of the areas without islands since no islands that can compete with them for the attraction of CuPc molecules are located there. The islands grow up- and downwards across step edges as can be observed in Fig. 5.19 (marked with blue arrows in (d) and (e)). This confirms the observations from Fig. 5.15 (d).

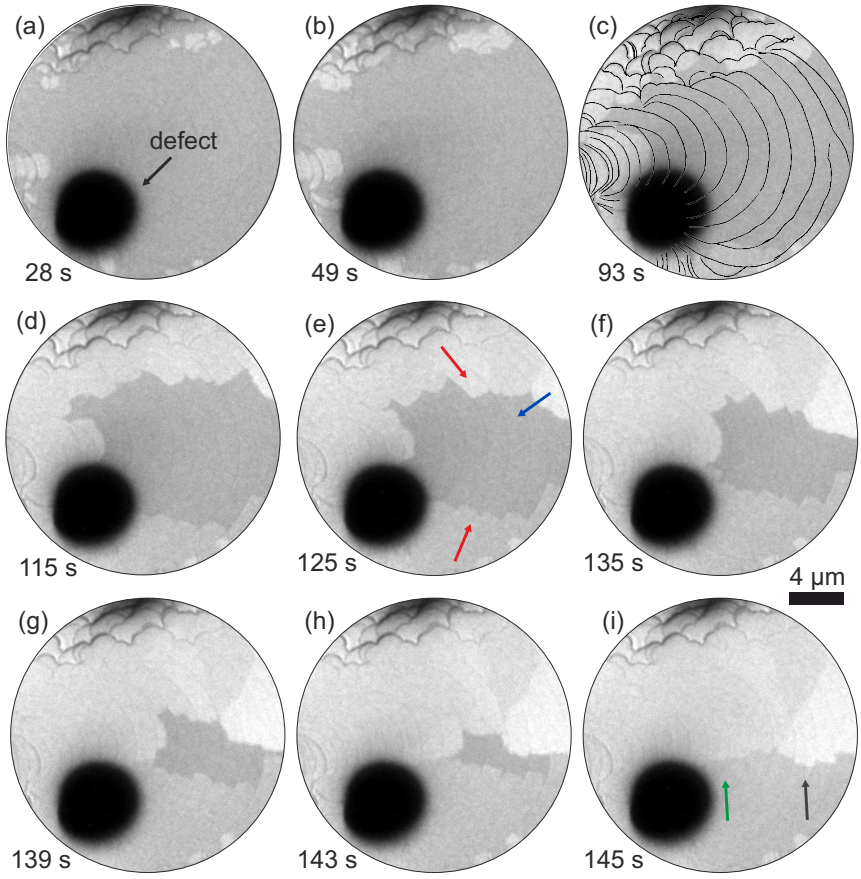

Fig. 5.19: LEEM image sequence of the growth of CuPc at a reduced deposition rate at a substrate temperature of 400 K ($U_{start} = 1.55$ V). The black area is a defect on the sample. The step edges of the Ag(111) substrate are superimposed in (c). The crystalline islands have a brighter contrast than the disordered phase. A detailed description of the growth can be found in the text.

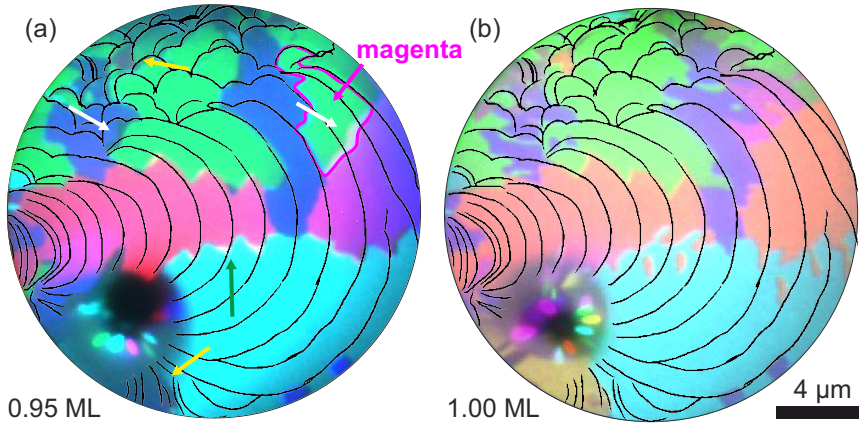

Fig. 5.20: Composite images of the orientational domains of CuPc deposited at 400 K. (a) DF-LEEM images taken in a time window between 4 min and 9 min after the deposition was stopped after 0.95 ML are deposited. It can be observed that the boundaries change in this time interval. (b) DF-LEEM images taken after more than 1.0 ML is deposited. The boundaries have changed drastically compared to part (a). ($U_{\text{start}} = 1.6$ V)

influence of step edges

The step edges do influence the growth but they do not strongly hinder the growth across them. The influence of the step edges can be seen more strongly when the islands grow parallel to them rather than perpendicular as is can be seen in Fig. 5.19 (b)-(h). The growth fronts that move parallel to the step edges (red arrows) exhibit much larger discontinuities in the growth fronts at the step edges than those growing perpendicular to them (blue arrows). This is a consequence of the geometry of the growth fronts with the orientation of the step edges as is was already discussed for the previous experiment.

boundaries during deposition

The last two images (Fig. 5.19 (h)+(i)) show how the crystalline layer is closed. The deposition was stopped right after the layer was closed which gives a total coverage of 0.95 ML. The domain boundaries between certain domains can be seen since the rotational domains have a slightly different contrast in this measurement. The boundaries look quite straight (green arrow) and only have few protrusions (black arrow). These protrusions can be explained by the shape of the growth fronts.

change of boundaries without continued deposition

DF-LEEM images were taken 4 to 9 minutes after the deposition was stopped and make up the composited image seen in Fig. 5.20 (a). The image of the green domain was taken 4 min, the cyan 6 min, the blue 7 min, and the red 9 min afterwards. The image consists of only these four colors since the other two were not observed in the limited time. It can be seen that two areas (marked with yellow arrows) do not exhibit any color which means that they belong to the one domain that was not found in the short time frame. The green domain in the upper right part of the image (marked with a magenta outline) belongs to the "magenta" orientation. The DF-LEEM image

where the green colored domains come from was not illuminated by just one spot but by two spots which lay very closely together, as is the case for the closely related mirror domains. These additional considerations give the six rotational domains. It can clearly be seen that the domains have changed a lot in the time interval used to record the DF images. The formerly straight boundary, which is marked by the green arrow in Fig. 5.19 (i) is already deformed when the image of the cyan domain was taken and became even more zig-zag shaped when the image of the red domain was recored (green arrow in Fig. 5.20 (a)). Another drastic change in the shape of the boundaries can be observed in the upper left of the image which is marked by a white arrow. The blue domain has shrunk while the green one grew. Another considerable shift of the domain boundaries is marked by a white arrow in the upper right part of the image. The boundary between the magenta domain, which is outlined by a magenta line, and the red domain shifted towards the magenta domain. These clear changes in the domain boundaries indicate a higher mobility of the molecules in this p.o.l. structure at a coverage of 0.95 ML than in the more densely packed 1.0 ML p.o.l. structure discussed in Fig. 5.16.

shape of domains

The peculiar domain shapes that were observed at a coverage of 1.0 ML in the previous experiment seen in Fig. 5.16 are not yet present in this 0.95 ML structure in Fig. 5.20 (a). This means that the irregular shapes observed before appear mostly during the deposition of the last 0.05 ML.

nucleation sites determine orientation

Another aspect these DF-LEEM images can help to elucidate is whether the orientation of the steps indeed influences the orientation of the islands. The two islands belonging to the red domain both nucleated at similarly oriented steps. The cyan colored domain consists of at least three islands that nucleated independently in an area with similarly oriented steps. These observations show that the orientation of the domain is determined by the orientation of the step edge the islands nucleated at.

deposition in DF-LEEM mode

The deposition of CuPc was continued after the previously discussed DF-LEEM images were taken. The growth was observed in DF-LEEM mode so that two domains appear bright, as can be seen in Fig. 5.21. The different time intervals between the images were chosen to demonstrate best the changes in the domain boundaries. The blue domain has the bright and the red domain a slightly darker contrast. The other domains appear dark. The bright areas become darker during the deposition due to molecules in the second layer that scatter some electrons out of the direction of the diffracted beam. The intensity of the dark areas is constant.

change in boundaries during deposition

It can be seen in Fig. 5.21 (a) that the domains are shaped differently than in the DF-LEEM image in Fig. 5.20 even before the deposition is started. This demonstrates again that the boundaries also change when there is no further deposition. Some significant changes compared to Fig. 5.20 (a) are marked by red arrows. Some boundaries change very quickly after the deposition is started, as can be seen in Fig. 5.21 (a)-(d). The most pronounced changes happen at the boundary that was the last to form when closing the first layer which is between the red and the cyan domain. A total coverage of 1.0 ML was reached after 75 s. The boundaries change more slowly after that, as can be seen in the images Fig. 5.21 (e)-(h) which were recorded with much larger time intervals.

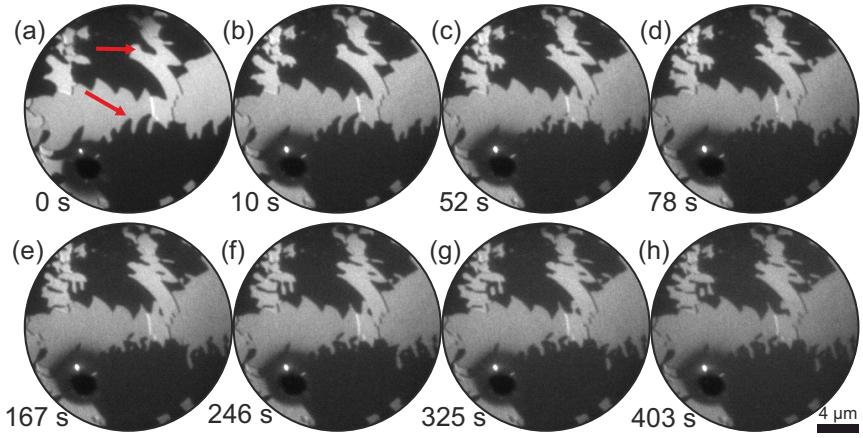

Fig. 5.21: Images taken in DF-LEEM mode during the deposition of CuPc on 0.95 ML of CuPc which are already present on the surface (U_{start} = 1.57 V). Strong changes of the boundaries can be observed during the completion of the first monolayer (top row). Changes happen more slowly afterwards (bottom row).

different transformation velocities

It can be seen in the images that some domain boundaries change very quickly while others are stable during the whole deposition process. A composite image of all six domains after the deposition can be seen in Fig. 5.20 (b) which can easily be compared to Fig. 5.20 (a). The orientations of all domains were determined to investigate if some domain boundaries change more rapidly than others due to their orientation to each other. The domains are colored using the same coding as Fig. 5.16. This means that the red and blue, the green and magenta, and the cyan and yellow domains are direct mirror domains of each other. The red, yellow, and magenta domains and the blue, cyan, and green domains can be transformed into each other by 120° rotation. An additional mirror operation is necessary to get from one group to the other. A rotation and a mirror operation are necessary to get from a blue domain to a magenta domain while only a rotation is necessary to go from a blue to a cyan domain. The symmetry operations necessary to get from one domain to another domain are summarized in the upper right part of Table 5.2. Whether the transformation at the boundaries takes place or not is indicated in the lower left part of Table 5.2. There are some indication that pure rotational transformations take place more easily, as can be seen by the strong changes in the blue-green boundary and the red-magenta boundary. The cyan-red boundary is a counter example to this. Although the strong changes at this boundary might be due to the fact that it was the last area on the sample that was covered by the crystalline CuPc layer before the deposition was stopped which might have lead to a slightly lower CuPc density there. It was already discussed that such a lower density would have lead to stronger changes of the domain boundaries. The red-green and the magenta-blue boundaries do not change much during the deposition.

	red	blue	yellow	cyan	magenta	green
red	x	m	r	r+m	r	r+m
blue	no	x	r+m	r	r+m	r
yellow	-	-	x	m	r	r+m
cyan	yes	no?	-	x	r+m	r
magenta	yes!	no	-	-	x	m
green	no	yes!	-	-	-	x

Table 5.2: Table of the transformation behavior between the different domains. The upper right part of the table gives the necessary symmetry operations to transform one domain into another domain. The letter "r" stand for a transformation consisting of a rotation and "m" for a mirror operation. The lower left part gives the changes of the boundaries observed during the deposition experiment shown in Fig. 5.21.

These are boundaries involving a rotation and a mirror operation. But the one blue-cyan boundary does not exhibit any strong changes, although it is very short and might not be representative for this boundary type. It seems that a reorientation is easier when only rotations are necessary. This was also observed in the data shown in Fig. 5.18. These observations give some indications for the aspects discussed although no strict conclusion can be drawn due to the low number of boundaries in these two experiments. Another explanation for the different changes in the domain boundaries could be the orientation of the CuPc molecules within the differently oriented unit cells. This hypothesis was checked, but it was found that it cannot be used to explain the observations.

destructive interference

Another interesting aspect to investigate is how the disordered phase behaves during the growth of the crystalline islands. The integrated LEEM intensity at $U_{start} = 2.00\,\mathrm{V}$ during the deposition of CuPc on a Ag(111) surface that is kept at 400 K is shown in Fig. 5.22 (a). The intensity decreases when the deposition is started and reaches a minimum at 0.5 ML. Then it increases again. This minimum in intensity can be explained by the destructive interference between electrons that are reflected at the Ag(111) surface and those reflected by the CuPc molecules. The difference in path length stems from the adsorption height of the molecules above the surface. This leads to maximal destructive interference when the surface is half covered with CuPc molecules. No significant change of the slope can be observed when the crystalline islands nucleate which can be explained by a similar reflectivity of the ordered and the disordered phases at the used start voltage. The slope changes when 0.95 ML are deposited since the whole surface is then covered by a crystalline layer. The crystal structure only becomes denser during the deposition of the last 0.05 ML which leads to a weak change in LEEM intensity. This shows that the density of CuPc can be monitored by measuring the image intensity of the Ag(111) surface.

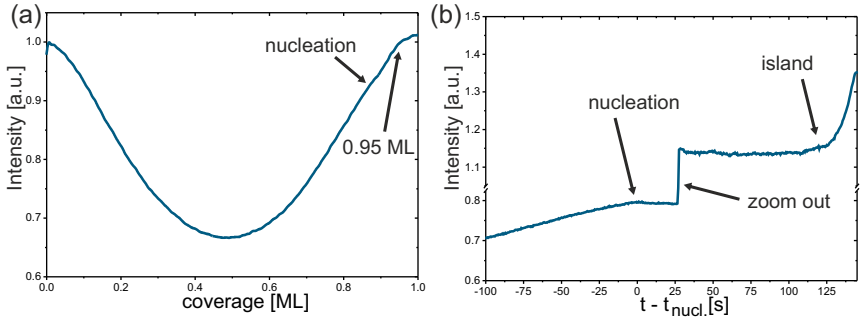

Fig. 5.22: (a) Intensity of the LEEM image during the deposition of 1.0 ML CuPc at $U_{start} = 2.0\,\mathrm{V}$. (b): Intensity of the area not covered by CuPc islands during the nucleation of those islands plotted against the time relative to the time of the first nucleation ($U_{start} = 1.55\,\mathrm{V}$). The data is taken from the experiment shown in Fig. 5.19. The intensity increases until the nucleation of the first island occurs. It stays constant until a crystalline island grows in the area where the intensity was measured. The strong increase in intensity is due to a zooming out at 25 s.

density in CuPc gas

The density of CuPc molecules before the nucleation and during the growth of the crystalline islands gives information about the growth process. To investigate this, the LEEM intensity at $U_{\mathrm{start}} = 1.55\,\mathrm{V}$ of the silver surface that is not covered by a CuPc island is shown in Fig. 5.22 (b). This start voltage was chosen since it allows a better contrast between the crystalline islands and the dilute phase while still exhibiting a similar trend as the one shown in Fig. 5.22 (a). It can be observed that the intensity increases until the first islands nucleate. The intensity then remains constant while the islands grow. An increase in intensity can only be observed when the area the intensity of which is measured is finally covered by a CuPc island. This constant intensity indicates that the density in the disordered gas phase of CuPc stays constant during the growth of the CuPc islands. The constant density during the nucleation as well as the fact that there is no increased intensity before the nucleation of the first islands indicates that the growth conditions are very close to the thermodynamic equilibrium and are not limited by a slow diffusion of the CuPc molecules. Another indication for this is that the growth of the CuPc islands stops as soon as the deposition is stopped.

6 Growth of heteromolecular layers consisting of PTCDA and CuPc

In the last two chapters, the growth of homomolecular films of the molecules PTCDA and CuPc were analyzed. The growth of heteromolecular structures consisting of these two molecules is discussed in this chapter.
Similar heteromolecular structures were already investigated by several different groups [CHC+08, BWBM03, ESBG+13, SYI03, DGLC+09, GMES+13, SSB+14, SLW+14, SWnSR14, KSSK14, GSP+15] and quite some information is already available about the geometric structure of such heteromolecular systems. Heteromolecular phases of the molecules PTCDA and CuPc were already investigated on Ag(111) [SSB+14, SLW+14] and Cu(111) [BWBM03]. On both substrates, they form long range ordered layers. Three different mixed phases were found on Ag(111), four on Cu(111) [SM14]. The stoichiometry in the unit cell of the layers depends on the deposited amount of the two molecules on the surface. By changing the deposited amount of molecules, it was possible to choose the heteromolecular phase that grew. previous studies
The influence of the strong molecule-substrate interaction on Cu(001) is investigated in section 6.1. The phases that grow there depend strongly on kinetic effects. The weaker interaction between Ag(111) and the molecules allows the study of thermodynamic properties as well as kinetic effects (section 6.2). content

6.1 Laterally mixed structures of PTCDA and CuPc on Cu(001)

The growth of laterally mixed structures of the molecules PTCDA and CuPc on Cu(001) is discussed in this section.
Although studies exist on the growth of heteromolecular structures of these two molecule on other surfaces, which were summarized at the beginning of this chapter, no laterally mixed heteromolecular phases have yet been published on Cu(001). previous studies
The formation of heteromolecular structures on Cu(001) is discussed in this section. content
The deposition of CuPc on a surface that is already covered by a submonolayer of PTCDA is discussed in section 6.1.1. It is found that this leads to a coexistence of the two homomolecular phases in separate domains. Annealing the sample does not induce a mixing of the two molecular types. The deposition order has to be reversed to achieve mixing and the results are discussed in section 6.1.2. Two heteromolecular phases are discovered. It is found that it is possible to dictate the heteromolecu-

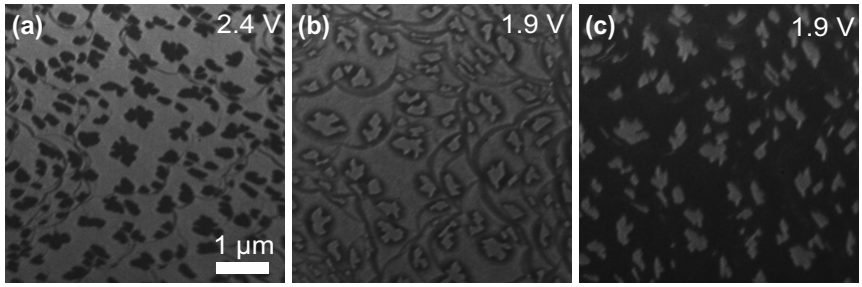

Fig. 6.1: LEEM images of the deposition of CuPc on a submonolayer film of PTCDA. (a) Dark PTCDA islands on the Cu(001) surface before the deposition is started. (b) PTCDA islands appear bright due to a change in start voltage from 2.4 V to 1.9 V. The halos around the islands are due to lensing effects. (c) The contrast on the terraces not covered by PTCDA islands gets darker until it is completely filled with CuPc molecules. A coexistence of both homomolecular phases is present on the surface.

lar phase by changing the initial coverage of CuPc. Additionally, the weak attractive interaction between the molecules is determined by analyzing STM images. The analysis of the island size distribution reveals that the nucleation theory, which can be applied to the system of PTCDA on a bare Cu(001) surface, is no longer valid in the case of heteromolecular growth.

6.1.1 Deposition of CuPc on submonolayer films of PTCDA

This section deals with the deposition of CuPc on a submonolayer of PTCDA on Cu(001).

deposition process

A submonolayer of PTCDA was deposited on a clean Cu(001) surface at 380 K until 20% of the substrate was covered. This can be seen in Fig. 6.1 (a). The PTCDA islands can be identified as the dark contrast while the fine dark lines are step edges of the copper substrate. Then CuPc was deposited on this submonolayer film of PTCDA at a substrate temperature of 400 K. After the deposition of 0.45 ML of CuPc, an image was taken which can be seen in Fig. 6.1 (b). To improve the visibility of the changes in contrast on the areas that are not covered by PTCDA islands, the start voltage had to be changed from 2.4 V to 1.9 V, which lead to an inversion of the contrast making the PTCDA islands now appear bright. Dark halos are visible around the PTCDA islands which are not present without CuPc on the surface. These finding suggest that the halos are due to a different density of CuPc around the island edges. But STM measurements discussed in chapter 6.1.2 show that this is not the case. These halos are rather due to lensing effects and are thus an artifact of the measurement technique. The area on the sample, where the images in Fig. 6.1 (b) and (c) were measured, differs from Fig. 6.1 (a) because LEED measurements were performed on the area of Fig. 6.1 (a) which can lead to beam damage in this area.

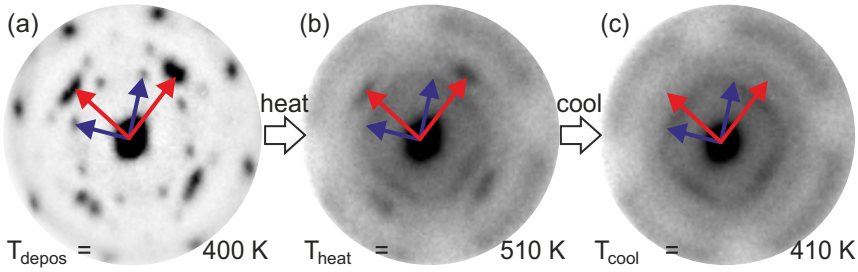

Fig. 6.2: LEED images of the annealing process of the sample from Fig. 6.1. (a) After the deposition of CuPc on a submonolayer of PTCDA, homomolecular phases of both molecules coexist on the surface. The red and blue arrows mark the unit cell vectors of the homomolecular PTCDA and CuPc phases, respectively. (b) The LEED spots become more blurry after increasing the temperature to 510 K. (c) After a maximum temperature of 520 K is reached, which makes the crystallinity even worse, the sample is cooled down to 410 K. The spots do not get their sharpness back. This experiment shows that mixing of the two molecules cannot be achieved by heating the sample.

The position on the sample was changed to make sure that beam induced effects did not play a role for the rest of the measurement. This is why the PTCDA islands in Fig. 6.1 (a) and (b) are not the same.

coexistence of homomolecular phases

The PTCDA islands do not change during the whole deposition process. They keep their shape and their crystal structure. Between the PTCDA islands, diffusing CuPc molecules are present and once a density equivalent to a crystalline homomolecular CuPc phase is reached, a homomolecular crystalline CuPc structure forms. The deposition of CuPc was stopped when the intensity in the area not covered by PTCDA islands no longer decreased since then the monolayer structure of CuPc is reached. LEED was performed to determined the crystal structure on the surface. It shows a superposition of the LEED pattern of the homomolecular PTCDA and the homomolecular ϵ phase of CuPc (Fig. 6.2 (a)). The red and blue arrows mark the basis vectors of the unit cells of PTCDA and CuPc, respectively. This proves that a coexistence of both homomolecular phases is present on the surface and shows that no mixing of the molecules is achieved when CuPc is deposited on a submonolayer of PTCDA at 400 K.

no thermal activation

Annealing to different temperatures was carried out to induce mixing of the two molecular species. The first annealing was done up to 520 K and can be seen in Fig. 6.2. Upon annealing, the LEED spots lose their sharpness (Fig. 6.2 (b)) but the PTCDA islands do not disappear which was verified by LEEM. Fig. 6.2 (b) was taken 10 K before the maximal annealing temperature was reached. The LEED image at the maximal temperature of 520 K matches the one shown in Fig. 6.2 (c). After cooling the sample back down (Fig. 6.2 (c)), the LEED spots do not get their initial sharp-

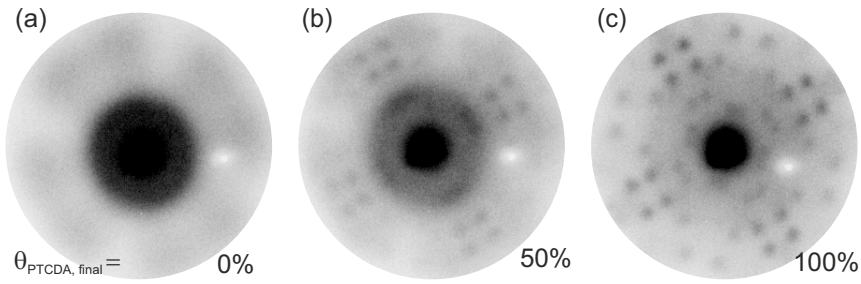

Fig. 6.3: LEED images taken during the deposition of PTCDA on a submonolayer of CuPc. (a) LEED pattern of the initial CuPc coverage of 0.5 ML. (b) Once the deposition is started, new LEED spots appear (c) which become more intense with increasing PTCDA coverage.

ness back. The crystallinity of the PTCDA and CuPc islands is strongly decreased by annealing to 520 K and no heteromolecular structure was created. Annealing to 740 K was then attempted since the PTCDA islands dissolve at this temperature. This leads to a complete destruction of any order in the film, and no islands existed anymore, even after cooling down the sample to room temperature. The heating of the sample only leads to the destruction of the molecules and, possibly, desorption from the surface, as could be observed in the homomolecular CuPc films on Cu(001) [vB14].

no mixing achieved

It seems that PTCDA islands, once they are formed, are bound so strongly to each other and to the substrate that CuPc cannot break the islands apart. This strong cohesion within one island is due to the high binding energy between the PTCDA molecules which is discussed in 4.1.1. Another reason why the PTCDA islands are not broken apart is the strong interaction of PTCDA with the underlying Cu(001) substrate. Some groups even suggested that at least one oxygen atom is removed from each end of the molecule [SA94, ATNIK08]. This stops the PTCDA molecules from leaving their adsorption site. A mixing of the molecules can be observed on the Ag(111) substrate at this deposition order which is discussed in section 6.2.2, where the interaction strength between the molecules and the substrate is weaker. To circumvent this problem and to achieve mixing, a reversal of the deposition sequence could be beneficial and is discussed in the next chapter.

6.1.2 Deposition of PTCDA on submonolayer films of CuPc

In this section, the deposition order of the two molecules is reversed. This means that PTCDA is deposited on a Cu(001) surface that is already covered by a submonolayer film of CuPc.

sample preparation

First, a submonolayer film of CuPc is deposited on a Cu(001) surface at 460 K. The coverage of CuPc was determined by looking at the LEED pattern, as was explained in section 5.1. The deposition of PTCDA is started immediately afterwards since the

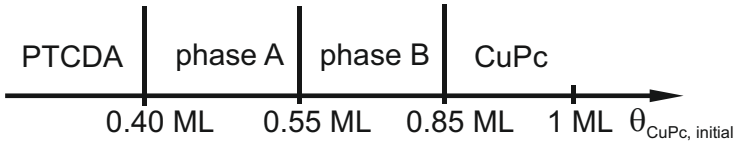

Fig. 6.4: Overview showing which structure the molecular islands have that grow when PTCDA is deposited on different coverages of CuPc. At low coverages, PTCDA islands grow and the CuPc molecules form a disordered dilute phase around them. Between 0.4 ML and 0.55 ML, the first heteromolecular phase, phase A, and, between 0.55 ML and 0.8 ML, islands of a second heteromolecular phase, phase B, grow. At higher CuPc coverages, CuPc already forms a crystalline phase and no mixing of the molecules can be observed.

CuPc molecules deteriorate after several hours on the 460 K hot surface. The initial coverage of CuPc was varied in these experiments and its effect on the growth of PTCDA is investigated. The deposition rate of PTCDA was of the same order as in the experiments performed in 4.1.

structure formation

LEED images, which can be seen in Fig. 6.3, were taken during the deposition of PTCDA on a Cu(001) surface covered by 0.50 ML of CuPc. Fig. 6.3 (a) shows the LEED pattern of the initial coverage of CuPc. After the deposition of PTCDA is started, LEED spots appear that do not belong to either the homomolecular phases of CuPc or PTCDA. The spots get more intense with increasing PTCDA coverage (Fig. 6.3 (b) and (c)) and the intensity of the diffuse CuPc signal from Fig. 6.3 (a) decreases. This decrease of the diffuse signal of CuPc indicates that the CuPc molecules no longer diffuse on the surface. The deposition was stopped after the diffuse signal around the (00)-spot started to increase again. This increase in the diffuse signal is likely due to molecules in the second layer.

influence of temperature

The structure, which belongs to the observed LEED pattern, is stable upon cooling down to room temperatures afterwards. At room temperature, this structure is stable for days. But if the sample is kept at 460 K, the crystallinity of the sample becomes worse quickly which can be seen by the disappearance of the LEED spots after just two hours. The best temperature for the formation of crystalline phases is around 460 K. At temperatures 50 K lower or higher, no growth of ordered structures could be observed. Therefore, all experiments discussed in this section were performed at 460 K.

6.1.2.1 Influence of CuPc coverage on growth

influence of θ_{CuPc} on occurrence of phases

The influence of the initial CuPc coverage on the growth is discussed in this section. Different crystalline structures are formed depending on the initial CuPc coverages when PTCDA is deposited on a submonolayer film of CuPc on Cu(001). At CuPc coverages below 0.40 ML, PTCDA islands grow while the CuPc molecules form a disordered dilute phase around them. Between 0.40 ML and 0.55 ML, a first hetero-

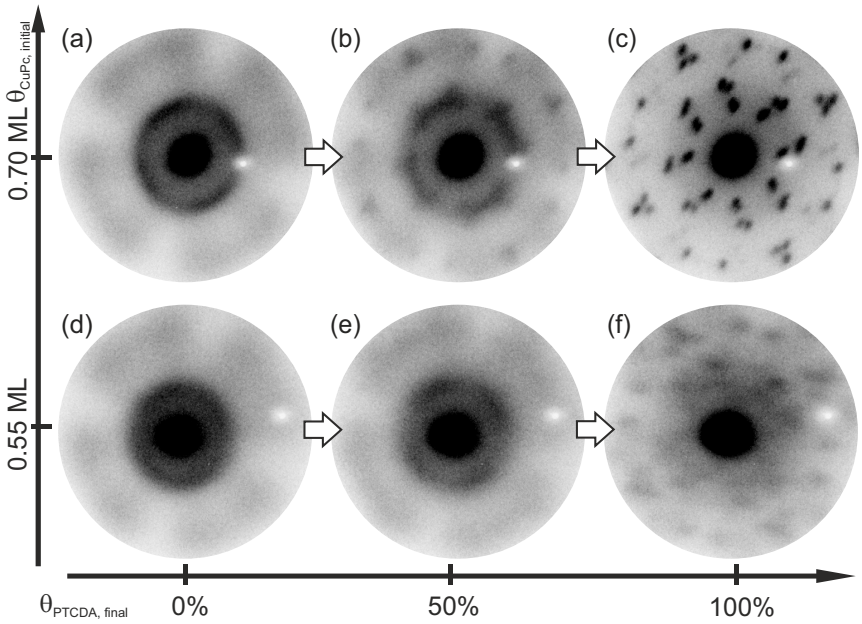

Fig. 6.5: LEED images taken during the deposition of PTCDA on a submonolayer of CuPc at two different initial coverages of CuPc. The quality of the structures changes significantly with a change in the initial CuPc density.

molecular structure, phase A, and, above 0.55 ML, a second heteromolecular phase, phase B, grows. CuPc forms a homomolecular crystalline structure and no mixing of the molecules is observed at CuPc coverages above 0.85 ML. A schematic overview of the coverages and phases is given in Fig. 6.4.

influence of θ_{CuPc} on crystallinity

The initial coverage of CuPc, $\theta_{\mathrm{CuPc,\,initial}}$, is not only crucial for the type of phase that forms, but also for the quality of its structure. In Fig. 6.5, LEED images of two deposition experiments are shown. The bottom and top row correspond to deposition experiments of PTCDA on an initial coverage of CuPc of 0.55 ML and 0.70 ML, respectively. The deposited amount of PTCDA increases from left to right. Both image sequences start with the LEED pattern of the initial CuPc coverages. Fig. 6.5 (b) and (e) depict the LEED pattern when 50 % of the final amount of PTCDA is deposited. Signatures of phase B are visible in both cases, but much weaker and more diffuse in the experiment with a lower CuPc coverage (Fig. 6.5 (b)). Fig. 6.5 (c) and (f) on the right show the LEED pattern of the final structures. Although the phase that appears is the same, the crystallinity of the structures differs strongly. The spots are well defined and sharp in Fig. 6.5 (c) at initial CuPc coverages of 0.70 ML, whereas the spots are very diffuse in Fig. 6.5 (f) in the experiment with a lower CuPc coverage. The same is true for phase A where the sharpness of the spots is the highest at an initial CuPc coverage of 0.4 ML and the crystallinity decreases when the initial

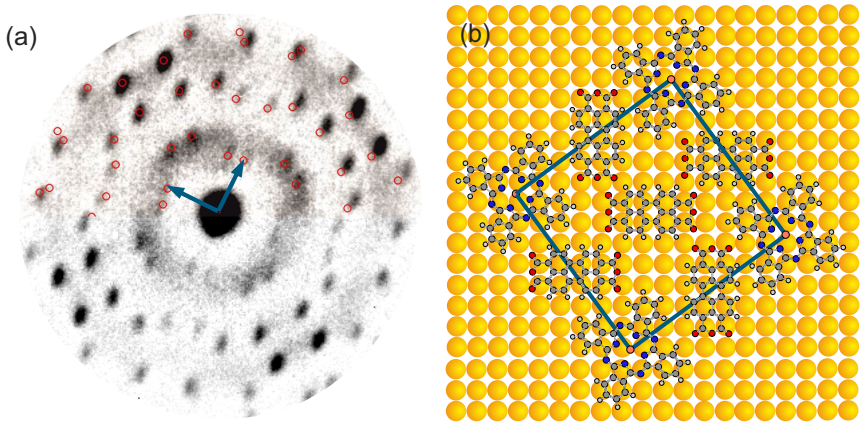

Fig. 6.6: Structure of the heteromolecular phase A. (a) Measured LEED pattern together with the simulated pattern of the determined unit cell vectors. (b) Proposed structure model with the arrangement of three PTCDA and one CuPc molecule in the unit cell.

CuPc coverage is further away from this value. Both of these observations show that, when the coverage of CuPc on the surface is slightly above the density of CuPc in the heteromolecular structure (discussed in section 6.1.2.2), the crystallinity is better and the crystallinity decreases when the CuPc coverage deviates from this value either to higher or lower values. This leads to a higher crystallinity for phase A at 0.40 ML and for phase B at 0.70 ML since these are coverages slightly above the density of CuPc in their respective unit cells. It seems to be very important that the intermolecular distance of the CuPc molecules is already similar to that in the heteromolecular unit cell before PTCDA is deposited since it allows the phase formation with minimal reorganization and diffusion of molecules.

6.1.2.2 Ordered heteromolecular phases

The two heteromolecular structures that were mentioned before are discussed in detail in this section.

Phase A

Phase A appears when PTCDA is deposited on Cu(001) surfaces which are covered with CuPc coverages between 0.40 ML and 0.55 ML. The ratio of the deposited amount of the two molecules is not important since this structure grows as soon as PTCDA is deposited on the surface and does not change with the amount of PTCDA deposited.

unit cell

An analysis of the LEED pattern results in an incommensurate superstructure matrix of

$$M_{\text{phase A, Cu(001)}} = \begin{pmatrix} 7.6 & 5.7 \\ -5.7 & 7.6 \end{pmatrix}.$$

Fig. 6.6 (a) shows the reciprocal unit cell vectors in the LEED pattern and the simulated spots corresponding to this superstructure matrix (red circles). The unit cell is quadratic with a vector length of 24.1 Å. The size of the unit cell of 579.5 Å^2 suggests that three or four molecules are present in the unit cell [SHS$^+$15].

structure model

The three heteromolecular phases that exist on Ag(111) all deviate very little from the packing density of the homomolecular films. If the same is true for Cu(001), the number of molecules of each type can be determined. If it is assumed that one PTCDA molecule occupies 132 Å^2 (half the unit cell size of the homomolecular layer) and CuPc 189 Å^2 (unit cell size of the ϵ phase), three PTCDA molecules and one CuPc molecule would fit best in this unit cell since they add up to an area of 585 Å^2. The heteromolecular structure would then be only 1% denser than the homomolecular films. Taking the area of two PTCDA and two CuPc molecules, a unit cell size of 643 Å^2 is obtained corresponding to a compression of 10%. This makes this constellation unlikely. A unit cell with the next best fit is one with two CuPc molecules and one PTCDA molecule. This gives a 12% more loosely packed structure than the homomolecular layers. Of the three discussed structures, the one with one CuPc molecule and three PTCDA molecules is the most likely. Another indication that the unit cell contains only one CuPc molecule is the density of CuPc on the surface when this phase grows. At coverages of 0.40 ML and 0.55 ML, the CuPc densities are 0.21 CuPc/nm^2 and 0.29 CuPc/nm^2, respectively. In a unit cell with one CuPc, the density is 0.17 CuPc/nm^2 compared to a unit cell with two CuPc molecules which corresponds to a density of 0.35 CuPc/nm^2. The density range of CuPc, when phase A grows, on the surface corresponds more closely to a unit cell with only one CuPc. A structure model with three PTCDA and one CuPc molecule is shown in Fig. 6.6 (b). The PTCDA molecules are oriented in the same way with respect to the substrate as in their commensurate homomolecular structure. The CuPc molecules are tilted by 21.8° with respect to the [110] direction since this is also their orientation in the densely packed homomolecular ϵ phase. This is of course a very tentative suggestion of the position and orientation of the molecules in the unit cell. STM investigations would be helpful for confirming or disproving this model.

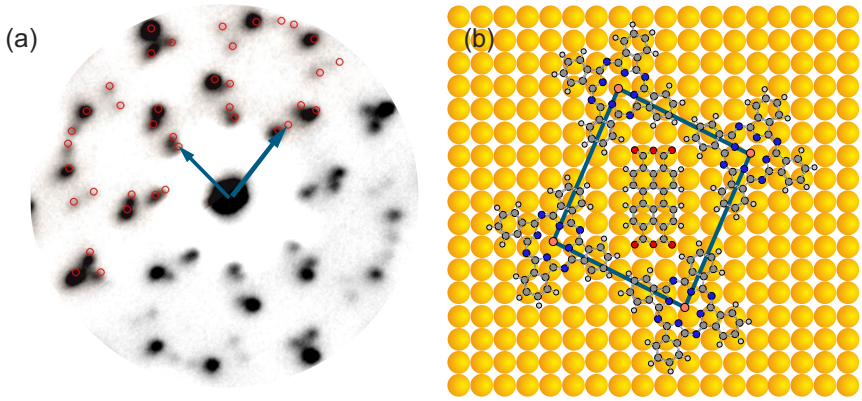

Fig. 6.7: Structure of heteromolecular phase B. (a) Measured LEED pattern together with the simulated pattern of the determined unit cell vectors. (b) Suggested structure model containing one PTCDA and one CuPc molecule in the unit cell.

Phase B

Phase B grows when PTCDA is deposited on a submonolayer of CuPc on Cu(001) in a CuPc coverage regime between 0.55 ML and 0.85 ML. As it was already the case for phase B, the deposited amount of PTCDA does not influence which phase grows.
The unit cell was determined by LEED and is given by the superstructure matrix unit cell

$$M_{\text{phase B, Cu(001)}} = \begin{pmatrix} 5.8 & 2.9 \\ -2.9 & 6.8 \end{pmatrix}.$$

The LEED pattern together with the simulated LEED spots (red circles) corresponding to the described superstructure are shown in Fig. 6.7 (a). This incommensurate structure is represented by the unit cell vectors $b_1 = 16.6\,\text{Å}$ and $b_2 = 18.9\,\text{Å}$ with an angle of 86.75° between them. With an area of $313.6\,\text{Å}^2$, the unit cell is much smaller than that of phase A.
At coverages of 0.55 ML and 0.85 ML, the CuPc densities are $0.29\,\text{CuPc/nm}^2$ and $0.42\,\text{CuPc/nm}^2$, respectively. In a unit cell with one CuPc molecule, the density would be $0.32\,\text{CuPc/nm}^2$. This lies right in the density range in which phase B grows. As it was discussed before, structures of the highest quality are achieved at a CuPc coverage of 0.70 ML. This corresponds to a CuPc density of $0.37\,\text{CuPc/nm}^2$, which is slightly above the CuPc density in the unit cell of the heteromolecular structure if it contains only one CuPc molecule, just as it is the case for phase A. The structures seem to prefer to grow with a slight density surplus of CuPc on the surface. This analysis suggests that there is only one CuPc molecule in the unit cell. Only one PTCDA molecule fits into the remaining space. This means that the proposed structure model structure model

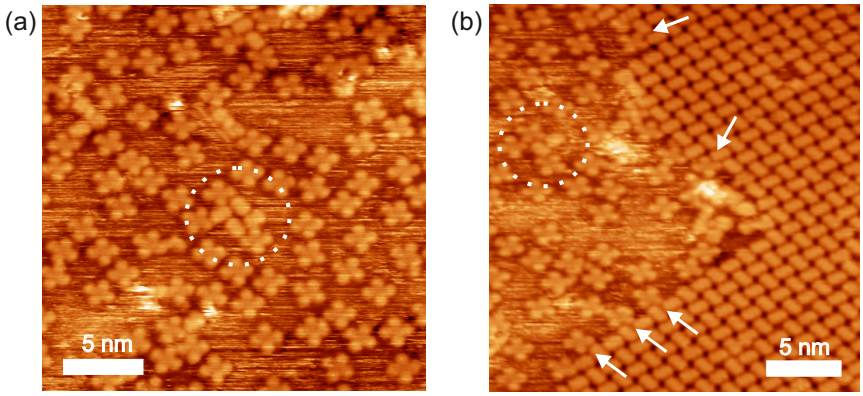

Fig. 6.8: STM images of the filled states. (a) PTCDA island consisting of four molecules surrounded by CuPc marked by the dashed circle. There is no preferred adsorption of CuPc at the PTCDA island edge. (b) Border between a PTCDA island and the dilute CuPc phase. The PTCDA island is not decorated by CuPc molecules showing that there is no dominant attractive intermolecular interaction between CuPc and PTCDA on Cu(001). A preferred adsorption geometry (marked by the white arrows and the white dashed circle) indicates a weak attraction between them. (Bias = 50 mV, Set Point = 0.033 nA)

for phase B contains one molecule of each kind as illustrated in Fig. 6.7 (b). The structure model proposed here is similar to the heteromolecular "One-to-one" structure of PTCDA and CuPc on Ag(111) [SHS+15]. The PTCDA molecule is oriented along the [110]-direction and the wings of CuPc are tilted by 21.8° with respect to the [110]-direction, very similar to the homomolecular phases and phase A.

6.1.2.3 Interaction between PTCDA and CuPc

STM images of the heteromolecular PTCDA-CuPc system are analyzed in this section and conclusions about the interaction between the molecules are drawn.

no strong attraction

It was already discussed that PTCDA islands grow when the deposition of PTCDA is started with a CuPc coverage below 0.40 ML. STM measurements were performed to investigate the interaction of PTCDA with CuPc at low coverages. PTCDA was deposited on a Cu(001) at 460 K surface that was already covered with 0.25 ML of CuPc. The sample was cooled down to room temperature afterwards and the measurements were performed at this temperature. Two of these measurements can be seen in Fig. 6.8. Fig. 6.8 (a) shows a small PTCDA island consisting of four molecules with CuPc molecules spread randomly across the surface. The CuPc molecules do not exhibit a preferred adsorption at the PTCDA island edge indicating that there is no preferred attachment at the PTCDA island. The edge of a large PTCDA island was

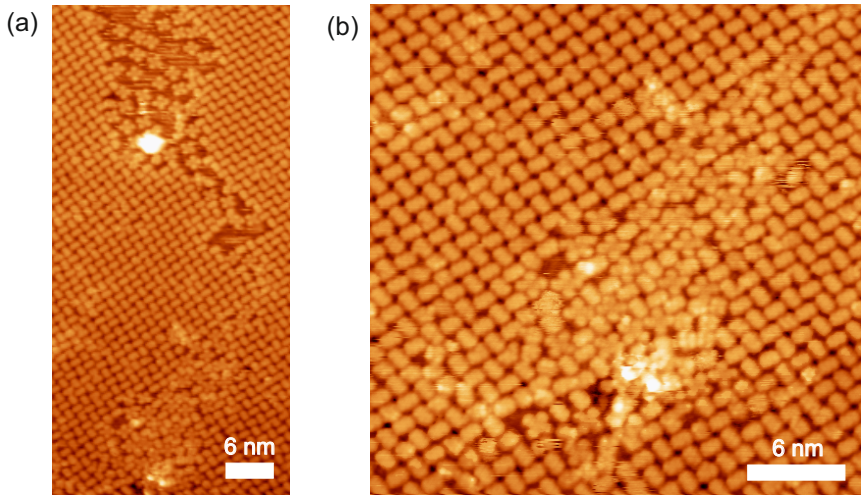

Fig. 6.9: (a) CuPc molecules get squished together when two PTCDA islands grow together and they cannot diffuse away (lower part). In the upper part, the CuPc molecules can diffuse away and thus the density of CuPc is not increased. (b) zoomed image of the molecules that are squished together. No long range order can be seen. (Bias = 50 mV, Set Point = 0.033 nA)

imaged (Fig. 6.8 (b)) to examine if the CuPc molecules preferably attach there. But also here no increased density of CuPc molecules close to the islands is found. This shows that there is no strong intermolecular attraction between the two molecular species on this surface.

weak attractive interaction

Looking at the CuPc molecules that are attached to the PTCDA island shows that most of them connect to the PTCDA border in a specific orientation. The molecules marked by white arrows in Fig. 6.8 (b) and the two CuPc molecules attached to the small PTCDA cluster of two molecules inside the dashed circle all exhibit the same orientation. The PTCDA molecules at the edge of the island are nestled between the wings of the CuPc molecule. This shows that there must be some attractive interaction between the molecules since the CuPc molecules apparently do not attach in a random way to the PTCDA island edge. These measurements indicate a weak intermolecular attraction. The mobility of CuPc at room temperature is so low that the molecules do not diffuse to the edges of the PTCDA island even if is energetically preferable due to a weak attraction.

influence of ρ_{CuPc}

The CuPc molecules are homogeneously distributed on those areas, which are not covered by PTCDA islands, as can be seen in Fig. 6.8. The PTCDA islands grow with continued deposition and hence reduce the area available for the CuPc molecules. This increases the local density of CuPc molecules, ρ_{CuPc}, in these areas as can be observed by a changing CuPc signal in LEED during the deposition of PTCDA. The signal stemming from the dilute phase of CuPc changes from a pattern belonging to

a low CuPc density to one of a higher CuPc density. Another proof that the growing PTCDA islands increase the density of the CuPc molecules on the empty terraces is given in Fig. 6.9 (a). It depicts an area where two PTCDA islands grew together. In the upper part, the CuPc molecules could diffuse away leading to a CuPc density that is identical to the one shown in Fig. 6.8 (b). In the lower part, the CuPc molecules were trapped by the two PTCDA islands leading to an increased density of CuPc. An enlarged image of this area can be seen in Fig. 6.9 (b). The CuPc molecules are packed closely together with the PTCDA molecules in a random distribution, not in an ordered heteromolecular structure even though it is expected that a heteromolecular structure forms at a CuPc density equivalent to 0.40 ML. One possible reason why this did not happen is that the amount of CuPc molecules was very small and the area was too restricted to allow a reorganization into an ordered heteromolecular phase. An additional LEEM experiment showed the formation of heteromolecular phases between PTCDA islands when PTCDA was deposited on 0.20 ML of CuPc. Phase A islands started to grow when a little more than half of the surface was covered by PTCDA islands. This coincides nicely with the necessary initial coverage of 0.40 ML for the formation of phase A and proves that not the absolute coverage of CuPc but the *local* density of CuPc in the dilute disordered phase is crucial for the formation of the heteromolecular phases. This should also lead to a coexistence of heteromolecular phase A and B when PTCDA is deposited on an initial CuPc coverage slightly below 0.55 ML, but such a coexistence was never observed. The order in both phases is bad in the range of 0.55 ML, which leads to very diffuse LEED patters. This might obscure diffuse spots of phase B even though this phase is present at a low fraction on the surface making it impossible to identify. These additional findings prove that the local density of CuPc is the decisive parameter for the formation of the different phases, not the initial coverage (compare Fig. 6.4).

6.1.2.4 Limits of nucleation theory

So far only the reciprocal space data of the measurements performed with the LEEM has been discussed. Now, the focus is on the real space data obtained with the LEEM.

high nucleation density

The islands that grow, when PTCDA is deposited on a submonolayer of CuPc on Cu(001), are very small and the noise of the images taken during the growth is too high to draw any conclusions about the growth from them. Here, the images taken after the deposition of PTCDA was stopped are analyzed. The size distribution of the islands is analyzed to determine the critical island size for this system if possible. The nucleation density of the islands of the heteromolecular systems is very high for the deposition temperatures used to form these structures. Many islands nucleate on each terrace very close to each other.

ISD of PTCDA in CuPc

Fig. 6.10 (a) and (b) show LEEM images of the PTCDA islands that were grown at a CuPc coverage of 0.25 ML. The islands appear bright or dark depending on the focusing conditions. The focusing conditions also drastically change the perceived size of the islands [DTKT14]. To check whether this has an influence on the analysis, both,

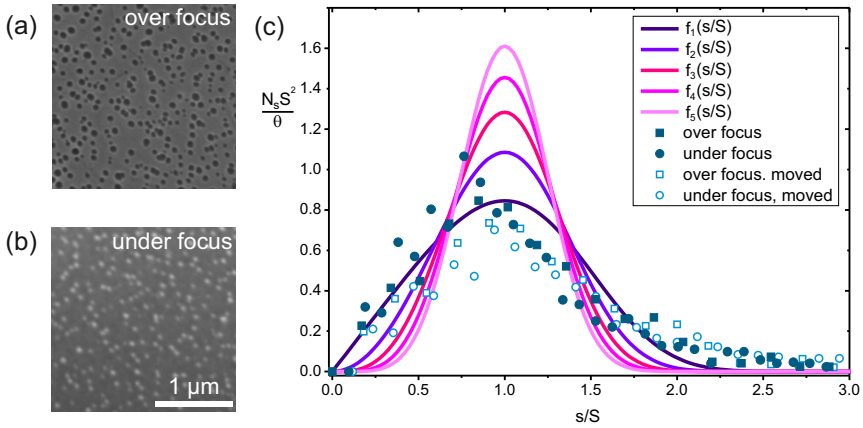

Fig. 6.10: (a) and (b) LEEM images of the PTCDA islands grown in a CuPc gas phase. Depending on the focusing conditions, the islands can appear dark (a) or bright (b). (c) The island size distribution was determined and can be seen as filled symbols. The unfilled symbols show data that was normalized by a different mean island size. This shifted the peak to 1. It can be seen that the shape of the data cannot be explained by the theoretical curves.

the over focus and the under focus images, are analyzed. The results can be seen in Fig. 6.10 (c) in the graph as filled dark blue symbols. It can be observed that both sets of data points show the same trend indicating that a change in focusing conditions has no effect on the shape of the island size distribution. It is obvious that the data is not described well by the theoretical curves. The peak of the data is shifted to the left compared to the theoretical predictions. For the normalization, the mean island size has to be determined (comp. (3.7)). It is calculated by averaging over all island sizes and therefore the additional shoulder at bigger islands sizes leads to an increase of the mean island size shifting the peak. In order to correct for this, the mean island size is determined from the peak position of the non-normalized data. This new mean island size for the normalization results in the open light blue symbols in Fig. 6.10 (c). The peak is now centered at 1. This transformation solves the problem of the shifted peak, but it does not change the overall shape of the curve and the shoulder at higher islands sizes is even more visible. It is not likely that this overestimation of island sizes for bigger islands is due to measurement errors since the uncertainties for island sizes due to different focusing conditions decreases for increasing island sizes. The amplitude, which matched the theoretical curve for $i = 1$ before the normalization, is now too low. It is clear that this data cannot be described by the standard model that was successfully applied to the growth of PTCDA on the bare Cu(001) surface in section 4.1.1. The reasons why the theory might fail to predict the shape of the measured curves are discussed at the end of this section. Ignoring the discrepancies

between the theoretical shape of the curves and the data, a critical island size of $i = 1$ could be suggested. This would indicate that the critical island size of PTCDA, which was already $i = 2$ at 390 K, decreased back to $i = 1$ at 460 K in the presence of CuPc.

comparison with PTCDA on bare Cu(001)

When the nucleation behavior of the PTCDA islands in the dilute CuPc phase is compared to the nucleation behavior of PTCDA on a clean Cu(001) surface (see section 4.1), strong differences can be observed. The nucleation density is two orders of magnitude higher when CuPc is present. At temperatures around 460 K on a clean Cu(001) surface, only one PTCDA island nucleates on each terrace. In the presence of CuPc, many PTCDA islands nucleate on each terrace. Equation

$$N \propto \left(\frac{F}{D}\right)^{\chi} \tag{6.1}$$

gives the island density's dependence on the deposition flux F, the diffusion constant D, and the exponent $\chi = \frac{i}{i+2}$. An increase in the island density could be due to a decrease in the diffusion length or critical nucleus size since the deposition rate was constant in the experiment where PTCDA was deposited on the clean Cu(001) sample and on the CuPc gas on Cu(001). The critical island size of PTCDA on a clean Cu(001) substrate at 460 K should be ≥ 2 since the critical nucleus size was already 2 at 390 K. If the critical nucleus size for PTCDA grown in a submonolayer of CuPc at 460 K were $i = 1$, as it is suggested by the ISD, a higher island density for PTCDA islands grown in the presence of CuPc would be the result. This is one contributing factor to the increased nucleation density. However, the main factor can be assumed to be the presence of CuPc on the surface. The CuPc molecules hinder the diffusion of PTCDA molecules on the surface and, thus, decrease their diffusion coefficient leading to a higher nucleation density. The CuPc molecules do not only represent objects that hinder the diffusion of PTCDA but might also influence the interaction of PTCDA with Cu(001). CuPc decreases the work function of the copper surface [vB14]. This should lead to a different interaction of PTCDA with the substrate. Both effects caused by the presence of CuPc on the surface could explain the increase in the nucleation density by at least two orders of magnitude.

ISD of phase A

The analysis of the ISD was repeated for islands of phase A that grew in a CuPc gas. The focusing conditions again influenced the perceived size of the small islands strongly. The analysis was further complicated by a worse image contrast (see Fig. 6.11 (a) and (b)) which made the differentiation between individual islands more difficult. To check if these two effects influence the analysis, the island size distribution was determined for two different focusing conditions (over focus and under focus) and another method for the determination of the island sizes was employed. A watershed algorithm [Sag08] as well as the standard thresholding method were used to determine the island sizes. The result of the analysis can be seen in Fig. 6.11 (c). It shows that the analysis seems to be robust against all these different factors since all evaluations show the same trend. When comparing the data to the theoretical curves, it can clearly be seen that they differ from them. The same differences are observed as in the case of PTCDA islands grown in a disordered CuPc phase. This shows that the standard nucleation theory cannot be applied to this system, either. Even if the

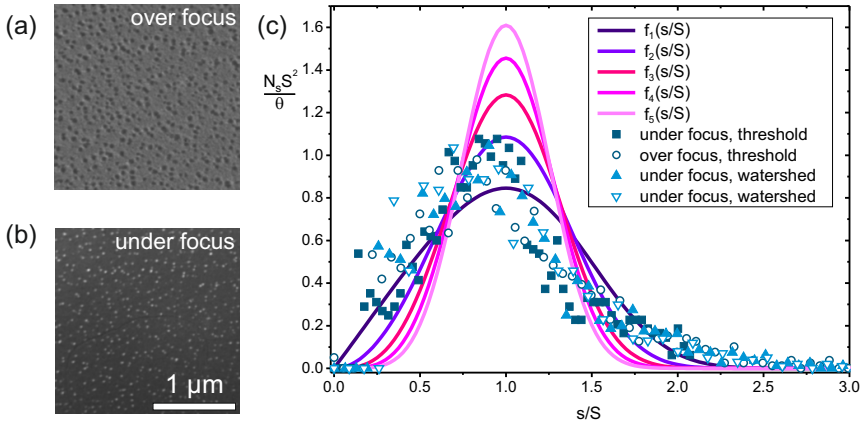

Fig. 6.11: (a) + (b) LEEM images of islands of phase A grown by depositing PTCDA on a submonolayer of CuPc measured in over focus (a) and under focus (b). (c) Island size distribution of phase A islands for different focusing conditions and different analysis methods. As it was already the case for PTCDA grown in a CuPc gas, the data cannot be described by the theoretical curves.

theory was applicable to the system, it is not clear what a critical island size of $i = 1$ would mean. Would it refer to the number of molecules or the number of unit cells that have to form?

limits of used nucleation theory

An important question to answer is: "Why does the theory fail to predict the form of the island size distribution?" There are several possible reasons for this. Firstly, equation (3.3) is extracted from rate equations for the limit of low adatom coverages. This is clearly violated here since there are already many CuPc molecules on the surface. Secondly, this theory was developed for atoms nucleating on a surface and not for molecules where steric effects might play an important role. The fact that the molecules have to arrange themselves in a certain direction does not seem to hinder the application of the theory to the PTCDA/Cu(001) system. This changes when CuPc is on the surface. The CuPc molecules seem to hinder the arrangement of PTCDA molecules so that it becomes more difficult for the PTCDA islands to grow at a rate which they would otherwise. Thirdly, the scaling function was developed for one-component systems, which is no longer valid for the growth of heteromolecular phase A. When only one type of atom/molecule is deposited on a surface, only entities that are the same interact with each other and form islands. There are two different types of molecules present in the case of heteromolecular systems. CuPc not only influences the movement of the PTCDA molecules and the growth of PTCDA islands but it is also incorporated into the growing heteromolecular islands. This is a fundamental difference compared to the homomolecular system. Fourthly, this incorporation of CuPc molecules also leads to a change in the local density of the

disordered CuPc phase which influences the growth of the islands further. The rate equations as well as the model for the shape of the ISD would have to be modified to describe this system quantitatively.

6.2 Laterally mixed structures of PTCDA and CuPc on Ag(111)

This chapter discussed the growth and the thermodynamics of laterally mixed layers of PTCDA and CuPc on Ag(111) up to coverages of one monolayer.
Three different heteromolecular phases were found for the PTCDA-CuPc system on Ag(111) [SHS+15, SLW+14, SSB+14]. The "Mixed Brick Wall" (MBW) phase has two PTCDA and one CuPc molecule in its unit cell which has a size of 449 Å^2. The "Mixed One-to-One" (M1^{2}1) phase has one molecule of each kind in its unit cell of a size of 333 Å^2. The "Mixed Zig-Zag" (MZZ) phase contains one PTCDA and two CuPc molecules and has a unit cell size of 520 Å^2. The superstructure matrices are

previous studies

$$M_{\mathrm{MBW}} = \begin{pmatrix} 8 & -2 \\ 3 & 7 \end{pmatrix} \quad M_{\mathrm{M1^21}} = \begin{pmatrix} 6 & -1 \\ 4 & 7 \end{pmatrix} \quad M_{\mathrm{MZZ}} = \begin{pmatrix} 8 & 0 \\ 2 & 9 \end{pmatrix}.$$

Incommensurate structures of the M1^{2}1 and the MZZ phases also exist. These structures, which deviate from their commensurate counterpart only slightly, are treated as identical phases for the majority of this section. It is only differentiated between the different structures within one phase when these small difference become relevant.
This chapter is divided into three parts. The first part discusses the growth process when PTCDA is deposited on a submonolayer film of CuPc. The influence of the CuPc concentration on the formation of different phases is analyzed. It is also found that the substrate temperature determines which phase grows when PTCDA is deposited on equal amounts of CuPc. The deposition order is reversed in the second part of this chapter where CuPc is deposited on a submonolayer film of PTCDA. A transformation of the PTCDA islands into MBW then M1^{2}1 and then MZZ islands is found with increasing amount of deposited CuPc. It is discovered that the CuPc density in the disordered phase is the determining factor for the nucleation of the MBW phase and that it depends on the temperature. The thermodynamic properties, which exist independently of the deposition order, are discussed in the third part. The key finding is a phase diagram of the different structures that exist at different coverages of PTCDA and CuPc at 300 K. It contains the results of 22 growth experiments performed in the full submonolayer coverage regime. The reversibility of temperature driven phase transformations is discussed next. The chapter concludes with a detailed analysis of the influence of the temperature on the critical CuPc density for the nucleation of the MBW phase and the nucleation energy of the MBW phase is determined.

content

6.2.1 Deposition of PTCDA on submonolayer films of CuPc

This section deals with the growth behavior when PTCDA is deposited on a submonolayer film of CuPc on Ag(111).
The growth was investigated at different coverages and temperatures. The deposition rate of the employed CuPc evaporator changed from deposition experiment to deposition experiment even though the same heating current was used. This made

sample preparation

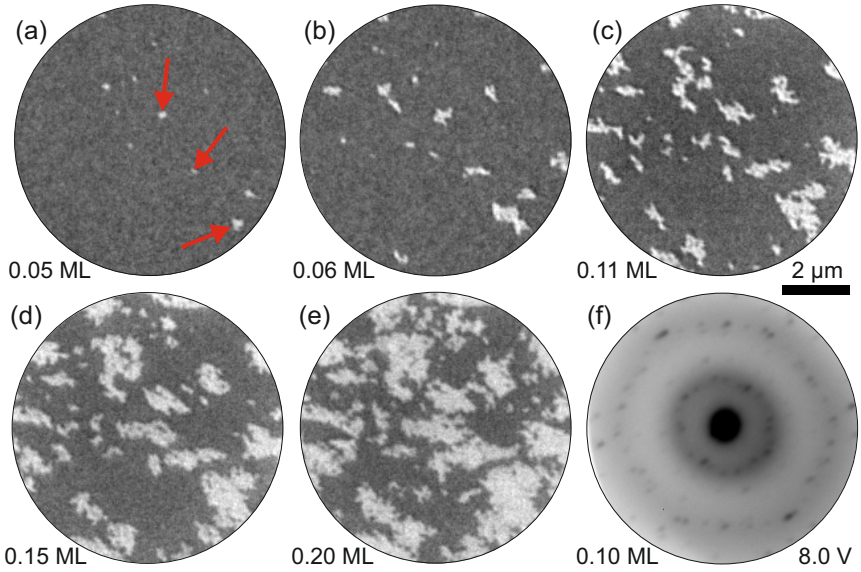

Fig. 6.12: Images of the growth of the M1^{2}1 phase when PTCDA is deposited on a 0.61 ML film of CuPc on Ag(111) at 300 K. (a)-(e): LEEM images taken at $U_{\text{start}} = 2.0$ V. The M1^{2}1 islands (red arrows) can be identified as the bright areas. (f): LEED pattern of the sample after 0.10 ML of PTCDA are deposited. A superposition of the LEED pattern of the crystalline M1^{2}1 phase and the diffuse signal of the CuPc gas can be observed.

it impossible to just use the deposition time as a measure of the CuPc coverage. It was rather determined by comparing the LEED patterns of the different coverages. Additionally, the intensity of the (00)-spot was monitored during the deposition which also depends on the coverage as is was already discussed in section 5.2.2. Even though these two methods were applied, there is still an uncertainty on the determined CuPc coverages of 10%. The PTCDA evaporator delivered constant deposition rates over several month and thus the uncertainty on the PTCDA coverages is much smaller with about 3%. There is also a relatively high uncertainty on the measured temperature for reasons discussed in section 2.3. The latter does not play an important role in the analyses shown in this chapter since most experiments were performed without heating at room temperature and the influence of the temperature on the growth is only analyzed qualitatively (except in section 6.2.3.3).

overview over growth

The growth process of the heteromolecular M1^{2}1 phase, when PTCDA is deposited on a 0.61 ML film of CuPc on Ag(111) at 300 K, is discussed first to give an overview over the whole deposition process. Fig. 6.12 shows five LEEM images measured during the growth of the M1^{2}1 phase. The intensity of the homogeneous gas-like phase increases after the PTCDA deposition is started (discussed in section 6.2.1.1). The first heteromolecular islands nucleate when a little less than 0.05 ML of PTCDA are

deposited, as can be seen in Fig. 6.12 (a). The M1^{2}1 islands (red arrows) can be seen as the bright contrast in the images. They grow in size but new islands also nucleate (Fig. 6.12 (b)-(e)). The dark shadows at the upper edges of the islands in Fig. 6.12 (c) are artifacts due to a slight tilt of the electron beam and do not stem from changes of the islands on the surface. The deposition is stopped when 0.31 ML of PTCDA were deposited (not shown here). The islands continue to grow for several seconds, which shows that the system is not in thermodynamic equilibrium during and right after the deposition, but that it is reached after a couple of minutes. This fact is important for the thermodynamic analyses in section 6.2.3. Fig. 6.12 (f) shows the LEED pattern after 0.10 ML of PTCDA are deposited.[1] The signature of the heteromolecular M1^{2}1 structure can be seen as well as the diffuse ring-like signal of CuPc on Ag(111). This indicates that there are still CuPc (and some PTCDA) molecules in a disordered gas-like phase between the M1^{2}1 islands. The intensity of the diffuse CuPc signal decreases during the deposition of PTCDA since an increasing surface area is covered by the M1^{2}1 phase. The islands exhibit the same LEEM contrast during the whole deposition experiment and it can be concluded that the first islands are already of the M1^{2}1 phase although the coverage was too low there to measure a clear LEED pattern. It can also be observed that the shape of the islands is strongly influenced by the substrate morphology. Details about this are given in section 6.2.1.3.

solution of PTCDA molecules in CuPc gas

A deposited amount of 0.20 ML of PTCDA should result in a coverage of 0.57 ML of the M1^{2}1 phase. The visible islands however cover only 43% of the surface which is much less than expected. This shows that a large number of the PTCDA molecules are not incorporated into the heteromolecular island. Only 0.15 ML of PTCDA are necessary to create a coverage of 0.43 ML of M1^{2}1 islands. These missing 0.05 ML of PTCDA can be explained partly by the amount of PTCDA molecules that is dissolved in the CuPc gas. In the CuPc gas phase, 0.05 ML of PTCDA are dissolved before the nucleation of the first islands starts. The total amount of PTCDA molecules that are dissolved in the CuPc gas becomes lower with increasing surface area covered by M1^{2}1 islands since it decreases the area of the disordered gas-like phase which can hold 5% of PTCDA. This leads to a reduced amount of 0.03 ML of PTCDA dissolved in the disordered phase at a coverage of PTCDA of 0.20 ML since 43% of the surface area is covered by islands. This gives a PTCDA coverage that is built into M1^{2}1 islands of 0.17 ML which would create an expected coverage of 0.49 ML of the M1^{2}1 phase. This value agrees much better with the experimental value of 0.43 ML. The discrepancies between the values can be explained by the uncertainties on the coverage of the M1^{2}1 phase of 0.03 ML and the PTCDA coverage of 3%.

6.2.1.1 Low coverage regime of PTCDA

Different crystalline structures appear depending on the coverages of PTCDA and CuPc. The growth, when coverages below 0.10 ML of PTCDA are deposited on top of a submonolayer film of CuPc on Ag(111), are discussed in this section.

[1] The LEED pattern was deskewed manually.

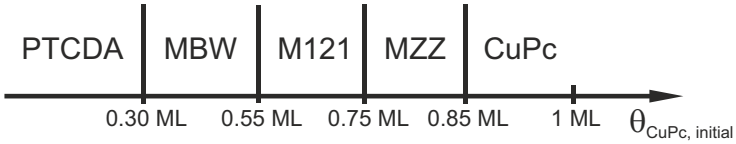

Fig. 6.13: Overview over the crystal structures of the first islands that are present when PTCDA is deposited on samples with different initial submonolayer coverages of CuPc on Ag(111) at 300 K.

influence of θ_{CuPc}

The influence of the CuPc coverage at low PTCDA coverages is discussed first. All experiments discussed in this paragraph were performed at room temperature. Fig. 6.13 gives an overview over the phase of the crystalline islands that exist when PTCDA is deposited on CuPc on Ag(111). It should be stressed again that this overview only give the phase of the *first* islands that are present when PTCDA is deposited. PTCDA islands start to grow when the CuPc coverage is below 0.30 ML while the CuPc molecules form a disordered gas-like phase around them. No crystalline heteromolecular structures are found at these coverages. The first heteromolecular structure, the MBW phase, requires an initial coverage of CuPc of at least 0.30 ML and maximal 0.60 ML. The unit cell of this phase contains two PTCDA and one CuPc molecule. The M1^{2}1 phase grows when the CuPc coverage is between 0.06 ML and 0.70 ML. One PTCDA and one CuPc molecule are in its unit cell. This shows that the relative area of CuPc in the unit cell increases with increasing initial CuPc coverage. This trend is continued for the MZZ phase containing one PTCDA molecule and two CuPc molecules per unit cell which grows at coverages of CuPc between 0.70 ML and 0.85 ML. Crystalline CuPc islands are already present before the deposition of PTCDA is started at CuPc coverages above 0.85 ML. The relative areas of CuPc in the unit cells of the MBW, the M1^{2}1, and the MZZ phase are 45%, 62%, and 76%, respectively. These values all lie within the range of the initial area covered by CuPc molecules when the different phases grow. This is in agreement with the finding on the growth of heteromolecular structures of these two molecules on Cu(001), as was discussed in chapter 6.1.2. Note that these observations are only true for low PTCDA coverages. How the structures change, when the deposition of PTCDA is continued, is discussed in the next section.

nucleation

It was already mentioned that a coverage of PTCDA of 0.05 ML is needed for the nucleation of the M1^{2}1 phase. The LEEM intensity of an area on the substrate, which is not covered by crystalline islands, before and after the nucleation of the first islands is shown in Fig. 6.14. It can be seen that the intensity increases strongly after the deposition is started at $t = 0$ s. This steep, linear increase stops as soon as islands start to nucleate and a slow decrease follows. This gradual drop in intensity after the nucleation of the M1^{2}1 phase can be explained by a change in the density of the molecules in the disordered phase consisting of CuPc and PTCDA molecules. The density of the CuPc molecules in the disordered phase changes when M1^{2}1 islands nucleate since these island have a higher CuPc density than the disordered phase present

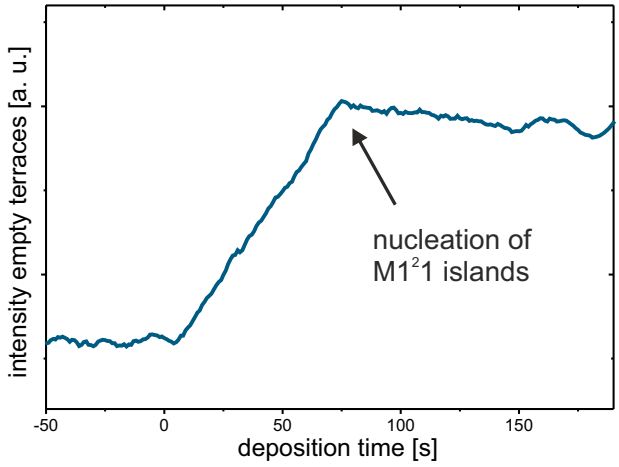

Fig. 6.14: Plot of the LEEM intensity of an area that is not covered by M1^{2}1 islands before and after the nucleation of the first M1^{2}1 island versus the deposition time. The intensity increases after the deposition of PTCDA is started and it starts to drop very slowly after the nucleation of the islands has occurred.

in this experiment of 0.61 ML. This decreases the CuPc density in the disordered phase with increasing coverage of the M1^{2}1 islands which decreases the intensity (compare section 5.2.2.3). Another explanation is that the density of the PTCDA molecules on the surface that was responsible for the increase in intensity before the nucleation is slowly reduced since they are slowly incorporated into the islands which occurs slightly delayed since the system is not in thermodynamic equilibrium. Both effects, the change in CuPc and PTCDA intensity, contribute to the change in intensity.

$\theta_{\mathrm{PTCDA,\,min}}$ necessary for nucleation

The observation that a certain amount of PTCDA is necessary for the nucleation is also true for the other heteromolecular phases. This amount varies between 0.02 ML and 0.15 ML depending on the initial CuPc coverage. This necessary amount of PTCDA for the nucleation of the first islands is much lower at CuPc coverages below 0.3 ML, a regime where PTCDA islands are found. Only a coverages < 0.01 ML are necessary there. Possible reasons for this behavior are discussed in section 6.2.3.1.

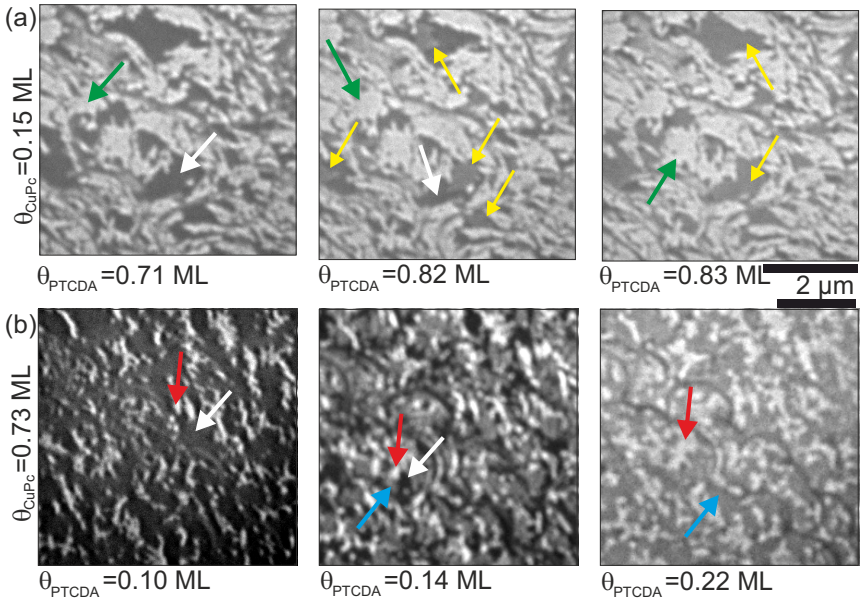

Fig. 6.15: LEEM images taken during the deposition of PTCDA on two samples with different CuPc coverages at 300 K until the whole surface is covered by crystalline islands: (a) θ_{CuPc} =0.15 ML: PTCDA islands (bright contrast, green arrows) grow until a PTCDA coverages of 0.72 ML is reached and the MBW phase (medium contrast, marked by yellow arrows) starts to grow as well. The gas-like phase (white arrows) has the darkest contrast. The PTCDA and the MBW islands grow until the whole surface is covered by them. (U_{start} = 1.6 V) (b) θ_{CuPc} =0.73 ML: M1^{2}1 islands (bright contrast, red arrows) grow until a PTCDA coverage of 0.13 ML is reached and MZZ islands (medium contrast, blue arrows) start to grow as well. (U_{start} = 0.5 V, 0.4 V, 2 V)

6.2.1.2 High coverage regime of PTCDA

The effect of a continued deposition of PTCDA on a submonolayer film of CuPc, up to the point when the whole surface is covered by crystalline islands, is discussed in this section.

high coverage regime

The deposition of PTCDA on CuPc-covered surfaces (initial coverages 0.15 ML and 0.73 ML) is shown in Fig. 6.15 (a) and (b). The deposition is continued until the complete surface is covered by a crystalline layer.

transition: PTCDA → PTCDA+MBW

PTCDA islands grow in the case of θ_{CuPc} = 0.15 ML and a LEEM image of the surface after 0.71 ML of PTCDA are deposited can be seen in the first image of Fig. 6.15 (a). Most of the surface is covered by PTCDA islands (bright contrast, green arrows). The CuPc molecules as well as a small amount of PTCDA molecules form a disordered

gas-like phase (dark contrast, white arrows) in the darker areas between the PTCDA islands. MBW islands (yellow arrows) start to nucleate at PTCDA coverages above 0.72 ML which can be seen in the second image in Fig. 6.15 (a). The MBW islands have a darker contrast than the PTCDA islands but are brighter than the disordered phase. These islands, as well as the PTCDA islands, continue to grow until the whole surface is covered by these two crystalline structures (last image of Fig. 6.15 (a)) and the deposition of PTCDA is stopped.

transition: $M1^21 \rightarrow M1^21$+MZZ

A similar trend can be observed when PTCDA is deposited on a 0.73 ML film of CuPc. Here $M1^21$ and MZZ islands are formed. The $M1^21$ phase (bright contrast, red arrows) starts to grow, as can be seen in the first image in Fig. 6.15 (b). MZZ islands (blue arrows) start to grow at a coverage of 0.13 ML and an image of both the $M1^21$ and the MZZ phase at a coverage of 0.14 ML can seen in the second image in Fig. 6.15 (b). The MZZ phase exhibits a darker contrast than the $M1^21$ phase but a brighter contrast than the disordered gas-like phase. Also here both crystalline phases continue to grow until the whole surface is covered by a crystalline layer, as can be seen in the last image in Fig. 6.15 (b).

CuPc richer phases with increasing θ_{PTCDA}

Both experiments shown in Fig. 6.15 demonstrate that CuPc-richer crystalline structures start to grow when the deposition of PTCDA is continued. The growth of PTCDA islands transforms into a growth of PTCDA and MBW islands at low CuPc coverages and instead of only growing the $M1^21$ phase, the MZZ phase also starts to grow at higher CuPc coverages. This counterintuitive trend of the growth of CuPc-richer structures with increasing PTCDA coverages is explained in section 6.2.3.1.

transition: MBW → PTCDA+MBW

A different type of transition occurs when PTCDA is deposited on a CuPc coverage of 0.40 ML, as is shown in Fig. 6.16 which is discussed in 6.2.1.3. Here, a growth of only the MBW phase turns into a situation where both the heteromolecular MBW and the homomolecular PTCDA phase grow. This type of transition is also explained in section 6.2.3.1.

3 phase region

Both experiments shown in Fig. 6.15 have one unusual aspect in common: a rather large coverage regime where two different crystalline phases and an additional disordered phase exist. Three coexisting phases appear in conventional phase diagrams only in one point, the eutectic point, and not in large areas. This coexistence of three different phases is not a kinetic effect since experiments, discussed in section 6.2.3.1, showed that the system is in thermodynamic equilibrium. The difference between the system analyzed here and conventional phase diagrams is discussed in section 6.2.3.1.

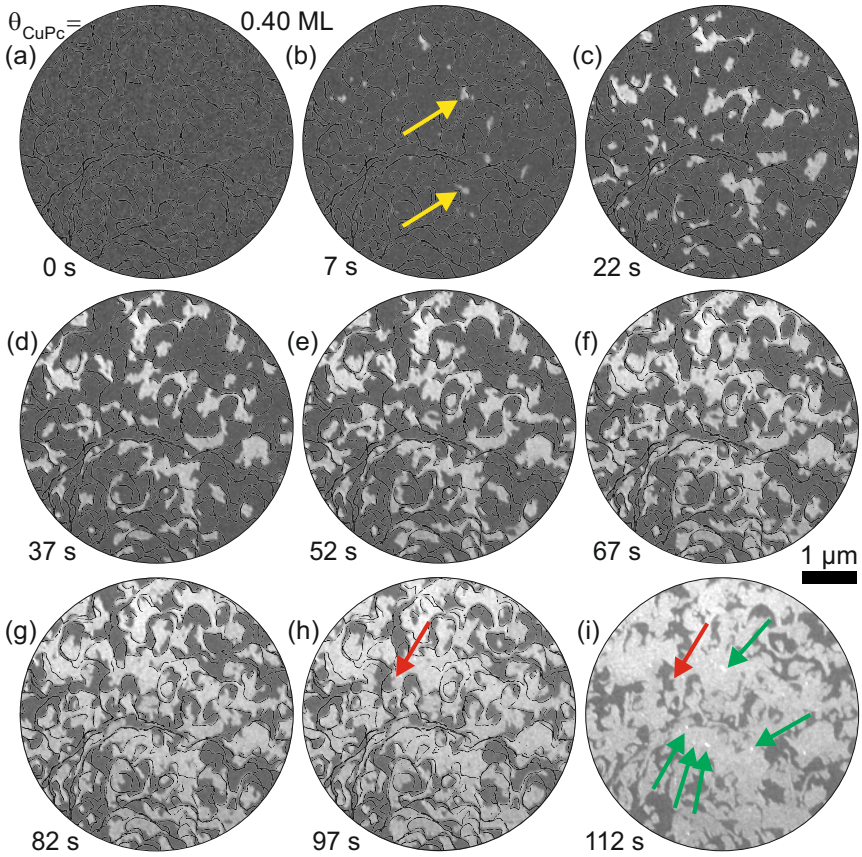

Fig. 6.16: LEEM images taken at different times during the growth of the MBW phase when PTCDA is deposited on a 0.40 ML film of CuPc. The MBW islands can be identified as the bright contrast in images (b)-(h).
(i) PTCDA islands appear which exhibit a brighter contrast than the MBW islands. Some of them are marked by green arrows. ($U_{\mathrm{start}} = 2\,\mathrm{V}$)

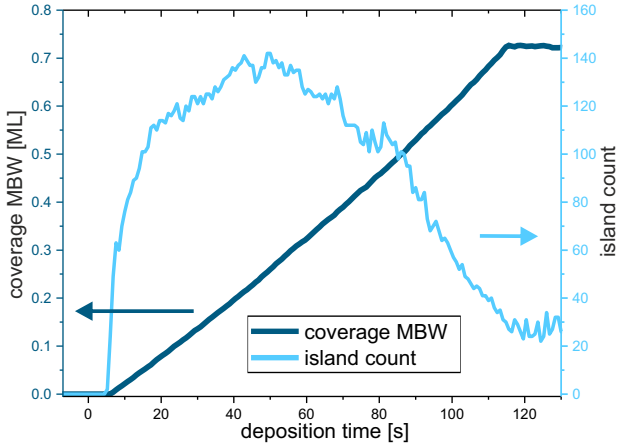

Fig. 6.17: The MBW coverage (dark blue curve) and the number of MBW islands (light blue curve) are plotted versus the deposition time of PTCDA. LEEM images of this deposition process are shown in Fig. 6.16.

6.2.1.3 Analysis of growth dynamics of MBW phase

One deposition process, where PTCDA is deposited on a submonolayer film of CuPc of 0.40 ML on Ag(111) at 300 K, is analyzed in detail on the next few pages.

overview over growth process

Fig. 6.16 shows several LEEM images taken during the growth process of the MBW phase with the step edges of the Ag(111) substrate superimposed in black. The whole surface is initially covered by a disordered gas-like phase (Fig. 6.16 (a)). When the deposition of PTCDA is started, MBW islands do not nucleate immediately but only after a PTCDA coverage of 0.07 ML is deposited, as shown in Fig. 6.16 (b). The MBW islands can be identified by their bright contrast. Two of them are marked by yellow arrows. The existing islands grow and new islands nucleate during the continued deposition of PTCDA (Fig. 6.16 (c)-(i)). Homomolecular PTCDA islands start to grow after 110 s and the deposition is stopped (Fig. 6.16 (i)). These PTCDA islands appear as bright dots in the image and some are marked by green arrows. The shape of the MBW islands is strongly influenced by the morphology of the Ag(111) surface since the islands cannot grow across step edges.

coverage MBW

The coverage of the MBW phase is plotted versus the deposition time as the dark blue curve in Fig. 6.17. The coverage of the MBW phase increases linearly, after the first islands nucleate after 6 s, until the deposition is stopped after 115 s. This leads to a coverage of 0.71 ML for the MBW phase.

island count

The islands are counted during the deposition process and plotted versus the deposition time (light blue curve in Fig. 6.17). There is a steep increase in the number of islands after the nucleation of the first islands and then a relatively constant number of islands between the coverages of the MBW phase between 0.1 ML and 0.5 ML. This constant number of islands is predicted by kinetic nucleation theory in this coverage

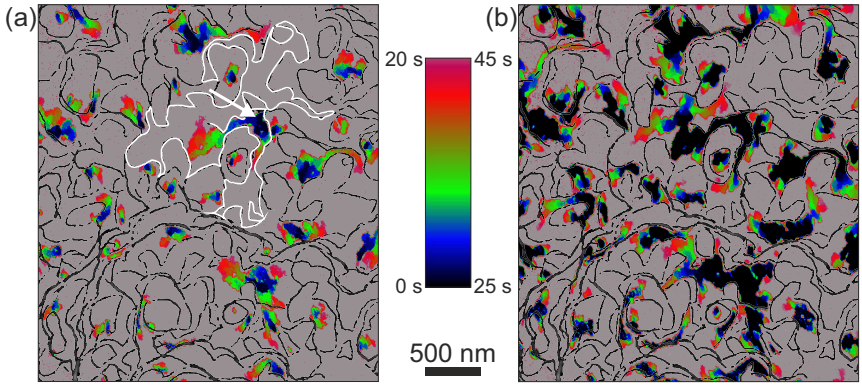

Fig. 6.18: The size of the MBW islands at different times during their growth. The step edges are superimposed as black lines. (a) The growth in the first 20 s after the nucleation and (b) between 25 s and 45 s after the nucleation of the first island.

regime, see chapter 3.1. Looking at the growth process in detail shows that a different phenomenon than the one discussed in chapter 3.1 leads to this constant number of islands. New islands continue to nucleate during the whole deposition process. This fact cannot be seen in the graph since islands also coalesce during this time which leads to a reduction of the number of islands and compensates for the nucleation of new islands. This leads to the almost constant number of islands in a certain coverage regime. The coalescence of islands becomes more pronounced at high coverages which leads to a smaller number of islands. This decrease in the number of islands at higher coverages agrees with the predictions by theory. It is found that the kinetic theory discussed in chapter 3.1 does not successfully describe the growth process even though the shape of the curve agrees well with the theoretical predictions. The reason for the ongoing nucleation of new islands is explained in the next paragraphs.

growth dynamics

The growth dynamics of the MBW phase is discussed in detail now. Fig. 6.18 depicts the growth dynamics of the islands at two different stages of the growth. The colors represent the size of the islands at different times according to the color coding defined in the middle of Fig. 6.18. The time is given in seconds after the nucleation of the first island. The step edges were determined by the threshold method (see section 2.5.3) and are superimposed as black lines. Several observations can be made in these images.

homo-nucleation

The islands do not nucleate at step edges but at random locations within the terrace. This homonucleation differs from the nucleation of the homomolecular phases of PTCDA and CuPc on Ag(111) (see chapters 5.2.2 and 4.2.1.1).

one island per terrace

Only one island nucleates on each terrace. This is valid even for very big terraces and for terraces that have narrow connections between different larger areas of them. One example of this is the island that is marked by the white arrow which grows on a large terrace the outer limits of which are indicated by the white lines. Molecules adsorbed

	ability of molecules to move across step edges			
observation	CuPc & PTCDA cannot	CuPc & PTCDA can	CuPc can & PTCDA cannot	CuPc cannot & PTCDA can
nucleation spread out	no	yes	yes	yes
growth in direction of largest areas of terrace	yes	no	yes	yes
MBW islands do not grow until whole terrace is covered	yes	no	no	yes
PTCDA islands nucleate in small areas surrounded by MBW	yes	yes	yes	yes
PTCDA does not nucleate otherwise	no	yes	no	yes

Table 6.1: Overview which scenarios fulfill which observations.

on the terrace have to diffuse as far as 2 µm assuming they cannot move across step edges in order to attach to the island. The distance is still 900 nm long if they can move across step edges.

step edge barrier

It can be seen that the islands do not grow across step edges. This shows that the step edges pose insurmountable barriers for the MBW islands at this temperature. Further experiments are necessary to check if this is still the case at higher temperatures since it might be that the energy barrier is just high making the growth across step edges only unlikely – not impossible – at this temperature. Such an energy barrier was for example observed for the growth of PTCDA islands on Ag(111), as was discussed in section 4.2.1.2.

additional observations

Several additional observations are given in this paragraph. Firstly, the nucleation of all islands does not occur at approximately the same time but is spread out over a large coverage regime. Secondly, the islands grow in the direction of the largest areas of their terrace that is not covered by islands. Thirdly, the MBW islands do not continue to grow until their whole terrace is covered by them. Fourthly, PTCDA islands start to grow in small areas that are completely surrounded by MBW islands but, fifthly, not in areas that are bordered by MBW islands and step edges. These observations are summarized in the left column of Table 6.1.

limited diffusion of molecules

It is checked in the next paragraphs if these observations can be explained by different abilities of the two molecular species to move across step edges. Four different scenarios, namely the assumption that neither, or both, or only one molecular species can

move across the step edges, are proposed. Two conclusions that are drawn in chapter 6.2.3.1 are used for the argumentation as well. The first is that a certain density of CuPc molecules is necessary for the growth of heteromolecular structures and the second is that the necessary density of PTCDA for the nucleation of heteromolecular phases varies with the density of CuPc.

growth direction

The growth direction of the islands depends on the available flux of the molecules to the growth front of the island. The density of CuPc in the MBW phase (45%) is higher than the initial density of CuPc on the surface (40%) before the deposition of PTCDA is started in this experiment. This leads to a gradient towards lower CuPc densities in the areas where a growth front of a heteromolecular MBW island is. The CuPc molecules move towards the growth front to compensate for this gradient in the CuPc density. This compensating flux depends on two thing. Firstly, the location of other islands on the surface influences the flux since the islands compete for the CuPc molecules. This leads to a increased flux, and thus growth speed, to the direction where no other growth fronts of islands are present. Secondly, the morphology of the sample could prohibit the diffusion of CuPc molecules to the growth front from certain directions. Step edges could pose as insurmountable barriers for the CuPc molecules leading to an increased flux, and thus growth speed, into the direction of the largest areas of the individual terrace that is not yet covered by islands. A gradient of the molecular density is also present for the PTCDA molecules since they attach to the growth front as well. Taking into account the fluxes of both molecules, the growth speed is higher towards the largest areas on the terrace that is not covered by islands if one or neither of the molecular species can move across step edges while it is higher into the direction without a growth front of another island on the surface if both molecules can cross the step edges.

neither can cross

The first scenario: Neither PTCDA nor CuPc molecules can cross step edges. A constant number of CuPc molecules and a constantly increasing number of PTCDA molecules should be on each terrace during the deposition of PTCDA. The necessary concentration of PTCDA for the nucleation of MBW islands should then be reached on all terraces at approximately the same time. This should lead to the nucleation of one heteromolecular island on all terraces at almost the same time. This is only possible since the nucleation of an island on a certain terrace does not change the molecular concentrations on the adjoining terraces because the molecules cannot move across step edges. The nucleation of all islands at approximately the same time is not observed in the experiment and this scenario can thus be rejected.

both can cross

A different growth behavior would be observed if both molecules could cross step edges unhindered (second scenario). The CuPc concentration is identical on all terraces before the PTCDA deposition is started. The concentration of the PTCDA molecules increases when the deposition is started. A soon as the necessary concentration of PTCDA for the nucleation of the MBW phase is reached, an island of the MBW phase nucleates. This leads to a slight drop in the density of the PTCDA molecules in the surrounding area since the nucleation of an island requires a certain supersaturation even if the supersaturation is very small and cannot be observed in LEEM, as is discussed later. This prevents the nucleation of additional islands in the regions close to

an existing growth front. A certain distance between nucleation centers is expected in this case, also (and in particular) across step edges. This is exactly what is observed in the experiment even if some counterexamples can be found (the nucleation of an island on the right of the island marked by the white arrow in Fig. 6.18 (a)). This decrease in the molecular densities, which prevents the nucleation of additional islands in the vicinity of growth fronts, would also lead to a large coverage regime, in which islands nucleate, as is observed in the experiment. This scenario would also lead to an increased growth speed in the direction of the areas on the surface without islands independent of whether or not step edges are located there. The island should grow in this direction until it reaches a step edge where the island's growth is stopped since islands do not grow across step edges at this temperature. The growth must also not slow down significantly before this happens. This partly disagrees with the observations. While the island often grow until the edge of the terrace is reached, their preferred growth direction is in the direction of the largest area of the terrace, not surface, that is not covered by islands. This scenario also demands that the islands should grow until the whole terrace is covered which is not observed in the experiment. An island in Fig. 6.16 (h)+(i) stops growing in one area marked by the red arrow before the deposition is stopped. Hence, this scenario can also be rejected.

CuPc can & PTCDA cannot cross

CuPc molecules can and PTCDA molecules cannot cross step edges in the third scenario. The CuPc concentration is the same on the whole surface in the beginning. The nucleation of the first islands leads to a slight drop in the PTCDA concentration only on the terrace where the island nucleated while the PTCDA concentration on the other islands should continue to increase. PTCDA molecules from the terrace and CuPc molecules from the whole surface move to the growth front of the nucleated island and the island grows. Here, the growth front should move more quickly into the direction of the largest areas on the terrace that are not covered by MBW islands since an increased PTCDA flux should come from there towards the growing island. This is observed in the experiment. The diffusion of the CuPc molecules from other terraces towards the growth front leads to a depletion of CuPc in the adjoining terraces which should stop the nucleation of additional islands there. This can explain the observation that the islands do not nucleate at approximately the same time on each terrace. New MBW islands can then only nucleate when there are no existing growth fronts of the MBW islands in the vicinity. Another conclusion that follows from this scenario is that the MBW islands should grow until the density of CuPc molecules is no longer high enough for the growth of the MBW phase. This occurs when there is no longer a flux of CuPc molecules from adjoining terraces and the CuPc molecules on the terrace are already build into the MBW structure. But this can only happen when an area is completely encased by MBW islands since these can be expected to represent a barrier for the diffusing CuPc molecules. Consequently, PTCDA islands should start growing, when the CuPc density drops below a certain value, as is discussed in section 6.2.3.1. The growth of PTCDA islands in small areas that are completely encased by MBW islands can indeed be observed (marked by the green arrows in Fig. 6.16 (i)). But no PTCDA islands start to grow in areas where the MBW islands stopped growing and that are not encased by MBW islands

(marked by the red arrow in Fig. 6.16 (h)+(i)). This disagrees with this proposed scenario, which has to be rejected also.

CuPc cannot & PTCDA can cross

Fourth scenario: CuPc molecules cannot and PTCDA molecules can cross step edges. The behavior up to the nucleation of the first island is the same as in the previous scenarios. Now, molecules that are being incorporated into the growth front of the MBW island can come from the terrace in the case of CuPc and from the entire surface in the case of PTCDA. This leads to a higher flux of CuPc from the direction of the largest areas of the terrace that are not covered by islands and, thus, a quicker growth in that direction which is in agreement with the experiment. It also explains the fact that only one island nucleates on each terrace since the density of CuPc on the terrace decreases after the nucleation, preventing the nucleation of more MBW islands. The MBW islands in this scenario continue growing until the density of CuPc becomes too low for their growth. Then, two different things can happen. The MBW island should stop growing since the PTCDA molecules can move away from the terrace to attach at a different growth front. This can be observed in the area marked by the red arrow in Fig. 6.16 (h)+(i). The other possibility is that the PTCDA molecules cannot move to a different terrace since they are completely encased by MBW islands. This should lead to the growth of PTCDA islands in this region. This is observed and can be seen in the areas marked by the green arrows in Fig. 6.16 (i).

limited diffusion of CuPc across step edges

This last scenario explains the observed growth behavior the best. These scenarios are of course oversimplified since it is assumed that the molecules can either cross the step edges or not. A scenario with different crossing probabilities for both molecules, higher for PTCDA and lower for CuPc would also explain the observations. Different probabilities for crossing a step edge in the upward or downward direction are not considered either. This analysis can nonetheless determine that the step edges pose a higher barrier for the CuPc molecules than for the PTCDA molecules. This agrees with the finding from chapter 4.2 where it was also found that PTCDA molecules can easily cross step edges of the Ag(111) surface at this temperature.

low supersaturation

The LEEM intensity on terraces with and without islands growing on them was measured to help verify this hypothesis for the growth behavior. But no significant difference in the intensity could be observed meaning that the density of the molecules in the disordered phase does not change very much since changes of both densities are observable at the used start voltage of 2 V. This proves that the supersaturation necessary for the growth of additional islands is low and that slight changes in the molecular densities influence the growth process strongly.

high mobility of molecules

This experiment also shows that the molecules have a very high mobility. The fact that only one MBW island grows on each terrace shows that the density of the diffusing molecules drops quickly enough in all areas of the surface preventing the nucleation of additional islands. The fact that the distance the molecules have to "feel" a nucleated island is up to 2 µm as demonstrated by the terrace the outlines of which are marked by the white line in Fig. 6.18 (a) requires a very high mobility of the molecules.

6.2.1.4 High mobility of heteromolecular clusters

This section analyzes the changes in island shape and island position during the deposition of PTCDA on a submonolayer film of CuPc on Ag(111). Conclusions about the mobility of clusters are drawn.

quick reorganization of islands

Fig. 6.19 (a) shows the growth of one island (bright contrast) between 16 s and 40 s after the deposition was started. The step edges of the silver substrate are superimposed in black. The small tail on the lower part of the island (marked by the red circle in Fig. 6.19 (a)) disappears after a couple of seconds, as can be seen in the second image. The island continues to grow and, in the fourth, image it grows again into the direction of the tail that had disappeared before. The growth of this single island shows that the islands can reorganize very quickly.

mobility of small clusters

The movement of two small clusters is tracked in Fig. 6.19 (b). They are marked with red circles. These two heteromolecular islands move during the deposition of PTCDA, as indicated by the black arrows. The larger island has a size of 650 nm^2 and moves 40 nm (upper circle) and the smaller island with a size of 380 nm^2 moves 60 nm (lower circle). This means that islands consisting of 450 and 250 molecules, respectively, move within 6 s across a distance that is comparable to their diameter or even bigger in the case of the smaller island.

mobility of large clusters

Further analysis shows that even larger clusters of a size of 3400 nm^2 consisting of more than 2000 molecules can move up to 110 nm in just 6 s, as can be seen in Fig. 6.19 (c). The cluster nucleates in the upper part of the terrace. It then moves towards the middle of the terrace where it stays and continues to grow. The island appears smeared out in the second and third image of this sequence. This is most likely due to the integration of the detector intensity during the acquisition time of 0.2 s and not due to different contrasts within the island at those times.

direction of movement

The direction of the movement of the two clusters in Fig. 6.19 (b) looks like it is towards the open surface while the movement of the cluster in Fig. 6.19 (c) seems to be directed towards the middle of the terrace. The analysis of the movement of another island (shown in Fig. 6.19 (d)) helps determining in which direction the islands move. This island moves away from the open area of the surface and towards the middle of the terrace it nucleated on. The growth direction seems to be a compromise between the two directions. This suggests that the movement of the islands is influenced by the gradient of both molecules. The flux of PTCDA molecules directs the islands to the open surface while the flux of CuPc molecules, which cannot cross step edges, directs the island towards the largest area on their individual terrace that is not yet covered by islands.

movement type

There are different ways in which a cluster can move [OLS+03]. One way is that the whole or large parts of the cluster move at once. This concerted movement can occur through different mechanism. The cluster moves as a whole in the gliding mechanism while only parts of the cluster move in the shearing mechanism. A different movement type is that the motion is accomplished by the motion of individual molecules only. The cluster can move with the evaporation-condensation mechanism by detachment of molecules from the back and a reattachment of these molecules or different molecules

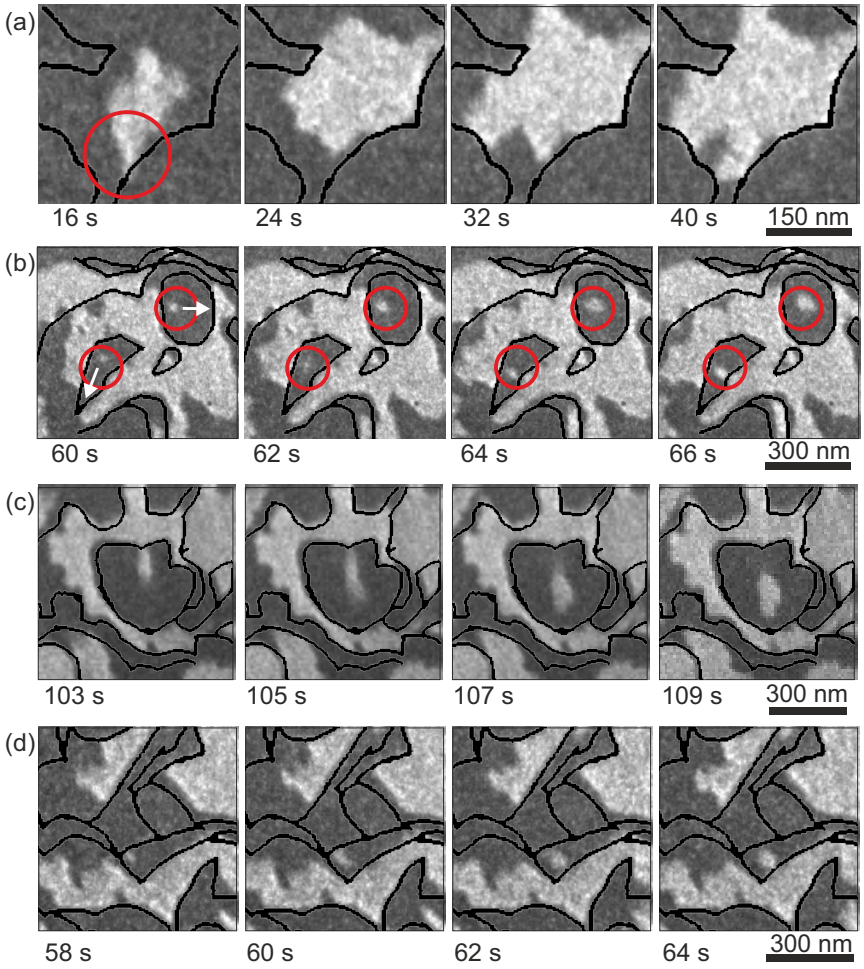

Fig. 6.19: Detailed images showing the growth of small islands during the deposition of PTCDA on a 0.40 ML film of CuPc on Ag(111). This is the same deposition process that was already shown in Fig. 6.16. The deposition time is given for each image. The step edges are superimposed in black in some images. (a) The shape of the island changes during the growth. (b) & (d) Small and (c) bigger clusters move on the surface.

at the front. The words "evaporation" and "condensation" refer the molecule's attachment to the islands and not to the surface since it does not leave the surface during this process. A motion of the cluster is also created when individual molecules diffuse along the edges of the island moving it in a certain direction. The first movement type seems unlikely since the shift of many hundred molecules at a time requires a large

amount of energy and it is unlikely that it is driven by a concentration gradient during the deposition. The second movement type is more likely. It costs less energy and also explains why the islands move towards the highest fluxes of PTCDA and CuPc molecules since there is an increased attachment of molecules from that direction. This also suggests that it is most likely the evaporation-condensation mechanism where the molecules from the back of the island detach and some molecules attach at the front. Further experiments would be necessary to get more data on the diffusion speed of the islands for determining the motion type [OLS+03]. Kinetic Monte Carlo calculations would also help to explain how the island moves exactly. The mobility of very small clusters consisting of only a few entities has been reported before [KE99, Kel96]. The motion of large homomolecular NTCDA islands during their deposition on Ag(111) was published in [Gro06] but no detailed description of the diffusion mechanism was given. This is the first time the motion of large islands, which consist of two species, is described in detail.

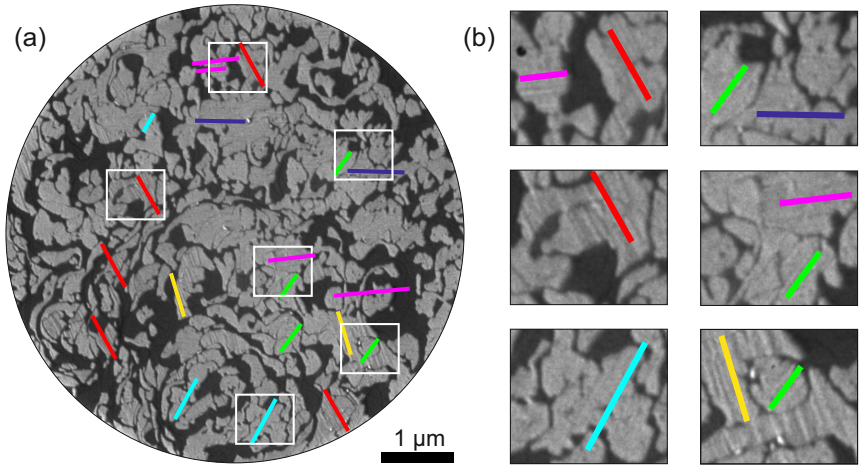

Fig. 6.20: LEEM image taken at $U_{start} = 2\,\mathrm{V}$ with a slight under focus. Straight lines of different orientations can be seen within the islands. (b) Enlarged images of the sections marked by white rectangles in (a). Lines with approximately the same orientation are indicated with the same color.

6.2.1.5 Line defects within heteromolecular islands

Line defects within the individual MBW islands are found in the islands of the experiment shown in Fig. 6.16. Their orientation and origin is determined by detailed LEEM, LEED, and DF-LEEM measurements which is discussed in this section.

description of lines

Lines within the islands became visible when LEEM images were taken at different focusing conditions. They get more pronounced in stronger over and under foci and are smallest close to the focus. An image at a slight under focus can be seen in Fig. 6.20 (a) where lines of different orientations can be seen. The lines are marked in different colors depending on their orientation. Fig. 6.20 (b) shows enlarged images of the areas marked by the white rectangles in Fig. 6.20 (a). The lines are clearly visible in these images and it can be seen that the lines are not equally spaced. The line direction does not change within one island even in islands that have grown around smaller terraces, as can be seen in the second image in the left column and the third image in the right column in Fig. 6.20 (b).

domain orientation determines line orientation

DF-LEEM images were recorded for this sample in order to determine a possible correlation of the orientation of the lines shown in Fig. 6.20 and the orientation of the domains. A composite image consisting of all six rotational domains superimposed over the LEEM image from Fig. 6.20 (a) is shown in Fig. 6.21 (a). All islands from Fig. 6.20 (a) are completely covered since the orientation of all islands could be determined. The step edges of the Ag(111) substrate are superimposed as black lines. It can be seen that no more than one orientation is present on each terrace. This shows again that only on island nucleated on each terrace. All islands which exhibit

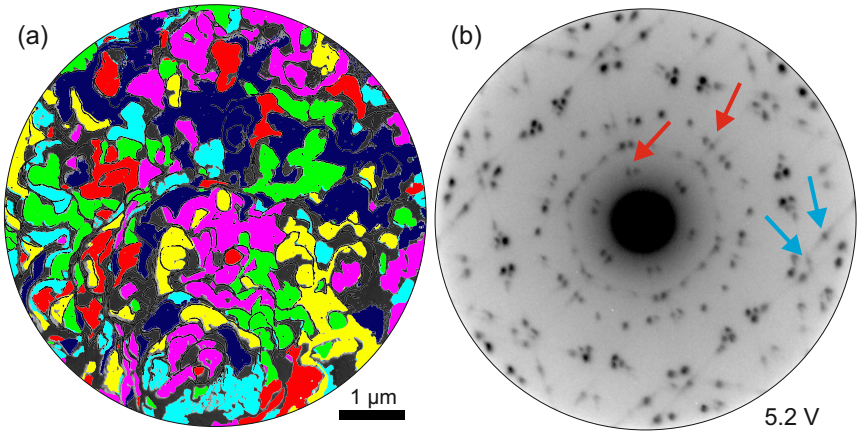

Fig. 6.21: (a) The colored rotational domains that were determined by DF-LEEM are superimposed over the LEEM image shown in Fig. 6.20 (a). The orientation of all domains could be determined and they correspond to the orientations of the lines in Fig. 6.20. (b) LEED pattern of the same sample. The MBW signature can clearly be seen. Some spots are smeared out indicating that the long axis of the unit cell is sometimes compressed or elongated.

the same orientation of the lines are of the same domain orientation as can be seen when Fig. 6.20 and Fig. 6.21 (a) are compared. The colors used for the domains in the composite image in Fig. 6.21 (a) correspond to the colors of the lines in Fig. 6.20. This proves that the orientation of the domain determines the direction of the lines.

lines along short axis of unit cell

The orientation of the lines of the islands belonging to a certain domain orientation were averaged. The six averaged orientations are depicted as the colored lines in Fig. 6.22 (a). They exhibit a sixfold symmetry just like the Ag(111) substrate. The angles between the orientations of the lines are measured and are given in Fig. 6.22 (a). The three small angles give an average value of 9° and the bigger angles of 51°. These angles are compared to the angles of the real space unit cell of the MBW phase. An STM image (taken from [Sta13]) of the MBW phase measured at low temperatures with the MBW unit cell and schematic PTCDA and CuPc molecules superimposed can be seen in Fig. 6.22 (b). The orientation of the substrate is indicated by the black lines. The angle between the short axis of the unit cell and the substrate is 25°. This means that the angle between the short axes of mirror domains is 50°. This value agrees nicely with the average of the bigger angles found between the lines in the LEEM image of 51°. This suggests that the lines in the LEEM image run in the direction of the short axis of the unit cell.

deviations of long unit cell vector

A LEED pattern was also taken of this sample and can be seen in Fig. 6.21 (b). The signature of the MBW phase is clearly visible. It can be observed that some spots are smeared out in two directions along a line. Some spots are smeared out radially with

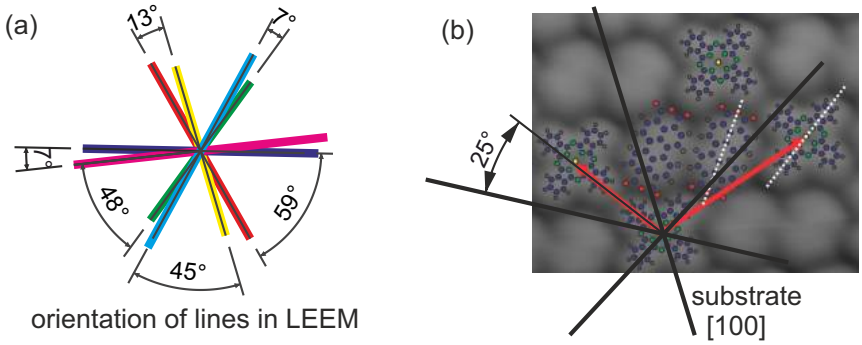

Fig. 6.22: (a) The average orientations of the lines of the same rotational domain found in LEEM are depicted and the angles between them measured. The two sets of small and large angles average to 9° and 51°. (b) STM image of the MBW phase taken from [Sta13]. The unit cell vectors are shown in red and the molecules as ball-and-stick models. The directions of the Ag(111) substrate are given by black lines. For details see text.

respect to the 00-spot (marked by red arrows) while higher order spots are smeared out in other directions (marked by blue arrows). Simulations of the LEED pattern revealed that all spot elongations can be explained by an uncertainty of the length of the long unit cell vector. Its length in the commensurate MBW structure is 26.5 Å. Varying the length from 23.7 Å to 27.6 Å explains the elongated spots in the LEED pattern. This shows that the compression of the unit cell is stronger than the elongation. But such distorted unit cells occur only rarely since the smeared out spots exhibit a sharp maximum at the value of the commensurate structure and a very low intensity on each side of the main peak. This fits nicely to the observation that the lines only appear with a certain distance from each other in the LEEM image.

line defects

A clear idea about the structure of the sample is obtained when both observations, the orientation of the lines in the LEEM image and the smeared out spots in the LEED pattern, are combined. The periodicity in the direction of the long axis of the unit cell is disturbed in some places and line defects appear which run in the direction of the short axis of the unit cell. Theses line defects are most likely caused by kinetic effects during the growth since they disappear after annealing the sample.

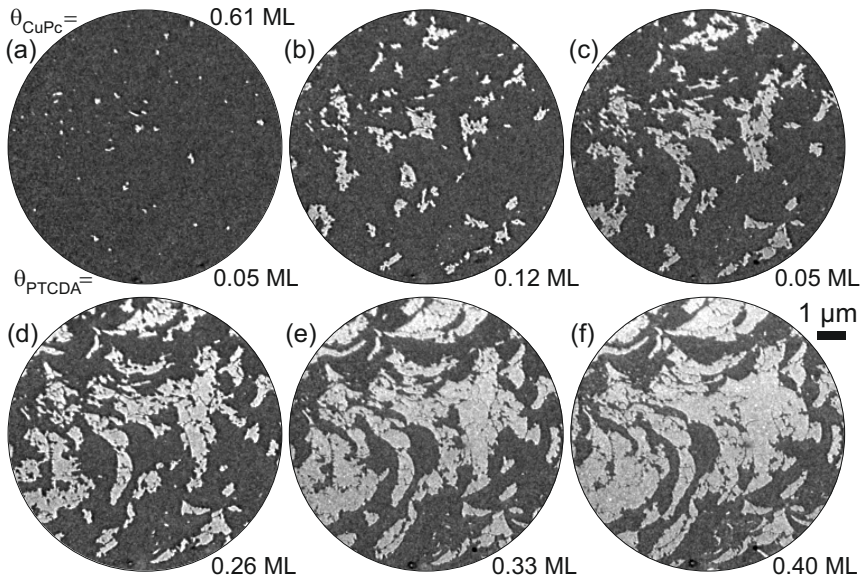

Fig. 6.23: LEEM images taken during the deposition of PTCDA on a CuPc film with a coverage of 0.61 ML at 380 K. The MBW islands can be identified as the bright areas. ($U_{\text{start}} = 2\,\text{V}$)

6.2.1.6 Influence of temperature on phase formation

The influence of the temperature on the growth of heteromolecular phases, when PTCDA is deposited on a submonolayer film of CuPc on Ag(111), is discussed now.

deposition at higher T

PTCDA was deposited on a 0.61 ML film of CuPc on Ag(111) at 380 K. The growth at this elevated temperature is shown in Fig. 6.23. The first islands nucleate after 0.04 ML of PTCDA were deposited and a corresponding image can be seen in Fig. 6.23 (a). The islands then grow in size and new islands nucleate as well (Fig. 6.23 (b)-(e)) until the deposition is stopped (Fig. 6.23 (f)).

MBW grows

LEED measurements, performed after the deposition, revealed the heteromolecular islands observed here are MBW islands. It can be said that the first islands that nucleated are also of the MBW phase since the LEEM contrast of the islands does not change during the deposition.

temperature changes phase

The coverage of CuPc used in the experiment was the same as in the first deposition experiment discussed in this section (seen in Fig. 6.12). However, M1^{2}1 islands grew there. This means that different phases appear during the deposition of PTCDA at the same CuPc coverage at different temperatures. This influence of the temperature on the phases is discussed in more detail in section 6.2.3.2.

6.2.2 Deposition of CuPc on submonolayer films of PTCDA

The growth process, when CuPc molecules are deposited on a submonolayer film of PTCDA on Ag(111), is discussed in this section.

sample preparation

All experiments in this section were performed in the following way: A submonolayer film of PTCDA was deposited on a Ag(111) substrate which was kept at a specific temperature. The PTCDA molecules form islands on the surface and the areas next to these islands only contain a very low density of diffusing PTCDA molecules, as was discussed in chapter 4.2. The CuPc molecules are deposited on top of this surface. This process is monitored in the LEEM and LEED mode.

6.2.2.1 Transformation of PTCDA islands at different temperatures

It was found that the PTCDA island on Cu(001) did not change when CuPc was deposited additionally. It is expected that the PTCDA islands can be restructured on Ag(111) since the molecule-substrate interaction is weaker. The deposition of CuPc on a submonolayer film of PTCDA at three different temperatures is analyzed in this section.

380 K

The deposition of CuPc on a Ag(111) substrate that is covered with a 0.17 ML film of PTCDA at 380 K is discussed first. A sequence of LEEM images can be seen in Fig. 6.24. The first image shows the PTCDA islands before the deposition of CuPc is started. The islands appear as bright areas and some are marked by green arrows. The CuPc molecules that are deposited on the surface form a gas between the PTCDA islands which leads to a decrease in intensity in these areas, as can be seen in Fig. 6.24 (b). PTCDA molecules start to get dissolved in the CuPc gas, as can be seen from the decreased island size in Fig. 6.24 (b) compared to Fig. 6.24 (a). Islands that exhibit a different contrast appear after the deposition of 0.33 ML of CuPc. LEED measurements show that these islands are of the MBW type. The surface after the deposition of 0.37 ML CuPc can be seen in Fig. 6.24 (c) where some MBW islands are marked by a yellow arrow. Almost all PTCDA islands are gone and many MBW islands can be seen. All PTCDA islands are gone after 0.39 ML of CuPc are deposited. The only bright spot visible in Fig. 6.24 (d) is a defect on the channel plate. Smaller islands with a similar contrast as the MBW islands, which belong to the $M1^21$ phase, nucleate after 0.52 ML of CuPc are deposited, while the MBW islands start to disappear (Fig. 6.24 (e)). The $M1^21$ islands can only be identified as the islands that were not present in Fig. 6.24 (d). One area with several $M1^21$ islands is marked by a red arrow while a cluster of some MBW islands is marked by a yellow arrow. All MBW islands have disappeared when 0.55 ML of CuPc are reached and the only islands present on the surface are $M1^21$ islands, as can be seen in Fig. 6.24 (f). The third type of heteromolecular islands, the MZZ phase, appears at a coverage of CuPc of 0.64 ML. It shows a slightly darker contrast than the previous two island types, and the islands are much larger than the very small $M1^21$ islands. One of the large MZZ islands is marked by a blue arrow in Fig. 6.24 (g). Some $M1^21$ islands are still visible (marked by a red arrow). Only MZZ islands are present on the surface when

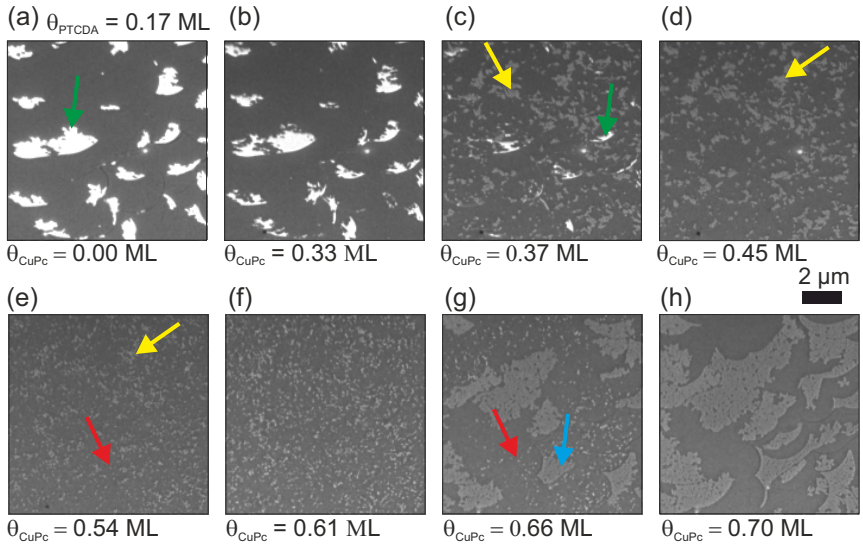

Fig. 6.24: LEEM images taken during the deposition of CuPc on a 0.17 ML film of PTCDA on Ag(111) at 380 K. (a) Bright PTCDA islands (green arrow) before the deposition is started. (b) PTCDA molecules from the islands become dissolved in the CuPc gas and (c) MBW islands (yellow arrow) start nucleating (d) until only MBW islands are present. (e) M1^{2}1 islands (red arrows) start growing and (f) become the only islands present on the surface. (g) MZZ islands (blue arrow) start growing and (h) the M1^{2}1 islands have disappeared completely leaving only MZZ islands. (U_{start} = 2 V)

0.67 ML of CuPc are deposited. The surface with 0.70 ML of CuPc can be seen in Fig. 6.24 (h).

complete transformation

The last experiment shows that the PTCDA islands undergo subsequent phase transitions when CuPc is deposited on the Ag(111) surface. The PTCDA islands disappear and MBW islands, which contain both PTCDA and CuPc, appear. These islands in turn transform, when the CuPc concentration reaches a certain limit, and islands of the M1^{2}1 phase appear, which contain a larger relative amount of CuPc in their unit cell. The MZZ islands appear at even higher CuPc coverages and the M1^{2}1 islands disappear. The phases that contain a larger relative amount of CuPc in their unit cell seem to be energetically preferable at higher CuPc coverages.

comparison to Cu(001)

This transformation of the PTCDA islands is in contrast to the experiments on Cu(001) where no transformation of the PTCDA islands was observed. The weaker molecule-substrate interaction indeed allows the transformation of the PTCDA islands. The occurrence of the phases on the surface do not seem to depend on the deposition order of the two molecules, as is the case for Cu(001). This independence of the occurrence of the phases on the deposition order is discussed in chapter 6.2.3.

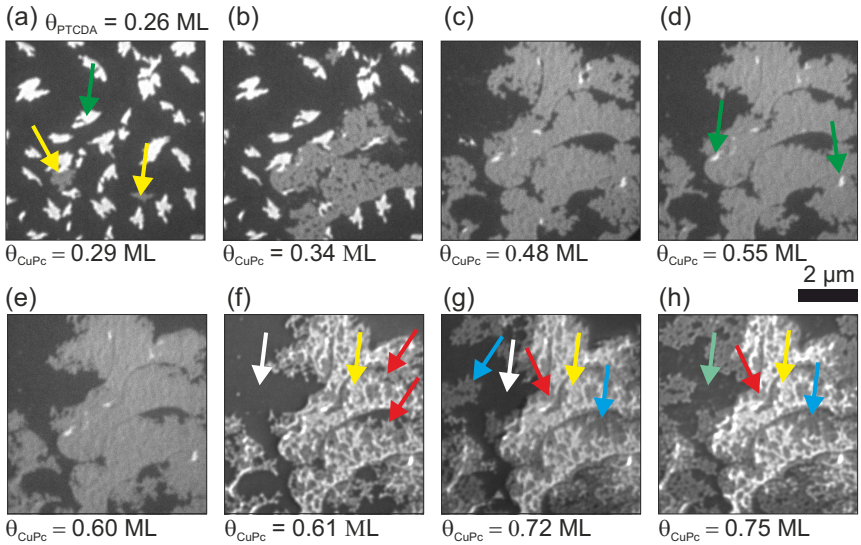

Fig. 6.25: LEEM images taken during the deposition of CuPc on a 0.26 ML film of PTCDA on Ag(111) at 300 K. The different phases are indicated by colored arrows: disordered (white), PTCDA (green), MBW (yellow), M1^{2}1 (red), MZZ (blue), and CuPc (teal). (a)-(d) PTCDA islands transform into MBW islands (e)-(f) which in turn partly transform into M1^{2}1 islands. (g) Then the MZZ phase appears and (h) finally a crystalline CuPc phase. Note that in (a)-(e): $U_{\text{start}} = 2.00\,\text{V}$ and in (f)-(h): $U_{\text{start}} = 0.42\,\text{V}$.

300 K The same experiment was performed at 300 K with an initial PTCDA coverage of 0.26 ML, see Fig. 6.25. The first image shows the surface after 0.29 ML of CuPc are deposited. Bright PTCDA islands (marked by green arrow) and already the first MBW islands, which exhibit a medium contrast and are marked by the yellow arrows, can be seen. These MBW islands appear at a CuPc coverage slightly below 0.29 ML. The PTCDA islands continue to disappear while the MBW islands increase in size with continued deposition of CuPc, as can be seen in Fig. 6.25 (b) and (c). Some PTCDA islands do not disappear since they are located at step edges or encapsulated by MBW islands so that CuPc molecules cannot reach them there (green arrows in Fig. 6.25 (d)). The edges of the MBW islands start to change strongly at 0.56 ML, as can be seen when comparing Fig. 6.25 (d) and Fig. 6.25 (e). It can be observed that the image changes very little between Fig. 6.25 (c) and (d), while it changes a lot between Fig. 6.25 (d) and (e) even though the CuPc coverage difference is almost the same. This shows that, once all reachable PTCDA islands are transformed, the growth of heteromolecular islands stops. The CuPc coverage has to increase again by a certain amount before the growth of islands of another phase starts. The start voltage was changed from 2.00 V (Fig. 6.25 (a) - (e)) to 0.42 V (Fig. 6.25 (f) - (g)) in order to obtain a strong contrast between the different phases within the islands

consisting of the MBW and the M1^{2}1 phase. There are three different contrasts visible in the image now (Fig. 6.25 (f)). The bright contrast belongs to islands of the MBW structure (yellow arrow) while islands of the M1^{2}1 phase (red arrows) appear darker. The gas-like structure (white arrow) consisting of CuPc and some PTCDA molecules appears darkest. It can be seen that the area close to the edges of the MBW islands are transformed into the M1^{2}1 phase while the centers of the islands remain mostly in the MBW structure. The reason for this is similar to the reason why some PTCDA islands do not disappear. The CuPc molecules do not seem to be able to reach the inside of the larger islands. A fourth contrast belonging to the MZZ phase appears when a coverage of CuPc of 0.71 ML is reached. These islands grow in size by transforming the edges of existing islands. An image taken at a coverage of 0.72 ML can be seen in Fig. 6.25 (g). The CuPc molecules on the terraces have become a homomolecular CuPc phase in Fig. 6.25 (h). The remaining dissolved PTCDA molecules in the disordered gas-like phase are built into small MZZ islands which can be seen as the small slightly brighter areas in the CuPc zones. Hence, islands of four different phases are present here and are marked by differently colored arrows: MBW (yellow), M1^{2}1 (red), MZZ (blue), and CuPc (teal).

incomplete restructuring

The experiment shows that even though the same phase transitions are found, the phases are not transformed completely into each other at this temperature. There are two possible reasons for this. Firstly, the reduced temperature could make the transformation slower. Secondly, the large size of the MBW islands could make is impossible for the CuPc molecules in the disordered phase to reach all areas inside the large MBW islands. This could be circumvented by using a higher deposition rate of PTCDA and CuPc, which should lead to more nucleation sites and, hence, to smaller islands.

450 K

The third experiment was performed at a substrate temperature of 450 K and an initial PTCDA coverage of 0.17 ML. The image sequence taken during the deposition of CuPc can be seen in Fig. 6.26. The PTCDA islands (green arrow) before the deposition is started can be seen in the first image. The intensity on the Ag(111) terraces decreases and the PTCDA islands start to disappear just as it occurred in the previous two experiments. The difference at 450 K is that the PTCDA islands disappear almost completely, as can be seen in Fig. 6.26 (b), before the nucleation of the MBW islands starts. This means that all PTCDA molecules are "solved" in the CuPc gas phase at this stage. The MBW islands nucleate at a CuPc coverage of 0.36 ML and the first MBW islands can be seen in Fig. 6.26 (c). All PTCDA islands are gone by this point. The MBW islands continue to grow and their maximal size is shown in Fig. 6.26 (d). The M1^{2}1 phase starts to grow after 0.47 ML of CuPc are deposited. Fig. 6.26 (e) is an image where both the MBW and the M1^{2}1 are present. All the islands that were not present in Fig. 6.26 (d) are of the M1^{2}1 type. Some are marked by red arrows while some areas of the MBW phase are marked by yellow arrows. The M1^{2}1 phase islands grow while the MBW islands continue to become transformed into M1^{2}1 islands until only small parts in the middle of the existing islands are of the MBW phase (marked by yellow arrows in Fig. 6.26 (f)). The MBW phase exhibits a slightly brighter contrast than the M1^{2}1 phase. The MZZ phase (blue arrows) starts

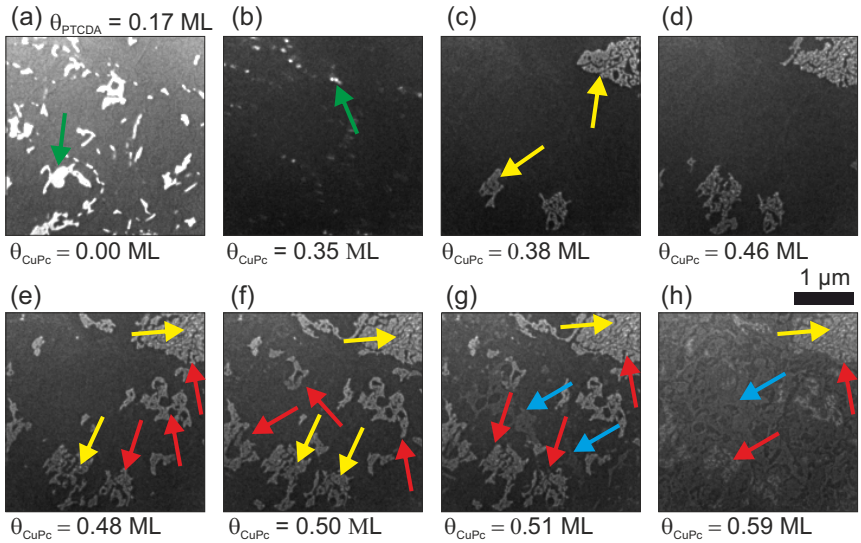

Fig. 6.26: LEEM images taken during the deposition of CuPc on a 0.17 ML film of PTCDA on Ag(111) at 450 K. (a) The PTCDA islands (green arrows) (b) almost completely disappear (c) before the nucleation of the first MBW islands (yellow arrows). (d) The maximal amount of MBW islands is present (e) before they start to disappear again during the nucleation of the M1^{2}1 phase (red arrows). (g) The MZZ phase starts to grow and all three phase can be seen. (h) The MZZ islands grow until the deposition is stopped. ($U_{\text{start}} = 2.00$ V)

to grow at a CuPc coverage of 0.50 ML. These island continue to grow while the M1^{2}1 phase disappears, as can be seen in Fig. 6.26 (g). The deposition was stopped at a CuPc coverage of 0.59 ML. The majority of the surface is covered by the MZZ phase at this stage. Only some M1^{2}1 islands are left which contain a little of the MBW phase in their middle. A couple of conclusions can be drawn from this experiment.

gas-like phase

The first is that there exists a configuration of coverages and temperature where all molecules are dissolved in a gas-like phase. This was previously only discovered for PTCDA coverages below 0.15 ML when PTCDA was deposited on a submonolayer film of CuPc at 300 K. Such a complete solution of molecular islands during the deposition of a second type of molecule has not been reported previously as far as it is known to the author.

incomplete transformation due to large islands size

The second observation is the fact that the phase transitions do not occur sequentially but in the final stage a mixture of three heteromolecular phases is found, although the areas covered by the M1^{2}1 and the MBW phase are very small. Two possible reasons for the incomplete transformation were suggested after the experiment at 300 K. The first was that a certain temperature is necessary for a complete transformation. This is disproved with this experiment since the temperature in this experiment was higher

than in the experiment where a complete transformation occurred at 380 K. The second explanation was that the islands of the MBW phase (or any other phase) were too big making it impossible for the CuPc molecules to reach the inside of the island. This encapsulation of the phases in the center of islands is the more likely reason since the large MBW islands in this experiment also do not become completely transformed.
The CuPc coverage during the nucleation of the first islands of the MBW phase was between 0.29 ML and 0.38 ML in the last three experiments. This discrepancy could be explained by the different initial PTCDA coverages and the different temperatures. Experiments performed at the same temperature but at different PTCDA coverages and at the same initial PTCDA coverage but at different temperatures have to be analyzed to investigate the influence of these two parameters. These experiments were performed and the results are discussed in the next two sections.

coverage and temperature influence transformation

6.2.2.2 Influence of initial PTCDA coverage on critical CuPc coverage for MBW nucleation

The influence of the initial coverage of PTCDA, θ_{PTCDA}, on the necessary CuPc coverage for the nucleation of the MBW phase is investigated in this section. Two experiments with initial PTCDA coverages of 0.14 ML and 0.48 ML at the same substrate temperature of 350 K are analyzed now.
The deposition of CuPc on a submonolayer film of PTCDA with a coverage of 0.14 ML is shown in Fig. 6.27. The first image shows the the surface before the CuPc deposition is started, Fig. 6.27 (b) after the deposition of 0.13 ML of CuPc. The intensity on the terraces has decreased, as is expected when CuPc is deposited on the Ag(111) surface at a start voltage of 2 V. A MBW island (medium contrast) already grows in the large hole in one PTCDA island in the upper left corner of Fig. 6.27 (b) marked by a yellow arrow. The island in the large hole grows and fills it out completely in Fig. 6.27 (c). The smaller holes in the PTCDA islands are also filled with the MBW phase at this point (marked by another yellow arrow). The presence of MBW islands (yellow arrow) outside of holes occurs at a CuPc coverage of 0.31 ML as is can be seen in the upper left corner of Fig. 6.27 (d). This MBW island spreads out on the surface but also new MBW islands nucleate (Fig. 6.27 (e)). This continues until all PTCDA islands have disappeared and the deposition is stopped (Fig. 6.27 (f)).

$\theta_{\mathrm{PTCDA}} = 0.14\,\mathrm{ML}$

This experiment shows that the nucleation of MBW islands in holes of PTCDA islands occurs at lower total CuPc coverages than on the large terraces. The reason is that the density of CuPc molecules is higher in the holes since additional CuPc molecules adsorbing on the surrounding PTCDA island diffuse into the holes. This effect is the stronger the smaller the hole and the larger the surrounding PTCDA island is. This suggests that a certain local CuPc density, not an overall coverage, is needed for the nucleation of the MBW phase. This means that the MBW islands should nucleate at a lower total coverage of CuPc when the initial coverage of PTCDA is increased since the CuPc molecules are then confined to a smaller area.

nucleation in holes at lower θ_{CuPc}

Such an experiment was performed with an initial PTCDA coverage of 0.48 ML. The substrate temperature of 350 K is the same as in the previous experiment. The depo-

$\theta_{\mathrm{PTCDA}} = 0.48\,\mathrm{ML}$

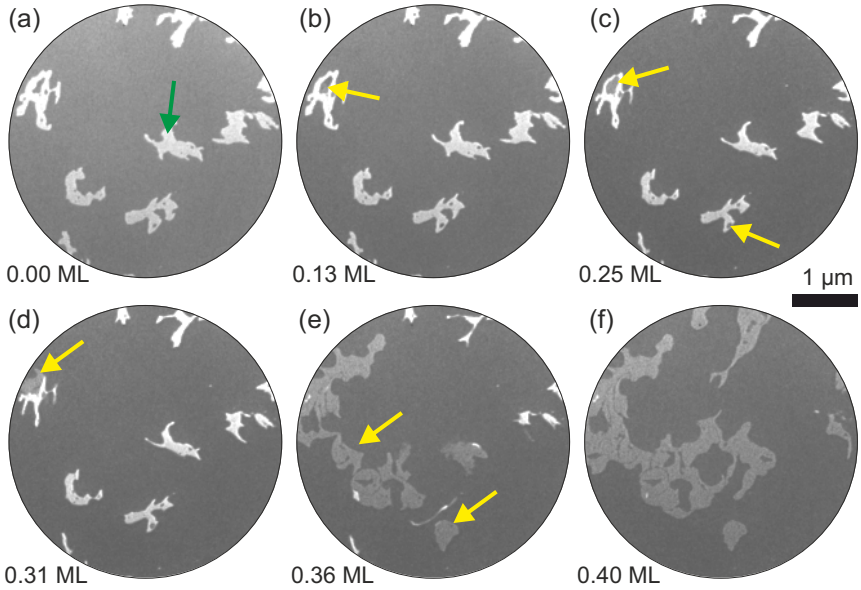

Fig. 6.27: LEEM image sequence taken during the deposition of CuPc on a 0.14 ML film of PTCDA on Ag(111) at a temperature of 350 K. The deposited amount of CuPc is given for each image. The PTCDA islands (green arrow) are completely transformed into MBW islands (yellow arrows). A detailed description is given is the text. ($U_{\text{start}} = 2.00\,\text{V}$)

sition process is shown in Fig. 6.28. The initial PTCDA coverage is seen in the first image. The intensity on the areas that are not covered by PTCDA islands decreases when the deposition of CuPc is started, as can be seen in Fig. 6.28 (b). The nucleation of the MBW phase in a small hole of a PTCDA islands is already completed when a CuPc coverage of 0.06 ML is reached (yellow arrow in Fig. 6.28 (b)). This observation alone is not an indication for a lower coverage of CuPc being sufficient for the MBW nucleation since the size of the PTCDA islands around the hole is larger compared to the previous case increasing the additional flux to the hole. Many holes are filled with MBW islands at a CuPc coverage of 0.21 ML, as can be seen in Fig. 6.28 (c). Some prominent holes are marked by yellow arrows. The first nucleation of the MBW phase outside of holes occurs at a CuPc coverage of 0.23 ML. This value is significantly lower than the coverage of 0.31 ML in the previous experiment. The MBW islands continue growing in Fig. 6.28 (e)+(f). M1^{2}1 islands start to grow at higher CuPc coverages (not shown) before the PTCDA islands have completely disappeared. The transformation of the PTCDA islands is not complete at this stage since the PTCDA islands are very large and encapsulated by MBW islands, so that the CuPc molecules could not reach the insides of the islands.

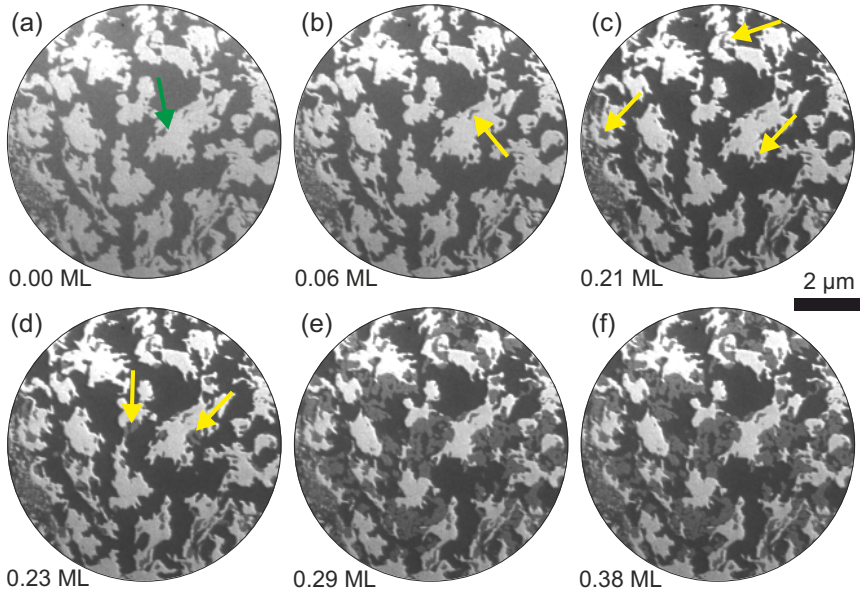

Fig. 6.28: LEEM images taken during the deposition of CuPc at 350 K on a submonolayer film of PTCDA of a coverage of 0.48 ML. The transformation of the PTCDA islands starts at lower CuPc coverages than in Fig. 6.27. This indicates that not the total coverage of CuPc but the density of CuPc in the disordered phase is crucial for the transformation. ($U_{\text{start}} = 2.00\,\text{V}$)

critical CuPc density

The CuPc density needed for the nucleation of MBW islands can be quantified. The deposited amount of CuPc lead to total densities of CuPc on the sample of 0.16 molecules/nm^2 and 0.12 molecules/nm^2 for the time when the nucleation of the first MBW islands was observed for the initial coverages of PTCDA of 0.14 ML and 0.48 ML, respectively. These total CuPc densities differ from each other, even when an experimental uncertainty of 10% is assumed, indicating that this parameter is not the decisive factor for the MBW phase nucleation. The situation changes when the area covered by PTCDA islands in subtracted, i.e. when it is assumed that all deposited CuPc molecules move down to the first layer forming a disordered phase there. Densities of the CuPc molecules in the disordered phases of 0.19 molecules/nm^2 and 0.23 molecules/nm^2 between the PTCDA islands are obtained for samples with PTCDA coverages of 0.14 ML and 0.48 ML, respectively. More details on the exact formula and its derivation are given in hypothesis 3 in section 6.2.3.1. Note that the experiment with the lower total CuPc density on the surface now has the higher CuPc density in the disordered phase showing how much the presence of PTCDA islands changes the CuPc density. The CuPc densities in the disordered phase are more similar and only deviate from their mean value by 8%, compared to 16% for the CuPc concentrations on the whole surface, which lies within the 10% uncertainty of the

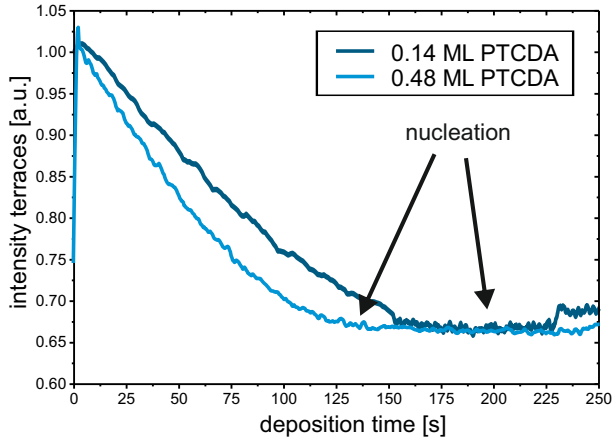

Fig. 6.29: The LEEM intensity of the disordered phase plotted against the deposition time. The dark blue and light blue curves belongs to the experiment where CuPc is deposited on 0.48 ML and 0.14 ML of PTCDA, respectively. The 0.48 ML-curve drops more quickly with time since the CuPc density in the disordered phase increases more quickly there.

CuPc coverages. This suggests that it is indeed the CuPc density in the disordered phase and not the total density of CuPc on the whole surface that determines the nucleation point of the MBW phase.

CuPc density in disordered phase

The LEEM intensity of areas of the disordered phase can be used as a measure of the density of CuPc molecules in the area, as was discussed in chapter 5.2.2. Fig. 6.29 shows the intensity on the terraces next to the PTCDA islands during the deposition of CuPc on 0.14 ML (dark blue) and 0.48 ML (light blue) of PTCDA. Both curves were normalized at $t = 0\,\mathrm{s}$. An additional scaling had to be applied to the data since different contrast apertures were used. The intensities during the nucleation of the first MBW islands were both set to the same value since the CuPc density in the disordered phase should be the same there. The LEEM intensity drops in both cases when the deposition of CuPc is started due to the destructive interference that was already explained in section 5.2.2. The curve belonging to the initial PTCDA coverage of 0.48 ML drops more quickly than the 0.14 ML-curve indicating that the CuPc density on those terraces increase more quickly. This agrees with the assumption that the CuPc molecules move down to the first layer, when they are deposited onto PTCDA islands, increasing the CuPc density in the disordered phase. The analysis of the LEEM intensity of the disordered phase gives further proof that the density of CuPc in the disordered phase is indeed the decisive factor for the nucleation of the MBW islands.

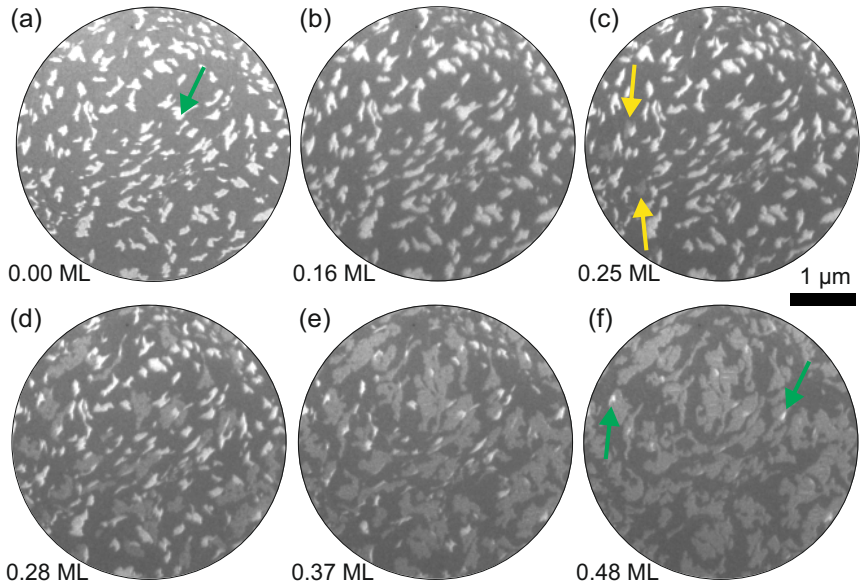

Fig. 6.30: Image sequence taken during the deposition of CuPc on 0.21 ML PTCDA on Ag(111) at 300 K. The PTCDA islands (green arrow) transform completely into MBW islands (yellow arrows). The first MBW islands nucleate at a CuPc coverage of 0.24 ML. ($U_{\text{start}} = 2.00$ V)

6.2.2.3 Influence of temperature on critical CuPc density for MBW nucleation

The influence of the substrate temperature on the critical CuPc density for the nucleation of the MBW phase is investigated in this section. CuPc is deposited on approximately the same initial coverages of PTCDA (0.22 ML) on a Ag(111) substrate at different temperatures.

In the first experiment, CuPc was deposited at 300 K. An image sequence of the whole deposition process is shown in Fig. 6.30. The first MBW islands nucleate after 0.24 ML of CuPc have been deposited and are marked by yellow arrows in Fig. 6.30 (c). This gives a CuPc density in the disordered phase between the PTCDA islands of 0.16 molecules/nm^2. The MBW islands grow in size and new MBW islands nucleate until almost all PTCDA islands are gone. Some remaining bright PTCDA islands are marked be green arrows in Fig. 6.30 (f). 300 K

The CuPc deposition was performed at 400 K in the next experiment. The whole deposition process can be seen in Fig. 6.31. The nucleation of the first MBW islands occurs in the holes of the PTCDA islands at coverages of 0.05 ML. The first MBW islands on the large terraces nucleate at a CuPc coverage of 0.37 ML which is significantly higher than at 300 K. This give a critical density of CuPc molecules in the disordered phase of 0.26 molecules/nm^2. 400 K

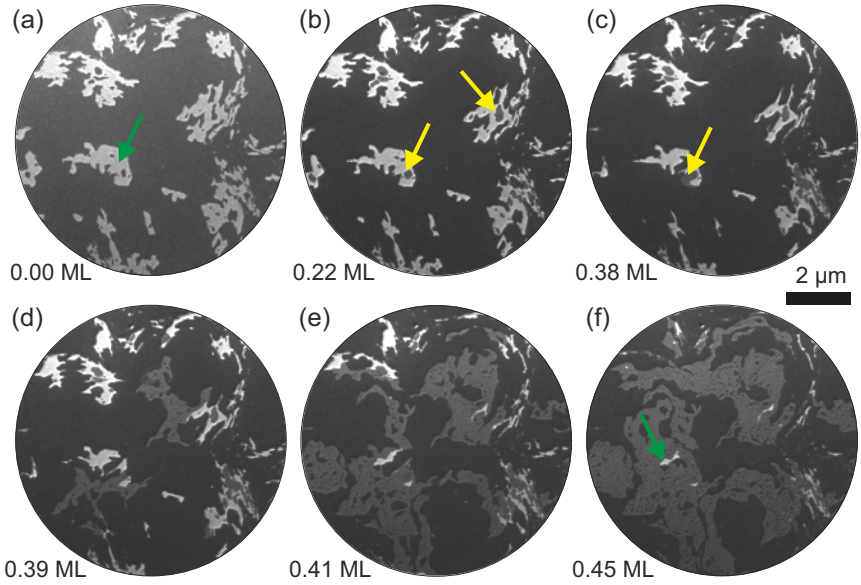

Fig. 6.31: LEEM image sequence taken during the deposition of CuPc on a submonolayer film of PTCDA of a coverage of 0.24 ML on Ag(111) at 400 K. The bright PTCDA islands (green arrows) are almost completely transformed into MBW islands (yellow arrows). The first MBW island appear at a CuPc coverage of 0.37 ML. ($U_{\text{start}} = 2.00\,\text{V}$)

CuPc density on terraces

The LEEM intensity of the disordered phase of both experiments is plotted versus the deposition time in Fig. 6.32. Both curves were normalized at $t = 0\,\text{s}$. Both intensities decrease in the same way when the deposition is started. This is expected since the PTCDA coverage is the same in both experiments leading to an equal density of CuPc molecules in the disordered phase with equal CuPc coverage. The MBW phase starts to nucleate after 85 s in the 300 K experiment. This leads to a slower decrease in intensity in that experiment which remains constant until all PTCDA islands are gone at 150 s. Then the intensity decreases more strongly indicating that the CuPc density on the terraces increases more quickly again since the CuPc molecules can no longer be incorporated into islands. The changes in LEEM intensity in the experiment at 400 K are different. The intensity continues to decrease until a minimum is reached after 175 s and then rises again. This minimum indicates that the terraces are covered with about half of the possible amount of CuPc molecules (see discussion on the LEEM intensity for CuPc/Ag(111) in chapter 5.2.2). The nucleation of MBW islands occurs after 225 s and the intensity stays approximately the same during the growth of the MBW islands. These intensity curves give further proof that a different CuPc density is necessary for the nucleation of the MBW islands at different temperatures.

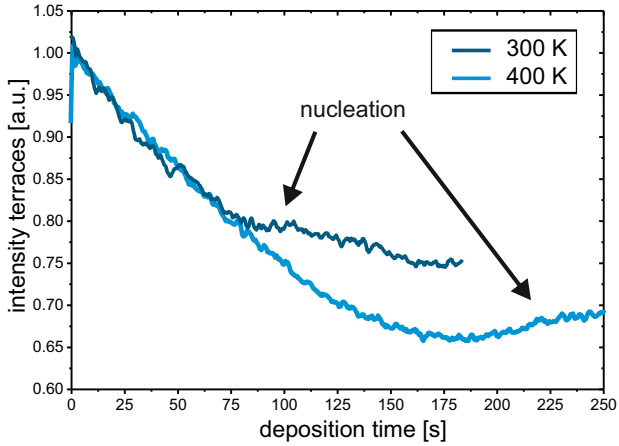

Fig. 6.32: The LEEM intensity of the disordered phase plotted versus the deposition time. The intensity drops in both experiments in the same way when the deposition is started. The nucleation of the MBW phase occurs after 85 s. The trend of the curves differ from this point on. The MBW phase nucleates only after 225 s when CuPc is deposited at 400 K.

higher critical CuPc density at higher T

The critical density for the nucleation of the MBW phase was 0.16 molecules/nm^2 at 300 K while is was significantly higher at 400 K with 0.26 molecules/nm^2. Taking into account the critical density observed in the experiments at 350 K from section 6.2.2.2, which resulted in 0.21 molecules/nm^2, gives a clear indication that the critical density of CuPc for the nucleation of MBW island increases with increasing temperature. This relation between the CuPc density and the temperature is discussed in detail in section 6.2.3.3.

6.2.3 Thermodynamic properties of the PTCDA-CuPc system

This section discusses the thermodynamic properties of the PTCDA-CuPc system on Ag(111). The first part analyzes the phase diagram of the binary system. The second part demonstrates the reversibility of the temperature-driven phase transitions for which indications were already found in section 6.2.1.6. The activation energy for the nucleation of the MBW phase is determined in the third part by analyzing the critical CuPc density during the nucleation of the first MBW islands at different temperatures.

6.2.3.1 Phase diagram at 300 K

The phase diagram of the binary PTCDA-CuPc system at 300 K is discussed in this section.

systems at constant volume

Many phase diagrams for binary systems at constant pressure exist, for example phase diagrams of metallic alloys [Kit93] or intermetallic compounds [Sau95]. But there are two fundamental differences to the system studied in this work: The studied system is two dimensional and it is at constant volume since the surface area is constant. The two-dimensionality changes the form of the phase diagram fundamentally. Here, not only the relative concentrations of the two components are important but the absolute values of both of them since they are spread out on the surface and not squished together due to gravity as in the case of constant pressure systems. This changes the conventional phase diagram which has two dimensions (the relative concentrations and the temperature) into a three dimensional phase diagram with the absolute concentration of both materials and the temperature as the three independent parameters. This three dimensional phase diagram is too large to be fully determined withing the framework of this work. Here, the focus is on the phase diagram at a certain (constant) temperature of 300 K where the two variables are the coverages of the two molecules.

thermodynamic equilibrium

It is a crucial prerequisite for a phase diagram that the system is in thermodynamic equilibrium. To ensure this, low deposition rates were applied in all experiments used for setting up the phase diagram and it was regularly waited for several minutes to ensure this. An aspect that still has to be checked is if the existing phases appear independently of deposition parameters during the growth.

form of phase diagram

Many deposition experiments were performed at 300 K to determine at which coverages of PTCDA and CuPc which structures are present. The results of the experiments can be seen in Fig. 6.33. The coverages of CuPc and PTCDA represent the abscissa and ordinate of the phase diagram. The triangular shape emerges since

$$\theta_{\mathrm{CuPc}} + \theta_{\mathrm{PTCDA}} \leq 1$$

must be fulfilled at all times. The line where the total coverage is equal to 1 is called the 1 ML-line in the following. Different deposition sequences were used for the experiments. PTCDA was deposited on a submonolayer film of CuPc in most experiments since a complete transformation of the islands does not always happen when CuPc is deposited on a submonolayer of PTCDA, as was already discussed in section 6.2.2.1.

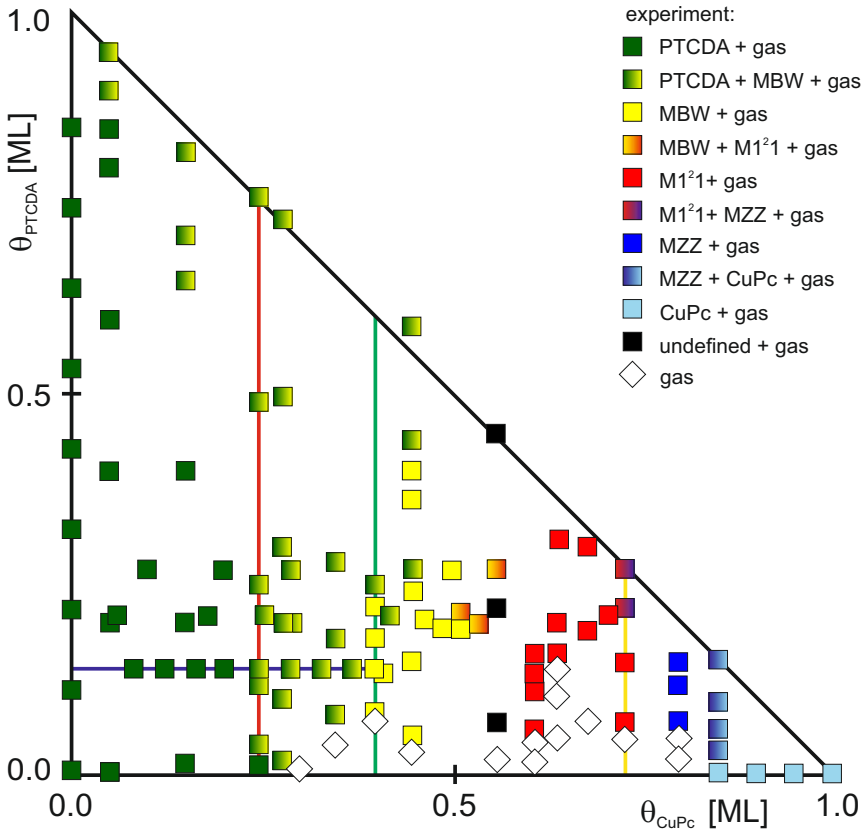

Fig. 6.33: Phase diagram of the different phases that are present at different coverages of CuPc and PTCDA at 300 K. The different colors indicate the different phases existing on the Ag(111) surface.

These experiments are represented by the data points aligned along vertical lines in the phase diagram. Three of those experiments are marked by a red, a green, and a yellow line in Fig. 6.33. Some experiments were performed with a reversed deposition order (CuPc on a submonolayer of PTCDA) to check if the final structure is indeed independent of the deposition sequence and they can be identified by the data points lying on horizontal lines in the phase diagram. Such a horizontal arrangement of data points of one experiment is marked by a blue line in Fig. 6.33. It can be seen in the phase diagram that the final structure is indeed independent of the deposition order which proves that the data is obtained in the thermodynamic equilibrium.

structure of diagram

Several different zones can be identified in the phase diagram in Fig. 6.33. The colors of the data points in Fig. 6.33 indicate which phases are present at this point. Data points that consist of only one color demonstrate that only one crystalline phase exists

at these coverages while data points with a gradient of two colors illustrate that a mixture of these different phases represented by the individual colors is present. Additionally, a disordered gas-like phase is always present as well except at the 1 ML-line where the whole surface is covered by crystalline phases.

eutectic regions

It can be seen that there are four eutectic regions where two crystalline phases and a gas-like phase are present. They were found for PTCDA + MBW + gas, MBW + M1^{2}1 + gas, M1^{2}1 + MZZ + gas, and MZZ + CuPc + gas. Eutectic *regions* are not present in constant pressure systems since they collapse into points there. The concept of eutectic regions is not new since they were also found for three dimensional binary systems of noninteracting particles at constant volume [BOP92, EMF93].

crystalline phase + gas zones

There are also five zones where one crystalline phase and the gas-like phase coexist. These zones are observed for all three heteromolecular phases as well as for the homomolecular PTCDA and CuPc phases. These types of zones exist in conventional three dimensional constant pressure as well as constant volume systems [Kit93, Sau95, BOP92, EMF93].

gas-like-phase-only zone

Additionally, there is also a zone with no crystalline phases present at high CuPc and low PTCDA concentrations. This gas-like-phase-only region, marked by the white diamonds in Fig. 6.33, is also observed for three dimensional constant volume systems of non-interacting particles with the difference that it is usually located at low coverages of both materials and in much larger areas of the phase diagram [BOP92, EMF93].

general trends

Some general trends can be observed in the phase diagram. Firstly, the system forms CuPc-richer structures when the coverage of CuPc is increased. This can be seen in the change from PTCDA to MBW to M1^{2}1 to MZZ islands with increasing CuPc coverage. Secondly, the system tends towards CuPc-richer or -poorer structures at higher PTCDA coverages. That both, CuPc-poorer and -richer, structures appear with continued deposition of PTCDA is surprising since CuPc-poorer structure are expected at higher PTCDA coverages. PTCDA islands and then PTCDA and MBW islands grow when PTCDA is deposited on a submonolayer film of CuPc which is marked by the red line in Fig. 6.33. An example, where the growth of the MBW phase turns into a growth of the MBW and the PTCDA phase with increasing PTCDA coverage, is marked by the green line in Fig. 6.33.

model

A model, which can explain the structure of the phase diagram, is developed on the next few pages. It was already shown in sections 6.2.2.2 and 6.2.2.3 that the phases are determined by the local density of CuPc in the disordered phase. This turns out to be indeed the defining parameter. Other possible models are disproved in the discussion in order to comprehensively understand the phase diagram and its origin.

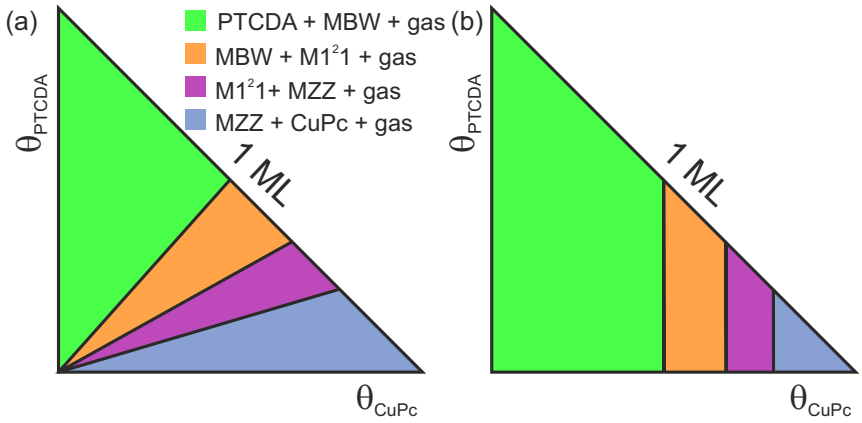

Fig. 6.34: The resulting phase diagrams from hypotheses 1 (a) and 2 (b).

hypothesis 1: ratio of molecules important

The first hypothesis is based on the assumption that the ratio of the two molecules determines which phase is found. This would in principle result in a phase diagram shown in Fig. 6.34 (a). The lines mark borders between different zones, which are colored according to the phases present there, and run from the origin to the 1 ML-line. The slope, s, of the lines is given by the relative area covered by PTCDA molecules within the unit cell of the heteromolecular phase i derivation

$$s_{\mathrm{i}} = \frac{A_{\mathrm{PTCDA}} \cdot \#_{\mathrm{PTCDA},i}}{A_i}$$

with $\#_{\mathrm{PTCDA},i}$ being the number of PTCDA molecules within the unit cell of phase i, and A_{PTCDA} and A_i being the size of a PTCDA molecule and the size of the unit cell of the heteromolecular phase i, respectively. This leads to

$$s_{\mathrm{MBW}} = 0.532 \quad s_{\mathrm{M1^21}} = 0.358 \quad s_{\mathrm{MZZ}} = 0.230$$

for the studied system.

On these lines, only the specified heteromolecular phase grows. A mixture of different heteromolecular phases grows at coverages that deviate from these lines. The lines cross the 1 ML-line where a complete coverage of one heteromolecular phase is expected. This model at the 1 ML-line is identical to the phase diagram at low temperatures of an intermetallic compound [Sau95]. description

Comparing this model with the experimentally obtained phase diagram (Fig. 6.33) shows that it describes the data well at high total coverages but deviates strongly from it at low coverages. This shows that the model developed for the intermetallic compound is only applicable for the studied system at monolayer coverages. A different approach is necessary to describe the data at low coverages. fits at high coverages

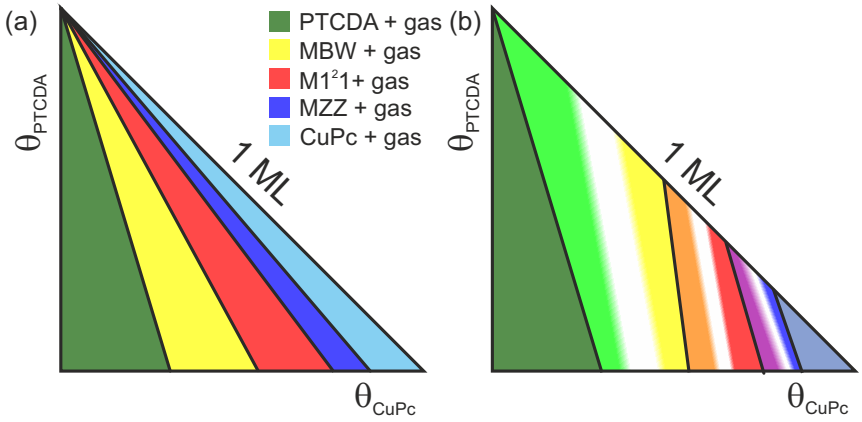

Fig. 6.35: The resulting phase diagrams from hypotheses 3 (a) and 4 (b). The color code of (a) is given in the image while the same color code as in Fig. 6.34 is used in (b).

hypothesis 2: initial coverage of CuPc important

The second hypothesis is that the initial coverage of CuPc determines which phase is present. This leads to vertical lines in the phase diagram, as is sketched in Fig. 6.34 (b).

description These vertical lines correspond to the CuPc coverage where only one heteromolecular phase grows and they intersect the 1 ML-line at the same positions as hypothesis 1. A mixture of two crystalline phases grows between those lines, as is indicated by the colors.

fits at high θ_{CuPc} It shows a relatively good agreement with the data at high total coverages. This is not surprising since it is similar to hypothesis 1 in this area. It also agrees nicely with the data at high CuPc coverages but it cannot explain why the growth of M1^{2}1 islands turns into a growth of M1^{2}1 and MZZ islands when PTCDA is deposited on a submonolayer film of CuPc (marked by the yellow line in Fig. 6.33) or why there are large areas with only one crystalline structure. There is also a big discrepancy between the model and the data at low CuPc concentrations. This model reflects the general trend that with increasing CuPc coverages more CuPc-rich phases grow, but it cannot explain the large areas of the phase diagram.

initial PTCDA coverage It is noted in this contest that the hypothesis that the initial coverage of PTCDA determines the phase is not realistic, since it would lead to horizontal lines in the phase diagram, which does not describe any part of it.

hypothesis 3: density of CuPc on surface important

The third hypothesis is that the density of CuPc on the surface is important. Only phase i is present in a certain CuPc density range, as was the case at low PTCDA coverages discussed in section 6.2.1.1.

derivation

Imagine that PTCDA molecules are deposited on a surface that is already covered by a submonolayer film of CuPc. The PTCDA molecules now take up space on the surface and compress the disordered CuPc gas phase increasing its density. This leads to the formation of different crystalline phases at higher PTCDA coverages. The coverages θ and the areas A are both measured in units of ML since they both give the fraction of the surface that is covered. This allows the substitution of areas by coverages in the formulas on the next few pages. The density of CuPc on the surface is calculated by

$$\rho_{\mathrm{CuPc}} = \frac{\theta_{\mathrm{CuPc}}}{A_{\text{not PTCDA}}} = \frac{\theta_{\mathrm{CuPc}}}{1\ \mathrm{ML} - \theta_{\mathrm{PTCDA}}} \tag{6.2}$$

and gives the amount of CuPc on "their" space on the surface. The unit of this equation does not give a density but it can be converted into one by using the size of the unit cell of the 1.0 ML structure of CuPc resulting in the factor 0.52 molecules/nm^2. This factor is omitted in all equations in this section for readability. The use of coverages instead of densities was chosen since it makes it easier to compare the values given in the equations to the phase diagram which gives the coverages of the molecules and not the densities. It is proposed that a certain critical density of CuPc, $\rho_{\mathrm{CuPc,\ crit}_i}$, is necessary for the formation of phase i. The index i obtains the "values" i = PTCDA, MBW, M1^{2}1, MZZ, CuPc, which also defines the sequence of the structures occurring with increasing CuPc density. The equation

$$\theta_{\mathrm{PTCDA}}\left(\theta_{\mathrm{CuPc}}\right) = 1\ \mathrm{ML} - \frac{1}{\rho_{\mathrm{CuPc,\ crit}_i}}\theta_{\mathrm{CuPc}} \tag{6.3}$$

follows from equation (6.2) which can be drawn easily in the phase diagram. The values for the critical densities taken from the experimental data are

$$\rho_{\mathrm{CuPc,\ crit}_{\mathrm{MBW}}} = 0.27\ \mathrm{ML} \quad \rho_{\mathrm{CuPc,\ crit}_{\mathrm{M1^21}}} = 0.55\ \mathrm{ML}$$

$$\rho_{\mathrm{CuPc,\ crit}_{\mathrm{MZZ}}} = 0.75\ \mathrm{ML} \quad \rho_{\mathrm{CuPc,\ crit}_{\mathrm{CuPc}}} = 0.85\ \mathrm{ML}.$$

description

A sketch of the proposed phase diagram can be seen in Fig. 6.35 (a). The lines i and $i+1$ border areas where the all islands are of phase i. A mixture of the phases $i-1$ and i are present on the line i.

fits at low θ_{PTCDA}

This model describes nicely the data at low PTCDA coverages. Especially, the line between the zone, where only PTCDA islands and that where PTCDA and MBW islands are present, fits well to the model even if the model requires the presence of the pure MBW phase instead of a coexistence of the MBW and PTCDA phase. But the model deviates strongly from the data at higher CuPc coverages and high total coverages. The 1 ML-line in the model should only consist of the MZZ phase and

the homomolecular CuPc phase according to this model which does not represent the data at all.

hypothesis 4: local density of CuPc in gas-like phase important

The fourth hypothesis is that the local CuPc density in the disordered gas-like phase and not the overall density of CuPc on the surface is important. The difference to hypothesis 3 is that not only a global PTCDA coverage is taken into account in the calculation of the CuPc density but the area and the composition of all crystalline phases, which are present, is explicitly considered.

derivation Imagine that CuPc is deposited on a surface that is already covered by a certain amount of PTCDA islands. The CuPc density in the areas not covered by PTCDA islands increases, when the CuPc deposition is started, until the density reaches a critical value. The MBW phase starts to grow then by the detachment of PTCDA molecules from PTCDA islands and the formation of heteromolecular islands with these PTCDA molecules together with the formerly diffusing CuPc molecules. This continues until all PTCDA islands have disappeared and only MBW islands are present. The CuPc density in the gas-like phase increase again at this point. Islands of the M1^{2}1 phase start to grow once a critical CuPc density in the gas-like phase is reached between the MBW islands. It should be stressed again that the consideration of not only the size of the PTCDA islands but also the coverage (and the composition) of phase i that is present when islands of the phase $i+1$ start to nucleate is the difference to hypothesis 3. The density of CuPc in the gas-like phase is defined as

$$\rho_{\text{CuPc, gas}} = \frac{\theta_{\text{CuPc, gas}}}{A_{\text{gas}}}. \tag{6.4}$$

$\theta_{\text{CuPc, gas}}$ is the amount of CuPc molecules that are in the gas-like phase. A_{gas} is the area covered by the gas-like phase which is given by $A_{\text{gas}} = A_{\text{total}} - A_{i-1}$. Only the area of phase $i-1$ has to be taken into account for the nucleation of phase i since it is the only one present at that point and has reached its maximal coverage there since all PTCDA molecules are built into islands of phase i. It is neglected that some PTCDA molecules are solved in the gas-like phase. The maximal area covered by phase $i-1$ islands, A_{i-1}, is determined by the initial coverage of PTCDA and depends on the coverage of PTCDA in the following way

$$A_{i-1} = A_{\text{PTCDA}} + A_{\text{CuPc},i-1} \tag{6.5}$$

where $A_{\text{PTCDA}} = \theta_{\text{PTCDA}}$ and $A_{\text{CuPc},i-1}$ is the surface area obtained by CuPc molecules that are build in the crystalline phase $i-1$, which depends on the structure of the phase and the initial coverages of PTCDA:

$$\theta_{\text{CuPc},i-1} = \theta_{\text{PTCDA}} \cdot \frac{\%_{\text{CuPc}(i-1)}}{\%_{\text{PTCDA}(i-1)}} \tag{6.6}$$

where $\%_{\text{CuPc}(i)\text{ or PTCDA}(i)}$ is the percentage of area covered by CuPc or PTCDA in the unit cell of phase i. An area of 191.8 Å^2 is assumed for the size of the individual CuPc molecule, which is equal to the unit cell size of the 1.0 ML structure on

Ag(111) [KSS+10], and 119.4 Å^2 for a PTCDA molecule which is half of its unit cell size on Ag(111) [Tau07]. The sizes of the heteromolecular unit cells are taken from [Sta13] which are given in the beginning of section 6.2. This gives an area of

$$A_{\text{gas}} = A_{\text{total}} - A_{i-1} = 1\ \text{ML} - \theta_{\text{PTCDA}} \cdot \left(1 + \frac{\%_{\text{CuPc}(i-1)}}{\%_{\text{PTCDA}(i-1)}}\right) \tag{6.7}$$

which is not covered by islands of phase $i-1$ when all PTCDA molecules are build in phase $i-1$ and phase i can start to grow. The amount of diffusing CuPc molecules in the gas-like phase can by calculated with

$$\theta_{\text{CuPc, gas}} = \theta_{\text{CuPc}} - \theta_{\text{CuPc},i-1}. \tag{6.8}$$

This give a final equation of

$$\theta_{\text{PTCDA}}\left(\theta_{\text{CuPc}}\right) = \frac{1\ \text{ML} - \frac{1}{\rho_{\text{CuPc, crit}_i}}\theta_{\text{CuPc}}}{1 + \frac{\%_{\text{CuPc},i-1}}{\%_{\text{PTCDA},i-1}}\left(1 - \frac{1}{\rho_{\text{CuPc, crit}_i}}\right)}. \tag{6.9}$$

This equation results in lines with a positive slope through the previously determined points on the 1 ML-line. The critical densities for the three heteromolecular phases can be obtained by fitting the lines to the data which is discussed later.

description

The resulting phase diagram is shown in Fig. 6.35 (b). Only islands of phase $i-1$ exist under the line, given by equation (6.9), at lower CuPc coverages, as indicated by the colors in Fig. 6.35 (b). A mixture of the heteromolecular phases $i-1$ and i exists above the lines and at higher CuPc coverages since islands of phase $i-1$ are transformed into phase i islands.

fits to data

It can be seen that the model describes the transitions from zones where only one crystalline phase exists to zones where two crystalline phases exist with increasing CuPc coverage reasonably well in all areas. There are some discrepancies at higher coverages but they lie within the experimental uncertainties of the measured coverages of PTCDA and CuPc. It can be seen however that there are still some lines missing. They have a positive slope and divide the areas where the system goes from an eutectic zone to a zone with only one crystalline phase with increasing CuPc coverage.

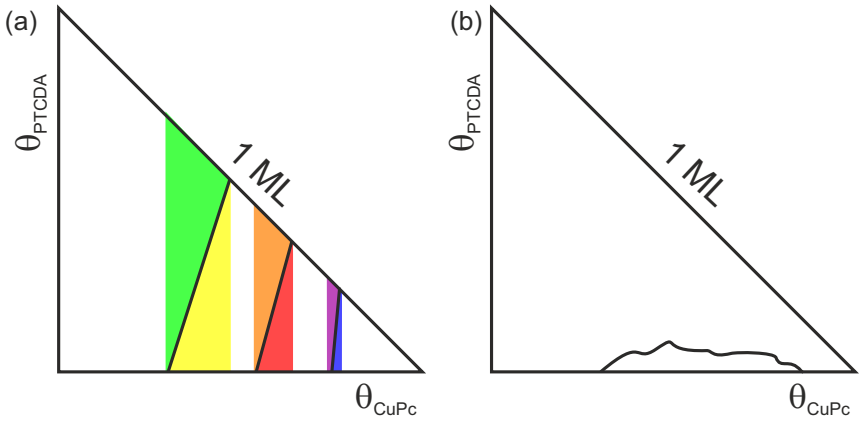

Fig. 6.36: (a) The resulting phase diagrams from hypotheses 5. (b) Sketch of the location of the gas-like-phase-only region.

hypothesis 5: CuPc density in gas-like phase decreases due to growing islands

The case of CuPc deposited on a surface covered with a certain amount of PTCDA was discussed in the last hypothesis. Here, the reversed sequence, the deposition of PTCDA on a submonolayer film of CuPc, is analyzed. Hypothesis 5 is in principle the same as hypothesis 4, in the sense that a certain density of CuPc in the gas-like phase has to be present for the growth of the different phases. But it is discussed as a separate hypothesis since it is analyzed from a different point of view. This differentiation is performed since it simplifies the necessary argumentation to obtain the resulting equations.

derivation Crystalline islands of only one heteromolecular phase grow when PTCDA is deposited on certain submonolayer coverages of CuPc on Ag(111). CuPc molecules are incorporated into these islands decreasing the number of freely diffusing CuPc molecules, $\theta_{\mathrm{CuPc,\,gas}}$. When PTCDA is deposited on a submonolayer film of CuPc, which has a lower CuPc density than the crystalline islands that grow, the density of CuPc in the gas-like phase decreases during the growth of these islands. For example, MBW islands, which have a CuPc density of 45%, grow when PTCDA is deposited on 0.35 ML CuPc. This means that, while the MBW islands grow, the density of CuPc molecules in the gas-like phase decreases until it drops to the critical value $\rho_{\mathrm{CuPc,\,crit_{MBW}}}$. PTCDA island as well as MBW islands start to grow at this point. A transition from the growth of one crystalline structure to two crystalline structures with increasing PTCDA coverage is explained by this. The resulting equation

$$\theta_{\mathrm{PTCDA}}\left(\theta_{\mathrm{CuPc}}\right) = \frac{1\ \mathrm{ML} - \frac{1}{\rho_{\mathrm{CuPc,\,crit}_i}}\theta_{\mathrm{CuPc}}}{1 + \frac{\%_{\mathrm{CuPc},i}}{\%_{\mathrm{PTCDA},i}}\left(1 - \frac{1}{\rho_{\mathrm{CuPc,\,crit}_i}}\right)} \tag{6.10}$$

is the same as equation (6.9) except that some indices shift by 1 since the islands that are present on the surface before the growth of phases $i-1$ and i are of phase i. The value for the critical densities for all heteromolecular structures as well as the CuPc phase can be obtained by fitting equation (6.10) to the data.

description

The resulting phase diagram can be seen in Fig. 6.36 (a). The lines have a positive slope and intersect the 1 ML-line at the same points as in hypotheses 1, 2, and 4. Only islands of one crystalline phase exist under (on the right side of) the lines while a mixture of two phases exists above the lines, as is marked by the colors in Fig. 6.36.

fits to data

These lines describe the lines missing in hypothesis 4 reasonably well within the experimental uncertainties. This shows that both types of lines, which were derived from the assumption that a critical CuPc density in the gas-like phase is crucial for the occurrence of the phases, describe the phase diagram.

final model

The final model is obtained by using both equation (6.9) and (6.10) and determining the optimal critical densities of CuPc in the gas-like phase for the combined equation system from data fitting. The resulting critical densities are

$$\rho_{\mathrm{CuPc,\,crit_{MBW}}} = 0.30 \text{ ML} \quad \rho_{\mathrm{CuPc,\,crit_{M1^21}}} = 0.55 \text{ ML}$$

$$\rho_{\mathrm{CuPc,\,crit_{MZZ}}} = 0.75 \text{ ML} \quad \rho_{\mathrm{CuPc,\,crit_{CuPc}}} = 0.85 \text{ ML}.$$

The values agree nicely with the ones already given in Fig. 6.13. The implications of these different values are discussed later. This fitting procedure results in the theoretical phase diagram which is plotted together with the experimental data in Fig. 6.37. It can be seen that the data is very well described by this model. It should be stressed again that only the four intersection points with the abscissa are fit results; the rest of the model is derived from ab initio assumptions. The intersections with the 1 ML-line come from the analogy of the intermetallic compound, which is also implicitly used in the derivation of the connection lines; that the lines connecting the points on the abscissa and the 1 ML-line are straight lines in turn stems from the assumption that a critical value of the CuPc density in the disordered gas-like phase is the crucial parameter. The very good agreement between the data and the model proves that the local density of CuPc in the gas-like phase determines the phase.

discrepancies

It was already mentioned that there are some discrepancies between the model and the data. The first is that a zone, in which the MBW and M1^{2}1 phase grow, when PTCDA is deposited on a submonolayer film of CuPc, is not found. A new phase with an undefined crystal structure was found there instead. This shows that this phase rather than a mixture of the MBW and M1^{2}1 phases is preferred. A second discrepancy is that the M1^{2}1 phase does not only appear at one point on the 1 ML-line. Both data points (marked by the red arrows in Fig. 6.37) were obtained at complete coverages of the surface and their deviation from the 1 ML-line can be explained by the uncertainty in the determined coverages. This second discrepancy can be explained by the variation in unit cell size for the M1^{2}1 phase since its most densely packed p.o.l. structure is 4% smaller than the commensurate structure.

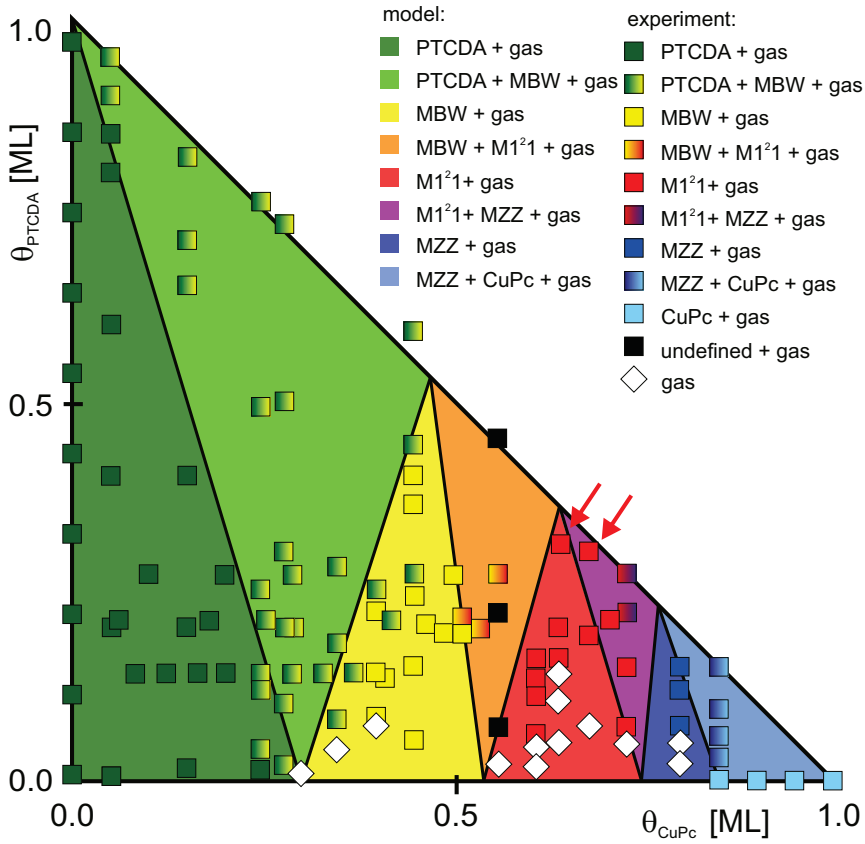

Fig. 6.37: The experimental data points superimposed over the final model of the phase diagram. The colors of the regions indicate the corresponding phases according to the developed model. A very good agreement between the experimental data points and the model can be observed.

repulsion between CuPc explains model

The interaction between the CuPc molecules can be used to explain why the density of CuPc is the defining factor in this system. The CuPc molecules exhibit a repulsive interaction, as was already discussed in section 5.2 and in [KSS+10, SHK+09]. The repulsion increases with increasing density of CuPc on the surface. When PTCDA is deposited on the surface, the CuPc molecules get pushed closer together increasing the repulsion between the CuPc molecules. When a certain density of CuPc is reached, it becomes energetically favorable for the system to form heteromolecular islands which decreases the density of CuPc molecules (or at least slows its increase) in the gas-like phase. Structures with more CuPc in their unit cell grow with increasing CuPc density since this leads to a stronger decrease of the CuPc density in the gas-like phase. A second aspect is that the CuPc molecules can obtain relative positions

to PTCDA within the heteromolecular islands facilitating attractive forces or even hydrogen bonding, which reduces the energy of the system significantly. These two processes can explain the phase diagram. It seems to be a battle between the entropy, which prefers the gas phase, and the mentioned energetic effects which reduce the inner energy and prefer the formation of islands.

interpretation of $\rho_{crit,i}$

The critical CuPc densities already give an idea of the relative strength of competing forces for the phase formation. An increase in the critical density could mean that the binding energy of the CuPc-richer phases is smaller since a higher repulsion between the CuPc molecules is necessary to make the crystallization energetically preferable. This agrees with the fact that CuPc-richer structures, which have a higher critical CuPc density, only grow at higher CuPc concentrations indicating that the binding energy gain in these structures is indeed smaller than, for example, in the MBW phase. They would otherwise already grow at lower CuPc densities since they would decrease the CuPc density in the gas-like phase more effectively than in the case of pure MBW island growth. A thorough quantitative description of the thermodynamic quantities, in particular the entropy and the inner energy, is still lacking and would lead to a better idea of the competing forces in the system.

gas-like-phase-only zones

There is still one part left of the experimental phase diagram that is not yet explained.

location and shape

It is located at CuPc concentration between 0.3 ML and 0.85 ML and at PTCDA coverages below 0.15 ML and indicated by the white diamonds in Fig. 6.37 and it is sketched in Fig. 6.36 (b). Only the disordered gas-like phase is present there. It can be seen that the necessary density of PTCDA for the nucleation of crystalline islands varies with the density of CuPc molecules. The exact relation between these two seems to be complicated since no clear trend can be observed in the measured data points. More experiments are necessary to draw definite conclusions about the correlation of the two quantities.

thermodynamic equilibrium

When PTCDA is deposited on a submonolayer film of CuPc in this coverage regime, the nucleation of islands does not occur immediately. It takes different amounts of PTCDA to start the nucleation of heteromolecular islands. The delay in nucleation is not because the system is not in thermodynamic equilibrium since the islands do not suddenly start to grow when the deposition is stopped at these low PTCDA concentrations and also not at after a long time. The presence of only the gas-like phase was also found at higher temperatures of 450 K when CuPc is deposited on a submonolayer film of PTCDA, see section 6.2.2.1. This also indicates that it is indeed a true phase of the system at these coverages and not an consequence of the experimental procedure. The "ultimate" proof would be the complete disappearance of PTCDA islands when CuPc is deposited on a surface covered by 0.07 ML of such islands. Unfortunately, this experiment was not performed.

small heteromolecular binding energy

Although this gas-like phase is not completely understood yet, it can be concluded from its existence up to PTCDA coverages of 0.15 ML that the binding energy gain by the formation of islands is overcompensated by the increased entropy in the gas-like phase. This indicates that the binding energy in the heteromolecular islands is lower than that between PTCDA molecules in their homomolecular islands since they already nucleate at much lower coverages. The driving force for the formation of the heteromolecular phases is therefore the interplay of energetic aspects and entropy of all different phases on the entire sample.

analogy: chemical solution of two materials

model system

The described system is similar to a solution of two substances in a solvent. The two substances A and B represent the molecule types PTCDA and CuPc. The solvent acts in place of the substrate and enables the motion of the two substances. The reaction

$$A + B \rightleftharpoons A_x B_y$$

represents the formation of heteromolecular islands and takes place in the solution.

solubility

Material A has a very low solubility leading to the formation of clusters of A in the solution just like PTCDA forms islands on the surface. Material B can get dissolved in the solvent up to very high concentrations just like the formation of a CuPc gas phase on the Ag(111) substrate. One assumption, which has to be made in order to continue this analogy, is that the solubility of A increases when there is already material B in the solvent. This describes the solution of up to 0.15 ML of PTCDA in the CuPc gas phase. Crystalline A_xB_y clusters appear only if no more of material A can be dissolved. This is analogous to the nucleation of heteromolecular islands at certain high enough PTCDA coverages.

different perspective

This analogy can describe the investigated PTCDA-CuPc system well but it does not give an explanation why the solubility of PTCDA is of a certain degree and why it is higher at higher CuPc coverages. It is given here to give a different view on the system.

6.2.3.2 Temperature-driven phase transition

This section deals with the influence of the temperature on the occurrence of the crystalline phases of the binary PTCDA-CuPc system. It was discussed in section 6.2.1 that two different heteromolecular structures grow when PTCDA is deposited at different temperatures on the same amount of CuPc. It is shown that the sample can be transformed from one of these stages into the other by changing the temperature after the deposition and that this phase transition is reversible. Possible reasons for this phase transition are also discussed.

heating and cooling

PTCDA is deposited on a 0.61 ML CuPc film on Ag(111) at 360 K. The MBW phase grows at this CuPc coverage and this temperature which can be seen as the large slightly brighter areas in Fig. 6.38 (a). These are the same islands the growth of which was shown in Fig. 6.23. The sample was heated first to 405 K and then to 640 K, as is discussed in the next two paragraphs.

reversibility

The sample is heated to 405 K after the deposition was stopped. The MBW islands (yellow arrows) start to dissolve during the heating process while small PTCDA islands (green arrows) appear at 375 K (Fig. 6.38 (b)). The PTCDA islands disappear and the MBW islands grow again when the sample is cooled down to 365 K, as can be seen in Fig. 6.38 (c). The complete disappearance of PTCDA islands and reappearance of MBW islands in the first heating/cooling step shows that the phase transition between the MBW and the PTCDA phase is reversible. It is assumed that this reversibility is also true for the other phases.

non-reversibility due to desoption of molecules

The sample is heated to 640 K in the next step. The MBW islands disappear again, as can be seen in Fig. 6.38 (d) and all MBW islands are gone at 460 K (Fig. 6.38 (e)). The area covered by PTCDA islands increases continuously during this time. The PTCDA islands start to disappear at temperatures above 505 K until they are all gone at 635 K (Fig. 6.38 (f)). The sample is cooled down again and PTCDA islands start to reappear at 605 K. This discrepancy of the last two temperatures could be explained by the high heating and cooling rates which lead to a difference in the measured and the actual temperature. Another explanation might be that some molecules desorbed at this high temperature leading to different coverages before and after the heating process which would influence the transition temperatures. More PTCDA islands nucleate and the existing islands grow while cooling down further (Fig. 6.38 (g)). The shape of the islands is different in Fig. 6.38 (g)-(i) compared to Fig. 6.38 (a)-(f) due to this change of position and also kinetic effects. The MBW islands start to appear again at 430 K. Again, there is a temperature difference of 30 K between the complete disappearance and the reappearance of the MBW islands probably for the same reasons as for the PTCDA islands. The MBW islands grow while the PTCDA islands shrink while the system cools down. The surface at 410 K can be seen in Fig. 6.38 (h) which shows PTCDA islands and MBW islands. Some PTCDA islands that were present in Fig. 6.38 (g) are no longer present while large MBW islands have reappeared. An image of the surface after reaching the initial temperature of 360 K can be seen in Fig. 6.38 (i). It shows clear differences in the coverages of PTCDA and MBW compared to Fig. 6.38 (a). The PTCDA islands are now still present at this

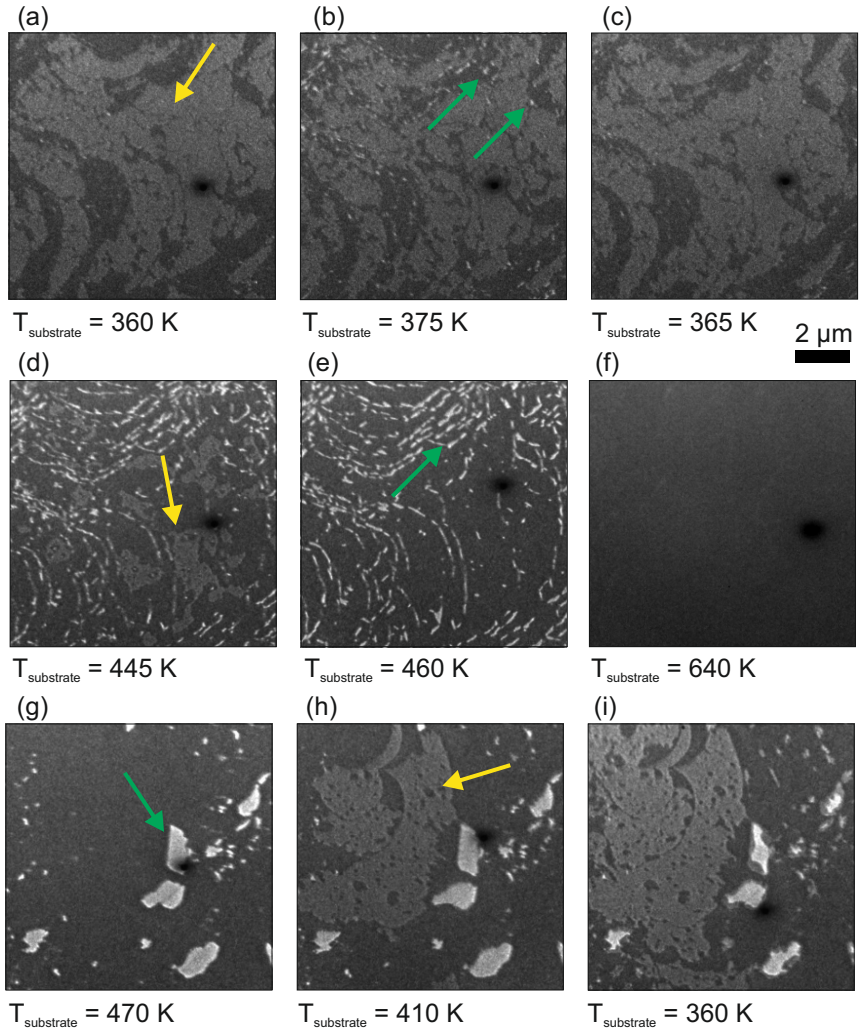

Fig. 6.38: LEEM images taken during the heating and cooling of a sample with 0.61 ML CuPc and 0.40 ML PTCDA. The PTCDA islands (green arrows), the MBW islands (yellow arrows), and the gas-like phase exhibit a bright, a medium, and a dark contrast,respectively. The MBW islands disappear and PTCDA island appear when the sample is heated. This transition is reversible as long as the temperature stays below the desorption temperature of the molecules. The dark spot in all images is a defect on the channel plate. ($U_{\mathrm{start}} = 2.0\,\mathrm{V}$)

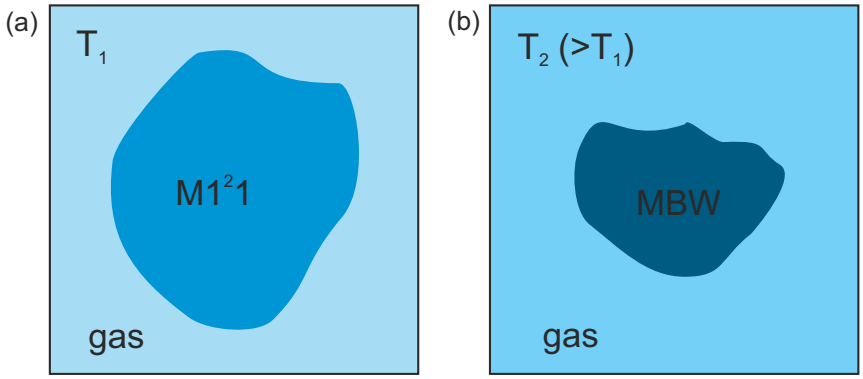

Fig. 6.39: Schematics of the heteromolecular phases occurring at the same coverages of CuPc and PTCDA at different temperatures. (a) The M1^{2}1 structure is present at lower temperatures (b) while the MBW phase is present at higher temperatures. Both islands are surrounded by a disordered gas-like phase.

temperature. This is not an effect of the difference in the measured and the actual temperature of the sample since the sample was kept at this temperature for a long time. This proves that molecules have desorbed from the surface during the heating process to 640 K, since the phase transformation was reversible when the sample was only heated up by 12 K (compare Fig. 6.38 (a)-(c)).

influence of entropy

It can be seen in Fig. 6.12 and Fig. 6.23 in section 6.2.1 that different structures grow when PTCDA is deposited at different temperatures on a sample covered with the same amount of CuPc. A sketch of the system when the same amount of PTCDA is deposited on the same amount of CuPc at different temperatures is shown in Fig. 6.39. It is illustrated that the area of the crystalline islands is smaller when the MBW is formed compared to that when the M1^{2}1 is present. This is clear since the same amount of PTCDA creates a bigger island when it is combined with more CuPc, as is the case for the M1^{2}1 structure. That entropy can play an important role in the temperature dependence of structures was already shown in section 5.2.1 [Ons49]. The entropy can also contribute to the understanding of the temperature-driven phase transition here. The entropy for both crystalline islands is very small and can be neglected.

entropy of gas-like phase

The entropy of the gas-like phase seems to be important though. When the M1^{2}1 phase forms at 300 K, the density of CuPc in the M1^{2}1 islands is very similar to that in the gas-like phase. This leads to a similar density in the gas-like phase before and after the island has grown. When the temperature is increased, the MBW structure is formed (either directly or by a phase transformation of the M1^{2}1 phase). The density of CuPc in the MBW phase is smaller than in the gas-like phase before the deposition of PTCDA. This means that more CuPc molecules are now free to diffuse in the gas-like phase, which also has a larger area available than at lower temperatures, where

the M1^{2}1 phase exists. Hence, the entropy of a system where more CuPc molecules form a gas-like phase that is spread over a larger surface area has to be quantified.

orientational entropy

The orientational entropy is the same for all diffusing molecules in the two systems since it is essentially independent of the density. This means that it increases with the number of molecules in the gas-like phase leading to a higher entropy in the MBW case since there are more diffusing CuPc molecules there:

$$S_{\text{orient., gas-like, MBW}} > S_{\text{orient., gas-like, M1}^2\text{1}}$$

This points to a preference for the MBW phase at higher temperatures.

positional entropy

The positional entropy for each molecule decreases with increasing molecular density since the individual molecules have less space to move. Hence, the positional entropy of one individual molecule is larger in the case of the M1^{2}1 phase since the molecular density of the gas-like phase is lower. However, this higher entropy per molecule is compensated by the lower number of molecules. It can therefore be assumed that the positional entropy is simmilar in both cases:

$$S_{\text{pos., gas-like, MBW}} \approx S_{\text{pos., gas-like, M1}^2\text{1}},$$

although no definite conclusions can be drawn since the relative strength of the positional entropies are not known for the two systems.

experimental consideration

The Gibbs free energies of the two systems should have a similar trend as shown in Fig. 5.10 in section 5.2.1. The curves of the p.o.l. and the commensurate system correspond to the MBW and the M1^{2}1 system, respectively, since it is known from the experiment that the MBW phase is preferred at higher temperatures. The influence of the pressure term in the Gibbs free energy is neglected for the system just as in the case of CuPc on Ag(111). This is a strong assumption since it is unclear if the temperature influences the pressure in this studied system. But assuming that it is justified, it allows the conclusion that the total entropy of the MBW system has to be higher than that of the M1^{2}1 system, to explain the observed occurrence of the two phases at different temperatures. This means that the orientational entropy term (rather than the positional entropy) is the dominant one, and hence responsible for the entropy-driven phase transition from the MBW to the M1^{2}1 phase.

6.2.3.3 Activation energy for MBW nucleation

This section deals with the influence of the temperature on the critical CuPc density for the formation of the MBW structure. The observation that the critical CuPc density increases with the temperature was already discussed in chapter 6.2.2. A quantitative analysis of this is given in this section.

prediction

Many processes are temperature activated. This means that they can usually be described by the relation

$$x = x_0 \cdot e^{-\frac{E_x}{k_B T}}, \tag{6.11}$$

where x is the observable, x_0 the pre-exponential factor, and E_x the activation energy of the investigated process. Diffusion on surfaces can be described well by this equation, as was discussed in chapter 3.2 in equation (3.2). The binding energy between molecules can also be determined with an identical formula, as was done in chapter 4.1.1 (equation (3.4)). It is proposed here that the density of CuPc, ρ_{CuPc}, also follows this dependency leading to

$$\rho_{\mathrm{CuPc}} = \rho_{\mathrm{CuPc},\,0} \cdot e^{-\frac{E_{\mathrm{nucleation}}}{k_B T}}. \tag{6.12}$$

The CuPc density in the disordered phase, ρ_{CuPc}, is determined by the coverage of PTCDA and CuPc with

$$\rho_{\mathrm{CuPc}} = \frac{\theta_{\mathrm{CuPc}}}{1\ \mathrm{ML} - \theta_{\mathrm{PTCDA}}}, \tag{6.13}$$

which is the same as equation (6.2) in chapter 6.2.3.1. The activation energy for the nucleation of the MBW phase is $E_{\mathrm{nucleation}}$. A theoretical model that derives equation (6.12) is necessary to determine the different contributions to this energy.

experiments

Many experiments were performed at different temperatures to investigate if this equation is fulfilled. The deposition order of PTCDA and CuPc was varied to make sure that the results do not depend on any kinetic effects. PTCDA was deposited first in 29 experiments while CuPc was deposited first in 4 experiments. The experiments were performed over a time period of more than 2.5 years. Furthermore, different Ag(111) crystals on different sample holders were used which creates a relatively high uncertainty on the temperature of at least 5 K at low temperatures and 10 K at higher temperatures. Different deposition rates were also used, some of which were very high (0.10 ML/min), giving an additional uncertainty on the CuPc coverage at the point of nucleation of the MBW phase since it occurs very quickly in this case. It was already explained that the uncertainty on the deposition rate of CuPc is around 10% and only 3% for the PTCDA coverage.

temperature dependence

The results of the experiments can be seen in Fig. 6.40 where the (natural) logarithm of ρ_{CuPc} at the time of the nucleation of the MBW phase is plotted versus the inverse of the substrate temperature in an Arrhenius-type diagram. It can be seen that the data scatters strongly as expected from the discussion in the previous paragraph. This strong scattering makes it difficult to decide if a linear fit really describes the data well. A line is fitted nevertheless to the data to determined the nucleation energy.

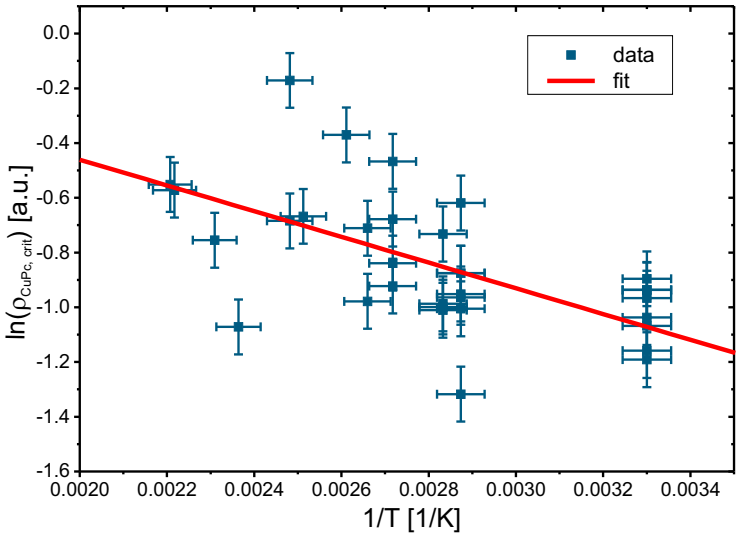

Fig. 6.40: Arrhenius-type plot of the density of CuPc during the first nucleation of the MBW phase. A line is fitted to the data resulting in an activation energy of $E_{\text{nucleation}} = 40 \pm 5\,\text{meV}$.

nucleation energy

The line has a slope of $-470 \pm 58\,\text{K}^{-1}$ and the intersect with the y-axis is 0.48 ± 0.17. This results in an activation energy of $E_{\text{nucleation}} = 40 \pm 5\,\text{meV}$. The uncertainty on this energy is only 13% although the data scatters strongly which is due to the large number of data points. This activation energy is very low compared to the binding energy between the PTCDA molecules on Cu(001) of 1.6 eV. A detailed comparison between the two energies is impossible since the exact contributions to the activation energy are unknown so far. It can still be said that this difference in the energies is the expected result. It was discussed in section 6.2.3.1 that the interaction energies between PTCDA and CuPc must be smaller since the PTCDA and the CuPc molecules only form MBW islands at sufficiently high coverages on Ag(111) in contrast to PTCDA islands that already form at very low coverages on Cu(001) and Ag(111). Although it is still unclear what the contributions to the activation energy are, the first step towards an understanding of the complex nucleation behavior of binary systems on a surface is made.

theoretical model

As it was already mentioned for the last two sections, theoretical work is necessary here as well to understand better the influence of the temperature on the system. A strict derivation of a relation between the critical CuPc density and the temperature would allow the determination of the energies that are responsible for the formation of heteromolecular islands.

7 Summary

A systematic study of the growth of a heteromolecular adsorbate system in the submonolayer regime is presented in this work. The properties of such systems are determined by the interplay between molecule-substrate and molecule-molecule interactions, and hence a careful selection of molecule on the one hand, and substrates on the other hand is essential. The molecules PTCDA and CuPc were chosen as adsorbates since they represent a donor-acceptor model system for organic electronics. Their intermolecular interaction is very different in the homomolecular phases with an attraction between PTCDA molecules and a mostly repulsive interaction in the case of CuPc. Consequently, these molecules form compact islands (PTCDA) or a dilute disordered gas-like phase (CuPc) which enables fundamentally different ways of preparing the heteromolecular films. Two different substrates, which were employed to investigate the influence of the metal-molecule interaction on the growth, are Ag(111) and Cu(001).

phase diagramm

The phase diagram of the heteromolecular PTCDA-CuPc system on Ag(111) at 300 K is the key finding in this work and is discussed in chapter 6.2.3.1. It contains eight different regions with one or two different crystalline phases which coexist with areas of a disordered phase of both molecules. Only the disordered phase is present on the surface in a ninth region. It is found that the local density of CuPc in the disordered phase is the decisive parameter for the occurrence of the different phases. Different phases exist when certain critical values of the CuPc density are exceeded. A number of other investigations have also been performed and most of their results are essential for the understanding of this phase diagram since its shape is determined by a complex interplay between different forces.

Homomolecular systems

The growth of the homomolecular systems is studied in the first part of this work since it is impossible to understand the growth processes of heteromolecular systems without first understanding the growth of the respective homomolecular systems. Detailed analyses were performed to determined the interaction between the molecules and the molecules and the substrate.

PTCDA: attraction

The attractive intermolecular interaction dominates the growth of PTCDA leading to the growth of crystalline islands already at very low coverages on both metal substrates.

binding energy

The island size distribution and the island density are used to quantitatively determine the binding energy between the molecules on Cu(001) to be 1.6 eV which is the energy required to detach one molecules from a molecular cluster. This high binding

energy can be explained by the strong hydrogen bonds which form between the three oxygen atoms at each anhydride end of the PTCDA molecule and the hydrogen atoms located at PTCDA's perylene backbone. This strong binding leads to the formation of only one crystalline structure in the whole submonolayer regime and a low concentration of diffusing PTCDA molecules between the PTCDA islands.

growth dynamics

The growth dynamics of PTCDA islands are analyzed for both substrates. The growth and the nucleation of islands is strongly influenced by the available flux of PTCDA molecules to the growth fronts of the islands. New islands are found to nucleate when there are no growth fronts of existing islands in the vicinity since this leads to an increase in the density of the diffusing molecules.

CuPc: repulsion

The weakly repulsive interaction between CuPc molecules leads to a very different growth behavior.

different phases

Many different phases exist for CuPc in the submonolayer regime. A disordered gas-like phase is present at CuPc coverage below 0.8 ML. Islands of different crystalline structures start to grow at higher coverages on each substrate. The first crystalline structure transforms without any intermediate phases into a second crystalline structure which changes continuously into a third structure on Cu(001). The different types of phase transitions and the multitude of different structures are explained by the interplay between the entropy, the molecular repulsion and the interaction between the molecules and substrate.

growth dynamics

The growth dynamics of the CuPc islands on Ag(111) are also studied in detail. The nucleation at step edges and the almost isotropic growth of the islands afterwards, independent of existing step edges, is discussed. It is found that the domain boundaries between the islands change strongly during, and shortly after, the deposition which is explained by the weak intermolecular and molecule-substrate interaction.

entropy-driven phase transition

CuPc islands start to grow only at high coverages, which means that a high density of diffusing CuPc molecules between the islands is present, in contrast to the growth of PTCDA at comparable temperatures. The crystal structure of the first islands that nucleate changes when the temperature is increased on Ag(111). This phase transition can be explained by the entropy of the disordered phase and the inner energy of the crystalline CuPc islands. It is hence an entropy-driven phase transition which cannot be explained by (binding) energy arguments alone.

Heteromolecular systems

The growth of the heteromolecular PTCDA-CuPc system is studied on Cu(001) and Ag(111) and is discussed in chapter 6. The interplay between the strong binding energy between the PTCDA molecules, which is the dominant factor for the homomolecular PTCDA system, and entropic effects, which play a large role in the growth of CuPc, is investigated.

stronger molecule - substrate interaction

The phase formation is strongly influenced by the deposition parameters when PTCDA and CuPc are deposited on Cu(001). Heteromolecular phases only grow when PTCDA is deposited on a submonolayer film of CuPc, while the PTCDA islands remain unchanged when the reverse deposition sequence is employed. This can be explained

by the strong molecule-molecule interaction within the islands, but also by the molecule-substrate interaction which is very strong on Cu(001). This significant influence of the substrate becomes particularly clear in comparison with the adsorption on Ag(111) as discussed below.

heteromolecular phases

Two different heteromolecular phases grow when PTCDA is deposited on CuPc coverage above 0.40 ML on Cu(001). The crystallinity of the film is better when the heteromolecular phases are prepared with a small CuPc surplus on the surface with respect to the stoichiometry on their unit cells. This density of CuPc molecules, which is distributed evenly across that surface, allows the formation of heteromolecular phases without the need for strong rearrangement or diffusion of the molecules.

critical CuPc density

Further studies find that the appearance of the different homomolecular and heteromolecular phases depends on the local CuPc density in the disordered phase and not on the ratio of both molecules. But the precise details of the influence of the CuPc density on the occurrence of the phases could not be investigated on Cu(001) since the molecule-substrate interaction is too strong leading to different phases depending on the deposition parameters and not only on the coverages of PTCDA and CuPc as it would be the case in the thermodynamic equilibrium.

weaker molecule - substrate interaction

The deposition experiments are repeated on Ag(111), where the weaker molecule-substrate interaction leads to different growth dynamics. PTCDA islands are transformed into three different heteromolecular phases with increasing CuPc:PTCDA stoichiometry during the deposition of CuPc on a Ag(111) surface that is covered by a submonolayer film of PTCDA. This transformation of PTCDA islands is not achieved on Cu(001) due to the stronger molecule-substrate interaction. It is found that the phases that are present on the surface only depend on the coverages of CuPc and PTCDA and on the temperature and no longer on other deposition parameters such as the deposition sequence or the deposition rates. This shows that the thermodynamically most stable phase is actually formed while the shape of the islands is still influence by kinetic effects.

growth dynamics

The growth dynamics, which are influenced by kinetic effects, are analyzed in detail. Different rates for the diffusion of the individual molecules across step edges are determined by analyzing the growth dynamics of heteromolecular islands such as the growth direction and the nucleation sites. A high mobility of heteromolecular islands is also found and can be explained by the fluxes of the different molecules to the island.

phase diagram

A complex phase diagram is determined in the complete coverage regime up to 1 ML. Its complete form can be explained by an ab-initio model with four fitting parameters. It is based on the model for an intermetallic compound at 1 ML coverages and includes the additional assumption that a critical density of CuPc in the disordered phase for each heteromolecular phase exists. These densities are obtained by fitting the model to the data. The existence of such a critical density of CuPc can be explained by the interplay between the interactions between PTCDA and CuPc molecules and the entropy of the entire system. With increasing CuPc coverage, the systems forms larger islands with a higher CuPc density and a disordered phase with a lower CuPc density instead of keeping the existing islands and increasing the CuPc

density in the disordered phase. The higher entropy in the disordered phase is thus overcompensated by the stronger repulsion between the CuPc molecules making the growth of heteromolecular islands with a higher CuPc density energetically favorable since it decreases the repulsion between the CuPc molecules in the disordered phase.

energy

The critical CuPc density in the disordered phase depends on the temperature. This critical density for the nucleation of the MBW phase is determined for different temperatures and an arrhenius-type plot revealed a nucleation energy for the MBW phase of only 40 eV which is much lower than the binding energy between the PTCDA molecules of 1.6 eV. This is an expected result since the entropy would otherwise not play such a decisive role in the phase formation in the heteromolecular system unlike in the case of the growth of homomolecular PTCDA islands.

relevance

The results of this work are an essential step forward in fundamentally understanding the phase formation of heteromolecular layers. They allow the tuning of the structure of the organic layer in a specific direction by changing the coverages of CuPc and PTCDA on the Ag(111) surface as it is defined in the phase diagram. This shows that understanding the self-assembly of molecules on surfaces enables the selective fabrication of heteromolecular thin films with desired properties which potentially influences the production of commercially used organic layers.

Outlook

Different avenues of investigation should be taken to study this topic further. The studied organic system should be modified and the presented system has to be analyzed from a different perspective by theoretical approaches in order to improve the understanding of such phase diagrams.

modified systems

A different organic system, for which this analysis should be repeated, is necessary to check if the developed model is of general validity. Exchanging CuPc by SnPc is the first logical step since the SnPc-PTCDA system forms almost identical heteromolecular structures on Ag(111) as it was found by current experiments in the institute. SnPc, unlike CuPc, is not a planar molecule with the Sn atom sticking out in an upward or downward direction when it is adsorbed on the Ag(111) surface[LH02]. This changes the interaction between the SnPc molecules and the substrate, which allows the investigation of the influence of a modified substrate-molecule interaction on the phase formation, since the other parameters are almost unchanged. Exchanging PTCDA by the weaker acceptor NTCDA enables the investigation of the influence of the electronic properties on the phase formation since NTCDA has a lower charge affinity than PTCDA. Additionally, more heteromolecular structures exist for this system [Sch15b] creating more regions in the phase digram. The substrate should also be exchanged since it strongly influences the phase formation. Preliminary experiments performed at the institute show that no heteromolecular phases form when PTCDA and CuPc are deposited on Au(111). Going to other substrates helps to determine what properties the substrate has to have to enable the formation of heteromolecular layers. But it should be kept in mind, when choosing the substrate, that the molecule-

substrate interaction has to be weak enough that the thermodynamic equilibrium can be reached.

theoretical approach

A fundamental thermodynamic description of the investigated system is necessary to completely understand the appearance of the different phases at different coverages of PTCDA and CuPc. This includes a basic description of thermodynamic entities such as the entropy and the inner energy. This is expected to allow the quantification of the competing forces on the structure formation. Kinetic Monte Carlo Simulations would help to better understand the kinetic processes occurring during the formation of the structures. The high mobility of the heteromolecular clusters during the deposition or the growth dynamics of the homomolecular and heteromolecular islands could then be explained.

Bibliography

[ACL98] M.S. Altman, W.F. Chung, and C.H. Liu. LEEM phase contrast. *MRS Bulletin*, 5(6):1129, 1998.

[AFL94] Jacques G. Amar, Fereydoon Family, and Pui-Man Lam. Dynamic scaling of the island-size distribution and percolation in a model of submonolayer molecular-beam epitaxy. *Physical Review B*, 50(12):8781, 1994.

[Alt10] M S Altman. Trends in low energy electron microscopy. *Journal of Physics: Condensed Matter*, 22(8):084017, 2010.

[ATNIK08] M. Andreasson, M. Tengelin-Nilsson, L. Ilver, and J. Kanski. Photoelectron spectroscopic studies of ultra-thin CuPc and PTCDA layers on Cu(100). *Synthetic Metals*, 158(1-2):45–49, January 2008.

[Bau14] Ernst Bauer. *Surface Microscopy with Low Energy Electrons*. Springer, 2014.

[BMW+12] Oliver Bauer, Giuseppe Mercurio, Martin Willenbockel, Werner Reckien, Christoph Heinrich Schmitz, Benjamin Fiedler, Serguei Soubatch, Thomas Bredow, Frank Stefan Tautz, and Moritz Sokolowski. Role of functional groups in surface bonding of planar π-conjugated molecules. *Physical Review B*, 86(23):1–11, 2012.

[BOP92] P. Bartlett, R. H. Ottwill, and P. N. Pusey. Superlattice Formation in Binary Mixtures of Hard-Sphere Colloids. *Physical Review Letters*, 68(25):3801–3805, 1992.

[Bru98] H Brune. Microscopic view of epitaxial metal growth: Nucleation and aggregation. *Surface Science Reports*, 31(3-4):125–229, May 1998.

[BTF00] Ma Baldo, Me Thompson, and Sr Forrest. High-efficiency fluorescent organic light-emitting devices using a phosphorescent sensitizer. *Nature*, 403(6771):750–3, 2000.

[BWBM03] C. Bobisch, Th. Wagner, A. Bannani, and R. Möller. Ordered binary monolayer composed of two organic molecules: Copper-phthalocyanine and 3,4,9,10-perylene-tetra-carboxylic-dianhydride on Cu(111). *The Journal of Chemical Physics*, 119(18):9804, 2003.

[CA98] W.F. Chung and M.S. Altman. Step contrast in low energy electron microscopy. *Ultramicroscopy*, 74(4):237–246, September 1998.

[CCMS07] Marcello Campione, Silvia Caprioli, Massimo Moret, and Adele Sassella. Homoepitaxial Growth of α-Hexathiophene. *Journal of Physical Chemistry C*, 111:12741–12746, 2007.

[CHC+08] Wei Chen, Han Huang, Shi Chen, Xing Yu Gao, and Andrew Thye Shen Wee. Low-temperature scanning tunneling microscopy and near-edge X-ray absorption fine structure investigations of molecular orientation of copper(II) phthalocyanine thin films at organic heterojunction interfaces. *Journal of Physical Chemistry C*, 112(13):5036–5042, 2008.

[CMG+12] J L Cabellos, D J Mowbray, E Goiri, L Floreano, D G De Oteyza, C Rogero, J E Ortega, and A Rubio. Understanding Charge Transfer in Donor-Acceptor/Metal Systems: A Combined Theoretical and Experimental Study. *The Jornal of Physical Chemistry C*, 116:17991–18001, 2012.

[CSS+03] L. Chkoda, M. Schneider, V. Shklover, L. Kilian, M. Sokolowski, C. Heske, and E. Umbach. Temperature-dependent morphology and structure of ordered 3,4,9,10-perylene-tetracarboxylicacid-dianhydride (PTCDA) thin films on Ag(111). *Chemical Physics Letters*, 371(5-6):548–552, April 2003.

[DGLC+09] Dimas G. De Oteyza, Juan M. García-Lastra, Martina Corso, Bryan P. Doyle, Luca Floreano, Alberto Morgante, Yutaka Wakayama, Angel Rubio, and J. Enrique Ortega. Customized electronic coupling in self-assembled donor-acceptor nanostructures. *Advanced Functional Materials*, 19(22):3567–3573, 2009.

[DTKT14] Thomas Duden, Andreas Thust, Christian Kumpf, and F. Stefan Tautz. Focal-Series Reconstruction in Low-Energy Electron Microscopy. *Microscopy and Microanalysis*, 20(2):968–973, 2014.

[Ein05] Albert Einstein. Über die von der molekularkinetischen Theorie der Wärme geforderte Bewegung von in ruhenden Flüssigkeiten suspendierten Teilchen. *Annalen der Physik*, 322:549, 1905.

[EMF93] M. D. Eldridge, P. A. Madden, and D. Frenkel. Entropy-driven formation of a superlattice in a hard-sphere binary mixture. *Nature*, 363:35, 1993.

[ES90] D.M. Eigler and E.K. Schweizer. Positioning single atoms with a scanning tunneling microscope. *Nature*, 344:524, 1990.

[ESBG+13] Afaf El-Sayed, Patrizia Borghetti, Elizabeth Goiri, Celia Rogero, Luca Floreano, Giacomo Lovat, Duncan John Mowbray, Jose Luis Cabellos, Yutaka Wakayama, Angel Rubio, Jose Enrique Ortega, and Dimas G de Oteyza. Understanding Energy-Level Alignment in Donor - Acceptor/Metal Interfaces from Core-Level Shifts. *American Chemical Society Nano*, 7(8):6914–6920, 2013.

[EST03] M. Eremtchenko, J. A. Schaefer, and F. S. Tautz. Understanding and tuning the epitaxy of large aromatic adsorbates by molecular design. *Nature*, 425(6958):602, 2003.

[FFG+99] R. H. Friend, R. H. Friend, R. W. Gymer, R. W. Gymer, a. B. Holmes, J. H. Burroughes, a. B. Holmes, J. H. Burroughes, R.N. Marks, C. Taliani, R.N. Marks, D. D. C. Bradley, C. Taliani, D. D. C. Bradley, D. a. Dos Santos, M. Lo, J. L. Bredas, M. Logdlund, W. R Salaneck, W. R. Salaneck, D. a. Dos Santos, J. L. Bre, and V. Slyke. Electroluminescence in conjugated polymers. *Nature*, 397:121–128, 1999.

[FK14] Jan Ingo Flege and Eugene E. Krasovskii. Intensity-voltage low-energy electron microscopy for functional materials characterization. *physica status solidi (RRL)*, 8(6):463–477, 2014.

[FKM+13] Jan Ingo Flege, Björn Kaemena, Axel Meyer, Jens Falta, Sanjaya D. Senanayake, Jerzy T. Sadowski, R. D. Eithiraj, and Eugene E. Krasovskii. Origin of chemical contrast in low-energy electron reflectivity of correlated multivalent oxides: The case of ceria. *Physical Review B*, 88(23):1–7, 2013.

[FM88] Fereydoon Family and Paul Meakin. Scaling of the Droplet-Size Distribution in Vapor-Deposited Thin Films. *Phys Rev Lett*, 61(4):428–432, 1988.

[FM89] Fereydoon Family and Paul Meakin. Kinetics of droplet growth processes: Simulations, theory, and experiments. *Physical Review A*, 40(7):3836–3855, 1989.

[For04] Stephen R Forrest. The path to ubiquitous and low-cost organic electronic appliances on plastic. *Nature*, 428:911–918, 2004.

[Fra14] Markus Franke. Bestimmung der lateralen und vertikalen struktur von kupferphthalocyanin auf cu(001) mit rastertunnelmikroskopie und stehenden röntgenwellenfeldern. Master's thesis, RWTH Aachen University, 2014.

[Fre94] D Frenkel. The simulation of entropic phase transitions. *Journal of Physics: Condensed Matter*, 6(23A):A71–A78, 1994.

[GEW+14] Matthew F B Green, Taner Esat, Christian Wagner, Philipp Leinen, Alexander Grötsch, F Stefan Tautz, and Ruslan Temirov. Patterning a hydrogen-bonded molecular monolayer with a hand-controlled scanning probe microscope. *Beilstein Journal of Nanotechnology*, 5:1926–1932, 2014.

[GFB+14] Stefan Gärtner, Benjamin Fiedler, Oliver Bauer, Antonela Marele, and Moritz M Sokolowski. Lateral ordering of PTCDA on the clean and the oxygen pre-covered Cu(100) surface investigated by scanning tunneling microscopy and low energy electron diffraction. *Beilstein Journal of Organic Chemistry*, 10(100):2055–2064, 2014.

[GMES+13] Elizabeth Goiri, Manfred Matena, Afaf El-Sayed, Jorge Lobo-Checa, Patrizia Borghetti, Celia Rogero, Blanka Detlefs, Julien Duvernay, J Enrique Ortega, and Dimas G de Oteyza. Changes in adsorption heights upon self-assembly of bicomponent supramolecular networks. *arXiv*, 1309.6440:1–15, 2013.

[GMN+00] M Gross, Dc Muller, Hg Nothofer, U Scherf, D Neher, C Brauchle, and K Meerholz. Improving the performance of doped π-conjugated polymers for use in organic light-emitting diodes. *Nature*, 405(6787):661–5, 2000.

[Gro06] Ullrich Groh. *Spektromikroskopische Untersuchungen an organischen Nanostrukturen*. PhD thesis, Julius-Maximilians-UniversitätWürzburg, 2006.

[GSL+00] M C Gerstenberg, F. Schreiber, T. Y. B. Leung, G. Bracco, S.R. Forrest, and G. Scoles. Organic semiconducting thin film growth on an organic substrate: 3,4,9,10-perylenetetracarboxylic dianhydride on a monolayer of decanethiol self-assembled on Au(111). *Physical Review B*, 61(11):7678–7685, 2000.

[GSP+15] Marco Gruenewald, Christoph Sauer, Julia Peuker, Matthias Meissner, Falko Sojka, Achim Schöll, Friedrich Reinert, Roman Forker, and Torsten Fritz. Commensurism at electronically weakly interacting phthalocyanine/PTCDA heterointerfaces. *Physical Review B*, 91(15):1–7, 2015.

[GSS+98] K. Glöckler, C. Seidel, A. Soukopp, M. Sokolowski, E. Umbach, M. Böhringer, R. Berndt, and W. Schneider. Highly ordered structures and submolecular scanning tunnelling microscopy contrast of PTCDA and DM-PBDCI monolayers on Ag (111) and Ag (110). *Surface Science*, 405:1–20, 1998.

[GXS+05] Byron D Gates, Qiaobing Xu, Michael Stewart, Declan Ryan, C Grant Willson, and George M Whitesides. New Approaches to Nanofabrication: Molding, Printing, and Other Techniques. *Chemical Reviews*, 105(4):1171–1196, 2005.

[HFGR+07] I. Horcas, R. Fernandez, J. M. Gomez-Rodriguez, J. Colchero, J. Gomez-Herrero, and A. M. Baro. Wsxm: A software for scanning probe microscopy and a tool for nanotechnology. *Review of Scientific Instruments*, 78:013705, 2007.

[HLWM96] K W Hipps, Xing Lu, X D Wang, and Ursula Mazur. Metal d-Orbital Occupation-Dependent Images in the Scanning Tunneling Microscopy of Metal Phthalocyanines. *Journal of Physical Chemistry*, 100:11207–11210, 1996.

[HPF+08] Gregor Hlawacek, Peter Puschnig, Paul Frank, Adolf Winkler, Claudia Ambrosch-Draxl, and Christian Teichert. Characterization of step-edge barriers in organic thin-film growth. *Science*, 321(5885):108–11, July 2008.

[HTS+10] a. Hauschild, R. Temirov, S. Soubatch, O. Bauer, a. Schöll, B. C C Cowie, T. L. Lee, F. S. Tautz, and M. Sokolowski. Normal-incidence x-ray standing-wave determination of the adsorption geometry of PTCDA on Ag(111): Comparison of the ordered room-temperature and disordered low-temperature phases. *Physical Review B*, 81(12):1–12, 2010.

[KB09] Joseph Kalowekamo and Erin Baker. Estimating the manufacturing cost of purely organic solar cells. *Solar Energy*, 83(8):1224–1231, August 2009.

[KE99] Kentaro Kyuno and Gert Ehrlich. Diffusion and dissociation of platinum clusters on Pt(111). *Surface Science*, 437:29–37, 1999.

[Kel96] G.L. Kellogg. Atomic view of cluster diffusion on metal surfaces. *Progress in Surface Science*, 53(2-4):217–223, 1996.

[Kit93] Charles Kittel. *Einführung in die Festkörperphysik*. R. Oldenbourg Verlag GmbH, München, 10 edition, 1993.

[KLS+09] H. Karacuban, M. Lange, J. Schaffert, O. Weingart, Th Wagner, and R. Möller. Substrate-induced symmetry reduction of CuPc on Cu(1 1 1): An LT-STM study. *Surface Science*, 603(5):L39–L43, 2009.

[Kro10] Ingo Kroeger. *Adsorption von Phthalocyaninen auf Edelmetalloberflächen*. PhD thesis, RWTH Aachen, 2010.

[KSS+10] Ingo Kröger, Benjamin Stadtmüller, Christoph Stadler, Johannes Ziroff, Mario Kochler, Andreas Stahl, Florian Pollinger, Tien-Lin Lee, Jörg Zegenhagen, Friedrich Reinert, and Christian Kumpf. Submonolayer growth of copper-phthalocyanine on Ag(111). *New Journal of Physics*, 12(8):083038, August 2010.

[KSSK14] Christoph Kleimann, Benjamin Stadtmüller, Sonja Schröder, and Christian Kumpf. Electrostatic Interaction and Commensurate Registry at the Heteromolecular F16 CuPc-CuPc Interface. *The Journal of Physical Chemistry C*, 118(3):1652–1660, 2014.

[KSW+11a] Ingo Kröger, Benjamin Stadtmüller, Christian Wagner, Christian Weiss, Ruslan Temirov, F. S. Tautz, and Christian Kumpf. Modeling intermolecular interactions of physisorbed organic molecules using pair potential calculations. *The Journal of Chemical Physics*, 135(23):234703, 2011.

[KSW+11b] Ingo Kröger, Benjamin Stadtmüller, Christian Wagner, Christian Weiss, Ruslan Temirov, F Stefan Tautz, and Christian Kumpf. Modeling intermolecular interactions of physisorbed organic molecules using pair potential calculations. *The Journal of chemical physics*, 135(23):234703, December 2011.

[KUS04] L. Kilian, E. Umbach, and M. Sokolowski. Molecular beam epitaxy of organic films investigated by high resolution low energy electron diffraction (SPA-LEED): 3,4,9,10-perylenetetracarboxylicaciddianhydride (PTCDA) on Ag(111). *Surface Science*, 573(3):359–378, December 2004.

[KUS06] L. Kilian, E. Umbach, and M. Sokolowski. A refined structural analysis of the PTCDA monolayer on the reconstructed Au(111) surface - "Rigid or distorted carpet?". *Surface Science*, 600(13):2633–2643, July 2006.

[LH02] Markus Lackinger and Michael Hietschold. Determining adsorption geometry of individual tin-phthalocyanine molecules on Ag(111) - A STM study at submonolayer coverage. *Surface Science*, 520(1-2), 2002.

[Lub15] Felix Lublasser. Kinetic monte carlo simulations of molecular island growth on metal surfaces. Master's thesis, RWTH Aachen University, 2015.

[Mar06] H. Marchetto. *High-resolution spectro-microscopic investigations*. PhD thesis, Frei Universität Berlin, 2006.

[MGS+06a] H. Marchetto, U. Groh, T. Schmidt, R. Fink, H. Freund, and E. Umbach. Influence of substrate morphology on organic layer growth: PTCDA on Ag(111). *Chemical Physics*, 325(1):178–184, June 2006.

[MGS+06b] H. Marchetto, U. Groh, Th. Schmidt, R. Fink, H.-J. Freund, and E. Umbach. Influence of substrate morphology on organic layer growth: PTCDA on Ag(111). *Chemical Physics*, 325(1):178–184, June 2006.

[MRT01] F.-J. Meyer zu Heringdorf, M. C. Reuter, and R. M. Tromp. Growth dynamics of pentacene thin films. *Nature*, 412(6846):517–20, August 2001.

[MS63] W. W. Mullins and R. F. Sekerka. Morphological Stability of a Particle Growing by Diffusion or Heat Flow. *Journal of Applied Physics*, 34(2):323, 1963.

[MS64] W. W. Mullins and R. F. Sekerka. Stability of a Planar Interface During Solidification of a Dilute Binary Alloy. *Journal of Applied Physics*, 35(2):444, 1964.

[Mul86] W. W. Mullins. The statistical self-similarity hypothesis in grain growth and particle coarsening. *Journal of Applied Physics*, 59(4):1341, 1986.

[OLS+03] K. Oura, V. G. Lifshits, A. A. Saranin, A. V. Zotov, and M. Katayama. *Surface Science - An Introduction*. Springer, 2003.

[Ons49] L Onsager. The effects of shape on the interaction of colloidal particles. *Annals of the New York Academy of Sciences*, 51(4):627–659, 1949.

[PLN+11] T. Potocar, S. Lorbek, D. Nabok, Q. Shen, L. Tumbek, G. Hlawacek, P. Puschnig, C. Ambrosch-Draxl, C. Teichert, and a. Winkler. Initial stages of a para-hexaphenyl film growth on amorphous mica. *Physical Review B*, 83(7):075423, February 2011.

[PS96] Douglas Philp and J Fraser Stoddart. Self-Assembly in Natural and Unnatural Systems. *Angewandte Chemie Internactional Edition Engl.*, 35:1154–1196, 1996.

[RNK+03] Ricardo Ruiz, Bert Nickel, Norbert Koch, Leonard Feldman, Richard Haglund, Antoine Kahn, Fereydoon Family, and Giacinto Scoles. Dynamic Scaling, Island Size Distribution, and Morphology in the Aggregation Regime of Submonolayer Pentacene Films. *Physical Review Letters*, 91(13):136102, September 2003.

[RNP+09] L Romaner, D Nabok, P Puschnig, E Zojer, and C Ambrosch-Draxl. Theoretical study of PTCDA adsorbed on the coinage metal surfaces, Ag(111), Au(111) and Cu(111). *New Journal of Physics*, 11(5):053010, May 2009.

[SA94] T. J. Schuerlein and N. R. Armstrong. Formation and characterization of epitaxial phthalocyanine and perylene monolayers and bilayers on Cu(100): Low-energy electron diffraction and thermal desorption mass spectrometry studies. *Journal of Vacuum Science & Technology A*, 12(4):1992, July 1994.

[SACF+12] Johannes Schindelin, Ignacio Arganda-Carreras, Erwin Frise, Verena Kaynig, Mark Longair, Tobias Pietzsch, Stephan Preibisch, Curtis Rueden, Stephan Saalfeld, Benjamin Schmid, Jean-Yves Tinevez, Daniel James White, Volker Hartenstein, Kevin Eliceiri, Pavel Tomancak, and Albert Cardona. Fiji: an open-source platform for biological-image analysis. *Nature Methods*, 9:676–682, June 2012.

[Sag08] Daniel Sage. Watershed segmentation. `http://bigwww.epfl.ch/sage/soft/watershed`, 2008.

[Sau95] Gerhard Sauthoff. *Intermetallics*. Wiley-VCH, 1995.

[SBF+99] H. Sirringhaus, P. J. Brown, R. H. Friend, M. M. Nielsen, K. Bechgaard, B. M. W. Langeveld-Voss, a. J. H. Spiering, R. a. J. Janssen, E. W. Meijer, P. Herwig, and D. M. de Leeuw. Two-dimensional charge transport in self-organized, high-mobility conjugated polymers. *Nature*, 401(6754):685–688, 1999.

[Sch94] T. J. Schuerlein. Formation and characterization of epitaxial phthalocyanine and perylene monolayers and bilayers on Cu(100): Low-energy electron diffraction and thermal desorption mass spectrometry studies. *Journal of Vacuum Science & Technology A: Vacuum, Surfaces, and Films*, 12(4):1992, July 1994.

[Sch01] A. B. Schofield. Binary hard-sphere crystals with the cesium chloride structure. *Physical Review E*, 64(5 Pt 1):051403, 2001.

[Sch12] Daniel Schwarz. *Visualization of nucleation and growth of supramolecular networks on Cu(001) and Au(111)*. PhD thesis, Universiteit Twente, 2012.

[Sch15a] Kathrin Schönauer. *Structural and electron investigations on homo- and hetero-organic layers involving CuPc on silver single crystal surfaces*. PhD thesis, RWTH Aachen University, 2015.

[Sch15b] Sonja Schröder. *Structural and electronic characterization of hetero-organic NTCDA-CuPc adsorbate systems on Ag(111)*. PhD thesis, RWTH Aachen University, 2015.

[SGE+00] F Schreiber, M C Gerstenberg, B Edinger, B Toperverg, S R Forrest, G Scoles, and H Dosch. Phase-sensitive surface X-ray scattering study of a crystalline organic-organic heterostructure. *Physica B*, 283:75–78, 2000.

[SHD+07] Fei Song, Han Huang, Weidong Dou, Hanjie Zhang, Yunwan Hu, Huiqin Qian, Haiyang Li, Pimo He, Shining Bao, Qiao Chen, and Wuzong Zhou. Electronic structures of CuPc on a Ag(110) surface. *Journal of Physics: Condensed Matter*, 19(13):136002, April 2007.

[SHK+09] Christoph Stadler, Sören Hansen, Ingo Kröger, Christian Kumpf, and Eberhard Umbach. Tuning intermolecular interaction in long-range-ordered submonolayer organic films. *Nature Physics*, 5(2):153–158, 2009.

[SHMH06] B. Stadlober, U. Haas, H. Maresch, and a. Haase. Growth model of pentacene on inorganic and organic dielectrics based on scaling and rate-equation theory. *Physical Review B*, 74(16):165302, October 2006.

[SHS+15] Benjamin Stadtmüller, Caroline Henneke, Serguei Soubatch, F Stefan Tautz, and Christian Kumpf. Tailoring metal-organic hybrid interfaces: heteromolecular structures with varying stoichiometry on Ag(111). *New Journal of Physics*, 17(2):023046, 2015.

[SKF+00] H. Sirringhaus, T. Kawase, R. H. Friend, T. Shimoda, M. Inbasekaran, W. Wu, and E. P. Woo. High-Resolution Inkjet Printing of All-Polymer Transistor Circuits. *Science*, 290:2123, 2000.

[SKKT11] S. Soubatch, I. Köger, C. Kumpf, and F. S. Tautz. Structure and growth of tetracene on Ag(111). *Physical Review B*, 84(19):1–16, 2011.

[SKRK11] Benjamin Stadtmüller, Ingo Kröger, Friedrich Reinert, and Christian Kumpf. Submonolayer growth of CuPc on noble metal surfaces. *Physical Review B*, 83(8):1–10, February 2011.

[SLW+14] Benjamin Stadtmüller, Daniel Lüftner, Martin Willenbockel, Eva M Reinisch, Tomoki Sueyoshi, Georg Koller, Serguei Soubatch, Michael G Ramsey, Peter Puschnig, F Stefan Tautz, and Christian Kumpf. Unexpected interplay of bonding height and energy level alignment at heteromolecular hybrid interfaces. *Nature communications*, 5:3685, January 2014.

[SM14] Johannes Schaffert and Rolf Möller. Heterogeneous organic layers. `https://www.uni-due.de/ag-moeller/heterogelayer.shtml`, 2014. accessed: 2015-02-03.

[SMS+10] C. H. Schwalb, M. Marks, S. Sachs, a. Schöll, F. Reinert, E. Umbach, and U. Höfer. Time-resolved measurements of electron transfer processes at the PTCDA/Ag(111) interface. *The European Physical Journal B*, 75(1):23–30, 2010.

[SPG00] F. Saija, S. Prestipino, and P. V. Giaquinta. Entropy, correlations, and ordering in two dimensions. *Journal of Chemical Physics*, 113(7):2806–2813, 2000.

[SPG+02] T. Schwieger, H. Peisert, M. Golden, M. Knupfer, and J. Fink. Electronic structure of the organic semiconductor copper phthalocyanine and K-CuPc studied using photoemission spectroscopy. *Physical Review B*, 66(15):1–5, 2002.

[SRE12] C.A. Schneider, W.S. Rasband, and K.W. Eliceiri. NIH Image to ImageJ: 25 years of image analysis. *Nature Methods*, 9:671–675, 2012.

[SSB+14] Benjamin Stadtmüller, Sonja Schröder, François C. Bocquet, Caroline Henneke, Christoph Kleimann, Serguei Soubatch, Martin Willenbockel, Blanka Detlefs, Jörg Zegenhagen, Tien-Lin Lee, F. Stefan Tautz, and

Christian Kumpf. Adsorption height alignment at heteromolecular hybrid interfaces. *Physical Review B*, 89(16):161407, April 2014.

[SSCA95] A Schmidt, T J Schuerlein, G E Collins, and N R Armstrong. Ordered Ultrathin Films of Perylenetetracarboxylic Dianhydride (PTCDA) and Dimethylperylenebis(dicarboximide) (Me-PTCDI) on Cu(100): Characterization of Structure and Surface Stoichiometry by LEED, TDMS, and XPS. *Journal of Physical Chemistry*, 99:11770–11779, 1995.

[SSM+09] Sönke Sachs, Christian H. Schwalb, Manuel Marks, Achim Schöll, Friedrich Reinert, Eberhard Umbach, and Ulrich Höfer. Electronic structure at the perylene-tetracarboxylic acid dianhydride/Ag(111) interface studied with two-photon photoelectron spectroscopy. *Journal of Chemical Physics*, 131(14), 2009.

[Sta13] Benjamin Stadtmüller. *Study of intermolecular interactions in heteroorganic thin films*. PhD thesis, RWTH Aachen, 2013.

[STS+00] V Shklover, F S Tautz, R Scholz, S Sloboshanin, M Sokolowski, J a Schaefer, and E Umbach. Differences in vibronic and electronic excitations of PTCDA on Ag(111) and Ag(110). *Surface science*, 456:60–66, 2000.

[SvGZP12a] Daniel Schwarz, Raoul van Gastel, Harold Zandvliet, and Bene Poelsema. Phase transformations of $4,4'-$biphenyldicarboxylic acid on Cu(001). *Physical Review B*, 85(23):1–10, June 2012.

[SvGZP12b] Daniel Schwarz, Raoul van Gastel, Harold Zandvliet, and Bene Poelsema. Phase transformations of 4,4'-biphenyldicarboxylic acid on Cu(001). *Physical Review B*, 85(23):1–10, June 2012.

[SvGZP13a] Daniel Schwarz, Raoul van Gastel, Harold Zandvliet, and Bene Poelsema. Growth Anomalies in Supramolecular Networks: 4,4'-Biphenyldicarboxylic Acid on Cu(001). *Physical Review Letters*, 110(7):076101, February 2013.

[SvGZP13b] Daniel Schwarz, Raoul van Gastel, Harold Zandvliet, and Bene Poelsema. Growth Anomalies in Supramolecular Networks: $4,4'$-Biphenyldicarboxylic Acid on Cu(001). *Physical Review Letters*, 110(7):076101, February 2013.

[SWnSR14] C. Sauer, M. Wieß ner, a. Schöll, and F. Reinert. Interface originated modification of electron-vibration coupling in resonant photoelectron spectroscopy. *Physical Review B*, 89(7):1–9, 2014.

[SYI03] Koji Suto, Soichiro Yoshimoto, and Kingo Itaya. Two-dimensional self-organization of phthalocyanine and porphyrin: dependence on the crystallographic orientation of Au. *Journal of the American Chemical Society*, 125(49):14976–7, December 2003.

[SZJ+04] A. Schöll, Y. Zou, M. Jung, Th. Schmidt, R. Fink, and E. Umbach. Line shapes and satellites in high-resolution x-ray photoelectron spectra of large π-conjugated organic molecules. *Journal of Chemical Physics*, 121(20):10260–10267, 2004.

[Tau07] F. S. Tautz. Structure and bonding of large aromatic molecules on noble metal surfaces: The example of PTCDA. *Progress in Surface Science*, 82(9-12):479–520, September 2007.

[TES+02a] F. Tautz, M. Eremtchenko, J. Schaefer, M. Sokolowski, V. Shklover, and E. Umbach. Strong electron-phonon coupling at a metal/organic interface: PTCDA/Ag(111). *Physical Review B*, 65(12):125405, February 2002.

[TES+02b] F.S. Tautz, M. Eremtchenko, J.a. Schaefer, M. Sokolowski, V. Shklover, K. Glöckler, and E. Umbach. A comparison of the chemisorption behaviour of PTCDA on different Ag surfaces. *Surface Science*, 502-503:176–184, April 2002.

[TKKT04] M. Tejima, K. Kita, K. Kyuno, and a. Toriumi. Study on the growth mechanism of pentacene thin films by the analysis of island density and island size distribution. *Applied Physics Letters*, 85(17):3746, 2004.

[TSS+00] F. Tautz, S. Sloboshanin, J. Schaefer, R. Scholz, V. Shklover, M. Sokolowski, and E. Umbach. Vibrational properties of ultrathin PTCDA films on Ag(110). *Physical Review B*, 61(24):16933–16947, June 2000.

[TV87] C. W. Tang and S. A. VanSlyke. Organic electroluminecent diodes. *Appied Physics Lettersied Physics Letters*, 51(12):913, 1987.

[UK08] Nobuo Ueno and Satoshi Kera. Electron spectroscopy of functional organic thin films: Deep insights into valence electronic structure in relation to charge transport property. *Progress in Surface Science*, 83(10-12):490–557, 2008.

[USF96] E. Umbach, M. Sokolowski, and R. Fink. and epitaxy of large organic adsorbates. *Applied Physics A*, 63:565–576, 1996.

[vB14] Jonas van Bebber. Untersuchung des wachstums von kupferphthalocyanin auf cu(001) mit niederenergetischen elektronen. Master's thesis, RWTH Aachen University, 2014.

[VF84] Tamas Vicsek and Fereydoon Family. Dynamic Scaling for Aggregation of Clusters. *Physical Review Letters*, 52(19):1669–1672, 1984.

[vS06] Marian von Smoluchowski. Zur kinetischen Theorie der Brownschen Molekularbewegung und der Suspensionen. *Annalen der Physik*, 326:756–780, 1906.

[vS16] Marian von Smoluchowski. Drei Vorträge über Diffusion, Brownsche Molekularbewegung und Koagulation von Kolloideteilchen. *Physikalische Zeitschrift*, 17:557, 1916.

[vS17] Marian von Smoluchowski. Versuch einer mathematischen Theorie der Koagulationskinetic kolloider Lösungen. *Zeitschrift für physikalische Chemie*, 92:129–168, 1917.

[VSH84] J. A. Venables, G D T Spiller, and M Hanbücken. Nucleation and growth of thin films. *Reports on Progress in Physics*, 47:399–459, 1984.

[WG02] George M Whitesides and Bartosz Grzybowski. Self-Assembly at All Scales. *Science*, 295(March):2418–2422, 2002.

[WMS91] G M Whitesides, J P Mathias, and C T Seto. Molecular self-assembly and nanochemistry: a chemical strategy for the synthesis of nanostructures. *Science*, 254(5036):1312–1319, 1991.

[WSx14] WSxM solutions. Wsxm solutions website. `www.wsxmsolutions.com`, 2014. visited December 2014.

[ZGS07] Dietrich R T Zahn, Gianina N. Gavrila, and Georgeta Salvan. Electronic and vibrational spectroscopies applied to organic/inorganic interfaces. *Chemical Reviews*, 107(4):1161–1232, 2007.

[Zhu04] X. Y. Zhu. Electronic structure and electron dynamics at molecule-metal interfaces: Implications for molecule-based electronics. *Surface Science Reports*, 56(1-2):1–83, 2004.

[ZKS+06] Y. Zou, L. Kilian, A. Scholl, T. Schmidt, R. Fink, and E. Umbach. Chemical bonding of PTCDA on Ag surfaces and the formation of interface states. *Surface Science*, 600(6):1240–1251, March 2006.

8 Acknowledgment

I would like to thank:

- Christian Kumpf: thank you for creating such a wonderful atmosphere in our group. You are a shining example of how one should lead a group. I always left your office in better spirits. I would also like to thank you for the countless discussions we had about my data.

- Frank Meyer zu Heringdorf: thank you for the discussions about my data and agreeing to co-referee my PhD thesis.

- Joachim Mayer: thank you for agreeing to co-referee my PhD thesis.

- Daniel Schwarz: thank you for showing me how to do science with the LEEM. You taught me how much information can be extracted from LEEM images. It was a pleasure to work with you.

- Thomas Duden: thank you for teaching me how to operate the LEEM. You seemed like a magician to me in the way you could fix almost any alignment problem within minutes if not seconds.

- Benjamin Stadtmüller: thank you for your never-ending patients in answering all my questions and helping me fix problems in the lab. You were the one I went to for the more difficult problems :) I am also grateful to you and your girlfriend Annemarie for driving me to Jülich every morning for the first two years.

- Sonja Schröder: thank you, Sonja. For your unwavering support. For the long discussions about my data. For a new perspective on how I could tackle problems. For your ability to get structure into my sometimes chaotic thoughts. For going on vacation with me and not complaining about me going to bed at nine o'clock instead of partying. The last years would only have been half as much fun without you.

- Janina Felter: thank you for your help during the last month of my thesis. I do not know what I would have done without you. I know the LEEM will be in good hands.

- Jonas van Bebber: thank you for your help during your year as a Master student at our institute.

- Christa Elsässer: thank you for measuring all STM images used in this work.
- Elmitec team: Thank you for your quick and reliable help with the LEEM. You never despaired when I needed descriptions like "the cylindrical things in the gray things next to the big blue thing" for finding the fuses on the circuit board.
- all members of the PGI-3: thank you for the nice atmosphere. Almost all of you helped me at one point or another by lending me equipment, by helping me with programming, or by fruitful discussions about my data. I would also like to thank Stefan Tautz for deciding to buy a LEEM :) and for the hard work he puts into providing the infrastructure we have at the institute.
- the SB20/SB11 gang: Martin, Sonja, François, Simon, and Kathrin: thank you for the entertaining discussions and all the fun we had riding in the bus from Aachen to Jülich and back. I feel like the two hours I spend in the bus each day were not lost. A special thanks to François for sometimes riding by bike with me to Jülich. Even at freezing temperatures.
- my friends Claudia, Dominik, Fabian, Jan, Katharina, and Lotte: thank you for your support. I could not hope for better friends. A special thanks to Lotte for reading large parts of my thesis and to Jan for his help in fitting the data with y- and x-errors.
- my family: thank you. I would not be the person I am today without you. You always supported me and I always knew that I could count on you. A special thanks to my brother for reading large parts of this work. I hope you understood more of my thesis than I did of yours ;)

Band / Volume 136
Manipulating the Structural and Electronic Properties of Epitaxial $NaNbO_3$ Films via Strain and Stoichiometry
B. Cai (2016), VI, 114 pp
ISBN: 978-3-95806-185-9

Band / Volume 137
Surface Potential of Metallic Surfaces and Self-Assembling Organic Monolayers in Various Electrolytes
J. Wang (2016), ii, 58 pp
ISBN: 978-3-95806-188-0

Band / Volume 138
Ab initio investigation of hybrid molecular-metallic interfaces as a tool to design surface magnetic properties for molecular spintronics
R. Friedrich (2016), 277 pp
ISBN: 978-3-95806-194-1

Band / Volume 139
Topological Matter – Topological Insulators, Skyrmions and Majoranas
Lecture Notes of the 48th IFF Spring School 2017
27 March – 07 April 2017, Jülich, Germany
ed. by S. Blügel, Y. Mokrousov, T. Schäpers, Y. Ando (2017), ca 1000 pp
ISBN: 978-3-95806-202-3

Band / Volume 140
In situ studies of the growth and oxidation of complex metal oxides by pulsed laser deposition
C. Xu (2017), iv, 159 pp
ISBN: 978-3-95806-204-7

Band / Volume 141
Intrinsic and extrinsic spin-orbit torques from first principles
G. Géranton (2017), 122 pp
ISBN: 978-3-95806-213-9

Band / Volume 142
Magnetic Proximity Effects in Nanoparticle Composite Systems and Macrocrystals
G. Wilbs (2017), III, 230 pp
ISBN: 978-3-95806-233-7

Band / Volume 143
Etablierung eines Systems aus Cysteinmutanten der Phosphoglycerat-Kinase für Entfaltungsstudien mit Einzelmolekül-FRET
A. Schöne (2017), 137 pp
ISBN: 978-3-95806-237-5

Band / Volume 144
Structural and electronic characterization of hetero-organic NTCDA-CuPc adsorbate systems on Ag(111)
S. Schröder (2017), vi, 154 pp
ISBN: 978-3-95806-239-9

Band / Volume 145
Tailoring Molecular Magnetism
T. Esat (2017), viii, 163 pp
ISBN: 978-3-95806-240-5

Band / Volume 146
Spin-wave excitations and electron-magnon scattering in elementary ferromagnets from *ab initio* many-body perturbation theory
M. C. T. D. Müller (2017), vi, 174 pp
ISBN: 978-3-95806-242-9

Band / Volume 147
Neutron Scattering
Lectures of the JCNS Laboratory Course held at Forschungszentrum Jülich and at the Heinz-Maier-Leibnitz Zentrum Garching
edited by T. Brückel, S. Förster, G. Roth, and R. Zorn (Eds.) (2017),
ca 400 pp
ISBN: 978-3-95806-243-6

Band / Volume 148
Neutron scattering
Experimental Manuals of the JCNS Laboratory Course held at Forschungszentrum Jülich and at the Heinz-Maier-Leibnitz Zentrum Garching
edited by T. Brückel, S. Förster, G. Roth, and R. Zorn (Eds.) (2017),
ca 200 pp
ISBN: 978-3-95806-244-3

Band / Volume 149
Kinetic and thermodynamic considerations on the formation of heteromolecular layers on metal surfaces
C. Henneke (2017), vii, 157, XIV pp
ISBN: 978-3-95806-245-0

Schlüsseltechnologien /
Key Technologies
Band / Volume 149
ISBN 978-3-95806-245-0